INEL-96/0212

April 1996

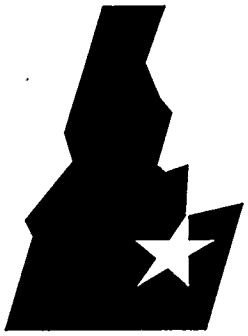

Idaho National Engineering Laboratory

An Accelerator-Based Epithermal Photoneutron Source for Boron Neutron Capture Therapy

Hannah E. Mitchell

Lockheed Idaho Technologies Company

An Accelerator-Based Epithermal Photoneutron Source for Boron Neutron Capture Therapy

A Thesis
Presented to
The Academic Faculty

by

Hannah Elizabeth Mitchell

In Partial Fulfillment
of the Requirements for the Degree
Doctor of Philosophy in Nuclear Engineering

Georgia Institute of Technology
April 1996

ACKNOWLEDGMENTS

This report is generated from thesis work completed in partial fulfillment of the requirements for the degree of Doctor of Philosophy in Nuclear Engineering at the Georgia Institute of Technology. The number of individuals who have given help and support during the course of my research and preparation of this thesis is so numerous that it is difficult to know where to begin. I would first like to acknowledge the technical as well as financial support I have received at the Idaho National Engineering Laboratory over the course of the past two years. I am grateful to the INEL for the opportunity to spend the past two years at this laboratory via an Associated Western Universities (AWU) graduate student fellowship and for the use of INEL equipment and computers. This study was performed under the auspices of the United States Department of Energy, Office of Energy Research, DOE Idaho Operations Office, Under Contract Number DE-AC07-94ID13223.

The author gratefully acknowledges Dr. Frank Harmon, of the physics department at Idaho State University, who was indispensible in both his help, time and financial support and for his invaluable comments during the writing phase of my thesis. In particular, I would like to recognize the support of Idaho State University for the use of the beam lab (linear electron accelerators, detectors, power supplies, foils, etc.). Additionally, I would like to recognize the help of several ISU graduate students (in particular

big Jim, little Jim and Lane for their patience and help during the irradiation experiments) and the support of the EML lab for their time and detectors.

In addition, much of this thesis would not have been possible without the help of researchers at the Technical Research Centre of Finland (VTT-Finland) for contributing sample filter bricks manufactured via a novel production process developed in Finland. The assistance of Iiro Auterinen, of VTT-Finland, in this matter is gratefully ackowledged, as are the interesting discussions with VTT-Finland graduate student Tiina Seppälä.

At Georgia Tech, Dr. Ratib Karam and my entire doctoral committee, have been more than helpful. I would also like to thank Claudette Noel of the Mechanical Engineering graduate office (who often went out of her way to help in details difficult to organize from the backcountry of Idaho) for her competence and patience. I would like to acknowledge the efforts of Arlene and Debbie of Georgia Tech's Neely Nuclear Research Center.

At the INEL, a huge thank-you goes to Dr. Dave Nigg, without whose support this work would simply never have been possible, for his encouragement and his amazing ability to explain just about anything. Additional thank-you's go to Yale Harker, James Jones, Woo Yoon and Floyd Wheeler for their inputs and suggestions in both experimental and calculational matters. I would also like to acknowledge Chuck Wemple for his enormous help in MCNP cross section calculations and comments during the writing of this thesis. And, additional credit belongs to Chris White for her patience and

help in scanning numerous photographs and figures.

The acknowledgments for this work would not be complete without thanking my friends and family. I would like to thank Carol for her spontaneity and enthusiasm and for putting up with me in her house for these few months (or....has it been years ?!!). I would also like to thank Gary for dragging me out skiing and hiking. And thanks! to Jeffery for the Lost Arts evenings. I am also grateful to my friends and climbing buddies in Idaho Falls, including Jason & Kim and Steve & Rene.

I would also like to mention George and Sadie in Atlanta for their kindness, and my friend and office-mate, Kate, for her help and support in Atlanta. I could never have made it through graduate school without the friendships of many individuals. In particular, thanks belong to David, Willi, Carl, Uffe, Iain, Angela, Jogy, Sara, Paul, Sándor, Laura and Martin (and his wonderful family!), as well as the whole Atlanta-crowd.

And, lastly, this section would not be complete without giving a special thanks to my family: including my four brothers (Phillip, Joe, Jay and Kevin) and especially my parents for their encouragement, support and confidence.

Hamm

TABLE OF CONTENTS

LIST OF TABLES

LIST OF FIGURES

SUMMARY

Boron neutron capture therapy is an experimental binary cancer radiotherapy modality in which a boronated pharmaceutical that preferentially accumulates in malignant tissue is first administered, followed by exposing the tissue in the treatment volume to a thermal neutron field. At present BNCT research in both the United States and Europe emphasizes the necessity of an epithermal beam to generate the necessary thermal neutron field at the desired depth. Through the use of an epithermal beam, deeper-seated tumors can be treated more effectively. Boronated cells are selectively destroyed via energy deposition resulting from the $^{10}B(n,\alpha)^{7}Li$ interaction.

Current usable beams are reactor-based but a viable alternative is the production of an epithermal neutron beam from an accelerator. Current literature cites various proposed accelerator-based designs, most of which are based on proton beams with beryllium or lithium targets. This dissertation examines the efficacy of a novel approach to BNCT treatments that incorporates an electron linear accelerator in the production of a *photoneutron* source. This source may help to resolve some of the present concerns associated with accelerator sources, including that of target cooling. The photoneutron production process is discussed as a possible alternate source of neutrons for eventual BNCT treatments for cancer. A conceptual design to produce epithermal photo-

neutrons by high energy photons (due to bremsstrahlung) impinging on deuterium targets is presented along with computational and experimental neutron production data. A clinically acceptable filtered epithermal neutron flux on the order of 10^7 neutrons per second per milliampere of electron current is shown to be obtainable. Additionally, the neutron beam is modified and characterized for BNCT applications by employing two unique moderating materials (an Al/AlF_3 composite and a stacked Al/Teflon design) at various incident electron energies.

If BNCT is to become a wide-spread treatment modality, more neutron beam centers are needed worldwide to meet the treatment needs of all patients. With only reactor-based beams available, there could be a significant shortage of epithermal neutron beam facilities. Accelerator-based beam designs should be considered for the ultimate future of BNCT as a radiotherapy modality.

CHAPTER I

INTRODUCTION

Due to the high incidence of cancer in our society, scientists have been researching methods of treating and curing cancerous tumors for decades. Gliomas offer particular therapeutic challenges. The most highly malignant and invasive forms of this type of brain tumor, high-grade astrocytoma or glioblastoma multiforme, are characterized by less than a year's life expectancy after detection. Conventional therapies consisting of surgery, photon radiation and chemotherapy have failed to produce significant indications of long-term tumor control. Surgery is difficult due to microscopic extensions of the tumor mass. In standard radiation therapy practices, the entire brain must be irradiated to attack the tumor, which allows relatively indiscriminate damage to both healthy and malignant tissues. Conventional radiotherapy, based in part on the presence of oxygen, is also less effective due to the hypoxic nature of cells in this particular brain cancer. Although more selective, chemotherapy is, by nature, toxic and almost always results in undesirable side effects. Whereas these treatments are effective for several other tumor types and have shown many successes, an ideal therapy would destroy tumor cells, leaving the healthy ones unharmed, and exhibit minimal side effects.

Boron neutron capture therapy offers an alternative treatment that is based on the selective destruction of malignant cells with minimal damage to adjacent normal tissues.[1] The basic premise of this treatment modality is to inject a patient with a tumor-seeking boron compound and follow this with thermal neutron irradiation of the tumor site. The effectiveness of the treatment is expected to increase as both the amount of boron in the cells and the neutron flux increase. Taken separately these two components are relatively harmless; taken together they can be designed to target malignant cells. Because normal unboronated tissue components are relatively insensitive to incident neutrons in an appropriate energy range, selective damage occurs. In this treatment, advantage is taken of the nuclear reaction between boron and thermal neutrons, resulting in cell death from the energy deposited along the paths of resultant alpha particles and lithium ions. Due to their short path lengths, these heavier particles give rise to closely spaced ionizing radiation events. Additionally, they are not as dependent, as compared to x-rays, on the presence of oxygen or cell division rates to enhance their effectiveness.

The main tasks are to deliver enough boron and thermalized neutrons to each tumor cell to ensure cell death. In order to realize the benefits of NCT (Neutron Capture Therapy), a sufficiently intense and pure epithermal neutron source is critical. An epithermal beam is required to yield deeper penetration of the neutrons and thus greater

---

1. Fairchild, R. G. and Bond, V. P., Eds., Workshop on Neutron Capture Therapy. Report BNL-51994, Brookhaven National Laboratory, Upton, NY, 1986.

therapeutic gain at the desired depth as well as better skin-sparing properties. Reactors are currently the only sources of epithermal neutrons available for NCT research. But, whether designing a reactor-based beam or an accelerator-based beam, the considerations are similar. A compromise must be made between the desired epithermal neutron flux intensity and the various beam contaminants. The designed beams are usually characterized through measurement as well as calculational methods. Beam parameters to be measured are the neutron flux densities for all appropriate energies and the fast neutron and gamma doses. Beam performance may be further discussed according to the advantage factor (the ratio of tumor dose to maximum normal tissue dose) and the therapeutic gain (the ratio of effective tumor dose to effective maximum normal tissue dose). Advantage depth is sometimes used to describe the depth at which the dose to the tumor equals the peak dose to normal tissue and the advantage ratio is the ratio of total therapeutic dose to total dose to the normal tissue at the advantage depth. Following beam characterization and boron drug selection, cell cultures and small animal studies and healthy tissue tolerance studies must be performed before proceeding to NCT's ultimate use as a human cancer treatment modality.

When atomic nuclei are hit by high-energy photons there is a slight chance that they will disintegrate, yielding photoneutrons. Although this process occurs with the highest probability in the heavier elements, deuterium, in for example heavy water, with a binding energy of about 2.2 MeV, can offer a photoneutron source of sufficient intensity. If a source of high-energy photons (bremsstrahlung for example) can be con-

veniently applied to a suitable D_2O target, a novel approach for production of an acceptable flux of filterable photoneturons for NCT use is possible. The purpose of this thesis work is to provide initial experimental proof-of-principle data for this approach to producing the necessary neutrons for boron neutron capture therapy using an electron linear accelerator. This type of accelerator is currently an acceptable and useful medical device in hospitals for producing gamma-rays for current radiation therapies. What this thesis proposes is an additional use for this class of accelerators that could offer a more cost efficient method, as compared to nuclear reactors, for treating tumors via NCT.

The ultimate intention of the work outlined here is the construction of an epithermal neutron beam with a spectral distribution suitable for human treatment. A proposed potential accelerator design, based on a related idea suggested in a paper by. Jones and Yoon,[2] is discussed in Chapter III. The general concept of this idea is to have multiple electron beams impinging inward onto tungsten targets located at the outer radius of a small cylindrical tank of heavy water. The neutron-producing target (heavy water) would offer the additional advantage of self-cooling of the targets by allowing the heat to be transported away via circulation of the D_2O.

---

2. Jones, J. L. and Yoon, W. Y., "Feasibility Study of the Application of a Linear Electron Accelerator to BNCT," Proceedings of the 12th International Conference on the Application of Accelerators in Research and Industry, University of North Texas, Denton TX, November, 1992.

This thesis examines the feasibility of an accelerator-based epithermal photo-neutron source for NCT. Experiments and corresponding calculations were carried out on a low-current benchtop linear electron accelerator at a variety of energies. The experiments included beam tailoring techniques, implementing two distinct filtering materials of varying thicknesses. The primary objective of these experiments was to validate the computational methods used in order that a scaled-up version of the photo-neutron concept could eventually be designed, based on beam performance from low current experiments. Projections as to viable neutron production at higher electron accelerator currents can reasonably be relied upon if the fundamental concept can be shown feasible.

This thesis offers an introductory examination of the electron-accelerator-based photoneutron production process as an alternative to reactor-based neutron capture therapy sources. Its feasibility and practicality from a physics and engineering stand-point is presented via experimental and computational analyses. Suggestions are made for further studies which could lead to a working clinical system.

CHAPTER II

LITERATURE REVIEW AND BACKGROUND

IIa. Background of Boron Neutron Capture Therapy

Boron neutron capture therapy (BNCT) is based on the selective destruction of malignant tissue via the introduction of a boron compound into the target tissue followed by thermal neutron irradiation. It is a binary modality based on the $^{10}B(n,\alpha)^{7}Li$ reaction. Boron-10 has a high thermal neutron capture cross section, meaning a relatively high probability of thermal neutron capture and consequent production of short range high Linear Energy Transfer (LET) particles. The ^{10}B interaction ($\sigma_{n,\alpha}$ = 3838 barns) is shown below:

$$^{10}B + n_{th} \rightarrow {}^{11}B^{*} \begin{cases} \nearrow\ {}^{7}Li\ (1.01\ MeV) + {}^{4}He\ (1.78\ MeV) \quad 6.3\% \\ \searrow\ {}^{7}Li\,(0.84\,MeV) + {}^{4}He\,(1.47\,MeV) + \gamma(0.48\,MeV) \quad 93.7\% \end{cases}$$

The maximum ranges of the alpha particles and lithium ions released are 10 and 5 μm respectively. The advantage of this reaction is that the resultant particles deposit their

energy along a path length on the order of a typical cell diameter. Because the thermal neutron capture probabilities for the major tissue components (H, N, C, O) are relatively low, the energy deposited, or dose, is preferentially localized in the boron-containing tissues. There are, however, doses which must be considered from $H(n,\gamma)$ and N(n,p) with respective reaction cross sections of 0.33 and 1.75 barns. For higher energy neutrons, the first reaction, elastic scattering with hydrogen nuclei, is predominant. Because neutrons can be thermalized as they travel through the tissue via scattering events, epithermal neutrons are considered advantageous for treating deeper-seated tumors. The preferred energy range for a neutron capture therapy epithermal neutron beam is between 1 eV and 10 keV (an ideal, uncontaminated beam being around 2 keV). An epithermal beam will deliver a much lower thermal neutron dose to surface tissues and will have a much greater penetration than a thermal beam.

The boron reaction, as a potential radiotherapy modality, was first suggested by Locher in 1936.[3] Locher's suggestion was followed by radiobiological studies conducted at the University of Illinois in 1938.[4] Boron neutron capture therapy chemical and biological research continued throughout the 1940s without many clinical successes. Renewed interest at Brookhaven National Laboratory Medical Department allowed treatment of three series of patients in 1951-1952 by Farr and Sweet.[5] In 1959

3. Locher, G. L., "Biological Effects and Therapeutic Possibilities of Neutrons." *American Journal of Roentgenology*, 36: 1-13, 1936.
4. Kruger, P. G., "Some Biological Effects of Nuclear Disintegration Products on Neoplastic Tissue." Proceedings of the National Academy of Sciences of the USA. 26: 181-192, 1940.

investigations at Brookhaven on the new 3 MW Medical Research Reactor[6] were performed on patients by reflecting the scalp and exposing the head to thermal neutron fluences of 10^{13} neutrons/cm^2. No significant improvements were seen in this work either. Additional attempts at the Massachusetts Institute of Technology and the Massachusetts General Hospital by Brownell, Soloway and Sweet[7] in the late 1950s yielded unsatisfactory outcomes with mean survival times of only a few months. The majority of this work concentrated on the treatment of glioblastoma multiforme, a tumor difficult to destroy via other modalities due to its continued recurrence if any tumor cells escape death.[8] Because the lives of these patients were not prolonged as a result of treatment, no significant advantages of BNCT were seen and clinical trials in the United States were consequently discontinued. The major problems incurred in these initial trials were due to insufficient boron concentrations in the tumor cells and prohibitively high boron concentrations in normal brain capillaries. In addition, the thermal neutrons used in the irradiations did not penetrate to the desired depths. Damage was seen in healthy brain tissues, in particular to the walls of blood vessels.

---

5. Farr, L. E., Sweet, W. H., et al. "Neutron Capture Therapy of Gliomas Using Boron-10." *Transactions of the American Neurological Association*, 79: 110-113, 1954.
6. Farr, L. E., "The Physics & Physiology of NCT." *Proc. National Acad. Sci.* 40: 1088-1093, 1954.
7. Brownell, G. L. and Sweet, W. H., "Studies on Neutron Capture Therapy." In: Proceedings of the Second United Nations International Conference on the Peaceful Uses of Atomic Energy, 26: 444-450, 1958.
8. Asbury, A. K., Ojeman, R. C., Nielsen, S. L., and Sweet, W. H., "Neuropathological Study of 14 Cases of Malignant Brain Tumor Treated by B-10 Slow Neutron Capture Radiation." *J. of Neuropath. & Expt. Neurol.* 31: 278-303, 1972.

Subsequent clinical trials using second generation tumor-specific boron compounds in conjunction with thermal neutrons and skull-reflecting surgeries[9] have lead to the treatment of over 150 patients in Japan[10] since the late 1960s, with apparent success in a majority of patient cases. One patient, a man of 50 years diagnosed in 1972 with glioblastoma multiforme, was still alive with no observable recurrences as of 1990. The initiative of the Japanese in treating these malignant gliomas has served to inspire rekindled interest in BNCT as a wide-spread treatment modality.

IIb. Boron Compound Development

From past and present treatment attempts with boron neutron capture therapy, two essential factors in successful treatment are found to be:

- *good epithermal neutron beam with low contaminations*
- *neutron capture compound capable of selectively delivering boron*

Thus, without a suitable boron compound (or other neutron capture compound) , even the best of epithermal neutron beams will be useless in the treatment of malignant tissues. Because the benefits of neutron capture therapy are based on a localization of the treatment radiations, a compound with the following characteristics is desirable:

9. Hatanaka, H., "Experience of Boron-Neutron Capture Therapy for Malignant Brain Tumours--with Special Reference to the Problems of Post-operative CT Follow-ups," *Acta Neurochir. Suppl. Wein.* 42: 187-192, 1988.
10. Nakagawa, Y., "Recent Study of Boron Neutron Capture Therapy for Brain Tumors," Proceedings of the First International Workshop on Accelerator-Based Neutron Sources for Boron Neutron Capture Therapy, Vol. I, 11, Jackson, Wyoming, Sept. 1994.

- sufficient cross section for neutron capture therapy
- non-toxic
- non-radioactive
- high LET resultant particles
- availability in sufficient quantities
- ease of synthesis into a convenient chemical structure for compound transport within the body

Although many compounds exist that meet the neutron capture constraints, most are either not available in sufficient quantities or have other undesirable qualities. Advantages of selecting boron as the compound of choice include the large amount of information available on boron chemistry as well as its abundance and convenience in handling. Also, approximately 20% of natural boron is comprised of ^{10}B, the neutron-capturing isotope. Many other compounds have been studied (including ^{6}Li, ^{235}U, ^{3}He, and $^{155/156}Gd$) as neutron capture agents, but boron is currently considered the ideal choice.[11]

As important as the selection of the proper neutron capturing agent is its synthesis into a suitable pharmacological compound. To benefit at all from neutron capture therapy, two important criteria of the compound must be met: tumor selectivity (tumor-to-

11. Soloway, A. H., "Presentation at the National Cancer Institute Board of Scientific Counsellors." In: Boron Compounds Suitable for Neutron Capture Therapy for the Treatment of Cancer. NCI: Bethesda, MD, 1988.

blood ratios) and low toxicity. In the initial trials at Brookhaven National Laboratory and MIT, several compounds were tested, all but one yielding fairly poor results.[12] The boron compound sodium perhydrodecaborate ($Na_2B_{10}H_{10}$) had the best overall tumor-to-blood boron concentration and a reasonably low toxicity. Others, including sodium pentaborate, para-carboxyphenylboronic acid and borax, were either highly toxic with negative side effects or had basically no tumor selectivity.

After the initial trials in the United States, the compound BSH ($Na_2B_{12}H_{11}SH$) was successfully used in Japan in the treatment of brain tumors by H. Hatanaka.[13] This drug still sees use in both treatments in Japan and in animal studies in the United States and Europe. Researchers at the University of Illinois initiated studies on boronophenylalanine (BPA), which is considered one of the best drug options currently available, especially as a compound suitable for treating melanomas. Although the clinical results obtained in Japan are encouraging, work continues in the search for a compound that provides an even higher tumor-to-blood ratio.

Attempts are being made to take advantage of the properties of various biomolecules which have significant possibilities in the transport of the boron within the

---

12. Fairchild, R. G., "Development of Boronated Compounds for NCT." In: Boron Compounds Suitable for Neutron Capture Therapy for the Treatment of Cancer. NCI: Bethesda, MD, 1988.

13. Yoshizaki, T., Ikeuchi, I. and Nagasawa, K., "Quality Control of $Na_2{}^{10}B_{12}H_{11}SH$ for Neutron Capture Therapy," In: Neutron Capture Therapy (Hatanaka, H. ed.), Norwell, MA: MTP Press, 1986.

body.[14] If a compound could be designed to incorporate itself into the bio-chemical building blocks of a cell, the boron could be concentrated in the nucleus which may greatly enhance the destructive effects of the boron neutron capture reaction.[15] Malignant cells have a propensity to take up nucleosides (which make up DNA) at a faster rate than healthy tissue cells which also may allow for boron concentration (thus a higher susceptibility to the BNCT reaction) within the actual cell nucleus. One such boron agent (a ^{10}B-labelled DNA ligand) was evaluated by A. Corder et al. and shown to have a high uptake by taking advantage of the ligand's DNA damage-locating properties.[16] Other compounds under consideration are porphyrins and promazines.

Another tactic in the delivery of boron to cancer cells is the possible attachment of the boron to particular antibodies which are then able to target tumor cells.[17] An additional consideration in boron delivery is the actual detection of the boron in the body and the measurement of the time required to attain maximum boron concentration within the tumor cells. Ideally, it is desirable to obtain pharmacokinetic data "live" and to have immediate feedback in monitoring the uptake of a particular boron-containing drug. Several imaging techniques are currently under investigation which would allow the monitoring of boron uptake directly. One method to conduct pharmacokinetic stud-

14. Fairchild, R. G., "Recent Advances in Neutron Capture Therapy (NCT)," In: Neutron Capture Therapy (Hatanaka, H. ed.), Norwell, MA: MTP Press, 1986
15. Barth, R. F., Soloway, A. H. and Fairchild, R. G., "Boron Neutron Capture Therapy for Cancer," *Scientific American* 100-107, October 1990.
16. Corder, A., Whittaker, A., et al. "Evaluation of a ^{10}B-Labelled DNA Ligand," In: Advances in Neutron Capture Therapy, New York: Plenum, 1993.
17. Ibid 15.

ies more quickly and noninvasively is that of boron-11 magnetic resonance imaging.[18] Because the effectiveness of BNCT is dependent, in part, upon the concentration gradient of boron in the healthy tissue compared to that in the tumor tissue, knowledge of the boron transport within the body is particularly important in determining the dosages given and the consequent proper irradiation time.

IIc. Reactor Beam Developments

The development of improved boron compounds and epithermal beams has lead to renewed consideration of boron neutron capture as a form of radiotherapy. With this resurgence of interest in BNCT as a treatment modality, much work has been done in the development of epithermal neutron beams with BNCT treatment purposes in mind. At present the only available epithermal neutron beams suitable for BNCT use are from reactors. Several beams at nuclear research centers around the world are currently employed in BNCT research. Although thermal neutrons are used in treatments in Japan, present designs focus on tumor treatment with beams of predominately epithermal neutrons.

To obtain an epithermal neutron beam from a reactor, the fission neutron energy must be reduced about 2-3 orders of magnitude. Unwanted gamma and fast neutron contaminants must be removed by moderating materials in the optimization process.

---

18. Glover, G.H., Pauley, J.M. and Bradshaw, K. M., "Boron-11 Imaging with a 3-dimensional Reconstruction Method," *J. Magn. Reson. Imaging*. 2:47, 1992.

Beam design entails several compromises between the neutron flux intensity and various beam contaminants.

Japanese medical doctors and scientists continue to use thermal beams for treatment in Kyoto at the Kyoto University Research Reactor (KURR) and at the JAERI Research Reactor (JRR-4),[19] the beam is currently undergoing alterations for an upgrade to epithermal energies. Thermal beams are still of interest due to the number of patients who have been and are currently undergoing treatment at these sites. In addition, thermal beams may prove useful in the treatment of superficial tumors. Improved beam designs at the Musashi reactor are also being considered for future thermal and epithermal treatments.[20] In the United Sates, beams at the Brookhaven National Laboratory in New York (Brookhaven Medical Research Reactor or BMRR) and the Massachusetts Institute of Technology Reactor (MITR-II) have been updated and redesigned to offer epithermal neutrons for BNCT purposes. Currently, the MITR-II offers a thermal neutron flux of about $4x10^8$ n/cm^2-sec at 2 cm depth in tissue. Plans have been presented to improve the beam to neutron fluxes greater than 10^9 n/cm^2-sec.[21] In Europe the High Flux Reactor at Petten has been installed and

19. Sakurai, Y., Kobayashi, T., Kanda, K., et al. "Improvement of Thermal Neutron Fluence for BNCT Treatment of Deep-seated Tumors: Simulation Calculation and Phantom Experiments." In: Advances in Neutron Capture Therapy. New York: Plenum, 1993.
20. Aizawa, O. and Yamada, H., "Study on the Best Design of Neutron Irradiation Facility for BNCT." In: Progress in Neutron Capture Therapy for Cancer. New York: Plenum, 1992.
21. Choi, J. R., Zamenhof, R. G., Yanch, J. C. et al. "Performance of the Currently Available Epithermal Neutron Beam at the Massachusetts Institute of Technology Reseaerch Reactor (MITR-II)." In: Progress in Neutron Capture Therapy for Cancer. New York: Plenum, 1992.

characterized[22] and will soon be employed in human clinical trials. Variations on the current design are also being considered, such as the possibility of employing a U-235 converter plate to boost neutron production.[23] Although not intended for human trials, another reactor in Sweden (R2-0 in Studsvik) is thought to be appropriate for BNCT studies in cell cultures and with small experimental animals.[24]

The epithermal neutron sources available to date are far from ideal. In addition to the beams presently available, several proposed beams are currently being designed and optimized for future BNCT use. Beams at three other reactor sites in Europe (Czech Republic,[25] Finland[26] and Italy[27]) offer possible BNCT epithermal neutron sources. In Finland plans are underway to begin beam characterization studies and small animal irradiations in late 1996. The HIFAR in Australia also seems a viable option.[28] In the United States three additional sites are of interest outside of the

22. Moss, R. L., "Progress Towards Boron Neutron Capture THerapy at the High-Flux Reactor Petten," Neutron Beam Design, Development and Performance for Neutron Capture Therapy, New York: Plenum Press, 1990.
23. Rief, H. et al. "Generating Epi-thermal Neutron Beams for BNCT at TRIGA reactors." In: Abstract Book - 5th International Symposium on Neutron Capture Therapy for Cancer. Columbus, OH, 1992.
24. Pettersson, O., Svensson, P., Larsson, B. and Grusell, E., "Studsvik Thermal Neutron Facility." In: Progress in Neutron Capture Therapy for Cancer. New York: Plenum, 1992.
25. Burian, J., Marek, M., and Rataj, J., "Neutron Beam Parameters on LVR--15 Reactor for Neutron Capture THerapy." In: Progress in Neutron Capture Therapy for Cancer. New York: Plenum, 1992.
26. Auterinen, I. and Hiismaki, P., "Epithermal BNCT Neutron Beam Design for a TRIGA II Reactor." In: Advances in Neutron Capture Therapy. New York: Plenum, 1993.
27. Rief, H., Van Heusden, R. and Perlini, G., "Generating Epithermal Neutron Beams for Neutron Capture Therapy in Small Reactors." In: Advances in Neutron Capture Therapy. New York: Plenum, 1993.
28. Storr, G. J., Allen, B. J. et al. "Design Considerations for the Proposed HIFAR Thermal and Epithermal Neutron Capture Therapy Facilities." In: Progress in Neutron Capture Therapy for Cancer. New York: Plenum, 1992.

MITR-II[29] and the BMRR. These proposed epithermal neutron beam sources are:

- GTRR - Georgia Tech Research Reactor[30]
- MURR - Missouri University Research Reactor[31]
- Washington State University research reactor beam

All of these proposed solutions appear to offer potentially adequate beams with epithermal neutron fluxes on the order of 10^9 n/cm^2-sec or greater. The GTRR design has less fast neutron contamination than other designs and offers better collimation with a current-to-flux ratio of 0.86.[32] Optimization and improvements in these neutron beams should continue as it is desirable to have several beam options as NCT research in the United States moves closer to clinical trials. Although research in reactor-based beam designs continues, and there are proposals to build new reactors (primarily TRIGAs at hospital sites) for the sole use of NCT,[33] the future appears to lie in the development of more flexible beam options, such as accelerators, which would be deployable to the hospital environment, or possibly radioisotope sources.

29. Harling, O. K. et al., "Boron Neutron Capture Therapy and Radiation Synovectomy Research at the Massachussetts Institute of Technology Research Reactor," *Nuclear Science and Engineering*, 110:330, 1992.
30. Klee, K., "Optimization of an Epithermal Neutron Beam and Beam Dosimetry for Boron Neutron Capture Therapy at the Georgia Tech Research Reactor," Doctoral Thesis, Georgia Institute of Technology, 1994.
31. Brugger, R. M., Shih, J. A. and Liu, H. B., "An Epithermal Neutron Beam for Neutron Capture Therapy at the Missouri Univerisity Research Reactor," *Nuclear Technology*, 98: 322-332, 1992.
32. Klee, K., Nigg, D., Wheeler, F. and Karam, R., "Conceptual Design for an Advanced Epithermal Neutron Beam for Boron Neutron Capture Therapy at the Georgia Institute of Technology Research Reactor," ANS Topical Meeting on Advances in Reactor Physics, Knoxville, TN, April 1994.
33. Whittemore, W. L., "A Compact TRIGA Reactor for Boron Neutron Capture Therapy." In: Progress in Neutron Capture Therapy for Cancer. New York: Plenum, 1992.

IId. Accelerator-Based Neutron Beam Developments

Currently, as NCT develops into an approved radiotherapy modality, accelerator-based sources are becoming more attractive neutron beam candidates. There are several reasons for this. Obvious advantages include the possible lower capital costs of accelerators as well as their convenience, deployability and compactness for hospital use. Research indicates that the neutron energy spectrum derived from an accelerator-based source may yield an improved neutron beam with less gamma contamination. A significant advantage of accelerator beams is that under some circumstances they can be more easily tuned to have fewer fast neutrons, with the majority less than 10 keV. Several accelerator-based sources for NCT use have been proposed in the past, largely based on the well-characterized $^{7}Li(p,n)^{7}Be$ reaction. Another possible approach utilizes a high-energy proton beam spallation reaction target design.[34] In general, the design ideas for an accelerator-based source attempt to maximize the neutrons produced per incident proton (which increases with proton energy) while minimizing degradation of the target.

Various feasibility studies based on proton accelerators have been considered, generally consisting of a lithium target in conjunction with a BeO or D_2O moderator system. One conceptual design recently under consideration consists of a proton beam with a maximum proton energy of 2.5 MeV incident on a Li-7 target, where

34. Crawford, J. F., Reist, H., Conde, H. B., Larsson, J. et al. "Neutrons for Capture Therapy Produced by 72 MeV Protons." In: Progress in Neutron Capture Therapy for Cancer. New York: Plenum, 1992.

there is a maximum in the cross section curve for the $^{7}Li(p,n)^{7}Be$ reaction. An advantage of this target material, in considering a (p,n) type reaction, is its low reaction threshold (1.88 MeV) which allows for a lower incident proton beam energy, leading to less target heating to be dissipated. Another advantage of the Li-7 target design is that it allows for a much smaller moderator (maximum neutron energy is approximately 0.8 MeV) as compared with that necessary for the 72 MeV proton spallation source. A possible accelerator-based neutron irradiation facility (ANIF) proposed by Wang and Blue appears to offer a viable alternative to reactor beams, if target cooling problems can be solved.[35] This design postulates the use of a Radio Frequency Quadrupole (RFQ) accelerator of 2.5 MeV protons at a current of 30 mA. Target size and geometry are optimized, resulting in the selection of a copper-backed lithium target, chosen for its high thermal conductivity. The neutron energy spectrum from the optimized moderator assembly yields a dose rate of approximately 23.4 cGy/min at 30 ppm boron-10, allowing for a long, but not unreasonable, treatment time. The ratio of absorbed neutron dose to fluence for this design was calculated to be 4.9×10^{-11} cGy-cm^2/neutron. In addition, useful neutron fluxes on the order of 10^7 n/cm^2-sec per mA of protons are shown to be possible.

---

35. Wang, C.-K. Ch., Blue, Th. E., Gahbauer, A., "A design study of an accelerator-based epithermal neutron source for boron neutron capture therapy." *Strahlentherapie und Onkologie* 165: 75-78, Februar/Marz 1989.

Another source based on this same reaction was designed by T. Wu and offers an epithermal neutron flux of $9x10^8$ n/cm^2-sec and a neutron current to flux ratio (J/ Φ) of 0.66.[36] Although in terms of beam directionality, intensity and fast neutron and gamma dose, this design does not perform as satisfactorily as the best reactor beam available, it is potentially competitive with the majority of NCT reactor beams. Experimental measurements at full-power are necessary to fully characterize the beam parameters.

Studies on a separate accelerator-based source conducted by Yanch et al. consider using a 10-mA 2.5-MeV Tandem Cascade Accelerator (TCA), with current experiments carried out on a 1-mA 3.7 MeV TCA.[37] Various forms of lithium were considered for the target design, resulting in the ultimate selection of a thin lithium metal layer (90 μm) on an aluminum substrate, which, at higher currents, could be important in facilitating heat transfer. A neutron yield of $8.98x10^{11}$ n/sec per mA was obtained in the energy range of 200-800 keV which was then moderated to therapeutically useful levels. The same investigators also optimized a moderator/reflector assembly consisting of a cylindrical D_2O moderator surrounded by a thin layer of ^6Li and a thick lead reflector. Dose rates were predicted and measured for various D_2O thicknesses.

---

36. Wu, H. T., "A Low Energy Accelerator-Based Neutron Source for Boron Neutron Capture Therapy," Dissertation in Nuclear Engineering Program of University of Missouri-Columbia, Aug. 1992.
37. Yanch, J. C., Zhou, X-L, and Klinkowstein, R. E., "Accelerator-Based Epithermal Neutron Beam Design for Neutron Capture Therapy," *Medical Physics*, 19:3, 709-721, May/June 1992.

Further work by Wu and Brugger indicates the possibilities of alternate target materials, such as H-3 or a H-3/Li-7 combination.[38] Their calculations show a higher dose rate for the H-3 target along with a higher neutron yield (almost double). The neutron energy values for the tritium target require more moderation in order to yield energies suitable for NCT. But, at the patient irradiation position, the experimental results indicate comparable neutron flux and gamma dose characteristics. In work conducted at the Science Research Laboratory, Shefer and Yanch investigated various charged particle reactions, most of which, except $^{7}Li(p,n)$ and $^{3}H(p,n)$, were considered inappropriate for NCT purposes due to relatively low reaction cross sections.[39]

Through joint research in Switzerland and Sweden, a spallation neutron source is being considered in which a lithium target is bombarded with 72-MeV protons produced with the 72-MeV Injector I Cyclotron at the Paul Scherrer Institüt.[40] When a high-energy primary particle interacts with a target nucleus, spallation will occur in two distinct stages. In the first stage high energy secondary particles and low energy "cascade" particles escape. The nucleus, left in an excited state, then relaxes with the emis-

38. Wu, T. H., Brugger, R. and Kunze, J. F., "Low Energy Accelerator-based Neutron Sources for Neutron Capture Therapy," In: Advances in Neutron Capture Therapy. New York: Plenum, 1993.
39. Shefer, R. E., Klinkowstein, R. E., Yanch, J. C., and Brownell, G. L., "A Versatile, New Accelerator Design for Boron Neutron Capture Therapy: Accelerator Design and Neutron Energy Considerations," In: Neutron Beam Design, Development, and Performance for Neutron Capture Therapy, New York: Plenum, 1990.
40. Crawford, J. G., Larsson, B., Reist, H., Conde, et al. "High Energy Accelerator Technology in Radiology," Presentationn at IEEE Particle Accelerator Conference, Washington, D. C., May 1993.

sion of low energy "evaporation" neutrons. The neutrons produced in this reaction at the PSI are of a peak energy of 2 MeV; they leak from the target and are then moderated with iron and carbon to energies useful for NCT treatment.

Currently, experiments are underway at Brookhaven National Laboratory and Los Alamos National Laboratory[41] which are designed to measure the neutron yield from tungsten and lead using a proton beam from BNL's Alternating Gradient Synchroton (0.8 to 2.0 GeV). These targets, unfortunately, produce some undesirable long-lived radioisotopes and are not a practical target solution for NCT purposes.

The possibilities of beryllium as a neutron target material have been researched by J. B. Marion and J. S. Levin.[42] Beryllium offers good thermal and chemical properties (not as reactive as lithium). Beryllium's melting point is higher than that of lithium (1278°C compared to 179°C) and has a thermal conductivity of 130 W/m°C as compared with lithium's 45 W/m°C. A problem to be overcome, however, with beryllium targets is its relatively low neutron yield. Higher incoming proton energies are required on a beryllium target.

---

41. Cokinos, D. M. and van Tuyle, G. J., "A High-Intensity Accelerator-Based Neutron Source," In: *Transactions American Nuclear Society* 69: 423-424, November 1993.
42. Marion, J. B. and Levin, J. S., "Investigation of the $^{9}Be(p,n)^{9}B$ and $^{9}Be(p,\alpha\gamma)^{6}Li$ reactions," *Physics Review*, 115:144, 1959.

A final accelerator-based epithermal neutron source considered is bombardment of a beryllium target with 20 MeV deuterons.[43] This source yields a forward-peaked spectrum with a maximum neutron intensity at 8 MeV. A calculational comparison of this source made with the lithium target and the spallation source yields comparable dose distributions,[44] although experiments have yet to confirm this design possibility. Further in-depth investigations on beryllium target designs for NCT treatment based on the $^{9}Be(p,n)^{9}B$ reaction with 4 MeV protons are presented by Wang.[45,46]

The selection of moderator material for the neutron beam is essential. The moderator should meet certain requirements while maintaining a large neutron flux:

- moderate scattering cross section with minimal absorption cross section
- low radiative capture neutron cross section
- larger cross section for fast neutrons to eliminate contamination
- as thin as possible so as not to reduce flux (relatively low mass number desirable)
- light nucleus to maintain angular directionality of beam

---

43. Cierjacks, S., ed. Neutron Sources for Basic Physics and Applications: Oxford, England: Pergamon Press, 1983.
44. Grusell, Erik, "Accelerator Based Neutron Sources for Neutron Capture Therapy." In: Progress in Neutron Capture Therapy for Cancer. New York: Plenum 1992.
45. Wang, C.-K. Ch., and Moore, B. R., "On the Study of Energy Spectra and Angular Distriibutions of the Neutrons Emitted from a Beryllium Target Bombarded with 4-MeV Protons for Neutron Capture Therapy," In: Advances in Neutron Capture Therapy. New York: Plenum, 1993.
46. Wang, C.K., "Thick Beryllium Target as an Accelerator-Based Neutron Source for Neutron Capture Therapy," Proceedings of the First International Workshop on Accelerator-Based Neutron Sources for Boron Neutron CaptureTherapy, 161, Sept. 1994.

Popular moderator candidates include D_2O, Al_2O_3, BeO and TiO_2. In work conducted by Yanch et al.,[47] D_2O was shown to have superior moderating qualities for neutrons in the 4 eV to 40 keV range. Moderator assemblies were also compared and analyzed in detail by Blue et al. In considering both the D_2O-MgO and BeO-MgO combinations, a higher useful neutron fluence per dose equivalent per source of approximately 30% was seen in the BeO-MgO assembly (for a small tissue volume in air). Monte Carlo studies were made using the well-known code MCNP at the Paul Scherrer Institüt to examine the properties of several moderator materials for tailoring appropriate beam energies and fluences.[48]

As can be seen from recent developments in accelerator-based epithermal neutron sources, one problem incurred in designing a source for NCT is that of obtaining an acceptable neutron flux with little fast neutron and gamma contamination, while addressing problems of target design and cooling. In the overall design process, target heat dissipation, desired neutron energy, angular distribution and proton current requirements must be considered. Several difficulties arise in the particular case of the $^7Li(p,n)^7Be$ reaction for epithermal neutron production. Since target design is simplified if the target does not exceed its melting point, lithium's melting temperature of 180°C leads to difficulties, especially when attempts are made to scale the design to

47. Yanch, J. C., Zhou, X-L, et al. "Design of an Accelerator-Based Epithermal Neutron Beam for Boron Neutron Capture Therapy." In: Progress in Neutron Capture Therapy for Cancer. New York: Plenum, 1992.
48. Ibid 34.

clinically useful beam strengths. The system pressure could possibly be increased to prevent this but then problems develop with the heat flux at the target/coolant interface. These thermal-hydraulic design criteria must be addressed in the target development and construction.

IIe. Additional Considerations in NCT Development

Additional areas of NCT research include dosimetry, microdosimetry and treatment planning. Biological studies on small animals and dogs are necessary in the determination of healthy tissue tolerance doses as well as the necessary tumor-killing doses. Radiation flux and dose distributions within an actual Labrador dog head were investigated using discrete-ordinate methods and then compared with the results from calculations in a standard homogeneous dog phantom.[49] Small animal studies are key in the process leading eventually to human clinical trials. Currently animal studies are being carried out at several reactors including Brookhaven Medical Research Reactor (BMRR), Petten's High Flux Reactor in Holland and in late 1996 at VTT in Finland. These studies aid in the determination of methods of measuring dose deposited within a patient and in the eventual treatment planning process.[50] Since the fall of 1994 human clinical trials are also underway in the United States at the BMRR.

49. Moran, J. M., Nigg, D. W., Wheeler, F. J. and Bauer, W. F., "Macroscopic geometric heterogeneity effects in radiation dose distribution analysis for boron neutron capture therapy," *Medical Physics* 19:3, 723-732, May/June 1992.
50. Nigg, D. W., Randolph, P. D. and Wheeler, F. J., "Demonstration of three-dimensional deterministic radiation transport theory dose distribution analysis for boron neutron capture therapy," *Medical Physics* 18:1, 43-53, Jan/Feb 1991.

Because NCT involves several different kinds of radiations interacting with various components of tissue, it becomes necessary to look at the effects on the cellular level. Microdosimetry is of particular importance because it deals with the deposition of energy on a cellular scale, taking into consideration the boron distributions within the cells. Microdosimetric models allow a theoretical prediction of both experimental dosimetry and of what occurs on a scale too small to allow measurements to be experimentally feasible. Looking at dosimetry on the microscopic level shows inhomogeneities in the boron distribution. An accurate analytical microdosimetric model could possibly provide insight into dose calculations for inhomogeneous boron distributions.[51]

Other NCT research of necessity is that of determining the Relative Biological Effectiveness (RBE) values associated with the boron neutron capture process. The predicted values for these factors vary greatly but are quite significant in calculating the total dose to the patient.[52] The RBE value is a multiplying factor which aids in comparing the relative dose effects from varying forms of radiation on tissues in a particular radiation process.

---

51. Vroegindeweij, C., "Micro-dosimetry Model: A Preparatory Study," ECN-I-93-010 ECN Netherlands Energy Research Foundation, March 1993.
52. Gabel, D., Bond, V. P., Kalef-Ezra, J. and Fairchild, R. G., "The Necessity of Stochastic Radiobiology in BNCT, or, What is the RBE of the $^{10}B(n,)^{7}Li$ Reaction?" In: Progress in Neutron Capture Therapy for Cancer, New York: Plenum, 1992.

IIf. Bremsstrahlung Production

In this work it is proposed to develop an alternate accelerator-based source of neutrons for NCT using photoneutrons produced by bombarding suitable materials with bremsstrahlung radiation generated by the slowing down of an electron beam in an appropriate target. For the photoneutron source proposed in this paper it is of interest to consider the production of bremsstrahlung and the various possible bremsstrahlung-producing targets which have been significantly studied in past experiments.

In order to produce photoneutrons, the energy of the high intensity photon source must exceed the binding energy of the neutrons in a particular target material. Although photons can be obtained from radioisotope sources, the majority of the isotopes with acceptable photon energies must be manufactured and have fairly short half-lives. In addition, the strength of these sources is usually not enough to produce the necessary neutron flux. The advantages of an X-ray source are its continuous spectrum and high energies. X-rays can be produced as either characteristic line spectra (not energetic enough for NCT use) or bremsstrahlung. When an electron slows down in the field of a target nucleus, the continuous electromagnetic X-ray spectrum called bremsstrahlung is produced. This radiation is a direct result of the electron being deflected by the coulombic field of a nucleus, although in some cases bremsstrahlung can be emitted in the field of an electron. When an electron undergoes a change in acceleration, electromagnetic radiation is emitted; the radiated energy is a continuous spectrum up to a maximum quantum energy equal to the total kinetic energy of the incident particle. The amplitude

of this radiation depends on the acceleration of the electron, proportional to Ze^2/M (where Ze is the nucleus charge and M the mass of the incident particle), in the vicinity of a nucleus, while the intensity varies as Z^2/M^2. Therefore, an electron will produce more bremsstrahlung than a heavier charged particle. The bremsstrahlung produced by heavy particles is negligible in comparison with the characteristic K and L X-rays produced by ionization. In general, for greater bremsstrahlung production, a higher Z target is also desirable due to the Z^2 dependence.

In the bremsstrahlung process, the electron can also be thought of in a quantum mechanical sense as a plane wave scattered by a nuclear field. The probability of bremsstrahlung radiation is on the order of 1/137 times the probability of elastic scattering. This factor, $2\pi e^2/hc$, is a result of the interaction of the electron with the electromagnetic field of the emitted photon and is called the fine-structure constant. In quantum mechanical theory, the probability that the photon will be emitted when a particle is accelerated is small but finite. But, when a photon *is* emitted, it is of a relatively large energy.

On the other hand, in classical considerations, bremsstrahlung is emitted in *every* inelastic collision. These two theories result in different energy spectra, with experiments confirming the quantum mechanical model. The two theories yield similar *average* values for cross sections, on the order of:[53]

(1)

$$\frac{Z^2}{137\left(e^2/m_o c^2\right)^2} cm^2/\text{nucleus}$$

The total radiative cross section, σ_{rad}, is given below and is defined as the fraction of the total (rest mass plus kinetic, T) energy of the electron which is radiated as the electron travels through a material of thickness 1 atom/cm^2.

(2)

$$\sigma_{rad} = \sigma_o Z^2 B cm^2/\text{nucleus}$$

where:

$$\sigma_o = \frac{1}{137}\left(e^2/m_o c^2\right)^2 = 0.58\text{mb/nucleus}$$

B = coefficient dependent on Z and T

The energy of the electrons considered in this work are highly relativistic ($T >> m_o c^2$) and the bremsstrahlung cross section approximation for these energies is given by Bethe and Heitler[54] to be:

---

53. Evans, R. D., "Radiative Collisions of Electrons with Atomic Nuclei," The Atomic Nucleus, New York: McGraw-Hill, 1955.
54. Bethe, H. A. and Heitler, W., *Proc. Roy. Soc. (London)*, A146: 83, 1934.

(3)

$$\sigma_{rad} = 4\left\{\ln\left(\frac{2(T+m_oc^2)}{m_oc^2}\right) - 1/3\right\}\sigma_o Z^2$$

Most theoretical analyses of bremsstrahlung deal with thin target spectra production from monoenergetic electrons. By a thin target it is assumed that the target is thin enough such that the electrons undergo no appreciable energy loss by ionization and no secondary radiative collisions. In the more realistic laboratory case of thick target bremsstrahlung production, the considerations become more complex. To some extent, the electron-photon transport in a thick target can be analytically considered as a superposition of thin target cases. Although the thick-target has not been as thoroughly studied as the ideal thin-target case, it has been shown that the total bremsstrahlung energy per electron absorbed can be given by:[55]

(4)

$$I = kZT^2$$

where k is a constant dependent on the target material and I and T are in MeV. The yield of bremsstrahlung production increases as both Z and T increase. In experiments conducted by Ulrey et al., the bremsstrahlung energy was measured on a thick tungsten target, demonstrating this T^2 dependence.[56] In this work it was deter-

55. Evans, R. D., "Stopping of Electrons by Thick Absorbers," The Atomic Nucleus, New York: McGraw-Hill, 1955.
56. Ulrey, C. T., *Physics Review* 11:401, 1918.

mined that the fraction of incident electron energy converted to bremsstrahlung radiation, I/T, to be approximately $7x10^{-4}ZT$.

Varied theoretical calculations of thick-target bremsstrahlung cross-sections are carefully outlined by Koch and Motz.[57] This overview discusses the bremsstrahlung cross-section formulae over various energy ranges as well as the utilization of several approximations and corrections which aid in the selection of the appropriate cross-section formula. Many of the discrepancies seen between analytical methods of determining bremsstrahlung cross-sections are a result of the complexity of the formulae and the approximations and simplifications that must be made to solve them. In addition, many of the methods take only the first electron stages into account, which can lead to inaccuracies when applied to thick targets.

Analytical methods of calculating bremsstrahlung spectra are supplemented by Monte Carlo electron-photon transport code calculations. These codes generate electron histories and follow individual electrons as they interact according to various stochastic sampling procedures. This method also involves generating a database of scattering and energy-loss cross sections and then determining the random sampling of particle histories. The results obtained through various Monte Carlo codes appear to yield reliable descriptions of the interaction processes consistent with analytical methods. One limiting factor

57. Koch, H. W. and Motz, J. W., "Bremsstrahlung Cross-Section Formulas and Related Data," *Review of Modern Physics*, 31:920-955, 1959.

is that of the accurate choice of bremsstrahlung cross-section values. The results of the Monte Carlo codes depend greatly on the selection of appropriate cross section data.

Although there are several candidate target materials for production of bremsstrahlung which may be appropriate for subsequent photoneutron production, tungsten is recognized as one of the best. Estimates of tungsten thick-target bremsstrahlung yields for varying electron energies (2 - 8 MeV) have been performed by Khandelwal et al.[58] using radiation yield tables for these energies from Berger and Seltzer.[59] They obtained a least-squares fit expression which can be integrated from the threshold electron energy to the incident energy to give an expression for the average radiation yield from a thick tungsten target:

$$Y(E) = (2.9E + 5.8)\,\% \tag{5}$$

where E is the total electron energy in MeV. This integration allows for consideration of only the electrons that are energetic enough to produce bremsstrahlung which is, in turn, energetic enough to produce photoneutrons from the chosen target material.

Berger and Seltzer performed Monte Carlo calculations of electron-photon cascades in thick tungsten targets bombarded by electrons of energies up to 60 MeV.[60]

---

58. Khandelwal, G. S., Pritchard, W. M. and Singh, J. J., "An Estimate of the Yield of Photoneutrons from Beryllium Using a LINAC as the X-Ray Source," *Nucl. Sci. Eng.*, 60:481-486, 1976.
59. Berger, M. J. and Seltzer, S. M., "Tables of Energy Losses and Ranges of Electrons and Positrons," NASA SP-3012, National Bureau of Standards, 1964.

The efficiency, angular distribution and spectra of the bremsstrahlung was obtained and then compared with experimental results. Bremsstrahlung beams from electron accelerators in which electrons of lower energies (but still in the MeV range) were incident on a tungsten target were also investigated.[61] They chose a target width to maximize the bremsstrahlung yield for the incident electron beam energy. Flux spectra were obtained at electron energies of 2, 5 and 10 MeV as a function of depth in a water phantom. Additional tungsten target measurements were conducted by Starfelt and Koch[62] in which they analyzed the shapes of the bremsstrahlung spectra from a 10 MeV monoenergetic electron beam.

Additional thick-target investigations were performed by Alsmiller[63] on a tantalum target with 13 MeV electrons and the results were in good agreement with those obtained by Berger and Seltzer. Further, Koch and Motz[64] analyzed the bremsstrahlung spectra from a platinum target, while targets of a composite tungsten/gold material were examined by O'Dell et al. for energies between 5.3 and 20.9 MeV.[65]

---

60. Berger, M. J. and Seltzer, S. M., "Bremsstrahlung and Photoneutrons from Thick Tungsten and Tantalum Targets," *Physical Review C*, 2:2, 621-631, August 1970.
61. Seltzer, S. M. and Berger, M. J., "Energy Deposition by Electron, Bremsstrahlung, and ^{60}Co Gamma-Ray Beams in Multi-Layer Media," *Appl. Radiat. Isot.* Vol 38:5, 349-364, 1987.
62. Starfelt, N. and Koch, H. W., *Phys. Rev.* 102:1598, 1956.
63. Alsmiller, R.G. and Moran, H.S., "Electron-Photon Cascade Calculations and Neutron Yields from Electrons in Thick Targets," Oak Ridge National Laboratory, Report No. ORNL-TM-1502, 1966.
64. Koch, H.W. and Motz, J.W., "Bremsstrahlung Cross-Section Formulas and Related Data," *Rev. Mod. Phys.* 31: 920, 19599.
65. O'Dell, A. A., Sandifer, C. W. et al. *Nucl. Instr. Methods* 61:340, 1968.

One method of analyzing the bremsstrahlung yield is given by Schiff in which an expression for the energy and angular distribution of the radiation from fast electrons in thin targets is obtained by integrating the differential bremsstrahlung cross section of Bethe and Heitler over the scattered electron angles.[66]

Hisdal[67] and Sirlin[68] have calculated thick target bremsstrahlung production based on the convolution of a multiple-scattering angular distribution for electrons with the bremsstrahlung cross section. Although experimental data are limited particularly in the electron energy range of moderately relativistic electrons, good agreement between analytical values and experimental results have been observed, especially in reference to spectral shape.

In order to accurately evaluate bremsstrahlung production, the entire electron-photon cascade must be known. Slowing down and scattering of primary and secondary electrons must be considered, including Compton scatter, pair production and photoelectric effects, as well as scattering and absorption of bremsstrahlung, characteristic X-rays and annihilation radiation. The target thickness should be optimized for maximum bremsstrahlung, taking into account that the bremsstrahlung production seen by the intended photoneutron production target will be reduced by attenuation within a thicker target.

---

66. Schiff, L. I., "Energy-Angle Distribution of Thin Target Bremsstrahlung," *Phys. Rev.* 83:2, 252-256, 1951.
67. Hisdal, E., *Phys. Rev.*, 105:1821, 1957.
68. Sirlin, A., *Phys. Rev.*, 106:637, 1957.

In addition to intensity measurements, angular dependence is of importance in bremsstrahlung analysis. The angular distribution is defined as the radiation emerging from the target per unit solid angle in direction with respect to the incident electron beam. The magnitude of the spectra is very sensitive with respect to the angle of emergence. Spectra from higher energy electrons are found to be harder at emergence directions parallel to the incident beam. The forward peaking is expected since bremsstrahlung is given off by electrons which have lost very little energy due to multiple scattering. Berger and Seltzer[69] have calculated angular dependence and compared their data to analytical results of O'Dell et al.[70] and good agreement was found. Experimental work by Jupiter, Hatcher and Hansen[71] showed the angular distribution of bremsstrahlung from a tantalum target, also indicating this forward peaking. These results were confirmed by researchers in this same citation, who measured the angular distribution of bremsstrahlung from tantalum targets bombarded with 29.7 and 57.4 MeV electrons. Although, for lower electron energies, the bremsstrahlung intensity at 90° is seen to be much greater.

A final subject to consider is the heating of the target by the incident electron beam. In work discussed previously, Berger and Seltzer give results of the energy

---

69. Ibid 60.
70. O'Dell, A. A., et al. *Nucl. Instr. Methods* 61:340, 1968.
71. Jupiter, C.P., Hatcher, C.R. and Hansen, N.E., "Measurement of the Angular Distribution of Bremsstrahlung Intensity for 10 MeV and 20 MeV electrons on Thick Targets," CONF-452-14, American Physical Society, Washington, D.C., April 1964.

deposited by electrons as a function of depth in a target for various incident beam energies. These results include the contributions of primary and secondary electrons. Although the energy deposited peaks at a relatively shallow depth in the target, energy is deposited to some extent by the exiting bremsstrahlung as well. Energy deposition resulting from an interaction is basically heat which must be dissipated in some way if the amount of heat could potentially damage the target.

IIg. Photoneutron Production

Photons can interact with matter through various mechanisms, being either scattered or absorbed. The type of interaction that takes place is mainly energy dependent and is independent of the origin of the photons. The interaction of photons in matter is an exponential attenuation process in which the photon may interact with atomic electrons, nucleons, or the electric or meson field associated with nuclei or electrons. The three most probable interactions are the Compton effect, photoelectric effect and pair production. Photodisintegration is the process by which a photon interacts with a nucleus, resulting in the ejection of either a neutron or a proton or, in the case of certain heavy nuclei, photofission. For the most part, this process is a relatively high energy effect seen mainly with photon energies greater than 8 MeV. Two exceptions are the interactions $^{9}Be(\gamma,n)$ and $^{2}H(\gamma,n)$. Although the most probable result of a photonuclear absorption is neutron emission, other processes can occur as well, including γ-ray and charged particle emission.

Photoneutron emission can occur with all elements as long as the photon energy is greater than the nuclear binding energy of the most loosely bound neutron. Due to the lower thresholds of the beryllium and deuterium interactions, these two materials are obvious choices for photoneutron targets of interest in BNCT. The photodisintegration reactions for beryllium and deuterium are:

$$ {}^{9}_{4}Be + \gamma \longrightarrow {}^{8}_{4}Be + {}^{1}_{0}n $$

$$ {}^{2}_{1}D + \gamma \longrightarrow {}^{1}_{1}H + {}^{1}_{0}n $$

with threshold energies of 1.67 and 2.18 MeV, respectively. The approximate energy of the ejected neutron is given by:[72]

(6)

$$ E_n = \frac{A-1}{A}\left(E_\gamma - Q - \frac{E_\gamma{}^2}{1862\,(A-1)} \right) + \delta $$

where E_n is in MeV, A is the mass number of the target nucleus, E_γ is the energy of the photons in MeV and Q is the threshold energy in MeV for the particular (γ,n) reaction. δ is a small energy spread dependent on the angle between the incident photon and the emitted neutron. The fractional spread in energy decreases as

72. Wattenberg, A., "Photo-Neutron Sources," *Preliminary Report No. 6 Nuclear Science Series*, July, 1949.

the neutron energy increases. Deuterium is more sensitive to the energy spread than is beryllium. But, at higher energies this energy spread is generally negligible and is only significant when a monoenergetic group of neutrons is desired. The actual useful energy of the photoneutron may be less than that calculated in the above equation due to collisions the neutron may suffer as it travels out of the target.

Photoneutron yields depend upon the target material, the strength and spectrum of the photon source and the geometry. Once the photon source spectrum is determined, the photoneutron yield will be determined by the cross section for the photodisintegration process which is dependent on the photon energy. Much work has been performed on the theoretical energy dependence of the deuterium cross section. The general shape of the cross-section as a function of photon energy above threshold shows a monotonically increasing function until a certain point (approximately 4.5 MeV) where it reaches a maximum then gradually falls off. This feature of the photoneutron cross section was first discussed in work by Bethe and Bacher.[73] Confirmatory calculations have also been performed by Rarita and Schwinger[74] and experimental measurements are in good agreement. In the case of beryllium, experimental evidence indicates a cross section which peaks about 100 keV above the threshold of 1.67 MeV and reaches two other maxima at approximately 2.95 and 4.6 MeV. The photoneutron cross-section

73. Beth, H.A. and Bacher, R.E., *Rev. Mod. Phys.* 8:125, 1936.
74. Rarita, W. and Schwinger, "Deuteron and Triton Methods", *Physical Review*, 1799-1801, Dec. 15, 1948.

for beryllium at just above the threshold has been examined in detail by Berman et al.,[75] in which it was attempted to experimentally characterize this excitation peak.

Because the photoneutron production process is a fairly unlikely process, even with an infinitely thick target, yields will not be greater than about 10^{-3} neutrons per incident photon. This is due to the fact that other gamma interaction processes such as the Compton effect (especially in the photoneutron production energy range) is approximately 10^3 times more probable than the photodisintegration process. The photonuclear absorption cross-section is usually on the order of a few millibarns per nucleon. In heavy water and beryllium, respectively, the mean free paths for the Compton effect for photons energetic enough to initiate the photonuclear reaction are approximately 25 cm and 10 cm. So, although a larger target will yield a greater photoneutron production, there exists a point at which the neutron production will peak due to the reduction of the photon flux through other competing interactions.

Both deuterium and beryllium have been carefully studied as a source of photoneutrons due to their low binding energy thresholds.[76] In experiments conducted by Jakobson,[77] a thick beryllium target was bombarded with the bremsstrahlung from a

---

75. Berman, B. L., Van Hemert, R. L. and Bowman, C. D., "Threshold Photoneutron Cross Section for Be^9," *Phys. Rev.* 163:4, 958-963, 1967.
76. Mobley, R. C. and Laubenstein, R. A., "Photoneutron Thresholds of Beryllium and Deuterium," Argonne National Laboratory ANL-4468, 1950.
77. Jakobson, M. J., "Photodisintegration of Be^9 from Threshold to 5 MeV," *Phys. Rev.* 123:1, 229-230, 1961.

monoenergetic electron source incident on a tantalum target. In these measurements, Jakobson looked at the angular distribution of the emitted photoneutrons and found the neutrons emitted from the peaks at 1.7 MeV and 4.6 MeV photon energies are isotropic but those at the 2.40 MeV and 2.95 MeV energies are not, showing a slightly higher production at 90° with respect to the photon beam.

The photoneutron yield from a target of atomic number Z is given as:

$$Y_n = \int \sigma(Z, \omega) W(\omega, E)\, d\omega \tag{7}$$

integrated over all photon energies above the reaction threshold, where ω is the energy of the photon quanta and E the energy of the electron. The values used for the cross-sections come from standard theoretical data while the X-ray radiation spectrum is a measured value dependent on orientation. A process for estimating the photoneutron yield from beryllium using a linear accelerator was performed by Khandelwal et al.[78] in which a thick beryllium target was exposed to bremsstrahlung from a tungsten target bombarded with electrons of energies from 2 to 8 MeV. The total photoneutron yield per electron is calculated taking into account both the bremsstrahlung and the photo-neutron target yields. The neutron production rate is calculated as:

$$R = \left(\#\ \text{impinging electrons}/cm^2 s\right)\left(Y_{ave} \times 10^{-3}\right)\sigma_{ave}\left({}^{9}Be\ \text{atoms}/cm^2\right) \tag{8}$$

78. Ibid 58.

where Y_{ave} is the average thick-target radiation yield and σ_{ave} the average photo-neutron cross section. This calculation assumes all photons are forwardly emitted and all reach the beryllium target normally. Another way to consider the photoneutron yield is to look at the photon track length in the target. If the track length per photon energy is summed up over the target, it can then be multiplied by the coefficient for photoneutron production per unit path length and integrated over all photon energies.

CHAPTER III

MOTIVATION AND PROCEDURES

IIIa. Motivation

The development of a practical accelerator-based source of epithermal neutrons for boron neutron capture therapy has been limited by several factors, including low beam intensities, target cooling difficulties and high neutron-capture gamma doses. The motivation of this work is the eventual construction of a clinically-useful accelerator-based epithermal neutron beam suitable for neutron capture therapy which may resolve some of these difficulties. The design is based on a photoneutron production process in which a high-atomic-number material is bombarded with electrons of energies sufficient to produce an appropriate bremsstrahlung spectrum. The resultant photon radiation is then directed on a neutron-producing material of high photoneutron production cross section and reasonably low threshold energy. This two-stage process is a well-known phenomenon but has yet to be applied in the medical field, in particular as a source for NCT (see Figure 1). The overall efficiency of this process for the NCT case studied (on the order of 10^{-4} neutrons/electron) is comparable to that obtained employing alternate methods of epithermal neutron production, including protons on lithium. If a prototype design can be shown to be a viable alternative to reactor-based

sources and if NCT as a radiation therapy modality continues to show promise, the advantages of such an epithermal neutron beam source are obvious. The compactness, relative simplicity, cost-effectiveness and multi-faceted uses of medical electron linear accelerators are all significant features which would make an accelerator-based epithermal photoneutron source an attractive design, especially in a clinical environment.

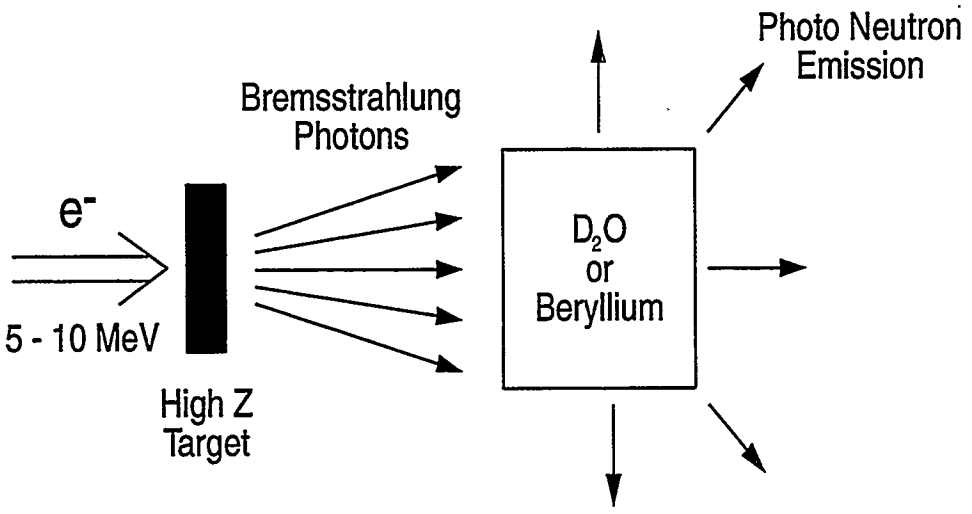

Figure 1: Photoneutron process for NCT use

Most existing non-medical photoneutron beams are of both high intensity and high energy. These fast neutrons must be moderated to useful NCT energy ranges, which, in the process, can result in unwanted loss of intensity in the filter/moderator assembly. A lower incident electron energy (still above the threshold energy for the production of bremsstrahlung) will yield slower neutrons more easily tailored for NCT with a lower, but still satisfactory, intensity and much less of a problem regarding bremsstrahlung contamination of the desirable neutron beam. The yield and intensity of this beam appear to be comparable with other accelerator-based systems proposed elsewhere. This low-energy electron beam photoneutron source offers several potential benefits over previous designs. The target for an electron accelerator-based neutron source can be designed for easy removal of the waste heat inevitable in accelerator targets. In addition, electron accelerators in this energy range are readily obtainable and are based on existing technology. Preliminary studies of the feasibility of this novel approach have been conducted. The purpose of this work is to propose an epithermal neutron source with sufficient flux intensity and satisfactory spectral distribution for clinical applications of NCT and to show, via calculation and experimentation on a low-current benchtop model, that the concept is viable.

A diagram illustrating a basic design for the proposed electron accelerator photoneutron source for NCT use is shown in Figure 2. It includes one or more electron beams incident on thin (1-5 mm) targets which surround a cylindrical tank of heavy water (a percentage of the tank possibly containing beryllium). An electron

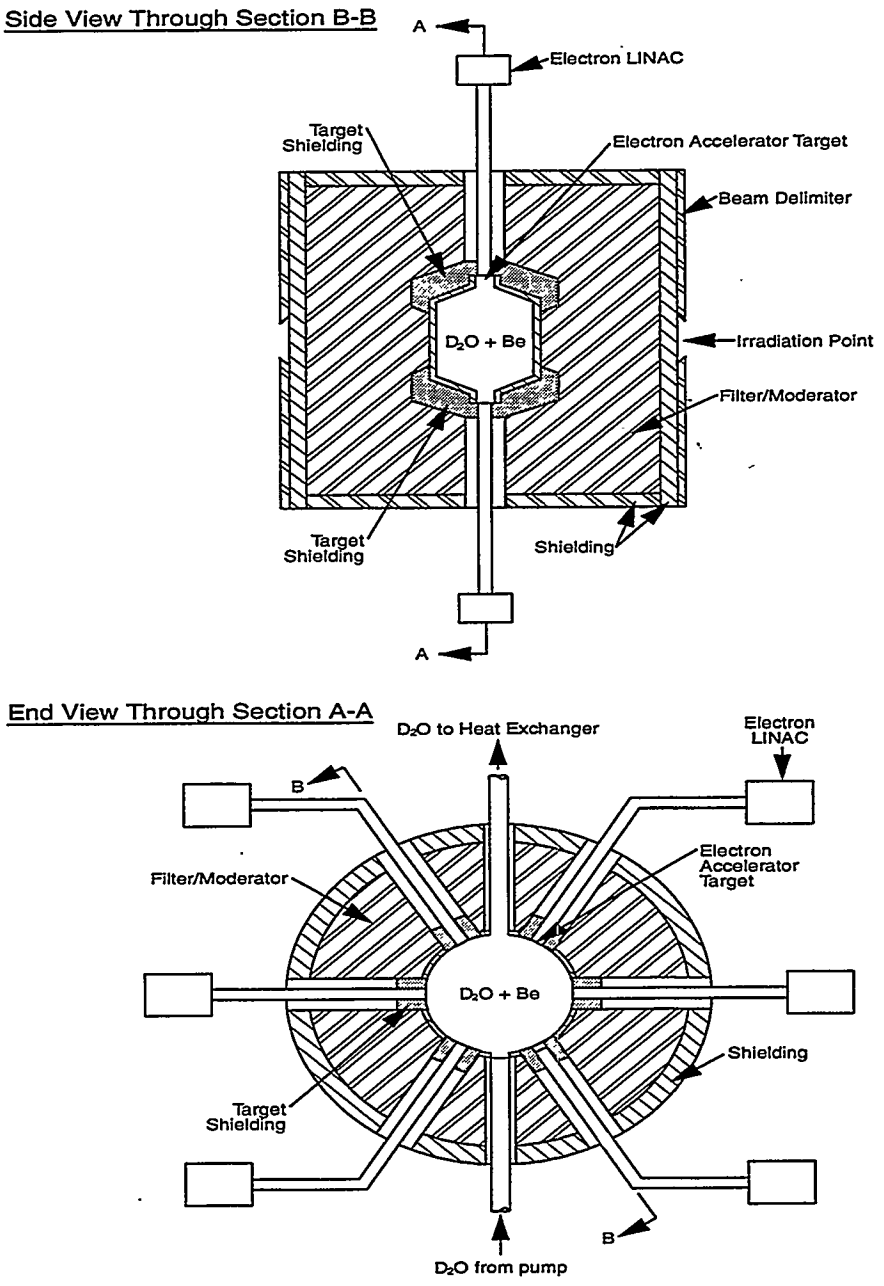

Figure 2: Proposed preliminary design of epithermal photoneutron source

beam in the 4 to 10 MeV range impinges on the targets yielding forward-peaked bremsstrahlung which is then absorbed in the D_2O/Be photoneutron target volume. The photoneutrons generated in this volume produce a strong neutron source which then passes through a filtering/moderating region where it is tailored to desired beam specifications. The neutrons will be moderated to some extent in the photo-neutron target volume. The materials in the moderating and filtering section of the assembly (possibly D_2O, metallic lithiated aluminum and aluminum trifluoride, AlF_3) are chosen such that the resultant beam spectrum at the patient location is strongly epithermal. Additional considerations must be made for shielding of the photons from the bremsstrahlung source and neutron-induced gamma rays. This shield could be composed of bismuth and lead. Final beam shaping is accomplished with beam delimiters, such as lithiated polyethylene. The complete assembly (excluding the treatment region) will be surrounded by additional concrete, lead and bismuth as patient shielding.

This idea is encouraged by the feasibility of such a design given existing technologies and the preliminary studies initially conducted at the Idaho National Engineering Laboratory on a related concept.[79] The work completed for this thesis was motivated by additional results calculated previously at the Idaho National Engineering Labora-

79. Jones, J.L. and Yoon, W.Y., "Feasibility Study of the Application of a Linear Electron Accelerator to BNCT", Proceedings of the 12th International Conference on the Application of Accelerators in Research and Industry, University of North Texas, Denton TX, November, 1992.

tory for the conceptual design shown in Figure 2. The computed nonselective proton recoil dose in hydrogenous tissue per unit useful epithermal neutron flux at the irradiation point is $1.6x10^{-11}$ cGy/neutron/cm^2 (radiobiologically-acceptable). Similarly, the incident gamma dose at this point due to neutron-capture reactions occurring before reaching the patient position is also on the order of 10^{-11} Gy/neutron/cm^2.

The preliminary design consists of an electron accelerator beam impinging on a tungsten target surrounding a tank of D_2O. The basic geometric configuration of this design is cylindrical and the moderator/filter region is composed of 90% AlF_3 and 10% lithiated aluminum. This mixture is believed to be an excellent epithermal beam shaper. Although preliminary studies were carried out assuming this type of filter material, the actual experiments and corresponding calculations for this thesis work employed two other materials (a similar $Al/AlF_3/LiF$ composite material developed by the Technical Research Centre of Finland[80] and a novel Aluminum/Teflon (Al/CF_2) design developed during this research). In this configuration it should be possible to treat with two or more opposing beams due to the symmetric geometry. Heat removal in this design could be accomplished by allowing the D_2O to flow through the cylinder, thus removing waste heat on a continual basis.[81] The assembly could be designed such that heat could be dissipated from the tungsten targets via

80. Ibid 26.
81. McEligot, D.M., "Accelerator Target Cooling for the BNCT Epithermal Source", In: J.R. Venhuizen (ed), 1995 INEL BNCT Program Annual Report, 1996.

transfer to the D_2O tank. The design is only proposed and it is intended that further investigations following the initial proof-of-principle work in this thesis be carried out in order to produce an optimized final design.

The calculated results using D_2O as the photoneutron source and lithiated aluminum and aluminum trifluoride as the moderating and filtering materials are shown in Figure 3[82] assuming a 1 mA electron beam current. These initial INEL calculations, carried out at an electron energy of 6 MeV, indicated the use of an electron accelerator-based neutron source as a promising alternative to previously investigated accelerator-based systems. These results were encouraging and were the initial motivation for the bulk of this thesis work.

Certain crucial proof-of-principle benchmark measurements essential to the design of a useful accelerator-based epithermal neutron source based on the photoneutron production concept are presented in this thesis. Because the results of these initial computations were encouraging, it was intended that this thesis work offer experimental verification of these calculational methods for the NCT photoneutron design concept. A workable "scaled-up" system modelled on the designed prototype is suggested with ultimate clinical use as the intended goal. The testing procedures included both calculational

82. Nigg, D.W., Mitchell, H.E., et al., "Epithermal Photoneutron Source Studies for BNCT," Proceedings of the First International Workshop on Accelerator-Based Neutron Sources for Boron Neutron CaptureTherapy, 373, Sept. 1994.

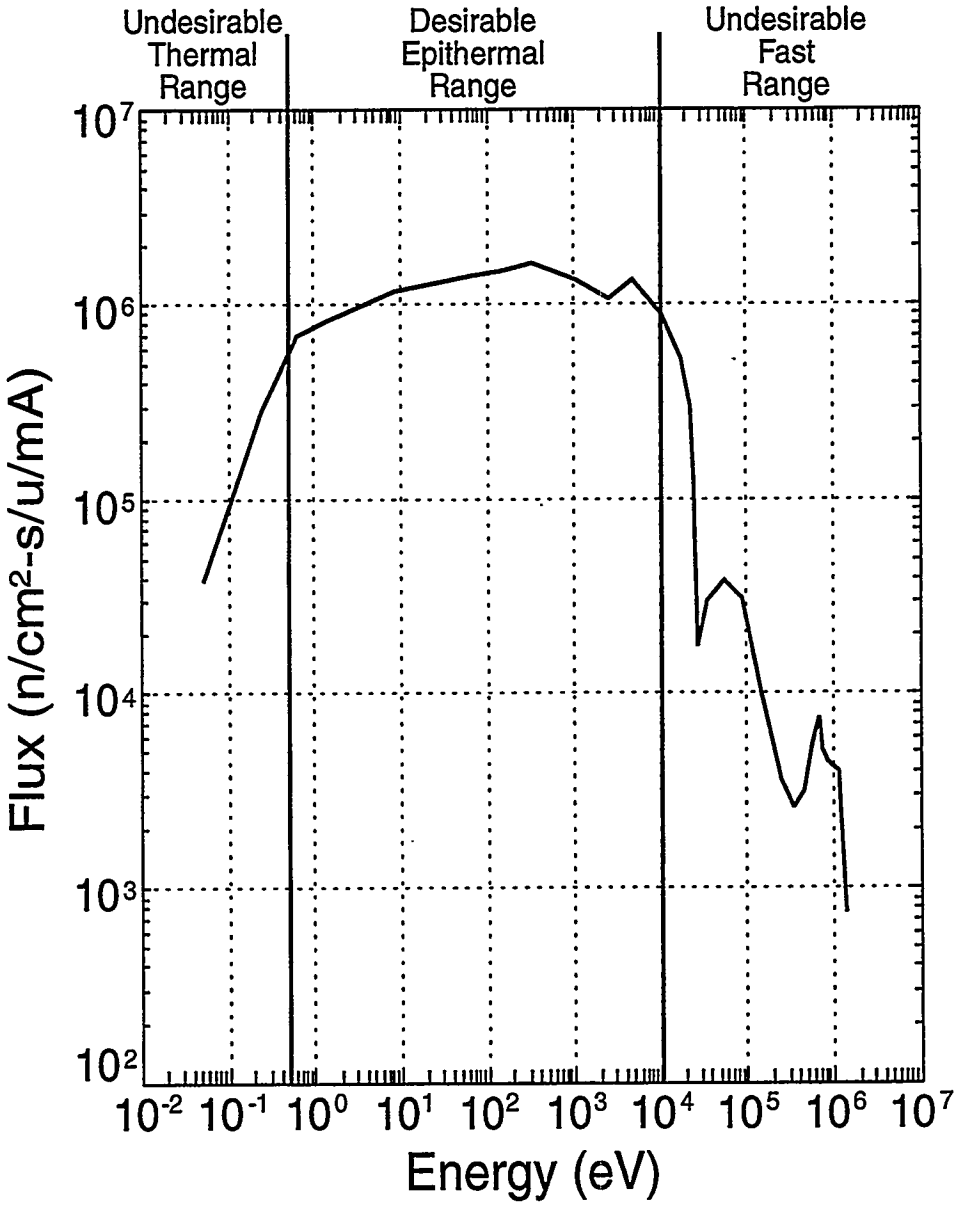

Figure 3: Flux spectrum of the initial trials for the conceptual BNCT source shown in Figure 4

and experimental verifications of the unfiltered photoneutron yield from a prototypical heavy-water target subjected to a bremsstrahlung beam of appropriate energy. Then, appropriate benchtop-scale filters were modelled and constructed, and measurements were taken of the resultant filtered neutron flux and energy spectra. Included in this work were preliminary studies of the selection of appropriate target thicknesses (both tungsten x-ray converter targets and neutron-producing D_2O) to maximize the photo-neutron yield. Initial Monte Carlo simulations of neutron production showed that available linear accelerators, target and filtering materials are adequate for further proof-of-principle applications. Yields from this proposed assembly were on the order of 10^{-4} neutrons per incident electron.

Calculations have been completed to estimate the performance of this neutron source. Electron-photon transport computations were conducted to obtain the bremsstrahlung production from the tungsten target and using these results photo-neutron production within the heavy water volume was calculated. It was of interest to characterize the filtering properties of the two aforementioned materials. In this way both source spectra and tailored energy spectra could be analyzed. Calculations were performed using both discrete ordinates and Monte Carlo methods in order to compare with the experimental results.

Proof-of-principle measurements were carried out using a simple 4-MeV medical accelerator and on a variable electron energy accelerator at energies from 4 to 8 MeV.

Photoneutron production measurements were taken and the experimental set-up was modelled and compared with the experimental results in order to provide benchmarking of the calculational techniques used in the original conceptual design studies. Dose rate measurements of the gamma dose in the accelerator room were made using ionization chambers in the vicinity of the accelerator with and without various shielding materials in place.

The results from this work demonstrate that neutron flux levels comparable to the levels produced by other accelerator-based epithermal neutron source concepts can be produced using the photoneutron technique. From preliminary calculations it is believed a flux output on the order of 10^7 n/cm^2/sec per milliampere of electron beam current is possible. With an electron beam current of 100 mA, a clinically-useful neutron flux intensity can be obtained on the order of 10^9 n/cm^2/sec. The research conducted demonstrates that the physics of this potential NCT neutron source will offer a competitive solution for ultimate use in clinical treatments.

IIIb. Procedures

The general approach taken in this work was to characterize and study the possibility of an accelerator-based photoneutron source implementing both computer modelling and experimentational methodologies. The bulk of the work consisted of designing low-current benchtop prototype experiments to collect neutron spectral and flux data followed by data reduction and finally, comparison with calculated theoretical results. A variety of experiments to study the unfiltered neutron flux as well as the filtered epithermal-neutron energy spectra were carried out in order to determine the feasibility of this electron-linear-accelerator-driven photoneutron production approach. These experiments and calculations served two primary purposes:

- *to determine whether the obtainable flux spectrum was comparable to that obtained using conventional reactor beams and to determine whether the overall efficiency of filtered photoneutron production is of a useful magnitude*
- *to obtain energy spectrum measurements that would indicate the possibility of an appropriate therapeutic beam of photoneutrons*

The calculations consisted of modelling various experimental set-ups as well as the modelling and tailoring of several additional geometries and materials. If these initial calculations are reasonably verifiable experimentally, then calculations of more advanced geometries may be assumed reliable for future design characterization

studies. Minor optimization studies were also completed varying several parameters, including target volumes, materials and energies.

The procedures and studies carried out were intended to characterize a variety of significant beam parameters. Of primary importance is the production of a *clinically-useful* flux of epithermal neutrons. To determine this feasibility, a number of beam characteristics, including intensity, spectrum and gamma contamination, are of interest. The experiments were designed to obtain information on these beam parameters.. Measurements included foil irradiation techniques and ionization chamber gamma detection. Of particular interest in describing the clinical usefulness are the neutron beam parameters such as cadmium ratios, spectral composition for impinging electron energies and currents, and epithermal flux intensity after neutron source filtration. For instance, thermal and non-thermal beam components were separated using cadmium to remove, or absorb, the thermal component.

The procedures section is divided into subsections, each addressing different aspects of the calculational and experimental approaches, apparatus used, data acquisition and data reduction techniques. The following sections will discuss the calculational and experimental methods employed and will describe in detail the apparatus utilized in describing the photoneutron production process. The procedures followed are outlined below along with considerations and difficulties encountered during the data collection process. Finally, the data analysis techniques of extracting useful beam parameters from measurements and computations will be detailed.

IIIb1. Calculational Methods

Since this neutron production process is basically a two-stage procedure (electron to gamma conversion followed by photoneutron production), knowledge and modelling of both steps is necessary. The calculational results were obtained using a variety of computational radiation transport tools. The various codes employed are described briefly below. In each case, the code selected for use was dependent upon the problem being solved and the differing capabilities offered by each code.

In general, radiation transport for NCT is more complex than is the case for standard photon therapy analysis. This is mainly due to the many physical radiation dose components associated with this treatment and the additional complications of transporting neutrons due to the increased importance of scattering interactions relative to the case with photons. The basic approach to all of the calculations completed in these studies relies on some method for solving or simulating the three-dimensional Boltzman transport equation for neutral particles:

$$\frac{\partial n}{\partial t} + v\hat{\Omega}\cdot\nabla n + v\Sigma_t n\,(r, E, \hat{\Omega}, t) = \int_{4\pi} d\hat{\Omega}' \int_0^{\infty} dE' v'\Sigma_s(E' \rightarrow E, \hat{\Omega}' \rightarrow \hat{\Omega}) n\,(r, E', \hat{\Omega}', t) + s\,(r, E, \hat{\Omega}, t) \quad (9)$$

Monte Carlo techniques and deterministic methods were both utilized in these studies. Discrete ordinates, or deterministic, methods solve the integro-differential transport

equation as shown above, with derivatives in space and time although for all calculations presented here, the time derivative is set to zero; i.e. a steady state source is assumed. In a Monte Carlo calculation, a simulation of particle transport is performed using the probability density functions to describe the particles in phase space.

A model must be constructed and defined geometrically, the initial source beam must be known and described, and finally a complete set of coupled neutron-photon cross section data must be available. For photoneutron production the coupled electron/photon transport throughout the system had to be computed. This allowed further calculations of the photoneutron production and the neutron transport within the system.

Although both Monte Carlo and deterministic methods were employed in these photoneutron studies, the deterministic method was considered adequate for most of the neutron transport calculations due to the relative simplicity of the geometry. Stochastic simulation would be the obvious method of choice in modelling biological systems where the associated geometries are quite complex. Comparisons were made between the Monte Carlo and discrete ordinates solutions and the results were comparable. The advantage of the deterministic model is its shorter run time while the major advantage of the Monte Carlo method lies in its ability to model complex geometries. Discrete ordinates methods differ from Monte Carlo methods in that the Monte Carlo methods do not explicitly solve the transport equation but obtains results by simulating

individual particles and looking at their average behavior as they travel through zones within the geometry. It uses sampling to solve the mathematical transport problem. Discrete ordinates solutions, on the other hand, solve the transport equation numerically by discretizing the variables in phase space. Monte Carlo requires no averaging in space, energy or time. It looks rather at transporting particles between events or interactions. As noted earlier, Monte Carlo methods yield an equation that describes the probability density of particles in phase space.

Monte Carlo codes are used to simulate a statistical process and are particularly useful when geometries become complex. But, with Monte Carlo codes, the main disadvantage lies in the fact that its precision depends critically on the number of histories run or the number of particles tracked in the region of interest. This can result in long run times in order to obtain reasonable statistics. Methods exist for reducing the computing time (such as complementary splitting and Russian roulette in which particles in particular regions are assigned "importance" weightings), but these can be complicated and can result in unwanted biasing in the system.

Additional calculational tools including small data manipulation programs, commercial software packages as well as hand calculations were employed to reduce and analyze the acquired data. These steps are outlined in the final section of this chapter,

indicating what was measured and how the data and calculations were analyzed to yield relevant results.

ACCEPT: Initially, calculations to estimate the photoneutron device's performance were completed using the ACCEPT[83] three-dimensional electron-photon coupled transport code to obtain the bremsstrahlung flux throughout the device. The 4 MeV electron head and the Varitron accelerator were both modelled using ACCEPT at various electron input energies. Given the computed bremsstrahlung production within the system, the actual neutron production in the heavy water volume was then calculated using a FORTRAN code developed previously at the Idaho National Engineering Laboratory. This code takes the output from an ACCEPT run (bremsstrahlung production within a particular system) and coverts it to neutron and gamma production within a specified volume. Thus, for a selected volume within the model, it was possible to obtain the neutron production as well as the gamma dose rate. Modifications to this program were also necessary to obtain the desired energy group structure format for input into DORT and MCNP for further calculations. Sample ACCEPT code inputs and outputs are listed in Appendix A.

---

83. Hablieb, J. A. and Mehlhorn, T. A., "ITS - The Integrated TIGER Series of Coupled Electron/Photon Monte Carlo Transport Codes", SAND91-1634, Sandia National Laboratory, March, 1992.

The ACCEPT code, developed at Sandia National Laboratories, offers a Monte Carlo solution of linear time-independent coupled electron-photon radiation transport problems. The basic premise of ACCEPT (and most electron/photon Monte Carlo codes) is to provide a description of the production and transport of the electron/photon cascade, which is based on microscopic photon transport and a macroscopic random walk for electron transport. The ACCEPT codes provide for three-dimensional multi-material geometries in which zones are designated and "built" out of a collection of geometric primitive bodies, as opposed to being defined in terms of bounding surface equations. Each of the input zones are defined as combinations of these bodies and the material for each zone is then specified. In specifying the materials, the description must be complete, including atomic densities and exact percentages of various elements within the material.

Although other codes can solve electron/photon cascades, the ITS[84] codes (of which ACCEPT is one) were deemed more effective in this case, particularly due to the code's improved, comprehensive database of electron/bremsstrahlung production cross sections. In order to run ACCEPT, cross sections must first be generated. The associated photon and electron cross section generating file used for this work was XGEN which selects its cross sections from the cross section data library

84. Ibid 83.

file XDATA. XDATAincorporates photon data from Biggs and Lighthill.[85] Electron data is taken from the ETRAN Monte Carlo code system.[86]

MCNP: Additional confirmatory neutron transport calculations were also performed using another Monte Carlo code, MCNP.[87] MCNP, like ACCEPT, allows the user to input exact geometries but is based on defining regions using geometric boundaries. It is a well-documented code with a wide range of features and capabilities. Employing MCNP entails defining regions, or cells, with geometry and material specifications, specifiying a source (defining probability distributions for source variables of energy, time, position and direction), and locating geometric surfaces or regions over which MCNP is instructed to perform particle tallies. MCNP also offers better error analyses, plotting options and error detection capabilities of input geometries. MCNP was mainly employed to confirm neutron transport results obtained through discrete ordinates methods by modelling the experimental geometries exactly. It was employed in modelling the initial Varitron geometries to obtain the neutron production within the indium foils. It was also employed in the processing of necessary foil cross section data in the construction of a simplified cylindrical geometry model of the activation foils and assembly. The geometries modeled using MCNP were completed using the

85. Biggs, F. and Lighthill, R., "Analytical Approximations for X-Ray Cross Sections II," SC-RR-71 0507, Sandia National Laboratories, December 1971.
86. Berger, M. J. and Seltzer, S. M., "ETRAN Monte Carlo Code System for Electron and Photon Transport Through Extended Media," CCC-107, Radiation Shielding Information Center, Computer Code Collection, Oak Ridge National Laboratory, June 1968.
87. Briesmeister, J. F., ed., "MCNP - A General Monte Carlo Code for Neutron and Photon Transport, Version 3B," LA-7396-M, Los Alamos National Laboratory, 1989.

same dimensions used in the input models for both DORT and ACCEPT. Sample MCNP input files are given in Appendix B.

DORT: In addition, the DORT[88] neutron-photon transport code was used to compute the transport of photoneutrons along with the associated neutron-capture gammas. DORT is a well-known two-dimensional deterministic code for the discrete ordinates solution of the neutron transport equation. DORT calculations performed utilized both the BUGLE-80[89] coupled neutron-photon cross section library (in the conceptual system design computations) and the COMBINE[90] code (with 27-group cross sections) in the experimental models. The geometry for the initial conceptual system design calculations is shown in Figure 4.

Both DORT and MCNP computations were performed for this geometry. The results obtained from these calculations were encouraging and suggested that experimental studies using scaled-down benchtop models of the concept would be of value. The actual geometries modelled for the experiments did not, however, include the beam delimiter or lead shielding. The experiments conducted were meant solely to provide basic proof-

88. Rhoades, W. A. and Childs, R. L., "An Updated Version of the DOT-4 One- and Two-Dimensional Neutron/Photon Transport Code, ORNL-5851, Oak Ridge National Laboratory, 1982.
89. Roussin, R. W., "BUGLE-80 Coupled 47-Neutron, 20 Gamma-Ray P_3 Cross Section for LWR Shielding Calculations", DLC-75, Radiation Shielding Information Center, Oak Ridge National Laboratory, 1980.
90. Grimesey, R.A., Nigg, D.W., Curtis, R.L., "COMBINE/PC - A Portable ENDF/B Version 5 Neutron Spectrum and Cross-Section Generation Program", EGG-2589 (Rev 1), Idaho National Engineering Laboratory, February, 1991.

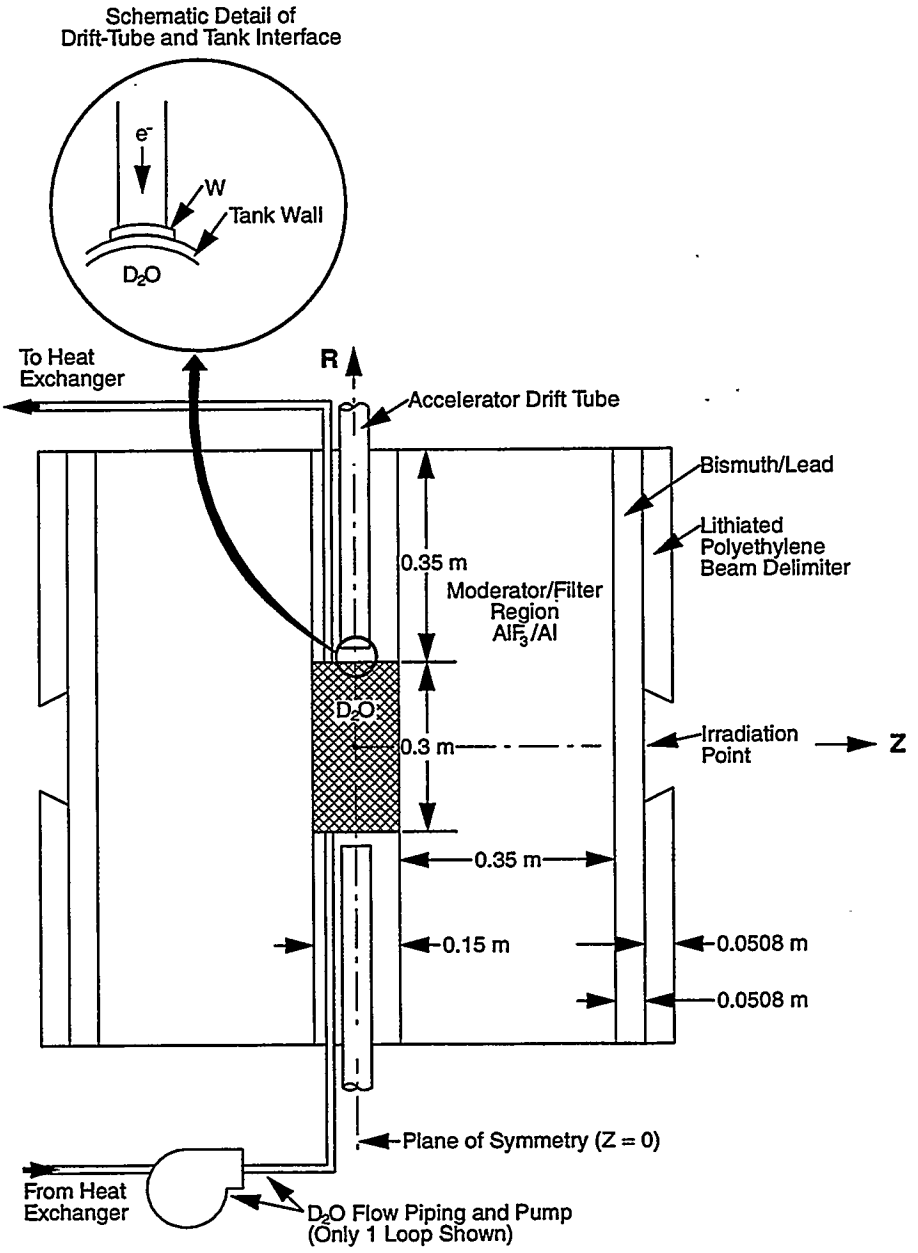

Figure 4: Calculational model for initial source calculations

of-principle data for the unfiltered and filtered neutron sources. A second example geometry modelled with DORT for the Varitron experiments is shown in Figure 5. Note that DORT geometry is two-dimensional (cylindrical) and is symmetric about the dashed line shown. Because of limitations in the code, geometries modelled in DORT were not necessarily geometrically accurate but the volumes, and thus total atoms, were preserved. The calculations made were completed for filtering assemblies composed of aluminum fluoride, aluminum and lithium fluoride, as well as a laminated Aluminum/Teflon (CF_2) filter design. A complete listing of the atomic densitites of other materials used is given in Appendix A. Sample DORT input files and calculations are given in Appendix C.

The DORT code, developed at Oak Ridge National Laboratory, provides a detailed numerical solution of the Boltzman transport equation for the direction-, space- and energy- dependent neutron intensity at all points in a calculational geometry. DORT partitions the particular geometry into a finite-difference mesh. It then integrates the computed angular flux over direction space yielding a scalar flux. DORT also requires the use of a separate cross section processing code which processes only the cross sections for the materials used from the cross section library. The DORT code, although limited in its geometry specification capabilities, provides calculated solutions to a given geometry in a relatively short period of time and for the purposes of this work was usually quite sufficient. In addition, some of the initial calculations performed to analyze the heavy water and tungsten target thicknesses as well as the electron energies were run using the one-

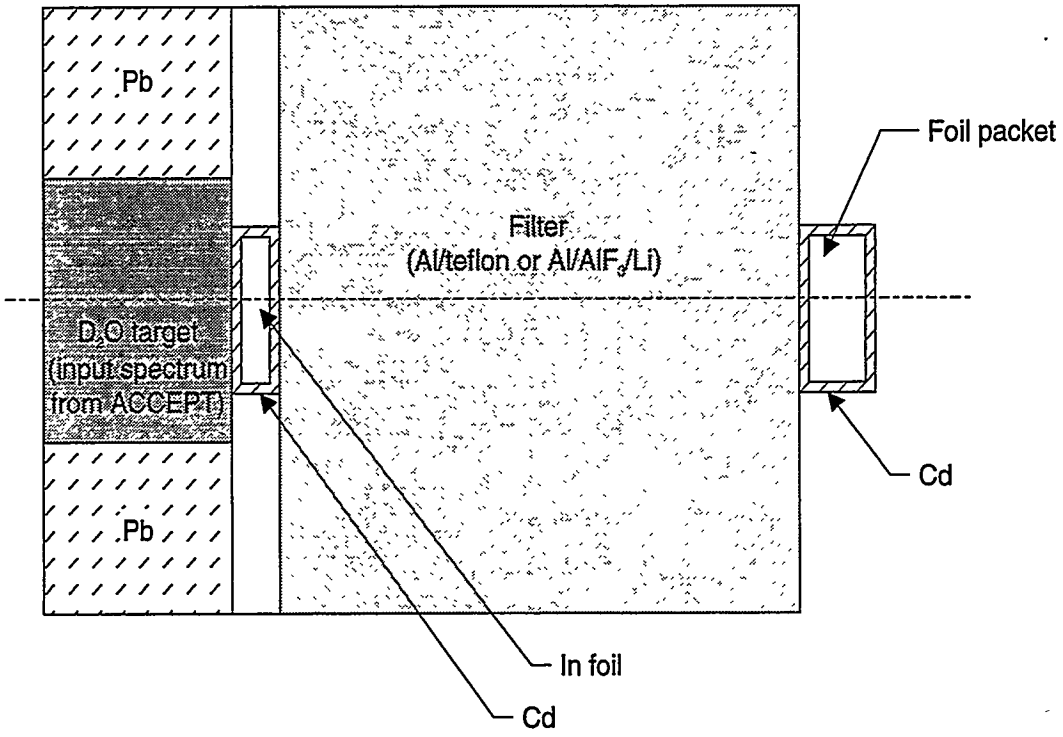

Figure 5: DORT geometry to obtain neutron production within foils for Varitron moderating experiments (Note: foil packet geometry is not to scale)

dimensional code ANISN,[91] also developed at Oak Ridge National Laboratory. Because these runs were not used in the final results presented in this thesis but mainly as a tool to modify parameters for quick indications and rough estimations on a simplified geometry, sample ANISN input files are not included in the appendices.

Additional computational tools employed include short FORTRAN and C codes. In addition to the standard transport codes mentioned previously, another code to convert the photon-production output from ACCEPT to a photoneutron yield using standard photoneutron production data (cross sections) was used. The neutron production in a particular volume was then transported using either Monte Carlo or discrete ordinates methods. Other computational tools, such as spreadsheet software and smaller programs were used and written to carry out hand computations and data reduction analyses. The majority of the larger computer calculations were completed on Hewlett Packard 9000s (Series 720) computers at the Idaho National Engineering Laboratory. Figure 6 shows a flowchart of the general calculational methods followed.

In addition a method was needed to combine related measurements and calculations in a consistent evaluation. The methodologies used and additional calculations required will be discussed in a later section of this chapter. Direct spectrum unfolding techniques

91. Parsons, D.K., "ANISN/PC Manual," EGG-2500, INEL, Dec. 1988.

and standard foil activation analyses were applied. Calculations to determine the beam current, cadmium ratios, stacked-vs.-single-foil effective cross sections and other parameters are described.

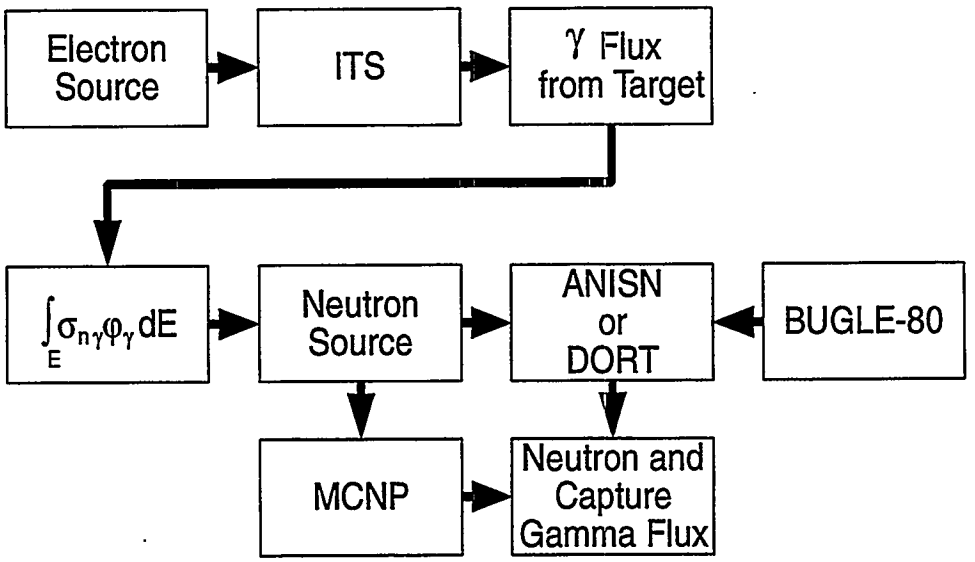

Figure 6: Flowchart of calculational procedures

IIIb2. Experimental Methods

The hardware apparatus used in the various experiments included a variety of equipment: activation foils, two electron accelerators, shielding materials, targets, detectors and counting equipment. The parameters, orientation and settings of the experiments were varied in accordance with the particular variable or quantity being measured.

Two separate electron accelerators were employed during the experimental runs. The electron accelerator initially used was essentially a standard 4 MeV side-coupled medical electron linear accelerator with a tungsten target. Following the original proof-of-principle experiments, a more sophisticated, tunable electron linear accelerator apparatus was installed which allowed greater flexibility, both in electron energy range and current. This accelerator, the Varitron, assembled by HESCO, incorporates an accelerator guide from the Varian Corporation and a water-cooled tungsten target for bremsstrahlung production from the electron beam. A photograph of the main drift tube and target assembly is shown in Figure 7.

A direct measurement of the electron current impinging on the target may be obtained with the Varian accelerator by magnetically diverting the electron beam from the tungsten target into a second drift tube terminated by a Faraday cup. This second drift tube can be seen in the photograph of Figure 7 to the right of the main drift tube. The average energy and spectral distribution of the electron beam can be directly esti-

mated by varying the magnetic field used to divert the electron beam into the second drift tube and correlating the measured beam current with the strength of the magnetic field as the beam is swept across the Faraday cup.

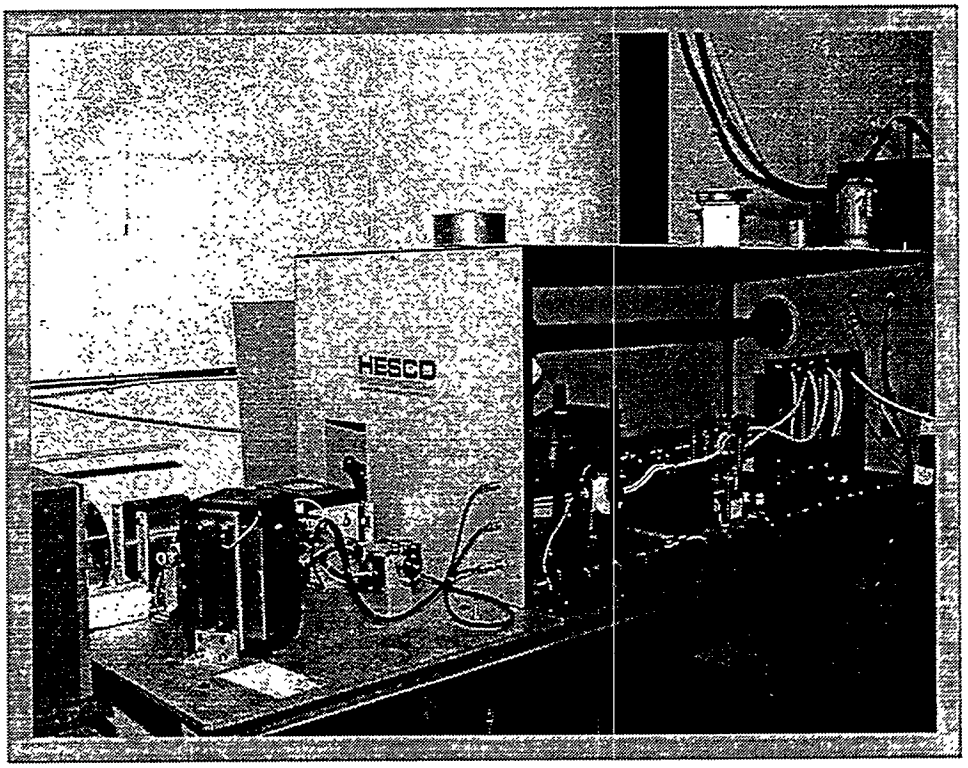

Figure 7: Main drift tube assembly of the Varian Corporation Varitron accelerator

Accelerator performance graphs for the Varitron are shown in Figures 8 and 9. The accelerator was designed to run at approximately 9 MeV. In order to obtain electrons at energies of 4, 6 and 8 MeV, it was necessary to alter the optimum operating parameters. Given a specified magnetron current, by increasing the electron gun filament voltage, and thereby the electron injection current, it was possible to lower the average electron beam energy because of increased loading of the RF field within the accelerating cavity. Operating parameters for the Varitron were set according to Figure 8.

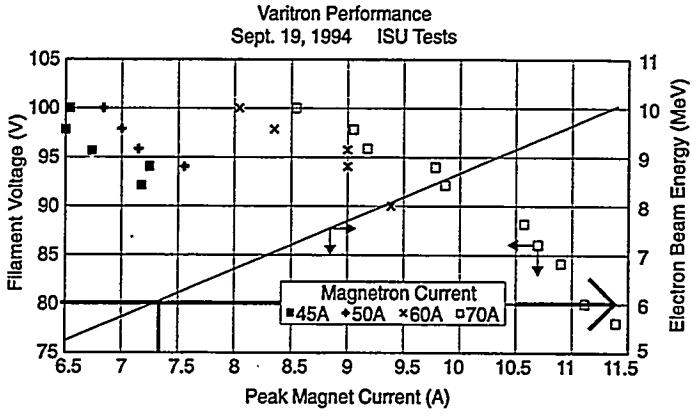

Figure 8: Varitron performance plot of magnet current vs. filament voltage and electron beam energy (arrow indicates operating parameters)

Typically, the filament voltage was set such that when the beam was diverted into the Faraday cup, the maximum current into the cup occurred at a diverting magnet current of 7.4 amperes, corresponding to a nominal electron beam energy of 6 MeV. These operating parameters are indicated in Figure 8 by the boldface line and arrow.

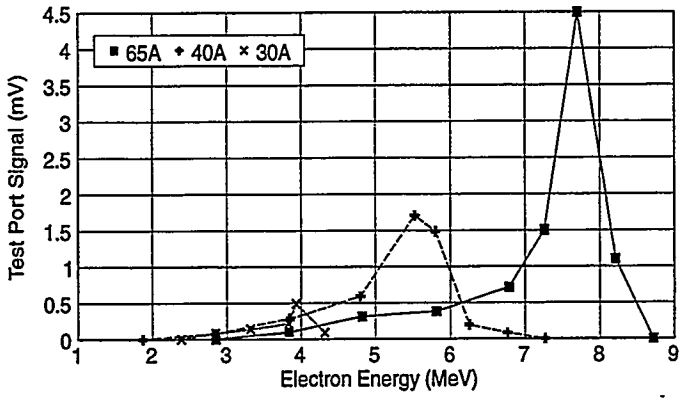

Figure 9: Varitron energy performance data

Due to the manner in which the electron beam average energy was manipulated, the obtained beam had a significant energy spread about the nominal value, as indicated in Figure 9. In regard to the data obtained throughout these experiments, this spread of the beam energy caused the bremsstrahlung source to be disproportionately skewed toward energies above the nominal value of electrons anticipated, resulting in a high energy tail in the photoneutron spectrum, that needed to be adjusted for in the experimental spectrum measurements. An ideal electron beam for the types of measurements done here would offer fewer electrons above the desired electron energy in order to maintain a well-characterized spectrum. As a practical matter for a clinical device, the spread in energy of the electron beam is not of consequence, although one would need to avoid excessively high-energy electrons, which could contaminate the neutron beam with photon radiation to a greater extent than accounted for in the system design.

In order to produce the neutron beam, the bremsstrahlung from the tungsten targets was directed into sealed cylindrical lucite tanks of D_2O. Although several thicknesses of D_2O cylinders were available, the tank with radius 76 millimeters (3 inches) and thickness 100 millimeters (4 inches) was found to offer the best neutron production of the available heavy water cylinders. The cylinder contained a D_2O mass of 1926 grams and was enclosed in 1/8 inch lucite. A photograph of the heavy water cylinder placed against the target assembly is shown in Figure 10. It can also be seen that the

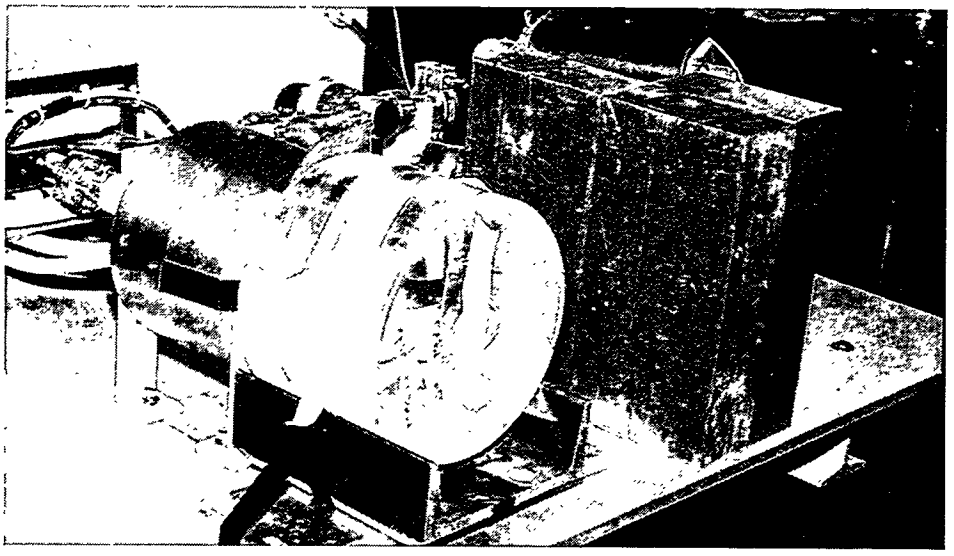

Figure 10: Cylindrical lucite tank against target assembly of Varitron

forward-peaked bremsstrahlung radiation emanating from the target is additionally collimated by a cylindrical tungsten shield. This tungsten collimation was significant and was included in the ACCEPT model of the target apparatus.

The primary measurement technique used in the beam spectrum characterization was foil activation spectrometry. Activation foils can be employed for the detection of neutrons of energies ranging from thermal to fast, depending on the foil material selected. The basic premise of this technique is to select a thin material that has an adequate capture cross section for the neutron energy of interest in detection. The foil is then exposed to a neutron field for a given period of time and the induced activation is counted using an appropriate (in this case, gamma) detector. The induced activity depends upon the number of atoms in the foil (determined from its mass and composition), the incident neutron flux (and its energy spectrum which can affect threshold foils) and the capture cross section of the nuclide of interest (also a function of energy).

Ideally, only one predominant isotope would contribute to an induced activity. Unfortunately, this is not always the case and various techniques are used to discriminate between decay lines. Irradiation and decay times are selected such that unwanted activities are allowed to decay away before counting. This was often the case in attempting to detect the weaker signal from the fast neutron component of the beam.

Corrections must be made for decay of activity between exposure and counting and during the counting and irradiation intervals as well. Additional necessary cor-

rections include those for self-absorption and for detector geometry and sensitivity. All detectors used were calibrated in a reproducible geometry with known calibration sources.

Neutron energy spectrum measurements were obtained through neutron activation of various foil materials for which the neutron activation cross sections were most sensitive to different energy regions of the neutron spectrum. Measurements in the epithermal energy region (0.5 eV to 10 keV) were undertaken using a set of activation foils, each with dominant resonance cross section peaks such that the majority of the detector response at a particular energy was due to the primary resonance. Throughout the series of benchmark experiments a variety of foil materials was employed. Of primary interest for simply determining the photoneutron source strength, or intensity, were indium foils. Two sets of indium foils were employed. The first set available consisted of a collection of seven indium foils of approximately one gram each and one inch in diameter. Because the foils were thin and fragile, they were mounted on an aluminum backing in order to give the foils additional support. The second set of indium foils used (manufactured by Reactor Experiments, Inc. of Sunnyvale, California) measured one inch in diameter, weighed approximately one-half gram each and, according to available specification sheets, were 99.9986% pure.

In order to measure the spectral properties of the resultant beam, additional foil materials with appropriate resonances were selected during the filter material experi-

ments. When activated and then analyzed, these foils (indium, gold, tungsten, copper) can provide a reasonably accurate broad-group energy description of the resultant filtered epithermal beam. The foil packages used were of varying weights and sizes, dependent on current availability and requirements. All foils were weighed to determine the actual number of atoms of interest in each individual foil package. The dimensions, thicknesses and densities of each foil material were also determined.

Throughout the majority of accelerator runs, the foils were placed in cadmium covers in order to reduce the thermal activation component seen by the foil. Additional foil materials were used in some of the experiments but they often proved to have cross sections that were too low for activation at the neutron fluences available with the obtainable LINAC currents. Foil count times were based on the strength of the induced activation and, for the long-half-life nuclides, it was necessary to count foils overnight. The foil materials used in most of the experiments, along with their half-lives and the gamma energies of interest, are tabulated in the following section. The raw foil data (counts and activation rates) are given in spreadsheet format in Appendix D. Figures 11 - 15 show the evaluated cross sections for the foils as placed on the downstream-side of the filtering material and surrounded by cadmium covers. Knowledge of the energy-dependent cross sections of the foils shows the energy regions at which each foil is sensitive.

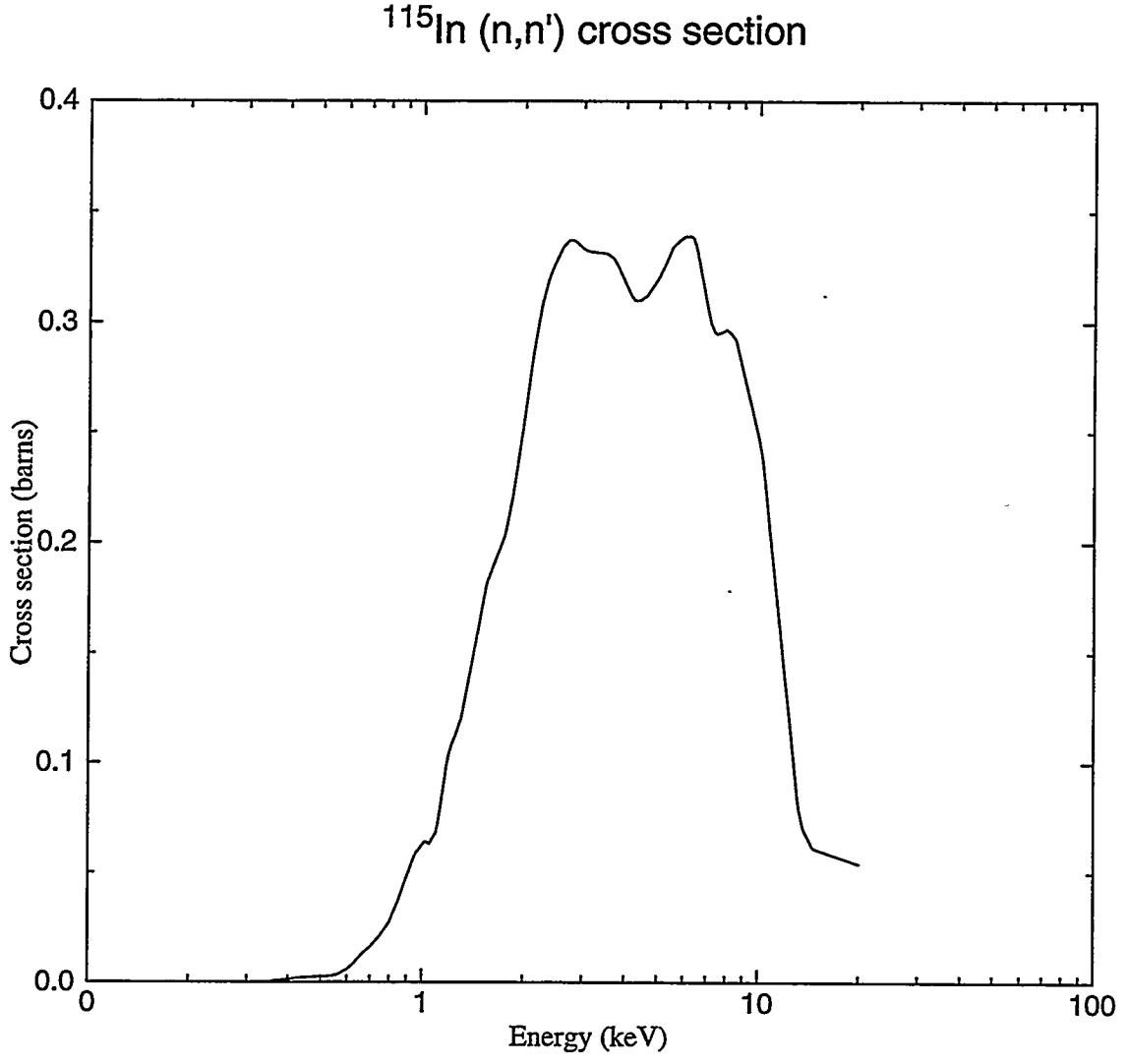

Figure 11: Cross section as a function of energy for indium foil

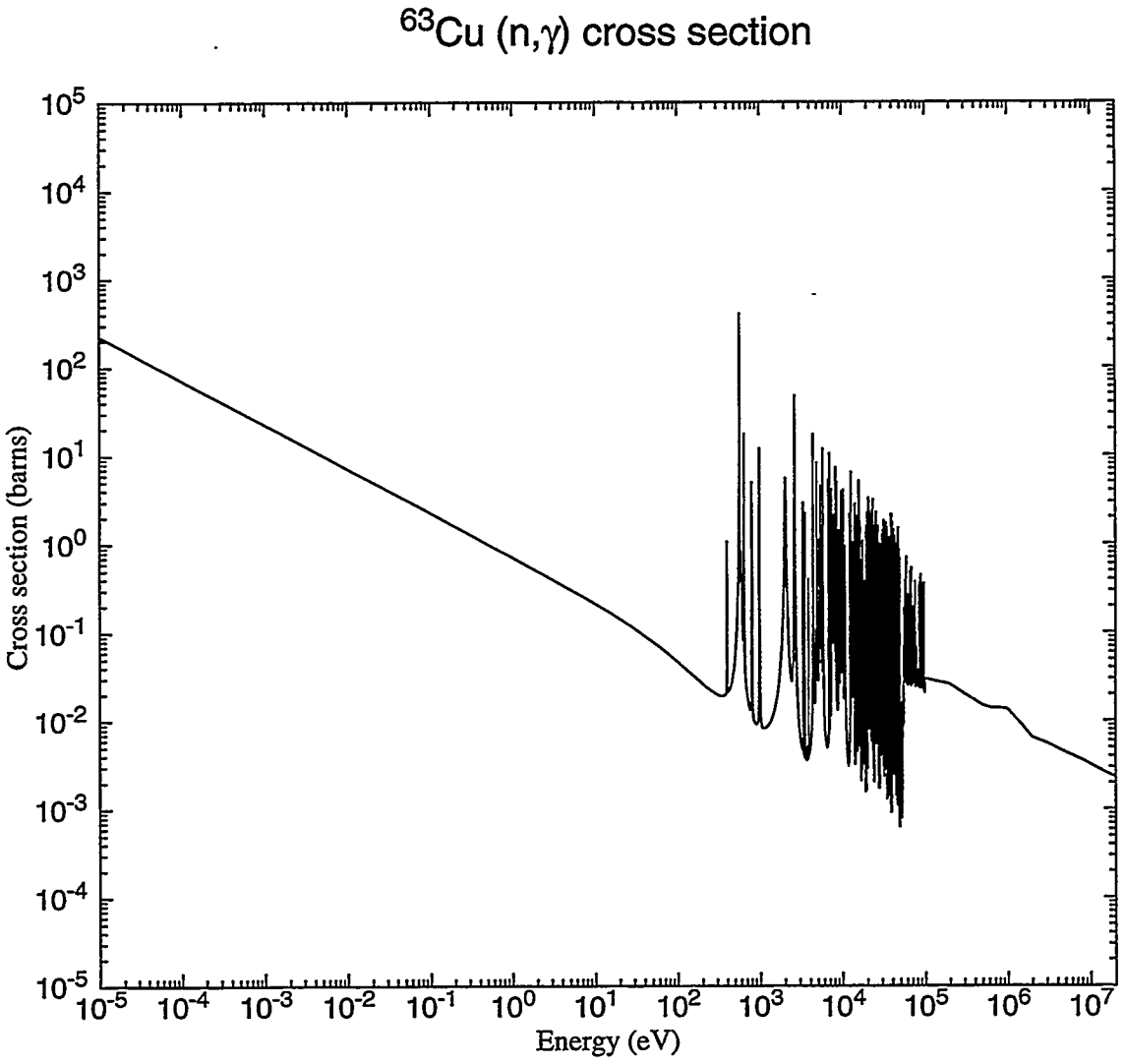

Figure 12: Cross section as a function of energy for copper foil

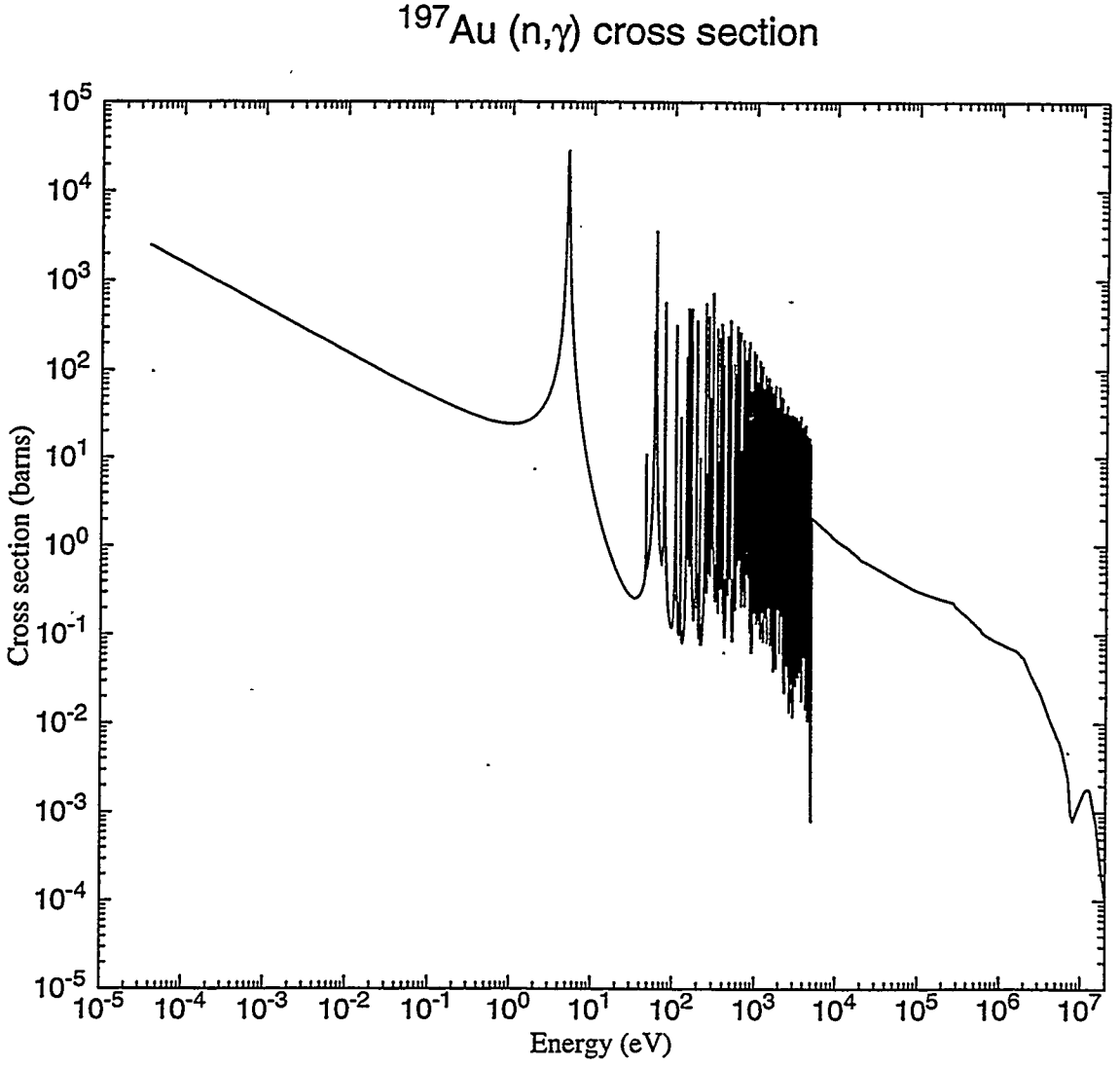

Figure 13: Cross section as a function of energy for gold foil

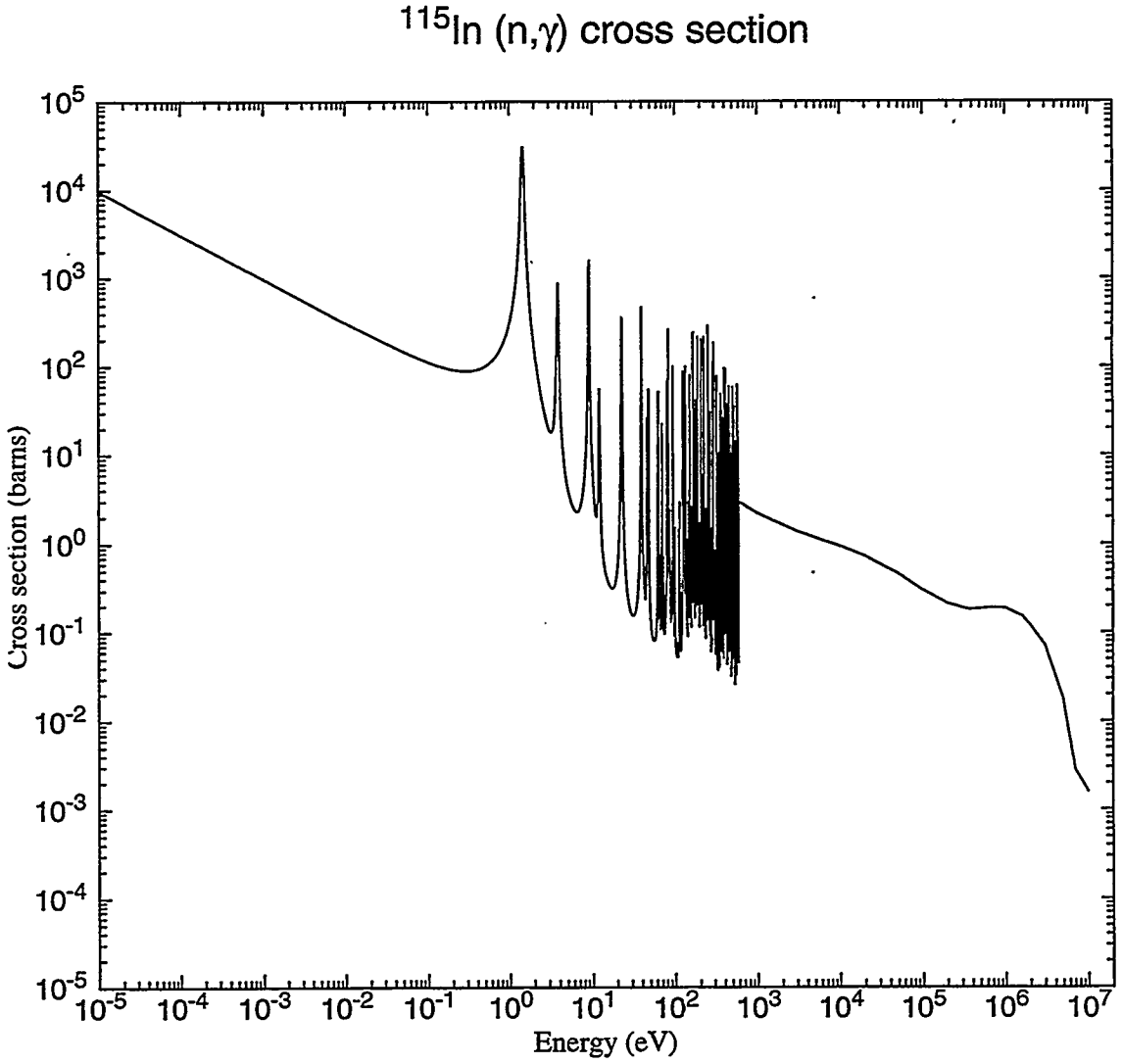

Figure 14: Cross section as a function of energy for indium foil

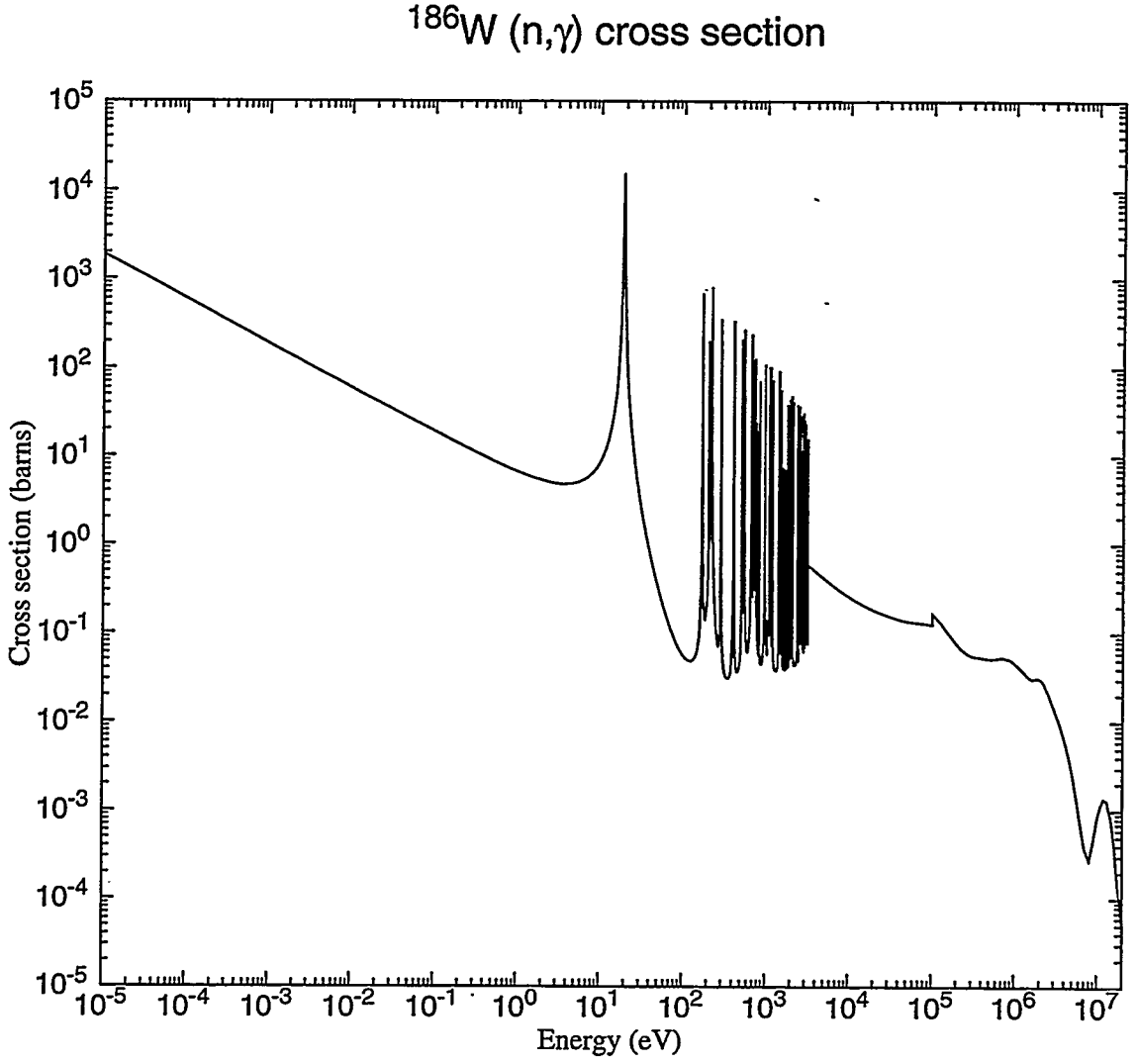

Figure 15: Cross section as a function of energy for tungsten foil

Experiments were performed with and without neutron filtering material. In the cases without filtering material, the objective was to measure the photoneutron source strength. For the experiments run with filter materials in place, two filter materials were tested for their effectiveness in filtering and moderating the source photoneutrons into the desired epithermal energy range. The first series of filter experiments were primarily to determine the spectral properties of the beam. In these runs a neutron moderator material patented in Finland[92] ($Al/AlF_3/LiF$ composite prepared by the Technical Research Centre of Finland, VTT-Finland) was placed along the beam line directly following the heavy-water cylinder. This particular material was specifically developed by VTT as an epithermal-neutron filter material for BNCT. Four blocks consisting of 30% (weight) aluminum, 69% (weight) aluminumfluoride and 1% (weight) lithiumfluoride were oriented such that two filter thicknesses were possible, 30 and 40 centimeters. The total mass of all four blocks was 107.8 kilograms, with a measured density (approximately 3.0085 g/cm^3) close to that of pure aluminum (2.7 g/cm^3). Two of the blocks measured 300 x 200 x 200 millimeters, while the second two measured 300 x 200 x 98.5 millimeters each. The blocks were prepared in early 1995 by VTT Chemical Technology, Finland for testing purposes at the Idaho National Engineering Laboratory and are shown in Figure 16 stacked against the target and heavy-water assembly.

---

92. Auterinen, I. and Hiismaki, P., "Epithermal BNCT Neutron Beam Design for a TRIGA II Reactor", Advances in Neutron Capture Therapy, R. Barth and A. Soloway, Editors, Plenum Press, New York, 81-84, 1993.

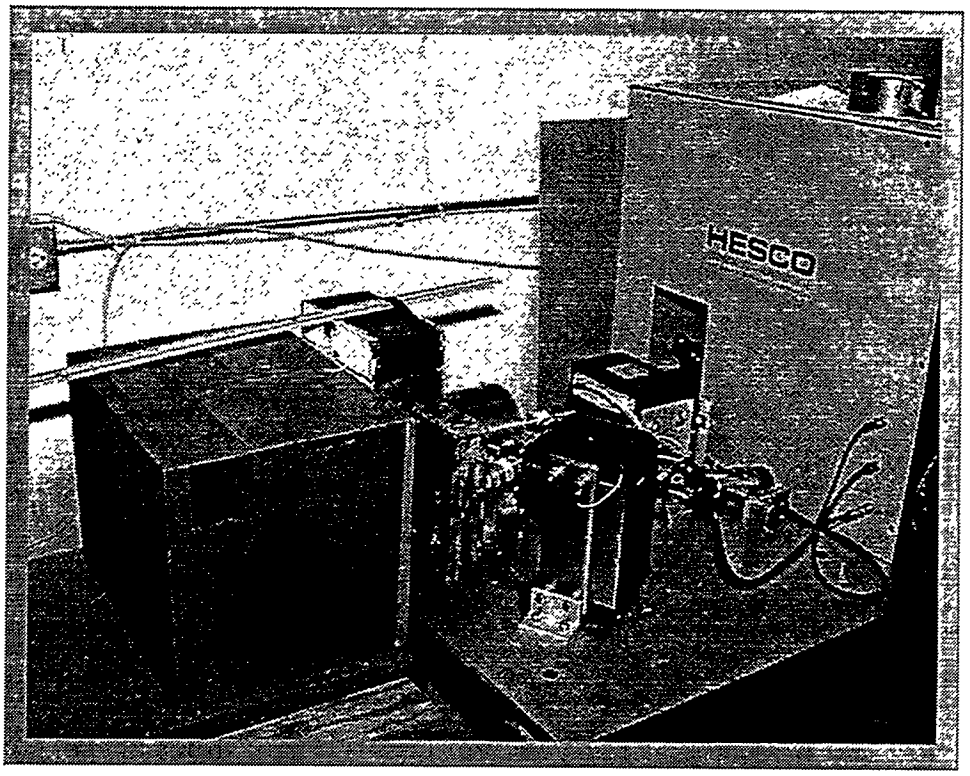

Figure 16: Aluminum fluoride filtering bricks in front of target assembly and D_2O cylinder

The second filter material trials were conducted using a novel "sandwiched" aluminum and teflon structure (Al/CF_2) designed at the INEL, fabricated at Idaho State University and incorporated into a test assembly as shown in Figure 17. The filter consisted of alternating 0.635 cm (0.25 inch) aluminum plates and teflon sheets to approximate a one foot filtering distance (excluding air gaps). Both the teflon and aluminum sheets were cut into approximate squares measuring 30.5 cm (1 foot) on an edge.

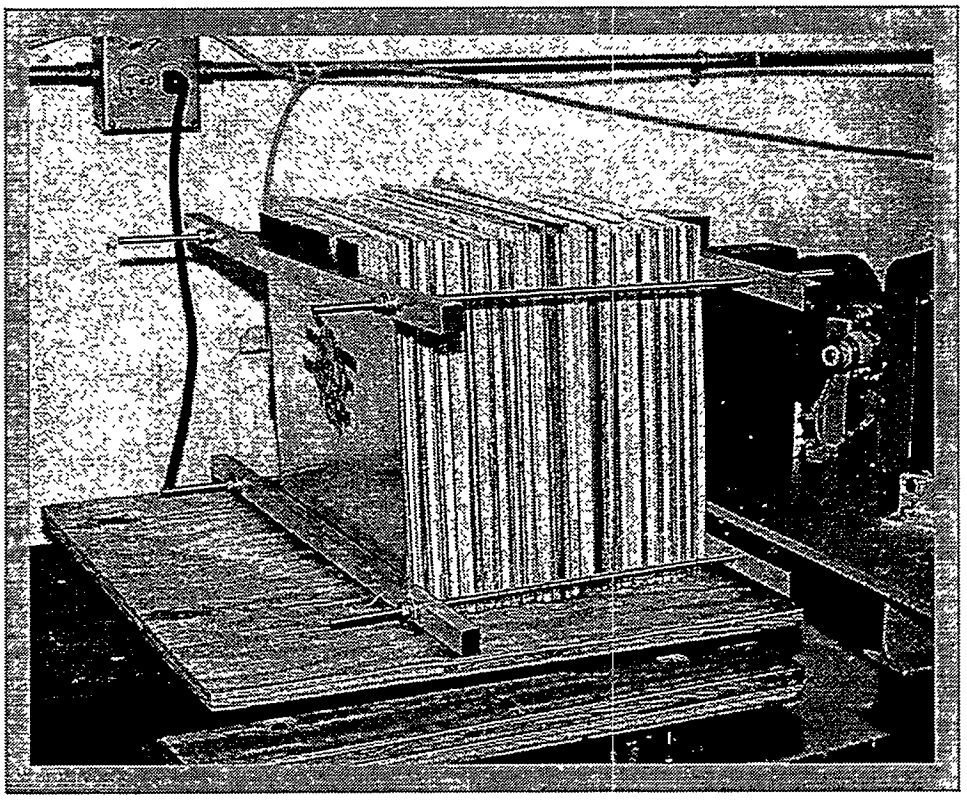

Figure 17: Aluminum/Teflon filtering assembly

These two filtering materials were examined as part of the studies on the neutron beam spectrum filtering. It was of interest to compare the moderating properties of both materials. Preliminary DORT calculations indicated that these two materials might offer comparable filtering properties. The Aluminum/Teflon arrangement was developed at the INEL as an alternate, high-efficiency, fluorine-based filter for epithermal neutron production. Teflon is an inexpensive, readily available, chemically-stable

fluorine-containing material, which, in combination with aluminum, was postulated to offer an effective filtering material, provided that there is not an unacceptable level of beam degradation by elastic scattering from carbon. Both filter materials contained fluorine which is known to have capabilities for moderating fast neutrons into the epithermal range. It is also a light nuclei and thus alters the beam directionality relatively little. Finally, fluorine has a cross section that tends to fill in some of the scattering minima in the aluminum cross section. Aluminum is also a very effective epithermal-neutron filtering material.

Data were collected both upstream and downstream of the filters. The experimental set-ups were also surrounded by both lead bricks and borated polyethylene to prevent unwanted scattering and reflecting effects. A small lead brick housing was constructed to shield the D_2O cylinder. Additionally, in an attempt to isolate the apparatus from room scatter during irradiations, the neutron moderatoring filters were surrounded in a borated polyethylene casing designed for the experiment. Other design considerations included the building of a stable cart for the positioning of the filter materials, as well as designing mounting devices for the D_2O and other materials. The beam table, heavy water target and filtering material in its housing are shown in Figure 18, also showing a closer view of the main electron drift tube which is terminated by a water-cooled tungsten target for converting the electron beam energy into bremsstrahlung radiation.

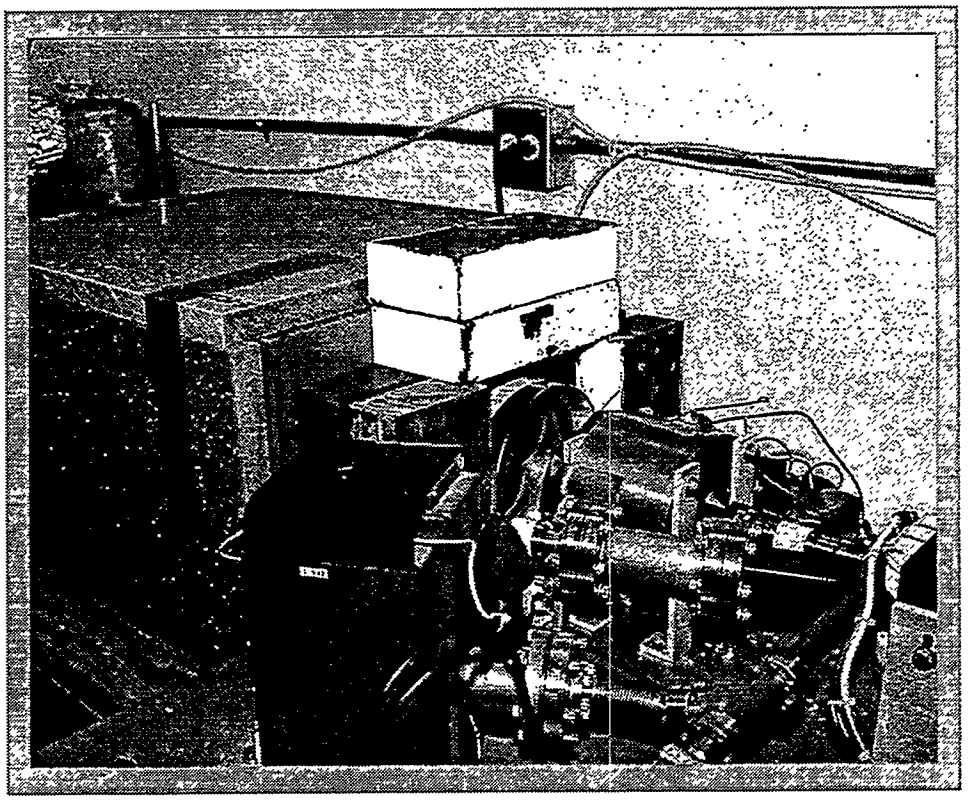

Figure 18: Experimental set-up with filter material surrounded by boronated polyethylene

Throughout all of the experimental trials, a calibrated ionization chamber was placed along the beam axis, allowing detection of the bremsstrahlung radiation down-stream from the tank (see Figure 19). The ionization chamber allowed a check on the direct electron beam current measurement method and was used to normalize the theo-retical calculations of the photoneutron source strength. Given the expected dose rate

in rads/sec/mA calculated from ACCEPT in the ionization chamber volume region and the actual measured dose rate from the detector, an approximation of the beam current is obtainable by dividing the calculated into the measured dose rates. For the initial experiments using the small 4-MeV medical accelerator, this yielded a current of

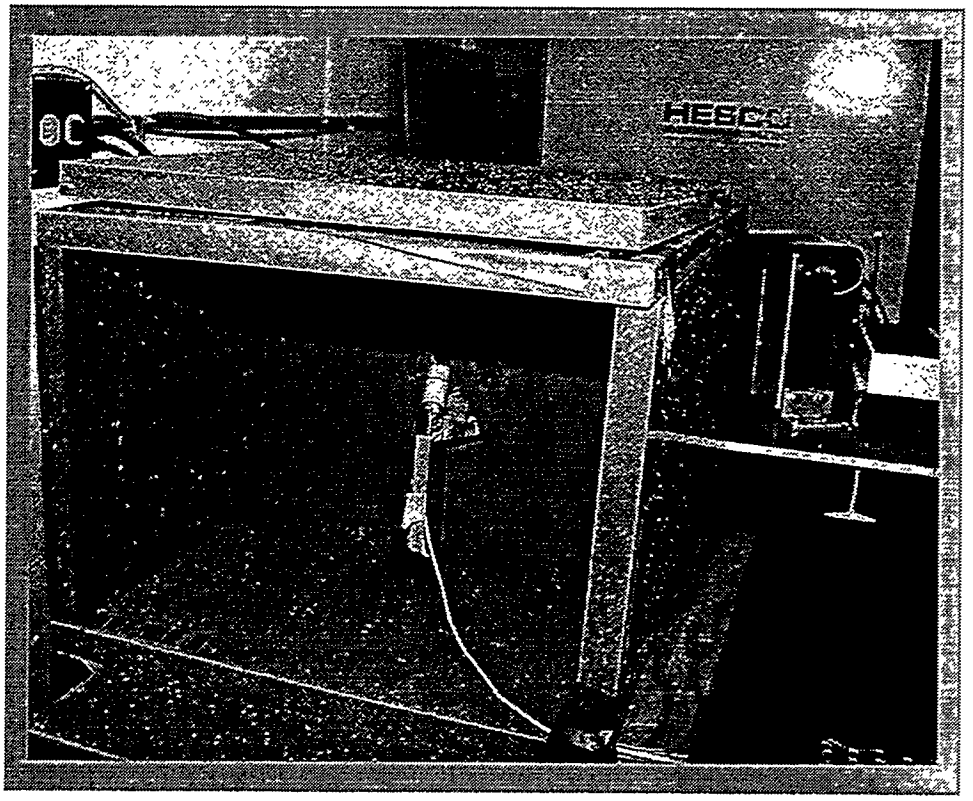

Figure 19: Ionization chamber as seen along the beam axis downstream from filter

approximately 15.2 μA when averaged over two runs (one at 3.5 and the other at 4 MeV). The detector was placed one meter from the bremsstrahlung target directly on the beam axis. With the filter material in place, the ionization chamber was positioned at times both outside and inside the borated polyethylene cover.

In addition, a pancake-type ionization chamber detector was placed along the beamline in all experiments which also monitored the gamma dose rate, but was intended more as a check on the first ionization chamber since it did not read an actual dose rate but rather an uncalibrated number proportional to the ionization chamber reading. In the case of the Varitron experiments, a third detector measured the total integrated current to ground from the accelerator target during an experimental run. This provided a third, direct measurement of the accelerator current. In addition, cameras were mounted before the irradiations such that the assembly and detectors could be monitored from the control room.

The induced gamma activity of the foils was measured employing standard gamma spectrometry techniques. In order to obtain the reaction rates of the irradiated foils, a variety of counting systems were employed, dependent upon availability at Idaho State University. The neutron activation rate was then derived from the measured gamma activity. The detection systems used were germanium crystal detectors, with the exception of one NaI detector.

Germanium detectors are semiconductor diodes in which intrinsic regions are sensitive to ionizing radiation, such as x-rays and gammas. Under reverse bias, an electric field extends across the depleted region. Photons interact within the depleted volume and charge carriers (holes and electrons) are produced and swept by the electric field to the respective p or n electrode. The charge recorded is proportional to the energy deposited in the detector by the incoming gamma and is converted to a voltage pulse and recorded. Due to a germanium detector's low band gap, the detector must be kept cool to reduce thermal generation of charged carriers, or reverse leakage current, to acceptable levels. Otherwise, noise destroys the energy resolution. In the systems employed for these experiments, liquid nitrogen at 77 K was used as a coolant. NaI detectors (excellent gamma-ray spectrometers because they are linear over a wide range of energies), in contrast to the semiconductor detection system, are based on utilizing a scintillation crystal. Fluorescent light intensity produced by the photoelectric interaction is directly proportional to the incident gamma energy. So, the electron pulse amplitude for the photometer due to a given gamma interaction should also be proportional to this energy. The pulses are sorted by amplitude and assigned to counting channels (see Figure 20). By plotting the count rate against the channel number, the counting spectrum is obtained. The channels are calibrated with a known source so that the net counts in a particular energy peak can be read.

The counting systems available included various Ge crystal detectors: Canberra Model GC1019, Canberra Model GC2520, Canberra Model GC3318 and an EG&G

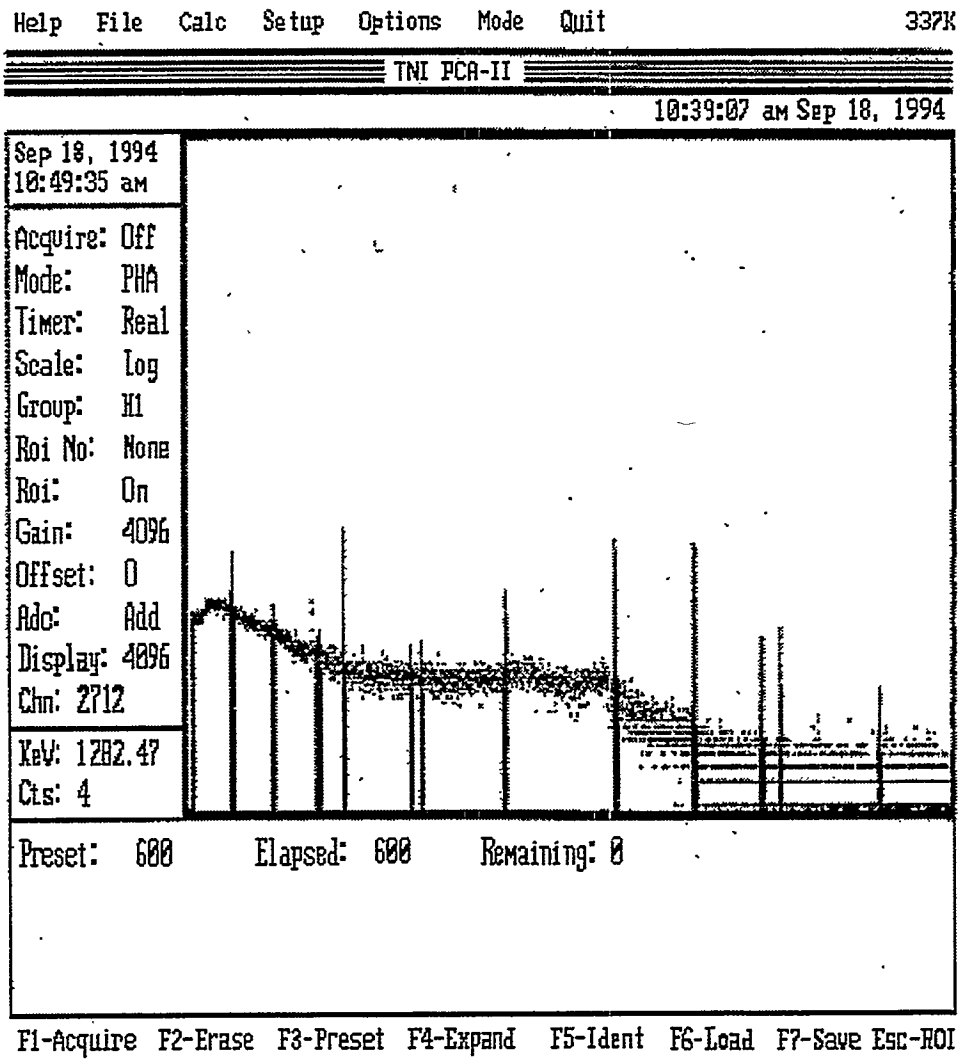

Figure 20: Sample screen dump from one of the counting software packages used

Ortec high-purity germanium coaxial detector system GEM-25195-P. A sample detector specification and performance data sheet is included in Appendix D, along with the raw data. The coaxial detector system is basically a cylinder of Ge with an n-type contact on the outer surface and a p-type contact on the surface of an axial well.

The calibration of these systems was carried out with multinuclide standard sources produced by Isotope Products Laboratories, California. In a few of the initial experiments, a Europium source (Nucleus Source MGS-1) of 1 μCi was used as well. Each of the detectors was calibrated and the efficiencies calculated. The efficiency was calculated by calculating the activity of a known source (corrected for decay to the day of measurement) and comparing it to the measured counts per second actually read by the detector. Several energy lines were analyzed and plotted to determine the detector's efficiency. In this way, the efficiency of the detector used can be determined for the energies of interest for a particular foil. A sample counter efficiency plot is shown in Figure 21.

Various counting software packages were used to analyze the acquired data. These include: the Norland 5700 MCA, Oxford PCA - version 3, Gamma Vision by Ortec and Canberra's Genie-PC QA, a quality assurance program for tracking and reporting on the performance of spectroscopy systems under the OS/2 operating system.

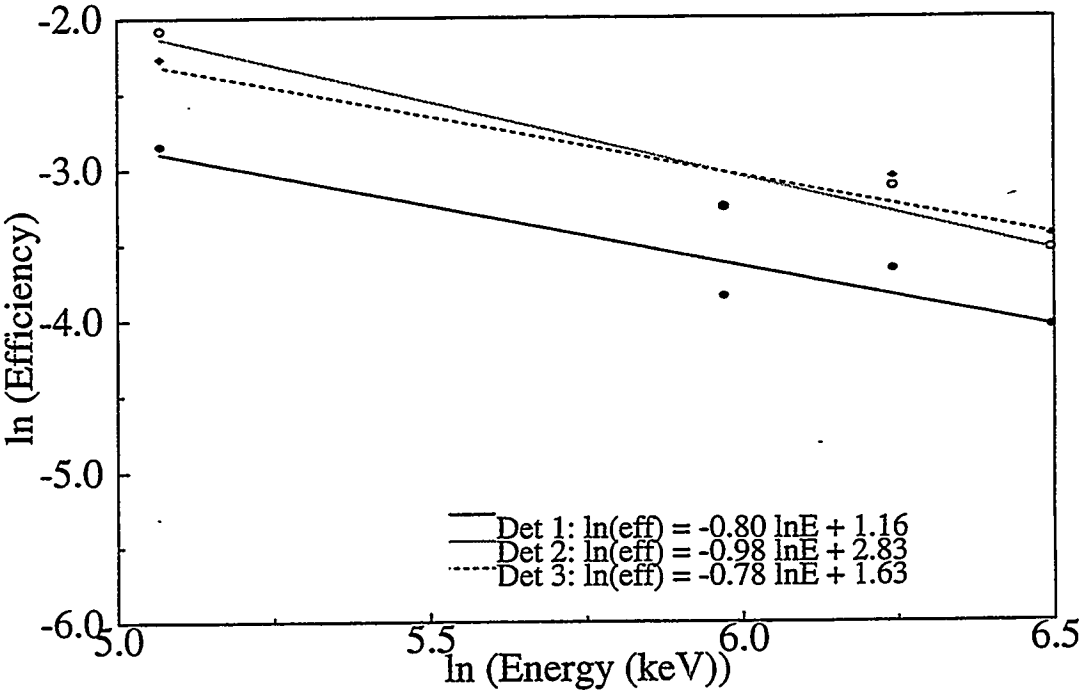

Figure 21: Efficiency vs. energy for three high purity Ge detectors

IIIb3. Data Acquisition, Reduction and Calculations

The various computational tools and experimental equipment have been described and the utilization of this apparatus and the methodologies will now be explained. The various experiments will be described in detail as well as the reasoning behind the various benchmark cases and the corresponding calculations. The experiments can be classified into basically three series. The initial series of experiments were performed to obtain data regarding the feasibility of this project. In the second and third series, more detailed and complete data were taken and analyzed computationally as well. The second and third series yielded spectral and filter/beam-tailoring information using a more sophisticated higher energy elecron accelerator. The experiments are described in detail below.

Series 1: The initial proof-of-principle experiments were performed using the medical linear accelerator at a fixed electron energy of approximately 4 MeV. The first series of irradiations were conducted with an experimental assembly as shown in Figure 22.

The cylinder of D_2O (4 inches thick) was placed flush against the accelerator target and centered on the electron beamline. Between the target and the D_2O volume, a thin aluminum barrier was added to reduce the effects of stray electrons. Indium foils in cadmium covers were taped at varying radial positions around the cylinder as well as on the downstream face. This positioning allowed for both axial and radial measure-

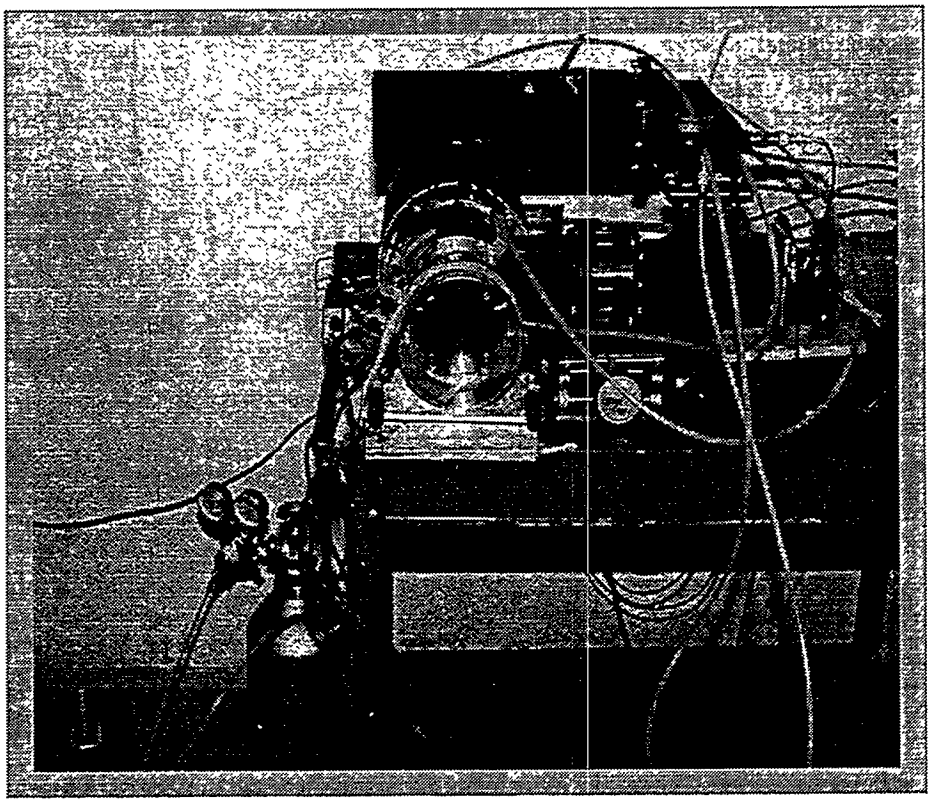

Figure 22: Fixed electron energy medical linear electron accelerator with D_2O tank

ments. In most of the runs during this series of experiments, a total of five indium foils were irradiated for between 45 minutes and one hour. The foil positioning will be described in the following section.

An ionization chamber was positioned at a known location downstream from the experimental set-up along the beam axis. This placement allowed the calculated photo-

neutron production rate to be normalized to a measured bremsstrahlung radiation field. During the irradiation at one meter from the tungsten target, the ionization chamber read approximately 20 rad/minute. The magnetron current was held at approximately 75 amps with an electron gun current of 3.7 amps.

One important point to note is that although the power supply parameters during individual runs fluctuated depending on the current operating requirements of the LINAC, the experimental parameters relevant for obtaining the desired measurement were recorded and held as constant as possible. In most instances, it was sufficient to have a successful run as long as the ionization chamber readings were stable and the electron energy and current of the beam constant. As long as all settings were known, differences in current and irradiation times between runs could be accounted for in the analysis calculations. The irradiation time is factored into the activation equation and in the final results, data is presented per milliampere of current. Because these experiments were carried out on a low current electron accelerator, it was often difficult to obtain the enough counts in a peak to yield good statistics. Restrictions in the power supply often resulted in lower electron beam currents than desired. In these instances, in order to obtain the required foil activities and necessary counts, a lower current simply required a longer irradiation time.

Three similar experiments using the 4 MeV medical head were carried out in order to collect as much data as possible. One of the initial runs was completed with a one

inch thick volume of heavy water but the neutron production in such a small volume was too low and yielded little information. The majority of the runs were then completed using the larger D_2O volume.

At times during experimentation beam current fluctuations caused difficulties in performing irradiations. The electron current would drop significantly and often fall completely to zero. In these instances, corrections were made during the analysis of the data such that these "down" times were factored into the foil activation results. For instance, if a break during the irradiation occurred, it was necessary to correct the measured activation rate by taking this "down" time into account. The foil activation was essentially treated as two separate irradiations and calculations performed accordingly. If the "down" time of the accelerator was long enough to significantly affect the foil data, the irradiation experiment was repeated. This was particularly significant in the case of the indium foils, with a half-life of 54.34 minutes.

The indium foils were counted for between ten and thirty minutes, depending on the strength of the induced activities. The peaks of interest in this first series of spectrometry experiments were gamma rays at 416, 1087 and 1293 keV, resulting from $^{115}In(n,\gamma)$ interactions. The neutron production was obtained by averaging the activation rates from these three decay lines for each foil. Given N target atoms, N' activated atoms, an activation rate $\sigma\varphi$ and decay constant λ, the induced foil activation during irradiation can be described in the following equation:

$$\frac{d}{dt}N' = N\sigma\varphi - \lambda N' \tag{10}$$

The activation rate per target nuclide for a particular decay reaction is then calculated according to the following formula, taking into account the irradiation, count and wait times while the foils are irradiated, counted and transferred following irradiation and before counting:

$$\sigma\phi = \frac{C\lambda}{\varepsilon b\gamma N} \cdot \left(1 - e^{-\lambda t_i}\right)^{-1} \cdot e^{\lambda t_w} \cdot \left(1 - e^{-\lambda t_c}\right)^{-1} \tag{11}$$

where

C = gamma peak area in units of counts

ε = efficiency of gamma dectector

$b\gamma$ = branching ratio of γ transition of interest

N = number density of target nuclide

λ = decay constant of activation product nuclide

ti = irradiation time

tw = wait time between end of irradiation and start of counting

tc = count time

Equation 11 is derived in Appendix D as it pertains to the experiments conducted in this thesis.

The four foils placed at the outer radius of the tank were expected to result in a similar activation rate since they were each offset by the same distance normal to the beamline. These four numbers were then averaged to yield a single radial neutron production rate. The measured activity of the individual foils was then used to infer a measured photoneutron production rate within the D_2O tank. This was accomplished with the aid of the two-dimensional discrete ordinance neutron transport code DORT.

To obtain the photoneutron production rate within the tank, corresponding calculations for this first series of experiments were completed with the codes ACCEPT, DORT and MCNP. The geometries were modelled as accurately as possible, within the limitations of the codes. The 4-MeV medical head geometry, including the target assembly and heavy water, was modelled in ACCEPT to obtain the photon production within the tank. The advantage of both ACCEPT and MCNP is that the actual experimental geometry can be modelled accurately. Several ACCEPT calculations at varying energies in the range of 4 MeV for this accelerator were run with 5000 particle histories each. Usually ten cases were performed and then averaged. Because the electron energy of this machine was not known precisely and was assumed between 3.5 and 4 MeV, ACCEPT calculations were performed at both 3.5 and 4 MeV and then averaged. The Monte Carlo ACCEPT runs were performed on the geometry of the target (80%

tungsten and 20% copper), and included the heavy water, lucite and detectors. The D_2O volume was also modelled as three concentric equal volume regions in order to more accurately describe the photoneutron production within the tank as it varied with distance from the center beamline.

The ACCEPT calculations provided the bremsstrahlung production in the D_2O tank volume which was then converted to photoneutron production spectra by employing a FORTRAN program and photoneutron cross sections. ACCEPT calculations also provide a measure of the rads/second in the ionization chamber volume region. The resultant output from both the ACCEPT (bremsstrahlung production) and the FORTRAN program (photoneutron production) runs were then converted to the proper energy structure compatible with the DORT and MCNP formats. ACCEPT calculations also yielded a gamma flux in $\gamma/cm^2sec/mA$ and a photon dose rate in rads/sec/mA or rads/sec/electron within a volume region of interest.

With the theoretical photoneutron production source spectrum obtained from Monte Carlo calculations, the foil activation per photoneutron produced can be calculated using DORT. This result is then used in the determination of the inferred measured neutron production rates. The DORT model was constructed similarly to the model shown in Figure 5 on page 62, including the lucite tank, heavy water and indium foils, but without the filter material in place and with additional indium foils placed radially at 90^o from the beamline.

Cross sections for all modelled materials in DORT were computed using the COMBINE[93] code. The DORT input required a 27-group energy structure. Measured photoneutron production rates from the experimental foil data were then compared with the theoretical photoneutron production rates from the computational sequence described above. The calculated neutron source was obtained by dividing the measured activation rate from the foils (averaged over the three decay lines) by the calculated activation per *unit* source. The photoneutron production was normalized to the estimated electron beam current of the accelerator, as obtained from the ionization chamber measurements described previously.

Additional experiments were run using this 4 MeV medical head in order to determine cadmium ratios for the unfiltered neutron source. Cadmium foil covers, causing any foil to behave as a pseudothreshold detector, were used basically as an aid in the measurement of the total epithermal flux. A cadmium cover surrounding a foil assembly will preferentially eliminate the thermal component of the beam by absorbing the slower neutrons in the reaction:

93. Grimesey, R. A., Nigg, D.W. and Curtis, R.L., "COMBINE/PC - A Portable ENDF/B Version 5 Neutron Spectrum and Cross-Section Generation Program", EGG-2589 (Rev 1), Idaho National Engineering Laboratory, February, 1991.

$$^{113}_{48}Cd + n_{th} \rightarrow {}^{114}_{48}Cd$$

with a thermal neutron capture cross section, σ_{cap}, of 27,000 barns. In these cases two foils (one with and one without a cadmium cover) were placed on the outer radius of the tank set at a 90° angle to each other (see Figure 23). The cadmium covers were 0.56 mm thick with a diameter of 3.2 centimeters. Bubble chambers (rated at 34 mrad/bubble) were placed to the left and right of the heavy water tank as an additional check on the dose at these points. A second run measured the cadmium ratio along the beam centerline. Two foils (again one with and one without a cadmium cover) were placed on the face as shown in Figure 23. The total run time for this irradiation was fifteen minutes.

Series 2: Once the initial series of experiments was completed and the data analyzed, the results indicated, as expected, an acceptable neutron production rate for this photoneutron concept. A second, more flexible electron linear accelerator manufactured by theVarian Corporation was employed for further studies which examined the photoneutron production at various electron beam energies as well as the spectral properties of filtered beams produced using filter materials.

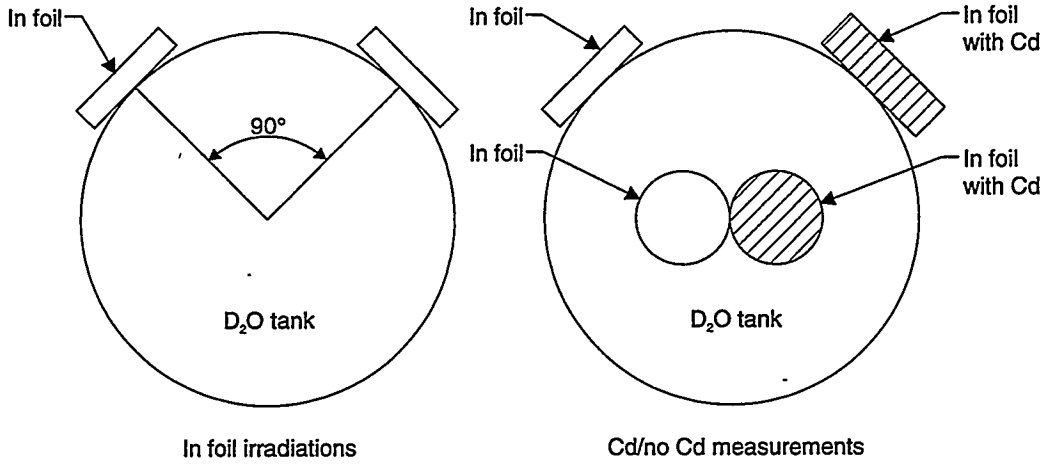

Figure 23: Foil placement for the first series of experiments using the 4 MeV fixed energy medical linear accelerator

During several trial runs and attempts, the Varitron's performance was characterized by making beam profile plots. Measurements were taken of the test port signal versus the electron energy for several magnet currents and used in the determination of LINAC's performance.

The foil irradiations for this second experiment series were performed without a moderating or filtering material in place. The experiental set-up is shown in the photograph of Figure 10 in the previous section. Four complete runs to obtain neutron flux information were conducted with parameters as shown in Table 1.

Table 1: Irradiations performed on variable energy Varitron linac to obtain initial neutron flux data

Electron energy (MeV)	Irradiation time (min)	Rad/min at 1 meter from target	Electron beam current (μamps)	Current on Magnetron (amps)	Foils packets irradiated
7.5	10.0	46.0	3.0	65	In (3): left, right, face
8.0	10.0	65.0	3.6	70	In (3): left, right, face
6.0	20.0	9.0	1.0	40	In (3): left, right, face
4.0	30.0	2.0	0.9	30	In (3): left, right, face

Each of these runs had foil positioning similar to those indicated in Figure 23. All three foils were cadmium covered, with one placed on the face and two placed radially along the beamline. Again, the resonance lines of interest were 416, 1097 and 1294 keV.

During all runs, the integrator detector was running to count the total charge in coulombs seen by the target. This reading was used to directly compute the exact coulombs per second, or current, of the electron beam. The target beam current could also be read from the oscilloscope by taking the voltage reading across a resis-

tor. For these runs, this method yielded a beam current of approximately 0.9 - 3.6 microamperes. The reflective power of the magnet was also monitored on the oscilloscope.

The corresponding calculations for this experiment were again completed with the previously-discussed codes. A model of the geometry input for the Varitron ACCEPT runs is shown in Figure 24. In order to compensate for variations in the photoneutron production within the heavy water volume as a function of radius from the beam axis, the modeled heavy water tank was divided into three equal volumes. By subdividing the neutron source input in this way, it is possible to more accurately describe the input for further calculations. Sample DORT and Monte Carlo runs are given in the appendices.

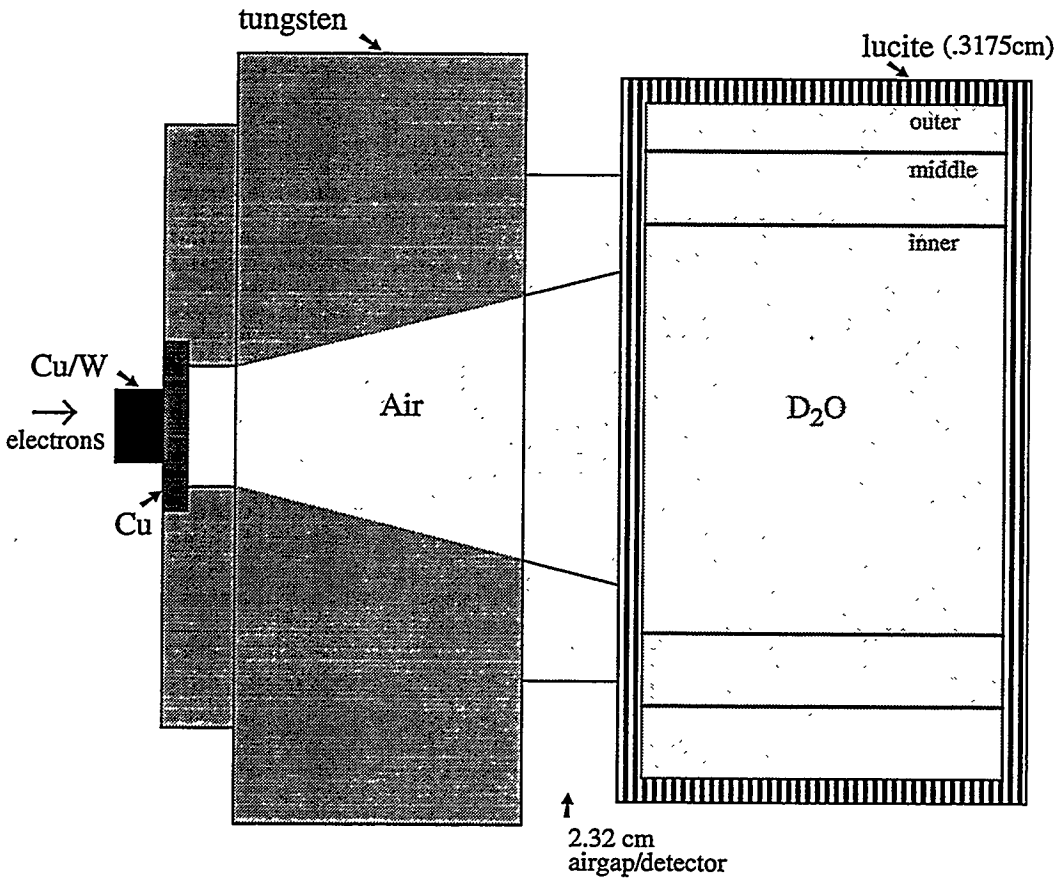

Figure 24: Sample geometry diagram used for ACCEPT Monte Carlo calculations of bremsstrahlung production from the Varitron electron linear accelerator

Series 3: The third series of data collection, reduction and computations was intended to measure the filtered epithermal neutron spectra produced implementing two separate neutron filtering materials. In order to understand the effects of the two filter materials chosen, spectral data were essential. The purpose of these experiments and calculations was twofold:

- *to analyze the filtering of the photoneutron beam produced from a variable electron energy linear accelerator*
- *to evaluate two new potential filter material ideas which may offer advanced, high-efficiency filtering capabilities for both accelerator and reactor beam technologies*

Other well-defined filter materials with good neutron moderating characteristics were considered (such as aluminum oxide) but it was decided to limit the scope of this work to advanced fluoride-based filtering materials.

Activation foil assemblies were selected and irradiated both on the downstream and upstream sides of the moderating material. Downstream foils were placed as close together as possible in a circle along the beam centerline. Foils were not positioned radially in these experiments. The upstream foil package consisted solely of indium foils but allowed for a direct comparison of the neutron flux intensity on opposing sides of the filter along the beam axis. Dominant resonances of particular activation reactions were used to measure neutron spectra. The fast neutron compo-

nent was measured by recording the 336 keV line of the indium foils which is produced by a threshold inelastic scattering interaction. Neutron spectral data were derived from the experimental and calculational data by obtaining the neutron flux values at the energies of the dominant or primary resonances of the epithermal activation reactions.

The first filter assembly tested consisted of bricks molded from a composite material developed by the Technical Research Centre of Finland ($Al/AlF_3/LiF$); the second assembly was constructed specifically for this experiment as a novel aluminum/teflon ($AlCF_2$) "sandwich" design. Each of the filtering materials was tested using a set of foils chosen to characterize a specific section of the energy spectra through the filtering materials. The decay reactions of interest are given in the following table:

Table 2: Foil reactions of interest

Reaction	Half-Life	Energy of Gammas (keV)
$^{115}In(n,\gamma)^{116}In$	54.2 min	416, 1097, 1294
$^{115}In(n,n')^{115m}In$	4.486 hr	336
$^{197}Au(n,\gamma)^{198}Au$	2.69 day	411
$^{63}Cu(n,\gamma)^{64}Cu$	12.70 hr	511
$^{186}W(n,\gamma)^{187}W$	23.9 hr	686

This set of experiments was meant to determine the filterable spectrum obtained through these two materials at several energies. Data were collected during irradiations from these sets of counting foils; the activation rate was then obtained for each foil and analyzed computationally. Data were also collected on the upstream side of the filter with indium foils to obtain basic information on the upstream spectrum as well as the neutron intensity entering the filter for each experiment.

As mentioned previously, each foil material used was intended to measure a particular part of the energy spectrum. The neutron interactions shown in Table 2 used for the measurements are, with one exception, insensitive to the gamma conponent of the neutron field. The ^{115}In(n,n') reaction in particular acts basically as a fast neutron threshold detector, sensitive to neutrons at incident energies above 430 keV. The activation product for this reaction is metastable ^{115m}In, which decays by gamma-emission. One problem encountered in attempting to measure this particular interaction was in distinguishing the fast neutron reaction from the photon activation of the isomeric state in ^{115}In by the strong bremsstrahlung field present along the beam axis. There is a competing decay gamma given off from the reaction ^{115}In(γ,γ')^{115m}In, which occurs at a similar gamma energy to that which is given off in the indium inelastic scattering.

The decay schemes are shown in the following diagram. Both metastable states decay to stable ^{115}In by giving off a gamma of 336 keV, which can then be detected.

Fast Neutron Threshold Detection Competing Decay Reactions:

$$^{115}In\,(\gamma,\gamma') \rightarrow {}^{115m}In$$

$$\searrow \quad 336\ \text{keV}\ \gamma$$

$$^{115}\text{In}$$

$$\nearrow \quad 336\ \text{keV}\ \gamma$$

$$^{115}In\,(n,n') \rightarrow {}^{115m}In$$

The signal from the photon-induced reactions in indium can often obscure the neutron-induced activity of the isomeric state. This effect was measured by replacing the heavy water target with an equal volume of distilled light water (H_2O). Foil data was then collected without the production of neutrons in order to determine the gamma-induced fraction of the measured activation signal, since with the light water there is no neutron production.

The initial filter material experiments were carried out using the Al/AlF_3/LiF composite material. Raw data is given in Appendix D for these experiments. The first sets of foils in these Al/AlF_3/LiF experiments were activated through a 30 cm filter thickness. During irradiations, the entire filter set-up was surrounded with borated polyethylene to reduce neutron room scatter in the foil data. In addition, the filter bricks were

offset to avoid streaming effects. Lead bricks were also utilized around the D_2O target to help reflect gammas and neutrons back into the system. The basic geometry set-up is shown in Figure 25.

In order to confirm the fluxes obtained in previous runs without the filter and to obtain initial indium foil data, a short 15-minute preliminary irradiation was performed with four indium foils only and at an electron energy of approximately 6.4 MeV from the accelerator. Further irradiations of foils with this material were performed with the parameters as listed in Tables 3, 4 and 5. It was of interest to increase the thickness of the Al/AlF_3 moderating material to 40 cm by rearranging the geometry of the bricks. The experimental runs performed are listed in Table 3.

A novel Al/Teflon filter design was then tested in order to compare its filtering properties with those of the Finnish material. A filter with a similar net thickness of approximately 30 cm was constructed and further investigations carried out to characterize this second moderating material. The experimental geometry was similar to that shown in Figure 25 except with Al/Teflon in place of Al/AlF_3 as the filter material.

Once the experiments were performed, the data was then reduced to obtain the foil activations. Because a clinically-useful neutron flux intensity was determined to be obtainable in the previous experiments, the ultimate goal of the filter work was to augment this information by unfolding a suitable epithermal neutron source incorpo-

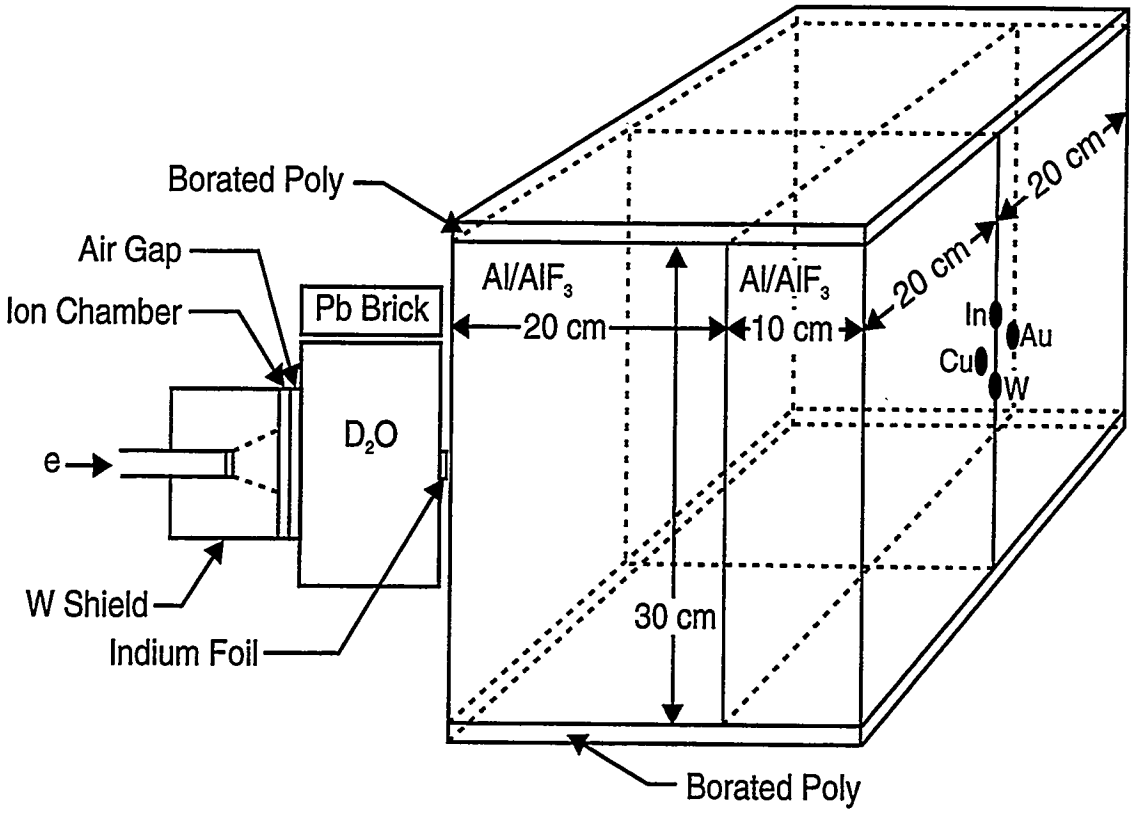

Figure 25: Drawing of Al/AlF_3 filter experimental geometry set-up

Table 3: Irradiations performed through 40 cm of Al/AlF_3 composite

Electron energy (MeV)	Irradiation time (min)	Rad/min at ~50 cm from target	Electron beam current (μamps)	Current on Magnetron (amps)	Foils packets irradiated
6.2	60.0	2.5	4.8	40	In(2), Au, W, Cu
8.0	60.0	3.45	2.9	50	In (2), Au, W, Cu
4.0	100.0	0.2	1.7	30	In(2), Au, W, Cu

rating both experimental and calculational filtering data. Following irradiations, the energy dependent neutron flux data from the measured activation rates can then obtained through data reduction and spectrum analysis/unfolding techniques. The next step, then, in analyzing this neutron source was to sort the data and to extract useful beam information.

In conjunction with the experiments, calculations were again run as in the previous series of experiments using MCNP, DORT and ACCEPT. The DORT geometry used is shown in Figure 5 on page 62. The computed neutron leakage from the tank of heavy water (from the 2-stage electron/photon transport and photoneutron production calculations) was used as input into the new DORT geometry with the filter material incorporated.

In the final DORT model, the computed photoneutron spectra inputs were actually weighted averages of separate spectra obtained at two individual initial electron

Table 4: Irradiations performed through 30 cm of Al/AlF_3 composite

Electron energy (MeV)	Irradiation time (min)	Rad/min at ~50 cm from target	Electron beam current (μamps)	Current on Magnetron (amps)	Foils packets irradiated
6.4	120.0	1.2	3.7	45	In(2), Au, W, Cu
7.7	90.0	13.0	3.3	60	In (2), Au, W, Cu
4.3	99.5	1.3	1.9	50	In(2), Au, W, Cu
6.4	60.0	9.5	5.0	45	In(2), Au, W, Cu, NaCl
8.0	90.0	11.0	3.0	55	In(2), Au, W, Cu
6.3	95.0	2.4	6.0	55	In(1 upstream) In(3 stacked dwn) Cu
6.3	31.5	2.1	5.6	55	In(1 upstream) In(4 stacked dwn)
6.4†	120.0	1.8	5.7	60	In(1 upstream) In(4 stacked dwn)
6.4	62.0	1.9	3.1	60	In(1 upstream) In(3 stacked dwn)

†run performed with distilled H_20 in target position (for test of fast neutron/γ component, nn')

Table 5: Irradiations performed through 30 cm of Al/Teflon filter design

Electron energy (MeV)	Irradiation time (min)	Rad/min at ~50 cm from target	Electron beam current (μamps)	Current on Magnetron (amps)	Foil packets irradiated
6.2	30.0	2.3	3.6	55	In(up: w/ & w/o Cd covers) In(dwn: w/ & w/o Cd covers)
6.3	81.0	1.4	2.1	55	In (2), Au, W, Cu
6.3	105.0	3.5	5.9	45	In(1 upstream) In(5 stacked dwn)
6.3	105.0	2.9	3.4	50	In(1 upstream) In(1 downstream)
6.3*	60.0	4.3	3.5	50	In(1 upstream) In(1 downstream)
6.3†	60.0	3.5	3.5	50	In(1 upstream) In(1 downstream)
6.3	120.0	4.3	6.2	55	In(1 upstream) In(5 stacked dwn) Cu

* run performed without D_20 target in place (for test of fast neutron/γ component, nn')
† run performed with distilled H_20 in target position (again for test of fast neutron/γ component, nn')

energy models in ACCEPT (using 7.67 MeV and 5.9 MeV incident electrons). This was done in order to account for the fact that the beam was comprised of electrons of many energies and most likely included more higher energy electrons than initially anticipated; this modification to the input file minimized the effects due to the fact that the electron beam from the accelerator was not comprised of electrons of one single energy hitting the tungsten target, but included a tail of higher energy electrons as well.

In order to offer a more complete description, two methods were employed in the spectra analyses. The first method utilized several foil materials to characterize the energy spectra, each foil being selected to characterize a specific section of the energy range. The second method was that of stacked-foil analysis.

By looking at the responses within specific energy regions from various foils, the total neutron spectrum can be reconstructed (limited by the foil activation analysis errors and by the number of foil energies selected). If it is of interest to determine the total neutron flux associated with a specific energy region, it is possible to employ suitable foils, subtracting the thermal contribution by means of a cadmium cover. A cadmium correction factor can be determined which relates the cadmium-covered foils to the bare foils. A second contribution which should be mentioned is the possible flux depression by the presence of the cadmium itself, which, in these experiments, was determined to be insignificant. Cadmium correction factors (defined as the ratio of the

reaction rates without cadmium to the reaction rates with cadmium) on the order of 1.5 to 2.5 were obtained. The purely thermal activation count on a foil (C_{th}) is obtained by subtracting the product of the cadmium correction ratio and the counts with the cadmium cover from the total counts, as described in the equation below:

$$C_{th} = C - (R \cdot C_{cd}) \tag{12}$$

Particular nuclear reactions occur only when the impinging neutrons are above a certain threshold energy at which they can overcome the binding energies and Coulomb barrier to allow ejection of a particle from the nucleus. These reactions can be used to determine the flux due to fast neutrons. Because typical cross sections for such reactions are on the order of millibarns, they can be difficult to detect. The threshold energy is that energy at which the reaction can first occur, just allowing the particle enough excess energy to escape. The cross section rises with energy above the threshold and then peaks, falling off at higher energies. The effective threshold energy is defined as the energy at which the cross section is the same as the average cross section value over a broad energy group spectrum. In these experiments, the threshold reaction of interest was the interaction of fast neutrons on indium foils.

If the cross section is significantly large, it may be necessary to describe a correction factor for self-shielding in the foils (unless the foil is thin when compared to the effective mean free path of the neutron) by using stacked-foil-analysis. By disturbing, or depressing, the incident flux, a foil can introduce errors, simply by its presence in the beam, that can result in a measured flux unrepresentative of the unperturbed neutron field.

The ultimate idea behind using the stacked foils is to obtain the incident neutron flux at the primary resonance energy. The primary resonance contribution is the dominant response within the first foil and is subsequently attenuated as a function of depth in the foil stack. The secondary resonance contributions, as well as possible neutron room return (although experiments were surrounded by borated polyethylene to reduce this effect), therefore, are more visible in foils situated further in the foil stack.

In the majority of the experiments performed, foils were individually placed in their cadmium covers (to remove the thermal component). But, in a few instances as described above, it was determined to be of interest to use this stacked-foil method to provide additional linearly-independent foil response functions, without changing foil materials. This approach relies on the fact that there is significant neutron self-absorption within the foil material at the dominant resonance energy as a function of depth in the irradiated material. In order to determine the actual unperturbed incident flux seen

by the foil assembly, it is necessary to individually measure, or count, the foils within the stacked assembly. The flux can then be corrected for self-absorption and secondary resonance contributions.

Indium foils were stacked and placed within one cadmium cover. Because the foils were stacked, those in front see a different neutron flux than the foils in back, due to severe depression of the resonance flux on the downstream side of the stack. It is necessary to take into account the flux-depression effects of these foils in front. To correct the indium cross sections which were calculated for single foils using COMBINE, MCNP was again run to determine depression factors for the stacked foil analyses, or simply ratios of the cross sections of foils within the stack to that of the first foil, i.e. the one directly in front of the filter. Sample stacked foil assemblies irradiated are shown in Figure 26.

The $\sigma\varphi$ values as calculated by MCNP for both the foil directly against the face of the filter material as well as the foil situated in between the other foils are plotted in the graph of Figure 27. This indicates the amount of depression by which the inner foil is reduced by being situated deeper in the stack. By examining these data, it is possible to determine the strength of the secondary resonances energies seen in the inner foils because the primary resonance neutrons are predominantly absorbed within the first foil. This method can then be used in the calculation of a more accurate final primary resonance incident neutron flux which will include a subtracted correction for the secondary resonances seen by the foils.

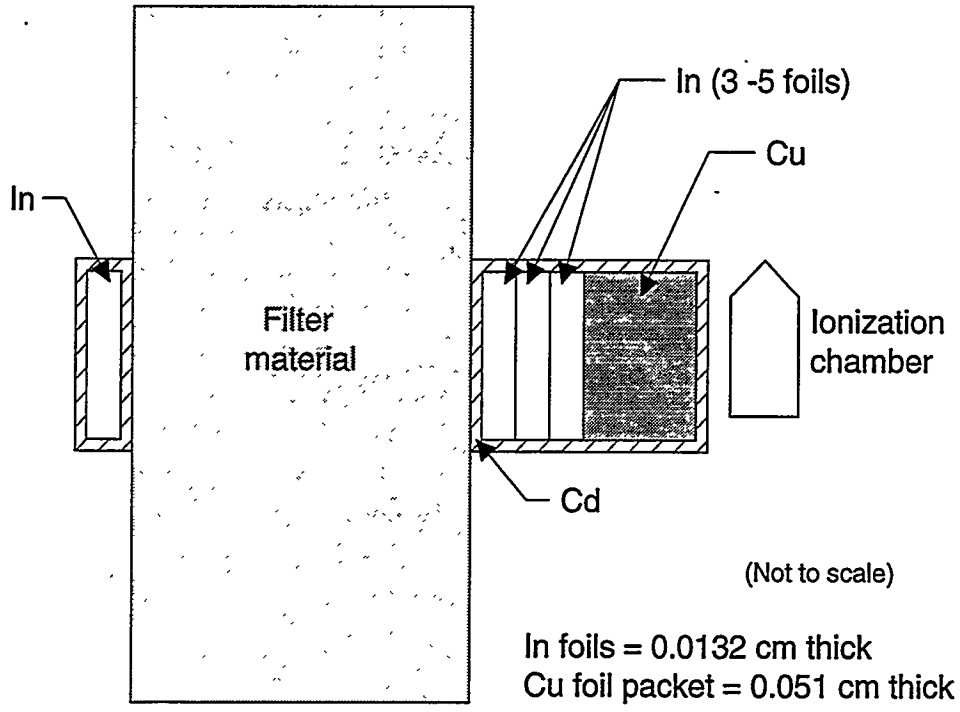

Figure 26: Geometry for stacked foil assembly technique

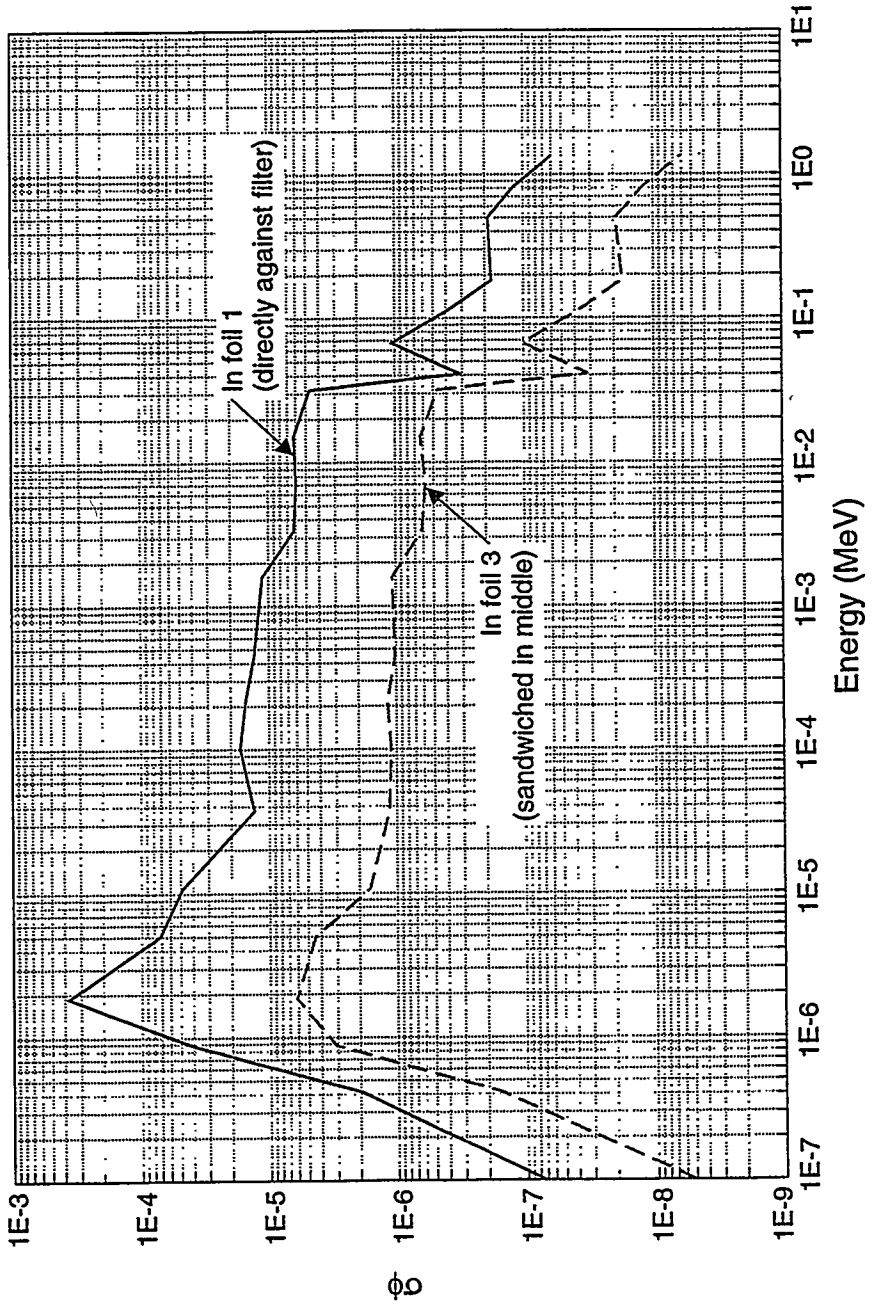

Figure 27: Plot of σφ as a function of energy for two foils in the stacked-foil assembly, as calculated using MCNP, indicating presence of secondary resonances

The number of different foil response functions determined the number of energy groups in a broad-group flux description. These broad-groups are basically collapsed energy groups selected to produce a well-conditioned, diagonally-dominant unfolding matrix, as indicated by the available foils. The energy group structures are given in Appendix D. The foils themselves were chosen such that the resonance peaks in the cross sections covered a reasonable range of the energies of interest and offered linearly-independent responses. The fast flux was characterized by the ^{115}In(n,n') reaction seen on the indium foils in which an incoming neutron scatters inelastically, giving off a gamma of approximately 336 keV in the process.

The goal in the spectrum analysis was to characterize the energy of the neutrons seen on the downstream side of the filtering material. This analysis was obtained through a direct matrix unfolding procedure involving the calculation of fluxes in the broad-groups, each corresponding to a particular foil reaction. A spectrum over a particular number of fine-group energy bins was calculated for comparison as well. Measured foil reaction rates were used to unfold a set of broad-group fluxes. In addition, calculations were performed to obtain neutron fluxes collapsed to the corresponding broad-group energy structure of the measurement data.

In analyzing the resonance foil reaction rate data, a calculated response matrix is derived in order to obtain the value of the incident flux for neutrons at the energy of each of the primary resonances. The data was analyzed by solving the matrices associ-

ated with these calculations by using a direct unfolding process. It was felt, given the number of measured data points, that this would offer a more direct and controlled approach than applying a least-squares adjustment technique. In order to unfold the spectrum data, it was first necessary to define the reaction rates within each foil over the total number of broad-groups, BG, as below:

(13)

$$R_f = \sum_{bg=1}^{BG} \varphi_{p(f,bg)} \tau_{(f,bg)}$$

where τ is the activation cross section for each foil averaged over the energy broad-group and φ_p is the perturbed broad-group flux in each foil. R_f is the measured foil activation for foil f. Perturbed and unperturbed refer to whether or not the flux seen is with or without the foil in place. Of ultimate interest is the unperturbed flux at the position of the foils downstream of the filter. If the *unperturbed* flux is then defined over all broad-groups as φ_u and a flux depression factor, or P-factor, is defined as:

(14)

$$P_{(f,bg)} = \frac{\varphi_{p(f,bg)}}{\varphi_{u}(bg)}$$

then the measured foil activation in each foil can then be rewritten as:

(15)

$$R_f = \sum_{bg=1}^{BG} P(f,bg)\,\varphi_u(bg)\,\tau(f,bg)$$

The P-factors as defined above can be determined using the a-priori calculation over the fine-group structure, which is, in this case, basically broken down into 27 energy groups all included within the broad-groups (dependent on the number of foils).

(16)

$$P(f,bg) = \frac{\sum_{fg} \Psi_p(f,fg)}{\sum_{fg} \Psi_u(fg)}$$

In the above equation Ψ_p and Ψ_u are the perturbed and unperturbed fine-group fluxes respectively, each summed over the fine-groups. The perturbed flux is known for each of the foils. The τ term, averaged over each of the broad-groups, can also be determined from a-priori calculations as:

(17)

$$\tau(f,bg) = \frac{\sum_{fg} \Psi_p(f,fg)\sigma_p(f,fg)}{\sum_{fg} \Psi_p(f,fg)}$$

where σ_p is the reaction cross section in each fine-group for each foil and is known from MCNP calculations as described earlier. The calculated reaction rate in each foil is defined as the perturbed flux multiplied by the averaged cross section over all the broad-groups:

(18)

$$R_c(f) = \sum_{BG} \varphi_p(f,bg)\tau(f,bg)$$

Finally, the measured activation rates are known from the data reduction of foil data. These are substituted into Equation 18, and the resulting system of equations is solved for the measured perturbed flux over the broad-group energies. The unperturbed flux is then simply the perturbed flux divided by the P factor.

The spectral unfolding technique is essentially the solution of a set of matrices. And, because the matrices solved in this direct unfolding process are diagonally-dominant, they can be considered well-conditioned. In addition, the foils for these experiments were selected in such a way that the foils produced linearly-independent responses.

IIIb4. Experiments Used in Photoneutron Source Presented

Lastly, it was of interest to look at the neutron production through the filter material at 90° off the beamline, since this would be the configuration used in an actual clinical device, where it is essential to reduce the photon component of the treatment beam to acceptable levels. In the original experiments both the radial and the axial neutron production was measured. It was trickier to design a method to look at the production through the filter materials and not simply off the D_2O tank.

Consequently, an experimental set-up as shown in the photo of Figure 28 was designed such that the foils were placed above the filtering material (in this case Al/AlF_3) and irradiated. The vertical filter configuration shown allowed an initial experimental confirmation of the postulate that a suitable neutron source could be produced with the apparatus aligned with the neutron and electron beam axes oriented at right angles. In addition, this measurement provided a preliminary indication of the photon content of the filtered neutron source.

Indium foils encased in cadmium were placed upstream and downstream of the neutron filter. The photon dose rate was measured with the ionization chamber positioned directly on top of the filter. Because the readings from the ionization chamber due solely to gammas through the filter material were obscured by gammas from air scatter of photons emitted sideways and backwards from the tungsten target, the

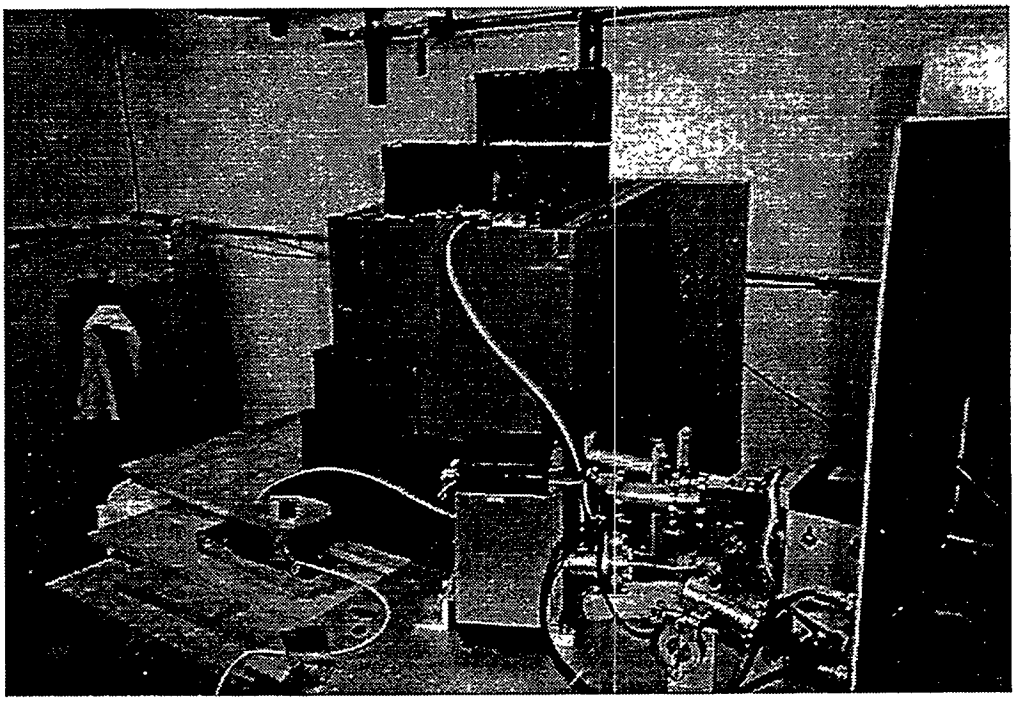

Figure 28: Photo of experiment to determine neutron production through filter material at 90^0 off beamline

detector positioned above the moderator was surrounded by a lead shielding (as indicated in the photograph) to prevent unwanted air-scattered photons from being detected. With sufficient shielding provided, the photon dose rate from radiation passing directly through the filter to the detection point was determined to be below detection limits of the chamber, as indicated in the instrumentation manual (1 mR per minute, or 1.67×10^{-5} cGy per second). Neutron production data from the foils was, however, measured. These results do appear to indicate that the photon component of the neutron source can be reduced to acceptable levels with appropriate shielding. Additionally, an extended beam guide to allow for treatment at distances further from the accelerator target would also aid in the reduction of gamma doses.

It should be noted that the above-described filtered and unfiltered neutron source experiments were designed to have a simple geometry that could be easily modeled in theoretical calculations. The experimental geometries were specifically arranged to have 2-dimensional symmetry and the on-axis photon flux was used in the normalization. All components in the neutron production and filtering apparatus were colinear with the electron beam axis, providing a high degree of azimuthal symmetry about this axis, although this is not the geometry intended for actual clinical use. The bremsstrahlung radiation produced by the electron LINAC is highly forward-peaked and is approximately an order of magnitude smaller at 90° to the beam axis. A right-angle treatment geometry would offer a patient irradiation point with minimal photon contamination in a clinical neutron source.

The electron beam energy used in the presentation of the final filtered neutron source measurements was taken at a nominal average electron energy of 6 MeV. As mentioned previously, the electron beam is believed to include a significant high-energy component of electrons in the 7-8 MeV range. Since the accelerator guide was designed to operate at 9 MeV, these higher energy electrons were not unexpected.

Measurements of the filtered neutron source intensity and spectral characteristics produced through each of the two separate moderating/filtering arrangements were performed using the standard resonance and threshold activation foil techniques described previously. The final two geometries presented in this work, the experiments on the AlF_3 filtering material and on the Aluminum/Teflon composite, were completed using two analysis methods. Spectral data were obtained for each experiment and are presented in the following chapter. The data were directly unfolded for sets of broad-group neutron energy intervals over the entire energy range of interest (from thermal energies up to 2.5 MeV).

In the Aluminum/Teflon case, the stacked-foil procedure was used which included both indium and copper foils located on the downstream side of the filter material and indium foil package. The interior indium foils were then shielded from resonance neutrons, forcing them to have linearly independent spectral responses relative to that of the first indium foil in the stack, unshielded from resonance neutrons. The copper foil was also shielded from neutrons by the intervening indium foils, forcing its spectral response toward the energy range of the primary resonance for this material as well.

In the case presented, five indium foils and one copper foil were counted. The measured inelastic scatter reaction rates of all five indium foils were added together to provide more sensitivity in the energy range above the threshold for this interaction. Four spectral response functions having a useful degree of linear independence were thus available from the downstream foil package. These response functions were: inelastic scatter in indium (experimentally corrected as described previously for photon activation of the 336 keV indium-115 isomer), neutron capture in the first indium foil, neutron capture in one of the interior indium foils (the center foil in the package of five was used), and finally, neutron capture in copper, shielded by indium. Effective shielded cross sections used in the spectral unfolding process for all foils in the stack were computed using an MCNP model of the filter and foil packages as described earlier.

In the results presented for the second material (from VTT), a multiple-material-foil irradiation technique was used, utilizing indium foils with and without cadmium covers, gold foils and copper foils (all with cadmium covers) to determine the spectral properties of this material. As in all experiments, indium foils were placed upstream of the filter as well. This method provided three linearly-independent foil response functions on the upstream side of the filter and five on the downstream side. Spectral information was then obtained over three broad-groups upstream and five broad-groups downstream over the energy range of interest. The broad-group and fine-group energy structures used are listed in Appendix D.

CHAPTER IV

RESULTS

Utilizing the various methods and tools, both experimental and calculational, described in the previous sections, results have been obtained for a low-current bench-top prototype of the epithermal photoneutron source concept. The theoretical computations as well as the experimental results indicate the feasibility of this promising alternate approach to the production of epithermal neutrons for BNCT. When scaled to existing, or feasible, electron accelerator technology, proof-of-principle experiments and calculations indicate that the concept can produce neutron fluxes in the desirable epithermal range which are competitive with other neutron production designs.

IVa. Series 1 Neutron Production Results

The first series of experiments was carried out on a standard 4 MeV side-coupled medical electron linear accelerator with a tungsten target. In these initial proof-of-principle experiments, the principle intent was to determine the *feasibility* of this neutron-production method, deriving basic performance data that would indicate a sufficient total neutron production. The measured activation of indium foils was used to infer a measured photoneutron production rate within the tank. Foil measurements were taken

both radially (at 90° to the beamline) and axially (along the beamline). Calculational results of the foil activation per photoneutron produced within the tank were obtained with the aid of the fine-mesh, 27-group, two-dimensional DORT discrete-ordinates neutron transport code, using the ACCEPT Monte Carlo code (to obtain photon production) in conjunction with the FORTRAN program (written to calculate photoneutron production) for calculating the theoretical photoneutron input source spectrum. The results are shown in Table 6. The estimated errors for these initial production rates are given with 68% confidence and, for the calculational result, are mainly due to the fact that the exact average electron energy of this particular accelerator was not precisely known. The measured production rate errors are a result of the various inaccuracies associated with data collection and activation rate measurement.

Table 6: Neutron production rates from initial photoneutron experiment

Foil Location	Inferred measured neutron production rate (n/sec)	Calculated neutron production rate (n/sec)
axial	$(2.51 \pm 0.9) \times 10^8$	$(6.1 \pm 1.1) \times 10^8$
radial	$(2.90 \pm 0.9) \times 10^8$	

The measured data were collected during experimentation at the fixed, estimated electron energy of this machine. Although the exact average energy of the electron beam generated inside the medical accelerator head was not precisely known at the point where the electrons impinge on the target, for calculational purposes, it was esti-

mated to be between 3.5 and 4 MeV. This estimation seems reasonable when compared with results obtained at an electron energy of 4 MeV on the Varitron tunable electron accelerator.

In Table 6, the neutron production rates are presented as both implied measured sources (obtained from actual measured foil activation rates together with the DORT-calculated foil activation rate per photoneutron) as well as purely calculational sources. In presenting the measured neutron production rate as an implied neutron source, it should be noted that although actual foil activation rates were used in obtaining the measured source, the numbers presented are normalized to calculated photoneutron source data and should not be considered purely measured results.

In addition, it should be noted that these results are presented as neutron production rates and not as production rates per milliampere. From the ionization chamber measurements, the electron current was estimated to be 15.2 $\pm$2.9 μA for this particular experiment. Using this estimated current, the unfiltered neutron production rate is determined to be on the order of 10^{10} neutrons/second per milliampere of electron beam current. It is important to note that these data were obtained without cadmium foil covers and thus include thermal neutrons. If obtaining electron currents on the order of 100 milliamperes is assumed feasible, the measured source before filtering can then be projected to be at least two orders of magnitude higher.

IVb. Series 2 Neutron Production Results

The second series of experiments performed was conducted on a tunable electron linear accelerator manufactured by the Varian Corporation. This more detailed experiment allowed data collection concerning the variation in photoneutron source strength, or production rate, at multiple incident average electron energies. Again, the calculated results are obtained using calculational codes while the implied measured production rates are obtained from foil analysis activation rates in conjunction with a calculated incident photoneutron source. Both the calculated theoretical and inferred measured unfiltered photoneutron source results from these experiments are shown in the graph of Figure 29 for three separate average electron beam energies. The measured data is normalized to the electron current inferred from the downstream bremsstrahlung flux measurements for each electron beam energy. The dose rate measured on the ionization chamber ranged from 2 to 65 rads per minute, with the accelerator running at currents of 0.9 to 3.6 microamperes. It was also possible to normalize to the second method of beam current determination (that of the directly-measured electron beam current) and this yielded similar results.

Because the experimental and calculational data shown in Figure 29 are in good agreement (within a factor of two), the computational methods used to estimate the beam performance can be said to predict realistic results for the absolute intensity of the photoneutron source, thus validating the use of these computational tools in further neutron beam analyses.

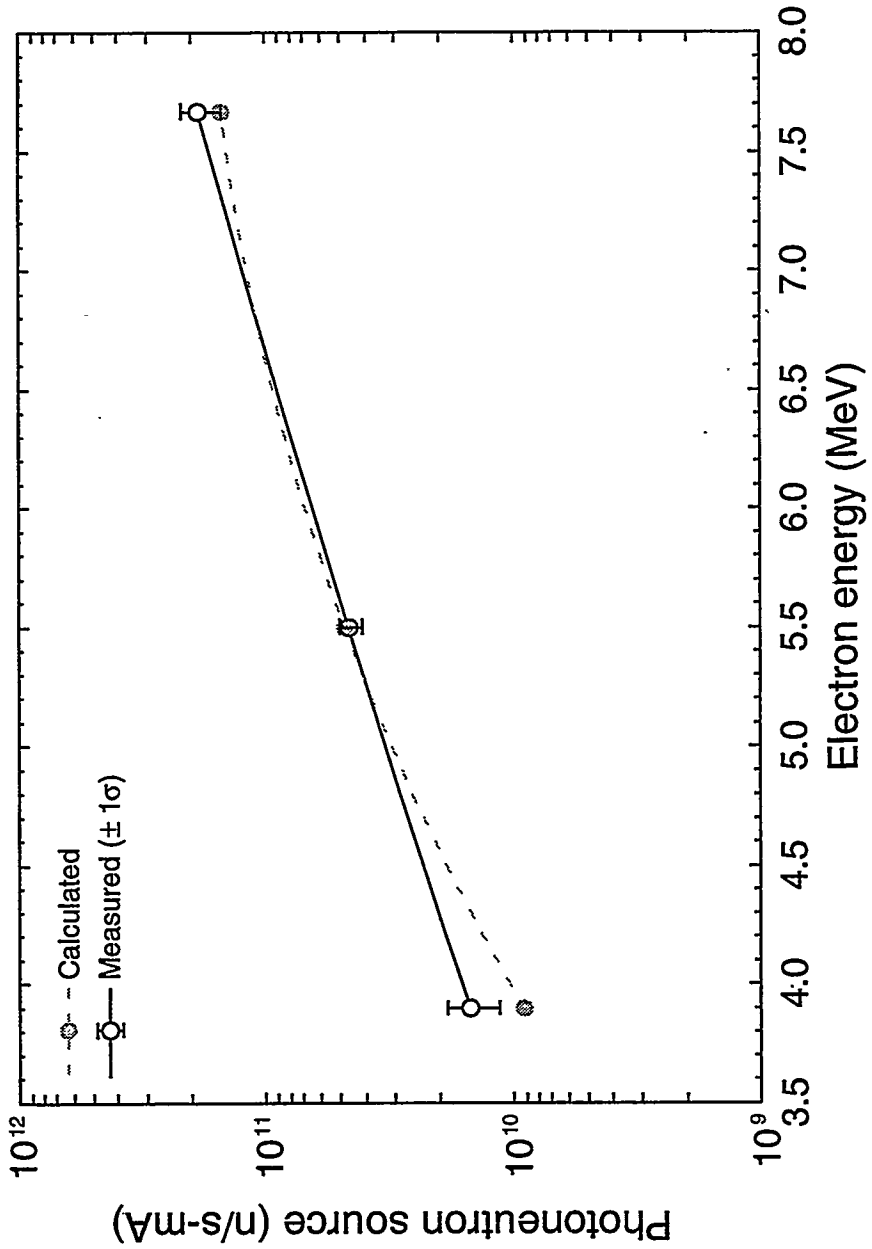

Figure 29: Photoneutron source at three electron energies of Varitron accelerator

These experiments also demonstrated how the unfiltered photoneutron source intensity varied as a function of incident electron energy. The information obtained during these studies was further used to determine the optimal energy at which to continue investigations into both viable moderating materials and the filtered spectrum. With the electron linear accelerator available, it was determined through the many irradiation experiments that the neutron production at the nominal 6 MeV electron energy (which most likely contained a significant number of electrons with energies greater than 6 MeV) offered the best neutron production results. Although an electron energy of 4 MeV is above threshold for both heavy water and beryllium photoneutron targets, it was determined, in this experiments carried out with the heavy water target, to offer a neutron production yield felt to be too low, while at higher incident electron energies, additional problems become apparent such as photon and fast neutron contamination, which would then require additional moderation. The prototype design presented in IIIa. was also modeled at this incident electron energy of 6 MeV, although it was modelled with a source consisting purely of 6 MeV electrons while the experimental system was not as ideal.

Both the initial experiments and calculations also served as a starting point for further studies. The pure neutron production order-of-magnitude results were encouraging. Because the beam will ultimately require filtration in its final optimization for treatment purposes, it was then of interest to investigate the quality of filtered spectra through selected materials.

If the beam is contaminated with neutrons of too high an energy and appreciable filtering becomes necessary, this may limit the practicality of the beam by not only the extra cost of the filter material but also in loss of neutron intensity in the beam. In the next series of experiments, the beam was analyzed for filterability with two moderator materials of two thicknesses and at incident average electron beam energies of from 4 to 8 MeV.

IVc. Series 3 Filtered Neutron Production Results

Although filtered beam characterization studies were conducted at three electron energies, for the remainder of the experimental and calculational data from the filtering material experiments, it was estimated that the optimal electron energy for epithermal neutron production without undue photon contamination of the neutron source occurred at approximately 6 MeV in the experimental design for these studies. The final results presented here were measured and calculated at this nominal 6 MeV electron energy.

The purpose of collecting these filtered spectral data was to characterize the neutron beam seen downstream in order to offer a reasonable starting point for eventual design of a clinical epithermal neutron beam. Of interest in this task was to quantify three major sections of the neutron beam spectrum: the slow or thermal energies, the desired epithermal range, and the undesirable fast neutron component. The foil activa-

tion data, along with ACCEPT, DORT and MCNP calculations, established the fast neutron component. The epithermal range was covered by the foil reactions listed in the previous chapter, while the thermal range was quantified with the aid of data collected utilizing cadmium-covered indium foils, acting as pseudothreshold detectors. Ultimately, an overall description of the filtered spectrum was obtained both experimentally as well as calculationally.

The results of the filtered photoneutron experiments are shown in the spectrum plots of Figures 30 and 31. Both the measured and calculated data were taken directly along the beam axis. The calculated spectral data in these graphs are plotted at the logarithmic midpoint in each broad energy group. Calculated neutron spectra for both upstream and downstream locations are indicated along with the inferred measured neutron flux data, unfolded from the foil activation rates using a direct matrix unfolding method. The measured neutron fluxes in these experiments are also obtained from actual measured foil data normalized to a calculated source, yielding an implied source which can then be compared with purely calculational results. The uncertainty in the fast neutron measured data is large but can be attributed to the low intensity of the fast neutron component. The measured downstream neutron source intensities for both materials offered neutron production rates actually higher than expected from calculations.

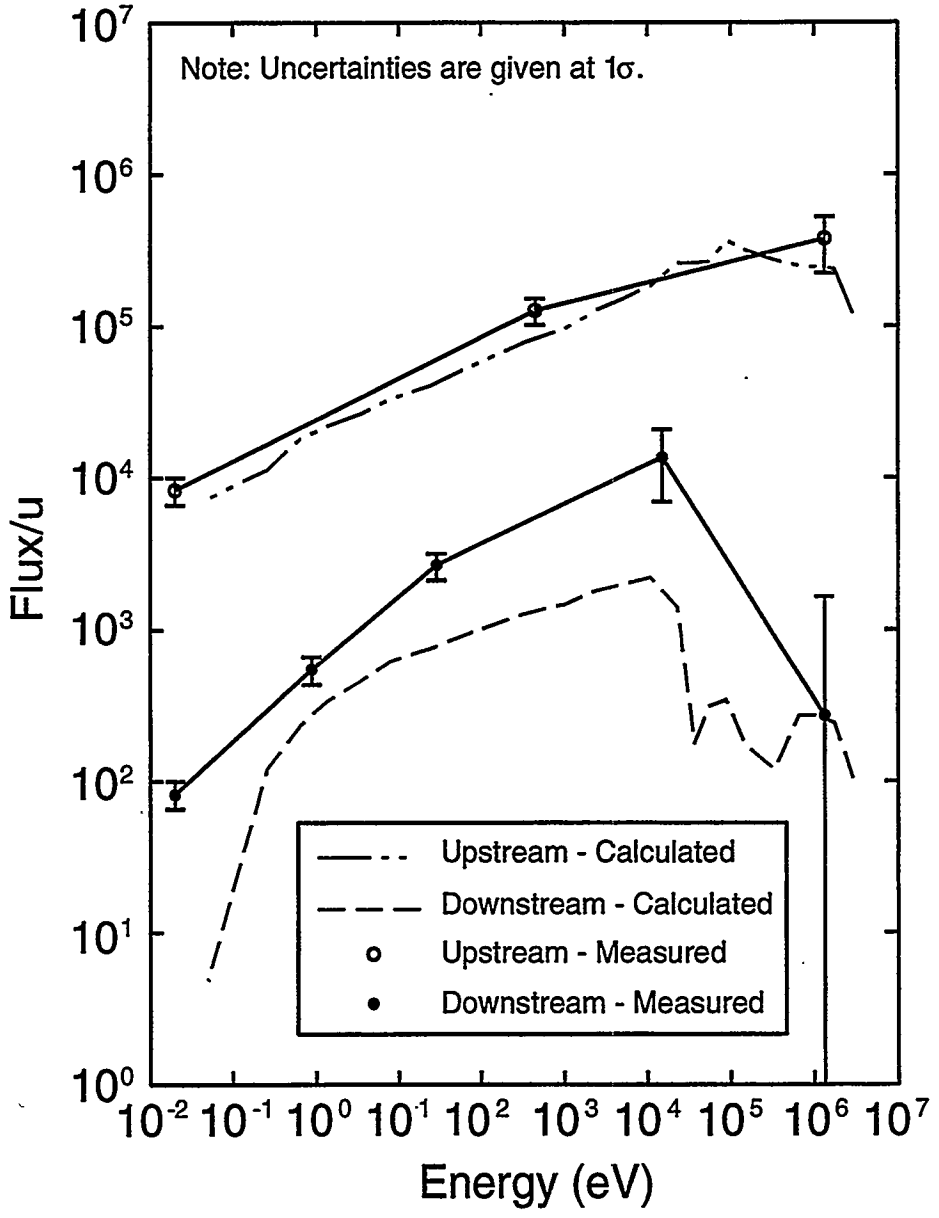

Figure 30: Inferred measured and calculated photoneutron spectra through 30 cm Al/AlF_3/LiF composite filtering assembly using multiple-material-foil method at an electron current of 5.99 μamps

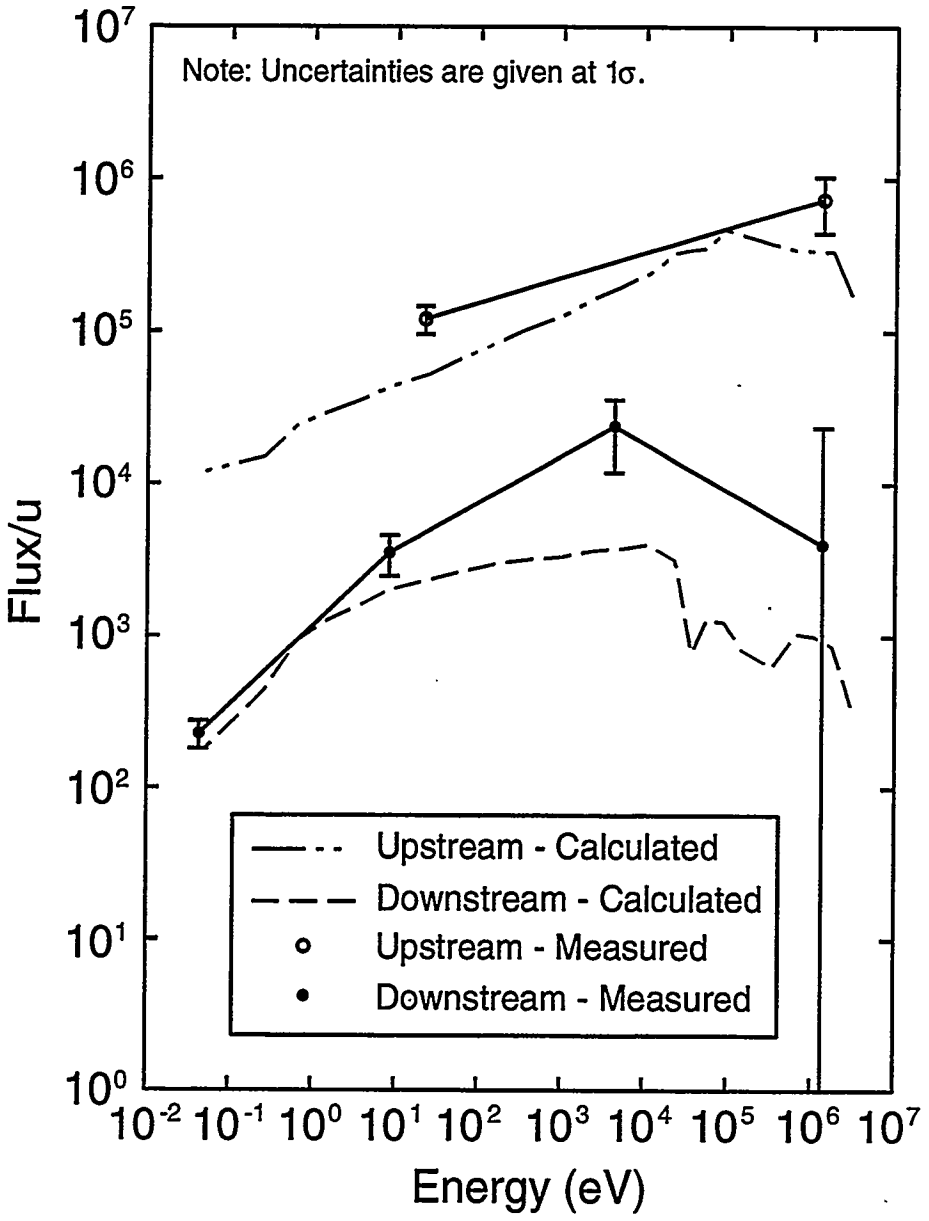

Figure 31: Inferred measured and calculated photoneutron spectra through 30 cm Al/Teflon filtering assembly using stacked-foil method at an electron current of 6.19 μamps

The histogram plots of Figures 32 - 35 show the integrated broad-group neutron fluxes as a function of energy upstream and downstream for both filter materials. These histograms compare the measured results with the DORT-computed fluxes over the energy broad-groups used in the final direct matrix unfolding. The number of broad-groups was determined by the foil interactions of interest employed in a particular experiment. For the AlF_3 composite filter, three and five broad-groups were applied in the upstream and downstream analyses, respectively. For the Al/Teflon filter, two and four broad-groups were used in the upstream and downstream flux determinations.

The foil activation data obtained and used in the neutron source determined experimentally was intended to confirm the calculational methods employed and to offer experimental support for the photoneutron source concept in neutron capture therapy.

The calculated spectra in all of these figures are normalized to the measured upstream indium foil activation rate, which is, in turn, in known proportion to the electron LINAC beam current and photoneutron production rate, as demonstrated by the unfiltered neutron source experiments described previously. A direct comparison of the measured and calculated downstream neutron fluxes, both normalized to the measured upstream flux, can be made.

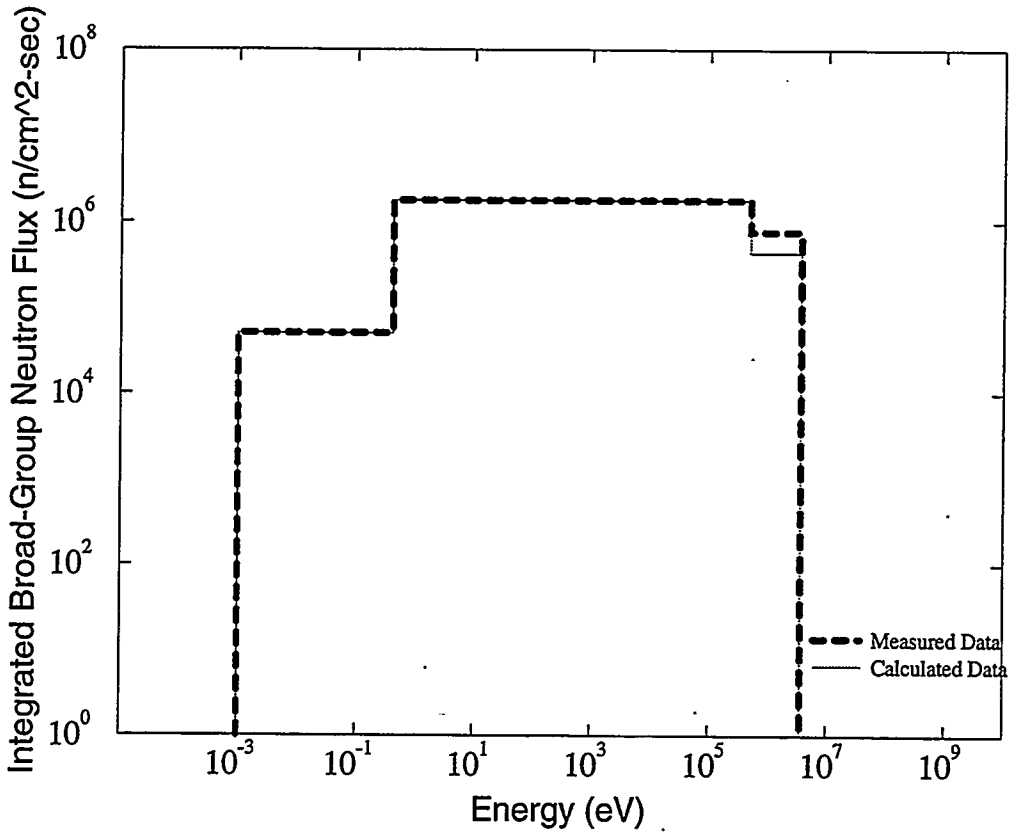

Figure 32: Upstream measured and calculated broad-group neutron fluxes through Al/AlF_3/LiF composite filter at an electron current of 5.99 μamps

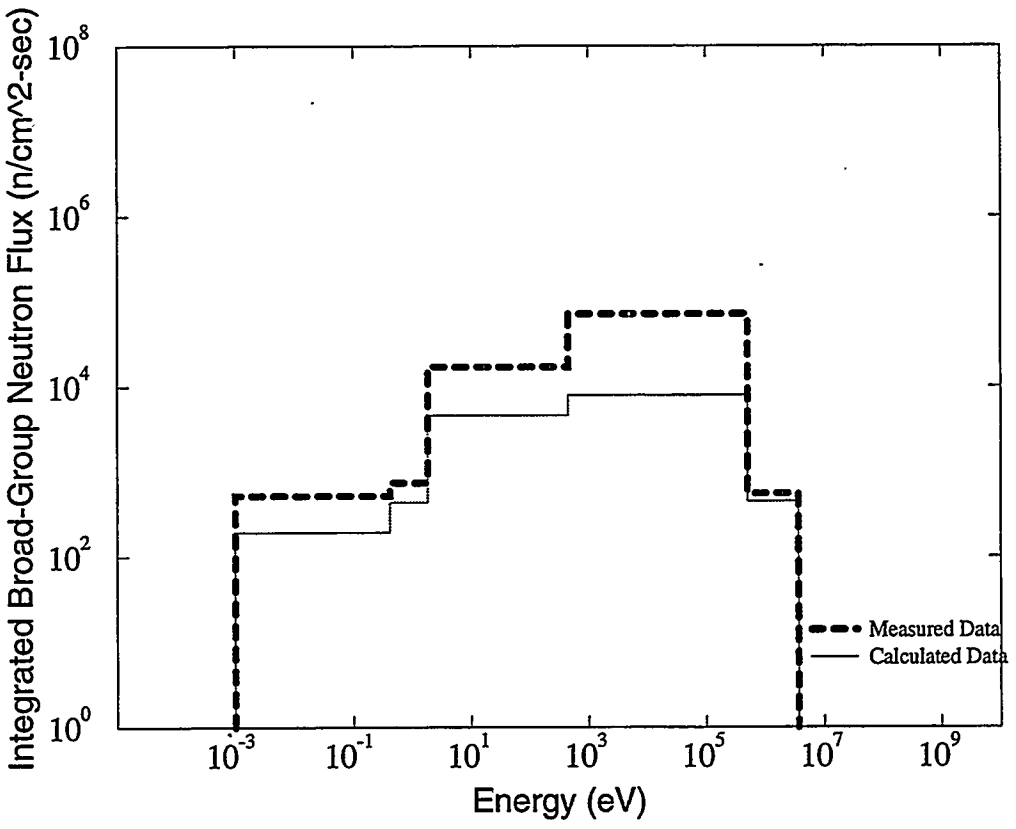

Figure 33: Downstream measured and calculated broad-group neutron fluxes through Al/AlF_3/LiF composite filter at an electron current of 5.99 μamps

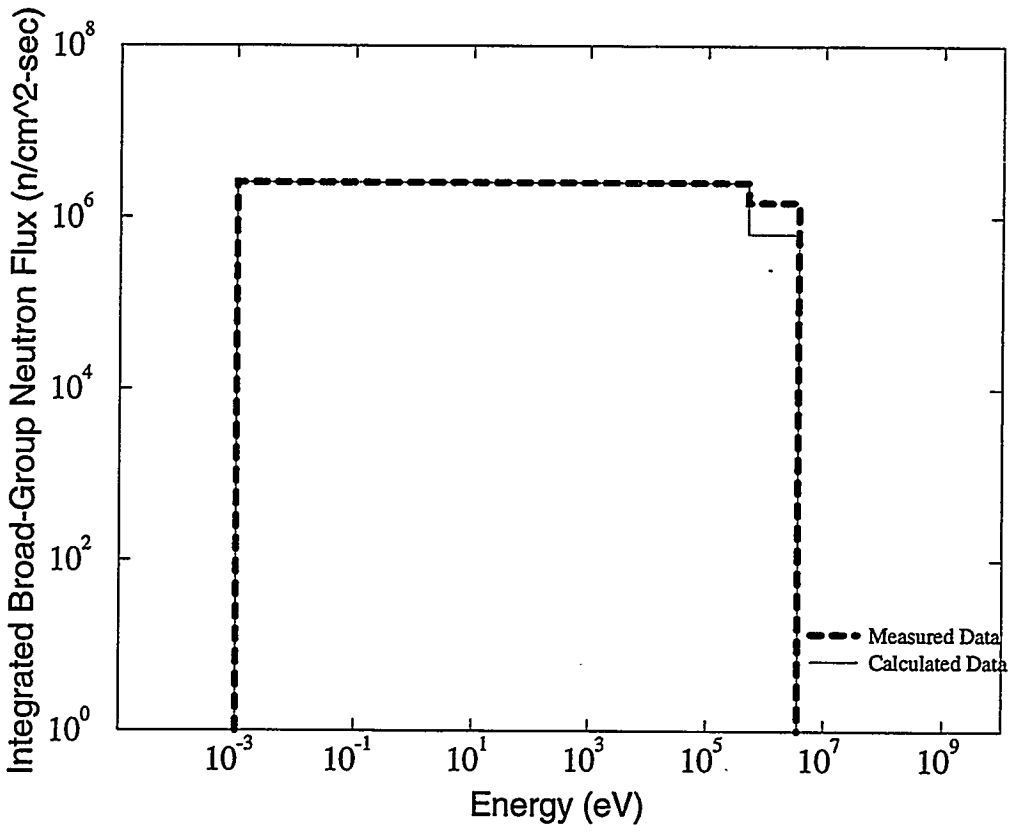

Figure 34: Upstream measured and calculated broad-group neutron fluxes through Al/Teflon filter at an electron current of 6.19 μamps

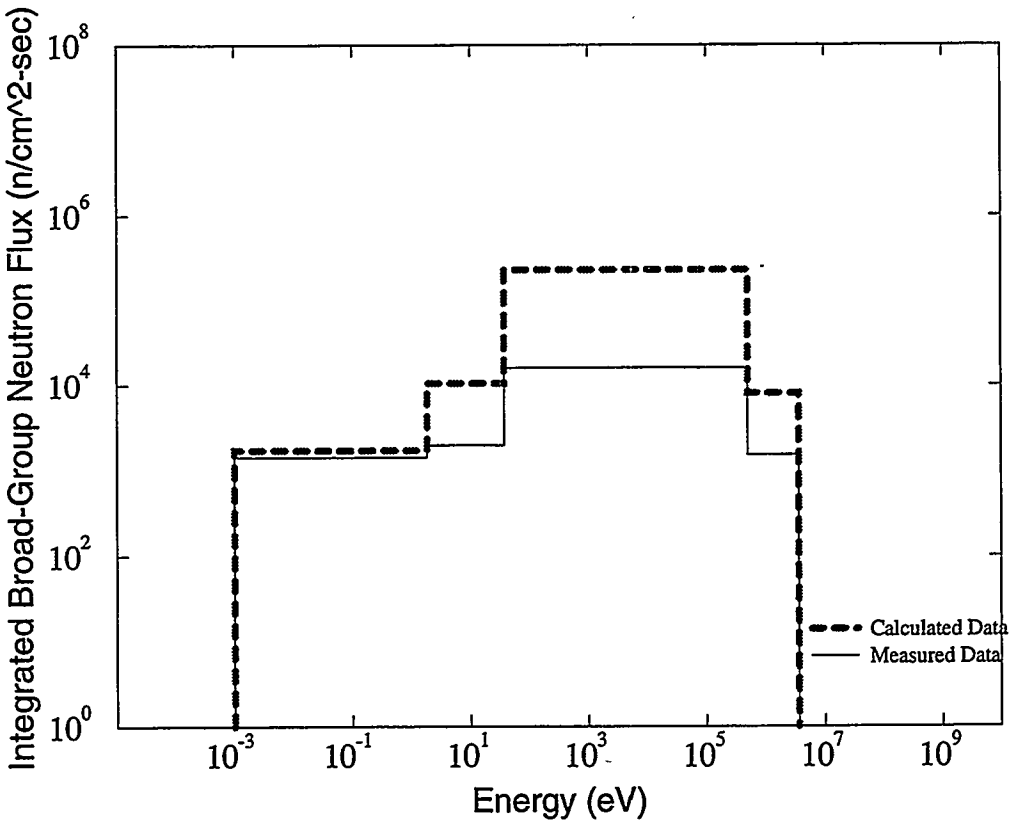

Figure 35: Downstream measured and calculated broad-group neutron fluxes through Al/Teflon filter at an electron current of 6.19 μamps

The results from these experiments not only indicate the feasibility of the photo-neutron process as a possible NCT epithermal source, but demonstrate the effectiveness of both filter/moderator materials, with the AlF_3 material being somewhat more effective in reducing the fast neutron component of the spectrum for a given filter thickness. The uncertainties given for this data are essentially due to experimental uncertainties (i.e.counting) and the fact that, in measuring the fast neutron component, the relative intensity was low, making it often difficult to measure this particular region of the spectrum.

The final model for the results presented in these figures is based on two methods of foil analysis. The 6-MeV data presented for the Aluminum/Teflon material was analyzed using the stacked-foil method, while similar results for the AlF_3 material were completed using the multiple-foil-material method. The results shown for the Aluminum/Teflon material include indium foil as well as copper foil data in the stack. The actual foil interactions of interest used in the final presentation of proof-of-principle data from experiments are shown in Table 7.

Table 7: Activation foil interactions used from experimental data for presentation of final epithermal neutron beam spectrum at 6 MeV

Interaction measured	Energy of maximum cross section	Gamma activation energy (keV) counted
$^{115}In(n,\gamma)^{116}In$	1 eV resonance, thermals	1293, 1097, 416
$^{115}In(n,n')^{115m}In$	430 keV threshold (fast)	336
$^{197}Au(n,\gamma)^{198}Au$	5 eV resonance	411
$^{63}Cu(n,\gamma)^{64}Cu$	1 keV resonance	511 (positron)

Selected data from this third series of experiments is presented for both filter materials at the 6 MeV electron energy in tables in Appendix D. Specifically, the calculated and measured reaction rates for foil reactions of interest for non-stacked foil packets irradiated with a neutron source produced by bremsstrahlung from a 6-MeV electron beam with both filter materials are listed in Appendix D. Stacked foil data results are shown as well for the two filtering/moderating materials tested. Note that these tables include the actual results used in the determination of the final photoneutron spectral results presented in this section.

Data, including the correction factors used, from the fast neutron component detection experiments for the AlF_3 material is given as an example in Table 8. The fast neutron component was estimated with the indium foil inelastic scattering reaction described previously. Once the fast neutron interactions were distinguished from the (γ,γ') reaction, the (γ,γ') portion was subtracted from the measured filter data, yielding the true reaction rate

due solely to neutrons. A correction factor was determined, which was simply the ratio of the activation rate actually due to incident neutrons to the reaction rate before subtraction, including the gamma component. The results listed in Table 8 include the reaction rate data obtained for determining the percentage of the fast neutron component line measured that is actually due to the neutron interaction. For the Al/Teflon filter material, a similar procedure was used, but it was necessary to infer the gamma activation with H_2O in place by using the ion chamber reading since the gamma activation of the foil itself, with H_2O in place was too low to produce a reliable signal.

Table 8: Reaction rate data for $^{115}In(\gamma,\gamma')$ and $^{115}In(n,n')$ determination on Al/AlF_3 filter

In foil reactions	With D_2O target in place (reactions/sec/ μA)	With distilled H_2O in target position (reactions/sec/μA)	fraction of interactions due to actual neutrons
Upstr. $^{115}In(\gamma,\gamma')/$ $^{115}In(n,n')$	$(1.16 \pm 0.16) \times 10^{-19}$	$(9.09 \pm 0.79) \times 10^{-20}$	0.22±0.07
Dwnstr. $^{115}In(\gamma,\gamma')/$ $^{115}In(n,n')$	$(2.33 \pm 0.27) \times 10^{-21}$	$(2.31 \pm 0.08) \times 10^{-21}$	0.009±0.111

In this work, spectral data were also used to derive integral performance data, including epithermal neutron flux and estimated absorbed gamma contaminant doses. The epithermal neutron flux is defined as:

$$\varphi_e = \int_{0.414\,\mathrm{eV}}^{10\,\mathrm{keV}} \varphi_n(E)\,dE \tag{19}$$

while the gamma dose per unit epithermal neutron flux, Dγ, is defined as:

$$D_\gamma = \frac{\int_0^\infty D_\gamma(E)\,\varphi_\gamma(E)\,dE}{\varphi_e} \tag{20}$$

where φ_γ is the gamma flux. Inferred results from experimental work are shown in Table 9. The absorbed gamma dose rates in this table are determined from the total measured neutron flux and the rad/minute measurements at a set distance from the foil positions. The numbers presented for the off-axis measurements are given to indicate more accurate figures for an actual clinical design geometry, which would be designed with the patient position at a right angle to the beam line. The majority of these initial experiments were conducted using the direct-beam-axis geometry.

For the actual design characterized in this work, the gamma doses were determined to be a maximum of 2.0×10^{-10} cGy per unit neutron fluence at the measurement point, above the filter material, and at a right angle off the beam line.

Table 9: Results of experimental beam parameters

Parameter of interest	6 MeV electrons through 30 cm Al/AlF_3	6 MeV electrons through 30 cm Al/Teflon
Epithermal neutron fluence rate, φ_u/mA (n/cm^2-sec)/ mA	$1.6x10^7$	$1.5x10^7$
Epithermal neutron fluence rate, φ_u. (n/cm^2-sec) at 90° off beam axis at electron beam current of 5 μA	$8.7x10^4$	n/a
Absorbed gamma dose per epithermal neutron fluence (cGy-cm^2/neutron)	$2.3x10^{-6}$	$1.7x10^{-6}$
Absorbed gamma dose rate, taken at 90° off beam axis (cGy-cm^2/neutron)	$< 2.0 \times 10^{-10}$	n/a

CHAPTER V

DISCUSSION AND CONCLUSIONS

With the beam characterized and an initial neutron beam proposal established, it is worthwhile to make comparisons with other beam designs in the literature. Although data were obtained at several energies and through two filter materials, the results shown for comparison in Table 10 are selected from data obtained for the nominal 6-MeV electron energy case through the Al/AlF_3 filtering material of thickness 30 centimeters. The parameters presented are standard beam quality parameters, including epithermal neutron fluence rates, neutron current to fluence ratios and absorbed fast neutron and gamma doses. The beams chosen for comparison include both lithium and beryllium target designs as well as two reactor sources, BMRR and GTRR.

It should be noted that the beam parameters presented for comparison are shown for essentially completed designs. The data presented on the photoneutron source concept are for an experiment meant to characterize the photoneutron process for NCT use and are not intended to represent final design parameters. The numbers listed for the BMRR are the most recent measured data (in air and before collimation). Parameters listed for the GTRR beam are calculated results for a filter design performed using accepted codes.

Table 10: Beam qualities for proposed photoneutron source as compared with other neutron sources: a lithium target beam, a beryllium target beam and two reactor sources

Beam quality parameters	6 MeV through Al/AlF_3	Li target design[a]	Be target design[b]	BMRR[c] @ 3MW	GTRR[d] @ 5 MW
Epithermal neutron fluence rate, φ_u/mA, (n/cm^2-sec)	$1.6x10^7$ (/mA)	$1.56x10^7$ (/mA)	$1.67x10^7$ (/mA)	$2.7x10^9$	$4x10^9$
Neutron-current-to-fluence ratio (J/φ)	n/a	0.94	0.94	0.56	0.86
Absorbed fast neutron dose per epithermal neutron fluence (cGy-cm^2/neutron)	n/a	$6.6x10^{-11}$	n/a	$4.3x10^{-11}$	$1.5x10^{-11}$
Absorbed gamma dose per epithermal neutron fluence (cGy-cm^2/neutron)	$2.3x10^{-6}$ (on-axis)	$1.4x10^{-11}$	n/a	$1.0x10^{-11}$	n/a

a. Wang, C.K., Eggers, P.E. and Crawford, H., "Accelerator neutron irradiation facility for hospital-based neutron capture therapy," in Advances in Neutron Capture Therapy, (A.H. Soloway and R.F. Barth, Editors), Plenum Press, New York, NY, 1993.

b. Wang, C.K., "Thick Beryllium Target as an Accelerator-Based Neutron Source for Neutron Capture Therapy," Proceedings of the First International Workshop on Accelerator-Based Neutron Sources for Boron Neutron Capture Therapy, 161, Sept. 1994.

c. Liu, H.B. and Wheeler, F., "An improved neutron collimator for brain tumor irradiations in clinical boron neutron capture therapy," (submitted to *Medical Physics* Jan. 1996).

d. Klee, K., Nigg, D., Wheeler, F. and Karam, R., "Conceptual Design for an Advanced Epithermal Neutron Beam for Boron Neutron Capture Therapy at the Georgia Institute of Technology Research Reactor," ANS Topical Meeting on Advances in Reactor Physics, Knoxville, TN, April 1994.

The GTRR results are calculated in air at the irradiation point, but include collimation effects. For the two accelerator designs indicated in the table, the parameters are also taken from computed data and are quoted with collimators in place for semi-finalized designs. For the photoneutron source, the gamma dose rate given is on the order of 10^{-6} but is for measurements taken directly along the beamline. As experiments performed at 90^{o} off the beamline indicated, the anticipated result in a final design would be far less than the dose seen directly along the beamline. The absorbed dose could then be further reduced by appropriate shielding, a few inches of lead being sufficient to reduce the dose to less than 10^{-11} cGy-cm^2/neutron.

After collimation, the beam quality may often be worsened due to additional induced gamma rays and the fact that fast neutrons may be more forward-directed than the desired epithermal neutrons in some designs. Collimation does, however, improve beam directionality (J_{epi}/φ_{epi}) which has the effect of more than overcoming any loss of spectral quality. For comparison, a totally isotropic beam will have a current to flux ratio of 0.5, while for an ideal parallel beam, the ratio is 1.0. The advantage of better beam directionality is deeper penetration and a higher thermal neutron flux at the tumor site, and a lower surface dose per unit useful thermal flux at depth.

The data for the two moderating materials are presented using two separate calculational methods, stacked-foil and multiple-material-foil irradiations. The results, however, should not be compared directly with the other designs as they are more complete, final design prototypes, while the data from these experiments were intended as initial benchtop experiments. Ultimate comparisons and conclusions can be drawn following further studies on a complete calculational model of a final design which would include multiple incident electron beams, collimators, a treatment room, and a phantom.

The results presented in Table 10 indicate that an accelerator-based photoneutron source would offer competitive neutron production, and could lead to the design of a competitive epithermal neutron source with comparable beam parameters and treatment times. Although gamma contamination and shielding are the major concerns in this design, the fast neutron and gamma doses shown are felt to be within acceptable levels. Additionally, the system yield (10^{-4} neutrons/electron) measured was as expected and comparable with other accelerator-based systems. This yield produces a useful neutron flux at the patient location on the order of 10^{7} per milliampere of current. Further investigations on more advanced geometries are expected to yield superior beam parameters.

It is important to note that the data collected and the results obtained are presented as proof-of-principle experimentation only. The intent was to verify the computational methods with experimental data and to obtain reasonable correlation between actual measured "real" neutron production and the neutron production obtained via accepted

computational tools. Within limitations of foil activation analysis techniques, a correlation was indeed seen, but it is further recommended that additional data be collected using time-of-flight and proton recoil measurements. These initial investigations were intended mainly to offer confirmatory measured data. Various assumptions were made (such as that of a uniform neutron flux across the foil) that may, to some extent, ultimately affect results. Eventually, it is planned to perform experiments on a higher current machine and to obtain data employing these additional techniques. Foil methodologies were deemed adequate for initial investigations. Additional neutron measurement techniques are described briefly in Appendix D.

The design utilizes existing electron accelerator technology to produce a strong photoneutron source which would be convenient for hospital installation, capable of dissipating its waste heat in an efficient manner, and which may circumvent several of the technological difficulties associated with other accelerator-based systems. Throughout this work it has also been assumed possible to scale results obtained from experimentation on a low current (microampere) electron LINAC to the 100 milliampere range necessary for treatment. Although a combination of electron LINACs with the desired current and energy range are obtainable, it is important to note that this linear scaling *is* an assumption and future experimentation on higher current machines is required to verify this presumption. No single presently available commercial electron accelerator has sufficient power to meet the requirements of this photoneutron concept,

several accelerators employed together would produce an acceptable epithermal neutron flux.[94] An additional advantage to electron LINACs is their current acceptability, as low-power machines, in therapeutic environments.

Theoretical computations as well as the initial experimental neutron source intensity and spectral data presented in this work indicate that, with some careful engineering, the proposed photoneutron source device could offer a promising alternate approach to the production of epithermal neutrons for NCT purposes. Clinically-useful neutron source intensity and spectral purity levels appear to be attainable by straightforward scaling using existing electron accelerator technology. Heat transfer studies performed to date[95] indicate that the accelerator target and photoneutron production components of the proposed device can be designed in such a manner that waste heat from the entire process is effectively removed. In addition, measurements indicate that photon contamination of the neutron source at the patient location appears to be controllable to acceptable levels. The data show the feasibility of reconciliation of the conflicting objectives found in accelerator-based systems of target cooling, neutron beam intensity and neutron beam spectral purity. It is felt that any unwanted beam contaminants can be safely lowered to acceptable levels by appropriate shielding. The final design proposes treatment of patients at off-beam-axes to fur-

---

94. Drewell, N.H., Lawrence, C.B., et al., "600 kW Electron Beam Power for Boron Neutron Capture Therapy (BNCT) with IMPELLA," Workshop on Accelerator-Based Neutron Sources for Boron Neutron Capture Therapy, CONF-940976, September, 1994, pp. 67-78.
95. Ibid 80.

ther increase patient safety while still retaining therapeutically-useful epithermal neutron fluxes. The results offer an encouraging solution to a practical clinical device based on the photoneutron concept.

Assuming the success of the current boron neutron capture therapy patient trials and with a possible reduction in the future in the number of reactors available for neutron capture therapy use, accelerators will ultimately become necessary alternatives to NCT reactor-based systems. In offering a new approach to accelerator-based epithermal neutron beam design, this research demonstrates the efficacy of the photoneutron source and fills a direct need in the neutron capture therapy community.

CHAPTER VI

RECOMMENDATIONS

The work presented in this thesis is intended to help fulfill the need for alternate solutions to the production of epithermal neutrons for boron neutron capture therapy. The ultimate intent is to engineer a neutron beam based on multiple electron beams impinging on a tank of heavy water, possibly supplemented with beryllium. Additional work on this project should yield a more in-depth look at this novel neutron production technique, including more prototypical neutron beam characterization studies, dosimetry calculations and treatment time recommendations.

Initial proof-of-principle experimentation was carried out and supplemented with computational models confirming the possibilities of this technology in a neutron-producing capacity. As a follow-up to this preliminary work, it is suggested that several additional aspects of the design be analyzed in further detail in order to thoroughly characterize and optimize photoneutron production as a possible alternate source for boron neutron capture therapy. Listed on the following page are recommendations for supplemental studies of this beam source, some of which are currently under consideration at both the Idaho National Engineering Laboratory and Idaho State University.

Recommendations for Future Studies on the Epithermal Photoneutron Source Concept:

- perform experiments utilizing a higher current accelerator (with less spread in the electron energy of operation), offering neutron beam flux magnitudes more proximate to those required for tumor treatments

- conduct additional experiments on the neutron beam at 90^{o} off the beamline, as this is the actual geometry to be used in the proposed final design (see Figures 2 and 4 of section IIIa.)

- construct and test a design incorporating beryllium rods as potential "spikes" to boost the neutron production, exploiting beryllium's lower neutron production threshold

- carry out complete dosimetry calculations and experimentations on phantom

- fully characterize gamma contamination within the beam and suggest appropriate shielding in patient treatment area

- perform experimentation with extended beam tubes to maximize distance from gamma source

- perform appropriate heat transfer studies to determine flow rate necessary within target to allow acceptable waste heat removal from clinical device

APPENDIX A

SAMPLE ACCEPT CALCULATION FILES

The following pages show sample input files used for Monte Carlo code runs using ACCEPT, along with their corresponding fortran code output from a program written to calculate the photoneutron production within a particular geometry volume.

The ACCEPT example input files given are shown with photoneutron outputs for incident electron energies for the Varitron experiment input at 5.5 MeV (page 140) and 4.0 MeV (page 148). An example of the initial clinical device geometry at an electron energy of 6.0 MeV is given on page 153. Each of these input files is followed by an example output file. Several outputs over particular selected volume regions were possible. A few selected regions are presented in this appendix section. To include all file outputs and input cases run would be too length. For the 5.5 MeV case, two photoneutron source output files are given over a heavy water region (the innermost concentric cylinder region closest to the beam axis) as well as the ionization chamber volume region, as indicated in the geometry diagrams of the procedures section. For the 4 MeV case file and the 6 MeV clinical device case shown, the example source outputs are shown over a heavy water region as well.

A.1 ACCEPT Input for 6 MeV Varitron Model (Monte Carlo Bremsstrahlung Determination within System)

```
TITLE
 Varitron accept model HEM  (exp6a1.inp)
********** GEOMETRY ******************************
GEOMETRY  1
 TRC        0.0     0.0      0.0      0.0      0.0   7.3279
        0.8255   2.8575
 RCC        0.0     0.0   -0.8509      0.0      0.0   0.1778
        0.9525
 RCC        0.0     0.0   -0.6731      0.0      0.0   0.127
        0.9525
 RCC        0.0     0.0      0.0      0.0      0.0   7.3279
         6.604
 RCC        0.0     0.0    -2.54      0.0      0.0    2.54
        2.2225
 RCC        0.0     0.0    -2.54      0.0      0.0    2.54
         6.604
 SPH        0.0     0.0      0.0    115.0
 SPH        0.0     0.0      0.0    116.0
RCC 0 0 7.3279 0 0 .1 6.604
RCC 0 0 7.4279 0 0 10.16 7.302
RCC 0 0 7.7454 0 0 9.525 6.985
RCC 0 0 7.7454 0 0 9.525 5.703
RCC 0 0 7.7454 0 0 9.525 4.03
RCC 0 2.5 100 0 -5 0 0.84
END
 Z1   +2
 Z2   +3
 Z3   +4   -1
 Z4   +6   -5
 Z5   +5   -2   -3
 Z6   +7   -4   -6 -9 -10 -14
 Z7 +9
 Z8 +10 -11
 Z9 +11 -12
 Z10 +12 -13
 Z11 +13
 Z12 +14
```

```
 Z13 +1
 Z14   +8   -7
 END
 0.50677 0.36198 955.9986 308.5993 38.527 4.1874e+4 13.7 241.89 486.66 486.66
486.66 11.08 48.056
* MAT  ECUT  PTCZ
 8
 9
 1
 1
 6
 6
 6
 7
 2
 2
 2
 6
 6
 0
****************** SOURCE *********************************
ELECTRONS
ENERGY 5.5
CUTOFFS 0.01 0.01
DIRECTION  0 0.0
POSITION  0.0 0.0 -0.851
RADIUS  0.2
****************** OUTPUT OPTIONS ***************************
PHOTON-FLUX
 NBINE 7 USER
  3.5 3.0 2.5 2.2 2.0
  1.0 0.01
****************** OTHER OPTIONS ****************************
HISTORIES  5000
BATCHES  5
*      XRAY PRODUCTION SCALING
 SCALE-BREMS 5000.
RANDOM-NUMBER
1326683
```

A.2 Output from Photoneutron and Gamma Production Computations in D_2O on ACCEPT File (6 MeV Case)

INPUT: exp6a1.out OUTPUT: exp6a1d2o1.pp
Max. E (MeV): 5.5000E+00 No. of E groups 7 Tot. Vols: 13
Target Vol.-of-Interest: No.= 11 ID= D CM3= 4.8666E+02 Ethres (g,n) (MeV)= 2.2000E+00 Ethres (g,f) (MeV)= .0000E+00
Number Density (#/cc)= 6.5789E+22
COMPOUND DATA: Density (g/cc) = 1.1000E+00 Mol. wt fraction= 2.0000E-01
Photon flux distribution for target volume 11

3.5000	1.161E+11	1
3.0000	3.196E+11	2
2.5000	4.576E+11	1
2.2000	6.236E+11	1
2.0000	7.740E+11	1
1.0000	1.442E+12	0
.0100	6.161E+12	0

Total gamma fluxe (#/cm2/mA)

Flux
8.5041E+12

Photon Dose (Rads/mA) = 4.20E+03

N production per mA in Volume-of-Interest
Thres. Energy (MeV) = 2.2000E+00 .0000E+00

(MeV)	(g,n)	(g,f)	Neu
3.5000	1.54E+10	.00E+00	.00E+00
3.0000	8.60E+09	.00E+00	.00E+00
2.5000	1.08E+10	.00E+00	.00E+00
2.2000	4.17E+09	.00E+00	.00E+00
2.0000	.00E+00	.00E+00	.00E+00
1.0000	.00E+00	.00E+00	.00E+00
.0100	.00E+00	.00E+00	.00E+00

Total (neutron/mA) = 3.89E+10 .00E+00

Integrated normalized prompt fission spectra = 1.0011E+00

GP	Neutron Energy (ev)	(g,n) Source (n/e)	%	(g,f) Source (n/e)	%	(g,total) Source (n/e)	%
1	1.73330E+07	.00000E+00	.00	.00000E+00		.00	
2	1.41910E+07	.00000E+00	.00	.00000E+00		.00	
3	1.22140E+07	.00000E+00	.00	.00000E+00		.00	
4	1.00000E+07	.00000E+00	.00	.00000E+00		.00	
5	8.60710E+06	.00000E+00	.00	.00000E+00		.00	
6	7.46820E+06	.00000E+00	.00	.00000E+00		.00	
7	6.06530E+06	.00000E+00	.00	.00000E+00		.00	
8	4.96590E+06	.00000E+00	.00	.00000E+00		.00	
9	3.67880E+06	.00000E+00	.00	.00000E+00		.00	
10	3.01190E+06	.00000E+00	.00	.00000E+00		.00	
11	2.72530E+06	.00000E+00	.00	.00000E+00		.00	
12	2.46600E+06	.00000E+00	.00	.00000E+00		.00	
13	2.36530E+06	.00000E+00	.00	.00000E+00		.00	
14	2.34570E+06	.00000E+00	.00	.00000E+00		.00	
15	2.23130E+06	.00000E+00	.00	.00000E+00		.00	
16	1.92050E+06	.00000E+00	.00	.00000E+00		.00	
17	1.65300E+06	.00000E+00	.00	.00000E+00		.00	
18	1.35340E+06	4.42038E+09	11.35	.00000E+00		.00	
19	1.00260E+06	5.42203E+09	13.93	.00000E+00		.00	
20	8.20850E+05	2.80916E+09	7.22	.00000E+00		.00	
21	7.42740E+05	1.20728E+09	3.10	.00000E+00		.00	
22	6.08100E+05	2.80094E+09	7.19	.00000E+00		.00	
23	4.97871E+05	3.81240E+09	9.79	.00000E+00		.00	
24	3.68830E+05	4.71153E+09	12.10	.00000E+00		.00	
25	2.97200E+05	3.10961E+09	7.99	.00000E+00		.00	
26	1.83160E+05	4.95072E+09	12.72	.00000E+00		.00	
27	1.11090E+05	2.56281E+09	6.58	.00000E+00		.00	
28	6.73790E+04	1.22927E+09	3.16	.00000E+00		.00	
29	4.08677E+04	7.45571E+08	1.92	.00000E+00		.00	
30	3.18280E+04	2.54221E+08	.65	.00000E+00		.00	
31	2.60580E+04	1.62268E+08	.42	.00000E+00		.00	
32	2.41760E+04	5.29270E+07	.14	.00000E+00		.00	
33	2.18750E+04	6.47104E+07	.17	.00000E+00		.00	
34	1.50344E+04	1.92376E+08	.49	.00000E+00		.00	
35	7.10174E+03	2.23088E+08	.57	.00000E+00		.00	
36	3.35463E+03	1.05379E+08	.27	.00000E+00		.00	

37	1.58461E+03	4.97778E+07	.13	.00000E+00	.00
38	4.53999E+02	3.17959E+07	.08	.00000E+00	.00
39	2.14454E+02	6.73666E+06	.02	.00000E+00	.00
40	1.01301E+02	3.18217E+06	.01	.00000E+00	.00
41	3.72665E+01	1.80083E+06	.00	.00000E+00	.00
42	1.06770E+01	7.47770E+05	.00	.00000E+00	.00
43	5.04348E+00	1.58430E+05	.00	.00000E+00	.00
44	1.85539E+00	8.96579E+04	.00	.00000E+00	.00
45	8.76430E-01	2.75310E+04	.00	.00000E+00	.00
46	4.13990E-01	1.30051E+04	.00	.00000E+00	.00
47	1.00000E-01	8.83026E+03	.00	.00000E+00	.00

Integrated (g,n) Production (#/e) = 3.8931E+10
Average (g,n) Neutron Energy (ev) = 5.0724E+05

Integrated (g,f) Production (#/e) = .0000E+00
Average (g,f) Neutron Energy (ev)= .0000E+00
Average number of neutrons per photofission (#)= .0000E+00

Integrated Total Neutron Production (#/e) = 3.8980E-06
Average Total Neutron Energy (ev) =

A.3 Output from Photon Dose Computation in Ion Chamber Region on ACCEPT File (6 MeV Case)

INPUT: exp6a1.out OUTPUT: exp6a1ion.pp
Max. E (MeV): 5.5000E+00 No. of E groups 7 Tot. Vols: 13
Target Vol.-of-Interest: No.= 12 ID= U238 CM3= 1.1080E+01 Ethres (g,n) (MeV)= 6.1000E+00 Ethres (g,f) (MeV)= 5.8000E+00
Number Density (#/cc)= 2.3021E+18
COMPOUND DATA: Density (g/cc) = 1.2050E-03 Mol. wt fraction= 7.5500E-01
Photon flux distribution for target volume 12

3.5000	2.990E+09	11
3.0000	1.149E+10	13
2.5000	1.436E+10	16
2.2000	1.573E+10	17
2.0000	1.898E+10	4
1.0000	3.258E+10	3
.0100	5.755E+10	2

Total gamma fluxe (#/cm2/mA)
Flux
1.1698E+11

Photon Dose (Rads/mA) = 7.48E+01

N production per mA in Volume-of-Interest

Thres. Energy (MeV) =	6.1000E+00	5.8000E+00
(MeV)	(g,n)	(g,f) Neu
3.5000	.00E+00	.00E+00 .00E+00
3.0000	.00E+00	.00E+00 .00E+00
2.5000	.00E+00	.00E+00 .00E+00
2.2000	.00E+00	.00E+00 .00E+00
2.0000	.00E+00	.00E+00 .00E+00
1.0000	.00E+00	.00E+00 .00E+00
.0100	.00E+00	.00E+00 .00E+00

Total (neutron/mA) = .00E+00 .00E+00

Integrated normalized prompt fission spectra = 1.0011E+00

GP	Neutron Energy (ev)	(g,n) Source (n/e) %		(g,f) Source (n/e) %		(g,total) Source (n/e) %	
1	1.73330E+07	.00000E+00	.00	.00000E+00	.00		
2	1.41910E+07	.00000E+00	.00	.00000E+00	.00		
3	1.22140E+07	.00000E+00	.00	.00000E+00	.00		
4	1.00000E+07	.00000E+00	.00	.00000E+00	.00		
5	8.60710E+06	.00000E+00	.00	.00000E+00	.00		
6	7.46820E+06	.00000E+00	.00	.00000E+00	.00		
7	6.06530E+06	.00000E+00	.00	.00000E+00	.00		
8	4.96590E+06	.00000E+00	.00	.00000E+00	.00		
9	3.67880E+06	.00000E+00	.00	.00000E+00	.00		
10	3.01190E+06	.00000E+00	.00	.00000E+00	.00		
11	2.72530E+06	.00000E+00	.00	.00000E+00	.00		
12	2.46600E+06	.00000E+00	.00	.00000E+00	.00		
13	2.36530E+06	.00000E+00	.00	.00000E+00	.00		
14	2.34570E+06	.00000E+00	.00	.00000E+00	.00		
15	2.23130E+06	.00000E+00	.00	.00000E+00	.00		
16	1.92050E+06	.00000E+00	.00	.00000E+00	.00		
17	1.65300E+06	.00000E+00	.00	.00000E+00	.00		
18	1.35340E+06	.00000E+00	.00	.00000E+00	.00		
19	1.00260E+06	.00000E+00	.00	.00000E+00	.00		
20	8.20850E+05	.00000E+00	.00	.00000E+00	.00		
21	7.42740E+05	.00000E+00	.00	.00000E+00	.00		
22	6.08100E+05	.00000E+00	.00	.00000E+00	.00		
23	4.97871E+05	.00000E+00	.00	.00000E+00	.00		
24	3.68830E+05	.00000E+00	.00	.00000E+00	.00		
25	2.97200E+05	.00000E+00	.00	.00000E+00	.00		
26	1.83160E+05	.00000E+00	.00	.00000E+00	.00		
27	1.11090E+05	.00000E+00	.00	.00000E+00	.00		
28	6.73790E+04	.00000E+00	.00	.00000E+00	.00		
29	4.08677E+04	.00000E+00	.00	.00000E+00	.00		
30	3.18280E+04	.00000E+00	.00	.00000E+00	.00		
31	2.60580E+04	.00000E+00	.00	.00000E+00	.00		
32	2.41760E+04	.00000E+00	.00	.00000E+00	.00		
33	2.18750E+04	.00000E+00	.00	.00000E+00	.00		
34	1.50344E+04	.00000E+00	.00	.00000E+00	.00		
35	7.10174E+03	.00000E+00	.00	.00000E+00	.00		
36	3.35463E+03	.00000E+00	.00	.00000E+00	.00		

37	1.58461E+03	.00000E+00	.00	.00000E+00	.00
38	4.53999E+02	.00000E+00	.00	.00000E+00	.00
39	2.14454E+02	.00000E+00	.00	.00000E+00	.00
40	1.01301E+02	.00000E+00	.00	.00000E+00	.00
41	3.72665E+01	.00000E+00	.00	.00000E+00	.00
42	1.06770E+01	.00000E+00	.00	.00000E+00	.00
43	5.04348E+00	.00000E+00	.00	.00000E+00	.00
44	1.85539E+00	.00000E+00	.00	.00000E+00	.00
45	8.76430E-01	.00000E+00	.00	.00000E+00	.00
46	4.13990E-01	.00000E+00	.00	.00000E+00	.00
47	1.00000E-01	.00000E+00	.00	.00000E+00	.00

Integrated (g,n) Production (#/e) = .0000E+00
Average (g,n) Neutron Energy (ev) = .0000E+00

Integrated (g,f) Production (#/e) = .0000E+00
Average (g,f) Neutron Energy (ev)= .0000E+00
Average number of neutrons per photofission (#)= .0000E+00

Integrated Total Neutron Production (#/e) = .0000E+00
Average Total Neutron Energy (ev) =

A.4 ACCEPT Input for 4 MeV Varitron Model (Monte Carlo Bremsstrahlung Determination within System)

```
ECHO
TITLE
 4.0 MEV 3-D BNCT-HEM electron-photon run (exp2d5.inp)
****************** GEOMETRY ******************************
GEOMETRY 1
 RCC        0.0     0.0    0.0     0.0     0.0    9.525
          6.985
 RCC        0.0     0.0    -0.3175     0.0     0.0    10.16
          7.302
 RCC 0.0    0.0    -2.318     0.0      0.0     -8.00 8.0
 RCC 0 0 -10.318 0 0 -2.0 6.50
 RCC  0 0 -12.191 0 0 -.127 0.55
 RCC 0 0 -10.318 0 0 -1.873 0.5
 RCC  0 0 -12.318 0 0 -.178 0.2755
 TRC 0 0 -2.318 0 0 -8.00 2.0 0.5
 SPH        0.0     0.0     0.0    100
 SPH        0.0     0.0     0.0    105
 TRC  0 0 -2.318 0 0 2.0 2.0 3.0
 RCC  0 0 -2.318 0 0 2.0 5.5
 RCC 0 0 0 0 0 0 9.525 5.703
 RCC 0 0 0 0 0 0 9.525 4.03
 END
  Z1       +14
  Z2 +13 -14
  Z3 +1 -13 -14
  Z4       +2 -1
  Z5     +3 -8
  Z6 +4 -5 -6
  Z7     +5
  Z8 +6
  Z9  +7
  Z10 +8
  Z11  +9 -1 -2 -3 -4 -5 -6 -7 -8 -12 -11 -13 -14
  Z12 +11
  Z13  +12 -11
  Z14  +10 -9
 END
```

```
486.66 486.66 486.66 241.89 1236.336 212.373 0.1207 0.5755 0.0424 40.069 1.0 55.0
135.0
* MAT  ECUT  PTCZ
2
2
2
8
1
1
9
6
10
6
6
6
6
0
****************** SOURCE **********************************
ELECTRONS
ENERGY 4.0
CUTOFFS 0.1 0.01
DIRECTION 0.0 0.0
POSITION  0.0 0.0 -12.495
RADIUS  .2755
****************** OUTPUT OPTIONS ***************************
PHOTON-FLUX
 NBINE 7 USER
  3.5 3.0 2.5 2.2 2.0 1.0 0.01
***************** OTHER OPTIONS ******************************
HISTORIES  5000
BATCHES  5
*      XRAY PRODUCTION SCALING
 SCALE-BREMS 5000.
 RANDOM-NUMBER
 3430081
```

A.5 Output from Photoneutron and Gamma Production Computation in D_2O on ACCEPT File (4 MeV Case)

INPUT: exp2d5wdet.out OUTPUT: exp2d5wdetd2o3.pp
Max. E (MeV): 4.0000E+00 No. of E groups 7 Tot. Vols: 14
Target Vol.-of-Interest: No.= 3 ID= D CM3= 4.8666E+02 Ethres (g,n) (MeV)= 2.2000E+00 Ethres (g,f) (MeV)= .0000E+00
Number Density (#/cc)= 6.5789E+22
COMPOUND DATA: Density (g/cc) = 1.1000E+00 Mol. wt fraction= 2.0000E-01
Photon flux distribution for target volume 3

3.5000	2.722E+05	99
3.0000	3.258E+07	50
2.5000	1.167E+08	49
2.2000	2.797E+08	27
2.0000	4.744E+08	6
1.0000	2.815E+09	4
.0100	1.230E+11	6

Total gamma fluxe (#/cm2/mA)

Flux
1.2481E+11

Photon Dose (Rads/mA) = 4.26E+01

N production per mA in Volume-of-Interest
Thres. Energy (MeV) = 2.2000E+00 .0000E+00

(MeV)	(g,n)	(g,f)	Neu
3.5000	8.46E+03	.00E+00	.00E+00
3.0000	8.77E+05	.00E+00	.00E+00
2.5000	2.76E+06	.00E+00	.00E+00
2.2000	1.87E+06	.00E+00	.00E+00
2.0000	.00E+00	.00E+00	.00E+00
1.0000	.00E+00	.00E+00	.00E+00
.0100	.00E+00	.00E+00	.00E+00

Total (neutron/mA) = 5.51E+06 .00E+00

Integrated normalized prompt fission spectra = 1.0011E+00

GP	Neutron Energy (ev)	(g,n) Source (n/e) %	(g,f) Source (n/e) %		(g,total) Source (n/e) %	
1	1.73330E+07	.00000E+00	.00	.00000E+00	.00	
2	1.41910E+07	.00000E+00	.00	.00000E+00	.00	
3	1.22140E+07	.00000E+00	.00	.00000E+00	.00	
4	1.00000E+07	.00000E+00	.00	.00000E+00	.00	
5	8.60710E+06	.00000E+00	.00	.00000E+00	.00	
6	7.46820E+06	.00000E+00	.00	.00000E+00	.00	
7	6.06530E+06	.00000E+00	.00	.00000E+00	.00	
8	4.96590E+06	.00000E+00	.00	.00000E+00	.00	
9	3.67880E+06	.00000E+00	.00	.00000E+00	.00	
10	3.01190E+06	.00000E+00	.00	.00000E+00	.00	
11	2.72530E+06	.00000E+00	.00	.00000E+00	.00	
12	2.46600E+06	.00000E+00	.00	.00000E+00	.00	
13	2.36530E+06	.00000E+00	.00	.00000E+00	.00	
14	2.34570E+06	.00000E+00	.00	.00000E+00	.00	
15	2.23130E+06	.00000E+00	.00	.00000E+00	.00	
16	1.92050E+06	.00000E+00	.00	.00000E+00	.00	
17	1.65300E+06	.00000E+00	.00	.00000E+00	.00	
18	1.35340E+06	.00000E+00	.00	.00000E+00	.00	
19	1.00260E+06	.00000E+00	.00	.00000E+00	.00	
20	8.20850E+05	2.50134E+03	.05	.00000E+00	.00	
21	7.42740E+05	2.65829E+03	.05	.00000E+00	.00	
22	6.08100E+05	1.36002E+05	2.47	.00000E+00	.00	
23	4.97871E+05	3.88686E+05	7.05	.00000E+00	.00	
24	3.68830E+05	6.67558E+05	12.12	.00000E+00	.00	
25	2.97200E+05	7.93311E+05	14.40	.00000E+00	.00	
26	1.83160E+05	1.26301E+06	22.92	.00000E+00	.00	
27	1.11090E+05	8.55053E+05	15.52	.00000E+00	.00	
28	6.73790E+04	5.51266E+05	10.01	.00000E+00	.00	
29	4.08677E+04	3.34350E+05	6.07	.00000E+00	.00	
30	3.18280E+04	1.14005E+05	2.07	.00000E+00	.00	
31	2.60580E+04	7.27690E+04	1.32	.00000E+00	.00	
32	2.41760E+04	2.37350E+04	.43	.00000E+00	.00	
33	2.18750E+04	2.90193E+04	.53	.00000E+00	.00	
34	1.50344E+04	8.62709E+04	1.57	.00000E+00	.00	
35	7.10174E+03	1.00044E+05	1.82	.00000E+00	.00	
36	3.35463E+03	4.72571E+04	.86	.00000E+00	.00	

37	1.58461E+03	2.23228E+04	.41	.00000E+00	.00
38	4.53999E+02	1.42588E+04	.26	.00000E+00	.00
39	2.14454E+02	3.02105E+03	.05	.00000E+00	.00
40	1.01301E+02	1.42704E+03	.03	.00000E+00	.00
41	3.72665E+01	8.07578E+02	.01	.00000E+00	.00
42	1.06770E+01	3.35336E+02	.01	.00000E+00	.00
43	5.04348E+00	7.10477E+01	.00	.00000E+00	.00
44	1.85539E+00	4.02069E+01	.00	.00000E+00	.00
45	8.76430E-01	1.23463E+01	.00	.00000E+00	.00
46	4.13990E-01	5.83211E+00	.00	.00000E+00	.00
47	1.00000E-01	3.95992E+00	.00	.00000E+00	.00

Integrated (g,n) Production (#/e) = 5.5098E+06
Average (g,n) Neutron Energy (ev) = 1.7645E+05

Integrated (g,f) Production (#/e) = .0000E+00
Average (g,f) Neutron Energy (ev)= .0000E+00
Average number of neutrons per photofission (#)= .0000E+00

Integrated Total Neutron Production (#/e) = 5.5167E-10
Average Total Neutron Energy (ev) =

A.6 ACCEPT Input for 6 MeV Prototype Design Run (Monte Carlo Bremsstrahlung Determination within System)f

```
ECHO
TITLE
 6 MEV 3-D BNCT-HEM electron-photon run (dbnct6.i1
****************** GEOMETRY ******************************
GEOMETRY 1
 RCC      0.0     0.0    -70.0     0.0     0.0    140.0
         5.0
 RCC      0.0     0.0    -65.0     0.0     0.0    130.0
         25.0
 RCC      0.0     0.0    -60.8     0.0     0.0    121.6
         50.0
 RCC      0.0     0.0    -55.0     0.0     0.0    110.0
         51.0
 RCC      0.0     0.0    -50.0     0.0     0.0    100.0
         52.0
 RCC      0.0     0.0    -20.0     0.0     0.0     40.0
         53.0
 RCC      0.0     0.0    -3.75     0.0     0.0      7.5
         54.0
 RCC      0.0     0.0     -4.0     0.0     0.0      8.0
         25.1
 RCC      0.0     0.0    -65.0     0.0     0.0    130.0
         51.0
 SPH      0.0     0.0     0.0     100.0
 END
  Z1      +2    +6
  Z2      +7    +8    -2
  Z3      +7    +3    -8
  Z4      +6    -7    +3    -2
  Z5      +5    +3    -6
  Z6      +4    +3    -5
  Z7      +3    -4    -1
  Z8      +1    +3    -4
  Z9      +9    -3
 Z10      +10   -9
 END
78539.816 70.92145 53532.5 160810.3 549778.7
```

```
 78539.82 90195.1 911.06 1.0 1.0
* MAT  ECUT  PTCZ
 2
 1
 0
 7
 3
 4
 5
 6
 6
 0
****************** SOURCE *********************************
ELECTRONS
ENERGY  6.0
CUTOFFS 0.01 0.01
DIRECTION 90.0 90.0
POSITION  0.0 -15.2 0.0
RADIUS  1.0
****************** OUTPUT OPTIONS ***************************
PHOTON-FLUX
 NBINE 21 USER
  5.5 5.0 4.5 4.0 3.5 3.0 2.5 2.2 2.0 1.5 1.0 0.8 0.7 0.6 0.4 0.2 0.1 0.06 0.03
  0.02 0.01
****************** OTHER OPTIONS ****************************
HISTORIES  1000
BATCHES  5
*      XRAY PRODUCTION SCALING
 SCALE-BREMS 5000.
RANDOM-NUMBER
 1234567
```

A.7 Output from Photoneutron and Gamma Production Computation in D_2O on ACCEPT File (6 MeV Prototype Case)

INPUT: dbnct6.o1 OUTPUT: dbnct6.r1
Max. E (MeV): 6.0000E+00 No. of E groups 21 Tot. Vols: 9
Target Vol.-of-Interest: No.= 1 ID= D CM3= 7.8540E+04 Ethres (g,n) (MeV)= 2.2000E+00 Ethres (g,f) (MeV)= .0000E+00
Number Density (#/cc)= 6.5789E+22
COMPOUND DATA: Density (g/cc) = 1.1000E+00 Mol. wt fraction= 2.0000E-01
Photon flux distribution for target volume 1

5.5000	1.100E-08	21
5.0000	7.870E-08	9
4.5000	1.740E-07	5
4.0000	3.460E-07	4
3.5000	5.410E-07	1
3.0000	9.150E-07	2
2.5000	1.360E-06	1
2.2000	2.010E-06	4
2.0000	2.400E-06	1
1.5000	3.550E-06	2
1.0000	6.530E-06	1
.8000	1.090E-05	2
.7000	1.440E-05	1
.6000	1.820E-05	1
.4000	2.830E-05	1
.2000	7.600E-05	1
.1000	2.810E-04	1
.0600	8.070E-04	1
.0300	1.270E-03	1
.0200	3.820E-04	1
.0100	8.490E-05	1

Total gamma fluxe (#/cm2/e)
Flux
1.3728E-04

Photon Dose (Rads/electron) = 2.42E-14

N production per incident electron in Volume-of-Interest

Thres. Energy (MeV) = 2.2000E+00 .0000E+00

(MeV)	(g,n)	(g,f)	Neu
5.5000	6.45E-08	.00E+00	.00E+00
5.0000	4.85E-07	.00E+00	.00E+00
4.5000	1.08E-06	.00E+00	.00E+00
4.0000	1.98E-06	.00E+00	.00E+00
3.5000	2.71E-06	.00E+00	.00E+00
3.0000	3.98E-06	.00E+00	.00E+00
2.5000	5.18E-06	.00E+00	.00E+00
2.2000	2.17E-06	.00E+00	.00E+00
2.0000	.00E+00	.00E+00	.00E+00
1.5000	.00E+00	.00E+00	.00E+00
1.0000	.00E+00	.00E+00	.00E+00
.8000	.00E+00	.00E+00	.00E+00
.7000	.00E+00	.00E+00	.00E+00
.6000	.00E+00	.00E+00	.00E+00
.4000	.00E+00	.00E+00	.00E+00
.2000	.00E+00	.00E+00	.00E+00
.1000	.00E+00	.00E+00	.00E+00
.0600	.00E+00	.00E+00	.00E+00
.0300	.00E+00	.00E+00	.00E+00
.0200	.00E+00	.00E+00	.00E+00
.0100	.00E+00	.00E+00	.00E+00

Total (neutron/electron) = 1.77E-05 .00E+00

Integrated normalized prompt fission spectra = 1.0011E+00

GP	Neutron Energy (ev)	(g,n) Source (n/e)	%	(g,f) Source (n/e)	%	(g,total) Source (n/e)	%
1	1.69046E+07	.00000E+00	.00	.00000E+00	.00	.00000E+00	.00
2	1.49182E+07	.00000E+00	.00	.00000E+00	.00	.00000E+00	.00
3	1.34986E+07	.00000E+00	.00	.00000E+00	.00	.00000E+00	.00
4	1.19125E+07	.00000E+00	.00	.00000E+00	.00	.00000E+00	.00
5	1.00000E+07	.00000E+00	.00	.00000E+00	.00	.00000E+00	.00
6	7.78801E+06	.00000E+00	.00	.00000E+00	.00	.00000E+00	.00
7	6.06531E+06	.00000E+00	.00	.00000E+00	.00	.00000E+00	.00
8	4.72367E+06	.00000E+00	.00	.00000E+00	.00	.00000E+00	.00

9	3.67879E+06	.00000E+00	.00	.00000E+00	.00	.00000E+00	.00
10	2.86505E+06	.00000E+00	.00	.00000E+00	.00	.00000E+00	.00
11	2.23130E+06	.00000E+00	.00	.00000E+00	.00	.00000E+00	.00
12	1.73774E+06	3.89026E-08	.22	.00000E+00	.00	3.89026E-08	.22
13	1.35335E+06	6.75530E-07	3.83	.00000E+00	.00	6.75530E-07	3.83
14	1.05399E+06	1.62451E-06	9.20	.00000E+00	.00	1.62451E-06	9.20
15	8.20850E+05	2.07663E-06	11.76	.00000E+00	.00	2.07663E-06	11.76
16	6.39279E+05	2.01502E-06	11.42	.00000E+00	.00	2.01502E-06	11.42
17	4.97871E+05	2.25972E-06	12.80	.00000E+00	.00	2.25972E-06	12.80
18	3.87742E+05	1.80465E-06	10.22	.00000E+00	.00	1.80465E-06	10.22
19	3.01974E+05	1.78607E-06	10.12	.00000E+00	.00	1.78607E-06	10.12
20	2.35177E+05	1.39101E-06	7.88	.00000E+00	.00	1.39101E-06	7.88
21	1.83156E+05	1.08331E-06	6.14	.00000E+00	.00	1.08331E-06	6.14
22	1.42642E+05	8.09850E-07	4.59	.00000E+00	.00	8.09850E-07	4.59
23	1.11090E+05	4.61575E-07	2.61	.00000E+00	.00	4.61575E-07	2.61
24	8.65170E+04	3.59479E-07	2.04	.00000E+00	.00	3.59479E-07	2.04
25	6.73795E+04	2.79963E-07	1.59	.00000E+00	.00	2.79963E-07	1.59
26	5.24752E+04	2.18035E-07	1.24	.00000E+00	.00	2.18035E-07	1.24
27	4.08677E+04	1.69806E-07	.96	.00000E+00	.00	1.69806E-07	.96
28	3.18278E+04	1.32245E-07	.75	.00000E+00	.00	1.32245E-07	.75
29	2.47875E+04	1.02993E-07	.58	.00000E+00	.00	1.02993E-07	.58
30	1.93045E+04	8.02109E-08	.45	.00000E+00	.00	8.02109E-08	.45
31	1.50344E+04	6.24673E-08	.35	.00000E+00	.00	6.24673E-08	.35
32	1.17088E+04	4.86503E-08	.28	.00000E+00	.00	4.86503E-08	.28
33	9.11882E+03	3.78888E-08	.21	.00000E+00	.00	3.78888E-08	.21
34	7.10174E+03	2.95079E-08	.17	.00000E+00	.00	2.95079E-08	.17
35	5.53084E+03	2.29807E-08	.13	.00000E+00	.00	2.29807E-08	.13
36	4.30743E+03	1.78973E-08	.10	.00000E+00	.00	1.78973E-08	.10
37	3.35463E+03	1.39385E-08	.08	.00000E+00	.00	1.39385E-08	.08
38	2.61259E+03	1.08553E-08	.06	.00000E+00	.00	1.08553E-08	.06
39	2.03468E+03	8.45425E-09	.05	.00000E+00	.00	8.45425E-09	.05
40	1.58461E+03	6.58408E-09	.04	.00000E+00	.00	6.58408E-09	.04
41	1.23410E+03	5.12762E-09	.03	.00000E+00	.00	5.12762E-09	.03
42	9.61117E+02	3.99347E-09	.02	.00000E+00	.00	3.99347E-09	.02
43	7.48518E+02	3.11011E-09	.02	.00000E+00	.00	3.11011E-09	.02
44	5.82947E+02	2.42214E-09	.01	.00000E+00	.00	2.42214E-09	.01
45	4.53999E+02	1.88638E-09	.01	.00000E+00	.00	1.88638E-09	.01
46	3.53575E+02	1.46910E-09	.01	.00000E+00	.00	1.46910E-09	.01
47	2.75364E+02	1.14415E-09	.01	.00000E+00	.00	1.14415E-09	.01
48	2.14454E+02	8.91053E-10	.01	.00000E+00	.00	8.91053E-10	.01
49	1.67017E+02	6.93956E-10	.00	.00000E+00	.00	6.93956E-10	.00
50	1.30073E+02	5.40454E-10	.00	.00000E+00	.00	5.40454E-10	.00

51	1.01301E+02	4.20906E-10	.00	.00000E+00	.00	4.20906E-10	.00
52	7.88932E+01	3.27804E-10	.00	.00000E+00	.00	3.27804E-10	.00
53	6.14421E+01	2.55292E-10	.00	.00000E+00	.00	2.55292E-10	.00
54	4.78512E+01	1.98821E-10	.00	.00000E+00	.00	1.98821E-10	.00
55	3.72665E+01	1.54844E-10	.00	.00000E+00	.00	1.54844E-10	.00
56	2.90232E+01	1.20591E-10	.00	.00000E+00	.00	1.20591E-10	.00
57	2.26033E+01	9.39168E-11	.00	.00000E+00	.00	9.39168E-11	.00
58	1.76035E+01	7.31421E-11	.00	.00000E+00	.00	7.31421E-11	.00
59	1.37096E+01	5.69639E-11	.00	.00000E+00	.00	5.69639E-11	.00
60	1.06770E+01	4.43640E-11	.00	.00000E+00	.00	4.43640E-11	.00
61	8.31529E+00	3.45495E-11	.00	.00000E+00	.00	3.45495E-11	.00
62	6.47595E+00	2.69077E-11	.00	.00000E+00	.00	2.69077E-11	.00
63	5.04348E+00	2.09556E-11	.00	.00000E+00	.00	2.09556E-11	.00
64	3.92786E+00	1.63204E-11	.00	.00000E+00	.00	1.63204E-11	.00
65	3.05902E+00	1.27103E-11	.00	.00000E+00	.00	1.27103E-11	.00
66	2.38237E+00	9.89872E-12	.00	.00000E+00	.00	9.89872E-12	.00
67	1.85539E+00	7.70920E-12	.00	.00000E+00	.00	7.70920E-12	.00
68	1.44498E+00	6.00389E-12	.00	.00000E+00	.00	6.00389E-12	.00
69	1.12535E+00	4.67587E-12	.00	.00000E+00	.00	4.67587E-12	.00
70	8.76425E-01	3.64153E-12	.00	.00000E+00	.00	3.64153E-12	.00
71	6.82560E-01	2.83605E-12	.00	.00000E+00	.00	2.83605E-12	.00
72	5.31579E-01	2.20870E-12	.00	.00000E+00	.00	2.20870E-12	.00
73	4.13994E-01	1.72015E-12	.00	.00000E+00	.00	1.72015E-12	.00
74	2.00000E-02	5.76374E-12	.00	.00000E+00	.00	5.76374E-12	.00

Integrated (g,n) Production (#/e) = 1.7652E-05
Average (g,n) Neutron Energy (ev) = 4.4452E+05

Integrated (g,f) Production (#/e) = .0000E+00
Average (g,f) Neutron Energy (ev)= .0000E+00
Average number of neutrons per photofission (#)= .0000E+00

Integrated Total Neutron Production (#/e) = 1.7652E-05
Average Total Neutron Energy (ev) = 4.4452E+05

APPENDIX B

SAMPLE MCNP CALCULATION FILES

The following are sample input files from the MCNP Monte Carlo code. Due to the length and complexity of many of the input, and particularly output, files and the number of varying cases run, a sample of representative, shorter input files are given below which indicate typical types of geometries modelled.

B.1 Sample MCNP Input for Varitron Experiment

```
bnct6.i, 3.5 MeV electron source
  1  1  -1.1       1  +17  -18              $D2O
  2  7   7.31     +4 -5 +3    $Indium
  3  7   7.31     +6 +10 -7
  4  7   7.31     +6 -9 +8
  5  7   7.31     +11 +12 -14
  6  7   7.31     +11 +15 -13
  7  8       +19 -1  +2 -3  $Lucite
  8  8      +2  -17 +19
  9  8     -3  +18 +19
  10 6 -1.205e-3    #1 #2 #3 #4 #5 #6 #7 #8 #9 +16  $air
  11 0           -16  $external void

 1    cz    7.3025
 2    pz   -5.08
 3    pz    5.08
 4    cz   1.27
 5    pz   6.0
 6    cx   1.27
 7    px   -7.62
 8    px   7.62
 9    px   8.54
 10    px   -8.54
 11    cy    1.27
 12 py    7.62
 13 py    -7.62
 14 py    8.54
 15 py    -8.54
 16     so    200.00
 17 pz    -4.7625
 18     pz    4.7625
 19     cz    7.62
mode n p
imp:n  1 9r 0
imp:p  1 9r 0
c    material #1 is D2O
m1     1002.55c -0.2 8016.50c -0.8
mt1   hwtr.01t
```

```
c   material #2 (0.15 D2O + 0.6 Al)
m2    1002.55c 9.8685e-3 8016.50c 4.935e-3 13027.50c 3.6144e-2
mt2   hwtr.01t
c   material #3 is LiAl/AlF3
m3    3006.50c 3.866e-5  3007.55c 4.769e-4
      9019.51c 5.580e-2 13027.50c 2.4624e-2
c   material #4 is Pb/Bi
m4   82000.50c 2.904e-3 83209.51c 2.555e-2
c   material #5 is Lithiated Polyethylene
m5    1001.50c 7.065e-2 3006.50c 6.432e-3
      3007.55c 3.385e-4 6012.50c 2.656e-2
c   material #6 is air
m6    7014.50c -0.755 8016.50c -0.232 18000.35d -0.013
c   material #7 is Indium
m7    49113.50c 1.6491e-3 49115.50c 3.6703e-2
c   material #8 is Lucite
m8    6000.50c .03611 1001.50c .05777 8016.50c .01444
f5:p  0.0 0.0 105.08 0.1
t5    1.0e+10
e5    1.0000e-7 4.1399e-7 8.7642e-7 1.8554e-6 5.0435e-6
      1.0677e-5 3.7267e-5 1.0130e-4 2.1445e-4 4.5400e-4
      1.5846e-3 3.3546e-3 7.1017e-3 1.5034e-2 2.1875e-2
      2.4176e-2 2.6058e-2 3.1828e-2 4.0868e-2 6.7379e-2
      1.1109e-1 1.8316e-1 2.9720e-1 3.6883e-1 4.9787e-1
      6.0810e-1 7.4274e-1 8.2085e-1 1.0026    1.3534
      1.653    1.9205   2.2313   2.3457   2.3653
      2.4660   2.7253   3.0119   3.6788   4.9659
      6.0653   7.4682   8.6071   10.0     12.214
     14.191   17.333
c f15:n  0.0 0.0 -55.1 0.1
c t15    1.0e+10
c e15    1.0000e-7 4.1399e-7 8.7642e-7 1.8554e-6 5.0435e-6
      1.0677e-5 3.7267e-5 1.0130e-4 2.1445e-4 4.5400e-4
      1.5846e-3 3.3546e-3 7.1017e-3 1.5034e-2 2.1875e-2
      2.4176e-2 2.6058e-2 3.1828e-2 4.0868e-2 6.7379e-2
      1.1109e-1 1.8316e-1 2.9720e-1 3.6883e-1 4.9787e-1
      6.0810e-1 7.4274e-1 8.2085e-1 1.0026    1.3534
      1.653    1.9205   2.2313   2.3457   2.3653
      2.4660   2.7253   3.0119   3.6788   4.9659
      6.0653   7.4682   8.6071   10.0     12.214
     14.191   17.333
c f25:p  0.0 0.0 55.1 0.1
```

```
c t25   1.0e+10
c e25   0.02 0.03 0.06 0.1 0.2 0.4 0.6 0.7 0.8 1.0
c       1.5 2.0 3.0 4.0 5.0 6.0 7.0 8.0 10.0 14.0
c f35:p 0.0 0.0 -55.1 0.1
c t35   1.0e+10
c e35   0.02 0.03 0.06 0.1 0.2 0.4 0.6 0.7 0.8 1.0
c       1.5 2.0 3.0 4.0 5.0 6.0 7.0 8.0 10.0 14.0
sdef  cel=1 pos=0. 0. 0. erg=d1 rad=d2 ext=d3
     axs=0.0 0.0 1.0
sp1   0.0       2.21280E-10 2.84127E-10 3.64827E-10 4.68446E-10
     6.01494E-10  7.72344E-10 9.91700E-10 1.27338E-09 1.63503E-09
     2.09944E-09 2.69574E-09  3.46133E-09 4.44450E-09 5.70694E-09
     7.32774E-09 9.40902E-09 1.20813E-08 1.55128E-08 1.99189E-08
     2.55764E-08 3.28407E-08 4.21678E-08 5.41453E-08 6.95239E-08
     8.92702E-08 1.14626E-07 1.47182E-07 1.88985E-07 2.42662E-07
     3.11580E-07 4.49086E-07  5.86439E-07 7.53011E-07 9.66873E-07
     4.70481E-07 5.13411E-072.34330E-08
si1   7.88932E+01 1.01301E+02  1.30073E+02  1.67017E+02 2.14454E+02
     2.75364E+02 3.53575E+02 4.53999E+02 5.82947E+02 7.48518E+02
     9.61117E+02 1.23410E+03 1.58461E+03 2.03468E+03 2.61259E+03
     3.35463E+03 4.30743E+03 5.53084E+03 7.10174E+03 9.11882E+03
     1.17088E+04 1.50344E+04 1.93045E+04 2.47875E+04 3.18278E+04
     4.08677E+04 5.24752E+04  6.73795E+04 8.65170E+04 1.11090E+05
     1.42642E+05 1.83156E+05 2.35177E+05 3.01974E+05 3.87742E+05
     4.97871E+05 6.39279E+05 8.20850E+05
si2  0.0 7.35
si3  4.8
nps   10000000
print
```

B.2 MCNP Input File for Obtaining Reaction Rate Data

```
message:  outp=6f12.o mctal=6f12.m runtpe=6f12.r srctp=6f12.s
xsdir=xsdirc
In-115 foil reaction rates in Varatron irradiation - ENDF/B-V XS
c
1  1 0.09969      -3  11 -12          imp:n=1.0  $ D2O
2  2 0.10825      -4  10 -13 (3:-11:12)  imp:n=1.0  $ lucite
3  3 0.033477   4  -5  10 -13          imp:n=1.0  $ lead
4  6 0.038352     -1  14 -15          imp:n=4.0  $ inner foil
5  4 0.04635      -2  13 -16 (1:-14:15)  imp:n=2.0  $ cadmium
6  0          2  -5  13 -16          imp:n=1.0  $ void
7  5 0.081139     -5  16 -17          imp:n=1.0  $ filter
8  6 0.038352     -1  18 -19          imp:n=16.0  $ outer foil
9  4 0.04635      -2  17 -20 (1:-18:19)  imp:n=4.0  $ cadmium
10 0          2  -6  17 -20          imp:n=2.0  $ void
11 0          6  -5  17 -20          imp:n=1.0  $ void
20 0          5:-10:20             imp:n=0.0

1  cx  1.27
2  cx  1.3208
3  cx  6.985
4  cx  7.3025
5  cx  19.5441
6  cx  5.0
c
10 px  0.0
11 px  0.3175
12 px  9.8425
13 px  10.16
14 px  10.2108
15 px  10.236
16 px  10.2868
17 px  40.2868
18 px  40.3396
19 px  40.3648
20 px  40.4176
mode   n
nps    200000000
prdmp  200000000 20000000 200000000 3
```

```
print
c
sdef  cel=1 rad=d1 ext=d2 pos=0 0 0 axs=1 0 0 erg=d3
si1   0.0  6.985
si2   0.3175 9.8425
si3   0.001e-6  0.1e-6   0.414e-6  0.876e-6  1.86e-6   5.04e-6      1.068e-5  3.73e-
5  1.013e-4  2.145e-4  4.54e-4   1.59e-3      3.36e-3   7.10e-3   1.50e-2   3.18e-2
4.09e-2   6.74e-2      0.111     0.183     0.498     0.821     1.35
sp3   0.0      2.26818e-7 3.34055e-7 7.07174e-7 2.303e-6  4.0695e-6      1.92076e-
5 4.6257e-5  8.17387e-5 1.73041e-4 8.16728e-4 1.27862e-3      2.70681e-3 5.73035e-
3 4.94146e-3 1.37198e-2 1.91511e-2 3.15756e-2      6.58296e-2 0.127167  0.298824
0.175114  0.252817
c
c     Heavy water   conc=0.09969
c
m1     1002.55c 0.06646    8016.50c 0.03323
mt1    hwtr.01t
c
c     Lucite   conc=0.10825
c
m2     1001.50c 0.0577     6012.50c 0.03611     8016.50c 0.01444
mt2    poly.01t
c
c     Lead   conc=0.033477
c
m3     82000.50c 0.033477
c
c     Cadmium   conc=0.04635
c
m4     48000.50c 0.04635
c
c     Filter   conc=0.081139
c
m5      9019.50c 0.04539    13027.50c 0.03505     3006.50c 5.243e-5        3007.55c
6.446e-4
c
c     Foil   conc=0.038352
c
m6     49000.60c 0.038352
c
c     Indium-115 in foil for tally
c
```

```
m12   49115.26y 1.0
c
c    Tally input
c
c      Flux in inner foil
c
f4:n   4
e4     0.1e-6    0.414e-6  0.876e-6  1.86e-6   5.04e-6   1.068e-5      3.73e-5   1.013e-
4  2.145e-4  4.54e-4   1.59e-3   3.36e-3       7.10e-3   1.50e-2   3.18e-2   4.09e-2
6.74e-2   0.111       0.183     0.498     0.821     1.35
c
c      Flux in outer foil
c
f14:n  8
e14      0.1e-6      0.414e-6   0.876e-6   1.86e-6    5.04e-6    1.068e-5        3.73e-5
1.013e-4   2.145e-4   4.54e-4    1.59e-3    3.36e-3        7.10e-3    1.50e-2    3.18e-2
4.09e-2    6.74e-2    0.111       0.183      0.498      0.821      1.35
c
c      Capture reaction rate in inner foil
c
f24:n  4
fm24   1.0  12  102
e24      0.1e-6      0.414e-6   0.876e-6   1.86e-6    5.04e-6    1.068e-5        3.73e-5
1.013e-4   2.145e-4   4.54e-4    1.59e-3    3.36e-3        7.10e-3    1.50e-2    3.18e-2
4.09e-2    6.74e-2    0.111       0.183      0.498      0.821      1.35
c
c      Inelastic reaction rate in inner foil
c
f34:n  4
fm34   1.0  12  51
e34      0.1e-6      0.414e-6   0.876e-6   1.86e-6    5.04e-6    1.068e-5        3.73e-5
1.013e-4   2.145e-4   4.54e-4    1.59e-3    3.36e-3        7.10e-3    1.50e-2    3.18e-2
4.09e-2    6.74e-2    0.111       0.183      0.498      0.821      1.35
c
c      Capture reaction rate in outer foil
c f44:n  8
fm44   1.0  12  102
e44      0.1e-6      0.414e-6   0.876e-6   1.86e-6    5.04e-6    1.068e-5        3.73e-5
1.013e-4   2.145e-4   4.54e-4    1.59e-3    3.36e-3        7.10e-3    1.50e-2    3.18e-2
4.09e-2    6.74e-2    0.111       0.183      0.498      0.821      1.35
c
c      Inelastic reaction rate in outer foil
```

```
c
f54:n  8
fm54   1.0  12  51
e54     0.1e-6     0.414e-6   0.876e-6   1.86e-6    5.04e-6    1.068e-5        3.73e-5
1.013e-4  2.145e-4  4.54e-4    1.59e-3    3.36e-3        7.10e-3    1.50e-2    3.18e-2
4.09e-2   6.74e-2   0.111      0.183      0.498      0.821      1.35
c
c      Surface source generation
c
ssw    17 (9 10)
```

B.3 MCNP Input File for Obtaining Reaction Rate Data

```
message:  outp=6t12.o mctal=6t12.m runtpe=6t12.r srctp=6t12.s
     wssa=6t12.src xsdir=xsdirc
In-115 foil reaction rates in Varatron irradiation - ENDF/B-V XS
c
1   1  0.09969        -3   11  -12            imp:n=1.0  $ D2O
2   2  0.10825        -4   10  -13  (3:-11:12)  imp:n=1.0  $ lucite
3   3  0.033477    4   -5   10  -13            imp:n=1.0  $ lead
4   6  0.038352       -1   14  -15            imp:n=4.0  $ inner foil
5   4  0.04635        -2   13  -16  (1:-14:15)  imp:n=2.0  $ cadmium
6   0            2   -5   13  -16            imp:n=1.0  $ void
7   5  0.0648864      -5   16  -17            imp:n=1.0  $ filter
8   6  0.038352       -1   18  -19            imp:n=16.0  $ outer foil
9   4  0.04635        -2   17  -20  (1:-18:19)  imp:n=4.0  $ cadmium
10  0            2   -6   17  -20            imp:n=2.0  $ void
11  0            6   -5   17  -20            imp:n=1.0  $ void
20  0            5:-10:20                    imp:n=0.0
1   cx   1.27
2   cx   1.3208
3   cx   6.985
4   cx   7.3025
5   cx  17.1965
6   cx   5.0
c
10  px   0.0
11  px   0.3175
12  px   9.8425
13  px  10.16
14  px  10.2108
15  px  10.236
16  px  10.2868
17  px  40.2868
18  px  40.3396
19  px  40.3648
20  px  40.4176
mode   n
nps    200000000
prdmp   200000000 20000000 200000000 3 print
c
```

```
sdef  cel=1 rad=d1 ext=d2 pos=0 0 0 axs=1 0 0 erg=d3
si1   0.0  6.985
si2   0.3175 9.8425
si3   0.001e-6  0.1e-6   0.414e-6  0.876e-6  1.86e-6   5.04e-6      1.068e-5  3.73e-
5  1.013e-4  2.145e-4  4.54e-4   1.59e-3      3.36e-3   7.10e-3   1.50e-2   3.18e-2
4.09e-2   6.74e-2      0.111     0.183     0.498     0.821     1.35
sp3   0.0      2.26818e-7 3.34055e-7 7.07174e-7 2.303e-6  4.0695e-6      1.92076e-
5 4.6257e-5  8.17387e-5 1.73041e-4 8.16728e-4 1.27862e-3      2.70681e-3 5.73035e-
3 4.94146e-3 1.37198e-2 1.91511e-2 3.15756e-2      6.58296e-2 0.127167  0.298824
0.175114  0.252817
c
c     Heavy water   conc=0.09969
c
m1     1002.55c 0.06646   8016.50c 0.03323
mt1    hwtr.01t
c
c     Lucite   conc=0.10825
c
m2     1001.50c 0.0577    6012.50c 0.03611    8016.50c 0.01444
mt2    poly.01t
c
c     Lead   conc=0.033477
c
m3    82000.50c 0.033477
 c
c     Cadmium   conc=0.04635
c
m4    48000.50c 0.04635
c
c     Filter   conc=0.0648864
c
m5     9019.50c 0.024851  13027.50c 0.02761    6012.50c 0.0124254
c
c     Foil   conc=0.038352
c
m6    49000.60c 0.038352
c
c     Indium-115 in foil for tally
c
m12   49115.26y 1.0
c
c    Tally input
```

```
c
c     Flux in inner foil
c
f4:n  4
e4    0.1e-6   0.414e-6  0.876e-6  1.86e-6   5.04e-6   1.068e-5     3.73e-5   1.013e-
4  2.145e-4  4.54e-4   1.59e-3   3.36e-3      7.10e-3   1.50e-2   3.18e-2   4.09e-2
6.74e-2   0.111      0.183     0.498     0.821     1.35
c
c     Flux in outer foil
c
f14:n  8
e14     0.1e-6     0.414e-6   0.876e-6   1.86e-6    5.04e-6    1.068e-5       3.73e-5
1.013e-4   2.145e-4   4.54e-4    1.59e-3    3.36e-3       7.10e-3    1.50e-2    3.18e-2
4.09e-2    6.74e-2    0.111      0.183      0.498      0.821      1.35
c
c     Capture reaction rate in inner foil
c
f24:n  4
fm24   1.0  12  102
e24     0.1e-6     0.414e-6   0.876e-6   1.86e-6    5.04e-6    1.068e-5       3.73e-5
1.013e-4   2.145e-4   4.54e-4    1.59e-3    3.36e-3       7.10e-3    1.50e-2    3.18e-2
4.09e-2    6.74e-2    0.111      0.183      0.498      0.821      1.35
c
c     Inelastic reaction rate in inner foil
c
f34:n  4
fm34   1.0  12  51
e34     0.1e-6     0.414e-6   0.876e-6   1.86e-6    5.04e-6    1.068e-5       3.73e-5
1.013e-4   2.145e-4   4.54e-4    1.59e-3    3.36e-3       7.10e-3    1.50e-2    3.18e-2
4.09e-2    6.74e-2    0.111      0.183      0.498      0.821      1.35
c
c     Capture reaction rate in outer foil
c
f44:n  8
fm44   1.0  12  102
e44     0.1e-6     0.414e-6   0.876e-6   1.86e-6    5.04e-6    1.068e-5       3.73e-5
1.013e-4   2.145e-4   4.54e-4    1.59e-3    3.36e-3       7.10e-3    1.50e-2    3.18e-2
4.09e-2    6.74e-2    0.111      0.183      0.498      0.821      1.35
c
c     Inelastic reaction rate in outer foil
c
f54:n  8
```

```
fm54   1.0  12  51
e54     0.1e-6     0.414e-6   0.876e-6   1.86e-6    5.04e-6    1.068e-5        3.73e-5
1.013e-4   2.145e-4   4.54e-4    1.59e-3    3.36e-3        7.10e-3    1.50e-2    3.18e-2
4.09e-2    6.74e-2    0.111      0.183      0.498      0.821      1.35
c
c      Surface source generation
c
ssw    17 (9 10)
```

APPENDIX C

SAMPLE DORT CALCULATION FILES

The following pages in this Appendix show actual DORT input files used in obtaining data presented in this thesis. Many additional runs were conducted as well but these files are felt representative of all used. The first file in C.1 is a DORT input file used for the Varitron 6 MeV modeling from September 1994, utilizing bremsstrahlung and photoneutron production input files from ACCEPT. The second file (C.2) included is the corresponding input file used in the processing of the necessary cross sections, subsequently used in the DORT run. Each DORT run of a different geometry required separate cross section generation. Because these files are quite lengthy as they are mainly tables of cross section data for the materials used, they are not included.

The last two files are the DORT inputs for 6 MeV runs of Al/AlF_3/LiF and Aluminum/Teflon geometries, respectively (C.3 and C.4). The Aluminium/Teflon DORT input file included here was used for the stacked-foil assembly method.

C.1 DORT Input for 6 MeV Varitron Run Without Filter Materials

```
Electron Accelerator Experiment pnv600d.inp
' Varitron Sept 23.  Nominal 6 MeV.
' Library from pne400g
'
61$$  0  0  8  0 19  0  0  0  0  0
    0  e
62$$   0  3  10 94 112 27  3  6 28  0
     10 20 20  0 48  1  1  0  0  0
      1 99 99  2  0  1  1  0  0  3
      0  0  0  0  0 10  0  0  0  0
      0  0  0 11  0  0  1  1  1  1
      4 100  2  0  5 80  1  0  0  0
      1  2  0  0  0  4 27  0  0  0e
63** 0.0 1.0 0.001 0.001 0.0 0.0 0.0 0.0 0.0 0.0
   1.0 1.0 -1.0 0.3 1.2 3.0-2 1.0-4 0.0 0.3 0.5
   1.0 0.6 0.0 1.0e-30 0.0 0.001 0.1 0.9 e
 t
 t
/ s  8 full symmetric
82*
 0 -30861- 5 0 -21822- 5 0 +21822- 5 0 -61721- 5 0 -57735- 5 0 -21822- 5
 0 +21822- 5 0 +57735- 5 0 -81650- 5 0 -78680- 5 0 -57735- 5 0 -21822- 5
 0 +21822- 5 0 +57735- 5 0 +78680- 5 0 -97590- 5 0 -95119- 5 0 -78680- 5
 0 -57735- 5 0 -21822- 5 0 +21822- 5 0 +57735- 5 0 +78680- 5 0 +95119- 5
 0 -30861- 5 0 -21822- 5 0 +21822- 5 0 -61721- 5 0 -57735- 5 0 -21822- 5
 0 +21822- 5 0 +57735- 5 0 -81650- 5 0 -78680- 5 0 -57735- 5 0 -21822- 5
 0 +21822- 5 0 +57735- 5 0 +78680- 5 0 -97590- 5 0 -95119- 5 0 -78680- 5
 0 -57735- 5 0 -21822- 5 0 +21822- 5 0 +57735- 5 0 +78680- 5 0 +95119- 5
83*
 3r-95119- 5 5r-78680- 5 7r-57735- 5 9r-21822- 5 3r+95119- 5 5r+78680- 5
 7r+57735- 5 9r+21822- 5
81*
 0 +   0+ 0 2r+30247- 6 0 +   0+ 0 0 +22685- 6 2r+22685- 6 0 +22685- 6
 0 +   0+ 0 0 +22685- 6 0 +23148- 6 2r+22685- 6 0 +23148- 6 0 +22685- 6
 0 +   0+ 0 0 +30247- 6 0 +22685- 6 0 +22685- 6 2r+30247- 6 0 +22685- 6
 0 +22685- 6 0 +30247- 6 0 +   0+ 0 2r+30247- 6 0 +   0+ 0 0 +22685- 6
 2r+22685- 6 0 +22685- 6 0 +   0+ 0 0 +22685- 6 0 +23148- 6 2r+22685- 6
 0 +23148- 6 0 +22685- 6 0 +   0+ 0 0 +30247- 6 0 +22685- 6 0 +22685- 6
```

```
 2r+30247- 6 0 +22685- 6 0 +22685- 6 0 +30247- 6
  t
1**  f0.0
2**  1i0.0 21i0.3175 3i3.7592 39i3.81 3i6.35 21i6.4008
     1i9.8425 3i10.16 7i10.2108 3i10.236 10.2868
4**  19i0.0 3i1.27 24i1.3208 14i4.0328 11i5.7032 1i6.9850 3i7.3025
     7i7.3533 3i7.3785 7.4293
9$$  1 5 5 5 9 13 17 9 13 17
31$$ 1 2 3 4 5 6 7 8 9 10
32** 0.0    0.0    0.0    0.0    0.0    0.0    0.0
     7.3025  7.3025  7.3533
33** 7.3025  6.9850  5.7032  4.0328  7.3025  1.3208  1.27
     7.4293  7.4293  7.3785
34** 0.0    0.3175  0.3175  0.3175  10.16   10.16   10.2108
     0.0    3.7592  3.81
35** 10.16   9.8425  9.8425  9.8425  10.2868  10.28666 10.236
     10.2868  6.4008  6.35
  t
96** 49r0.8135 15r0.1637 12r0.0228 f0.0
  t
97** 2r0.0 92r1.0 f0.0
  t
98**
 .00000e+00
 .00000e+00
 .00000e+00
 .00000e+00
 .00000e+00
9.84241e+09
6.81738e+09
1.16335e+10
4.95072e+09
2.56281e+09
1.22927e+09
7.45571e+08
5.34126e+08
1.92376e+08
2.23088e+08
1.05379e+08
4.97778e+07
3.17959e+07
6.73666e+06
```

3.18217e+06
1.80083e+06
7.47770e+05
1.58430e+05
8.96579e+04
2.75310e+04
1.30051e+04
8.83026e+03
t

C.2 GIP Input File for Processing Cross Sections

```
Gip Input For Electron Accelerator Experiment pne400g.inp
'
1$$ 27 3 6 28 36 100 0 120 0 3 0 2 2 60 e t
'
' COMBINE-6 Micros:
'
' 1  Hydrogen free atom
' 5  Deuterium in D2O
' 9  Carbon-12 free atom
' 13 Oxygen free gas
' 17 Natural Cadmium
' 21 Indium-113 at 300K
' 25 Indium-115 at 300K
' 29 Reserved
'
' Macros at 101
'
10$$  101 102 103 104 2q4      /Lucite

    105 106 107 108 1q4      /D2O

    109 110 111 112          /Void

    113 114 115 116          /Cadmium

    117 118 119 120 1q4 e    /Indium

11$$   1 2 3 4          /H
       9 10 11 12       /C
       13 14 15 16      /O

       5 6 7 8          /D
       13 14 15 16      /O

       1 2 3 4          /H

       17 18 19 20      /Cd
```

```
    21 22 23 24       /I113
    25 26 27 28 e     /I115

12**  0.05777 .1731 .2885 .4039     /H
    0.03611 .1083 .1806 .2528     /C
    0.01444 .0433 .0722 .1011     /O

    0.06646 .1994 .3323 .4652     /D
    0.03323 .0997 .1662 .2326     /O

    0.0    .0   .0   .0       /H

    0.04635 .1391 .2318 .3245     /Cd

    0.001649 .00495 .00825 .0115     /I113
    0.036703 .11011 .18352 .2569 e t /I115
'
'
' Materials from COMBINE
'
14**   +2.95399e-05    +.00000e+00    +6.68197e-01  2r+0.00000e+00
     +1.92332e-01 22r+0.00000e+00    +3.36331e-05    +.00000e+00
     +1.18868e+00  2r+0.00000e+00    +2.11116e-01    +1.82336e-01
    21r+0.00000e+00    +3.69201e-05    +.00000e+00    +1.70407e+00
     2r+0.00000e+00    +3.37566e-01    +3.78172e-01    +1.12789e-01
    20r+0.00000e+00    +3.33384e-05    +.00000e+00    +2.37007e+00
     2r+0.00000e+00    +4.68919e-01    +5.32284e-01    +2.32527e-01
     +6.98137e-02 19r+0.00000e+00    +3.50240e-05    +.00000e+00
     +3.14508e+00  2r+0.00000e+00    +6.63340e-01    +7.43768e-01
     +3.25647e-01    +1.42879e-01    +4.30720e-02 18r+0.00000e+00
     +3.19472e-05    +.00000e+00    +4.14555e+00  2r+0.00000e+00
     +8.56206e-01    +9.73282e-01    +4.53528e-01    +1.99027e-01
     +8.75326e-02    +2.64604e-02 17r+0.00000e+00    +3.95134e-05
      +.00000e+00    +5.39751e+00  2r+0.00000e+00    +1.12638e+00
     +1.29160e+00    +5.92171e-01    +2.76169e-01    +1.21356e-01
     +5.34469e-02    +1.61864e-02 16r+0.00000e+00    +5.33028e-05
      +.00000e+00    +8.12338e+00  2r+0.00000e+00    +2.63663e+00
     +2.69763e+00    +1.26175e+00    +5.78650e-01    +2.70031e-01
     +1.18774e-01    +5.23632e-02    +1.58819e-02 15r+0.00000e+00
     +5.94109e-05    +.00000e+00    +1.11809e+01  2r+0.00000e+00
     +2.29214e+00    +2.15774e+00    +6.18812e-01    +2.89439e-01
     +1.32764e-01    +6.19787e-02    +2.72772e-02    +1.20330e-02
```

+3.65309e-03 14r+0.00000e+00 +9.97547e-05 +.00000e+00
+1.33944e+01 2r+0.00000e+00 +2.77133e+00 +3.49624e+00
+1.30942e+00 +3.75512e-01 +1.75641e-01 +8.05701e-02
+3.76172e-02 +1.65584e-02 +7.30591e-03 +2.21864e-03
13r+0.00000e+00 +1.66451e-04 +.00000e+00 +1.53763e+01
2r+0.00000e+00 +3.20864e+00 +4.17881e+00 +2.12127e+00
+7.94449e-01 +2.27824e-01 +1.06563e-01 +4.88842e-02
+2.28250e-02 +1.00482e-02 +4.43397e-03 +1.34674e-03
12r+0.00000e+00 +2.01762e-04 +.00000e+00 +1.66289e+01
2r+0.00000e+00 +1.90150e+00 +2.69098e+00 +1.42521e+00
+7.23468e-01 +2.70947e-01 +7.76989e-02 +3.63430e-02
+1.66722e-02 +7.78483e-03 +3.42729e-03 +1.51244e-03
+4.59419e-04 11r+0.00000e+00 +2.96215e-04 +.00000e+00
+1.78747e+01 2r+0.00000e+00 +5.22644e+00 +7.77013e+00
+4.99987e+00 +2.64804e+00 +1.34420e+00 +5.03415e-01
+1.44362e-01 +6.75244e-02 +3.09768e-02 +1.44646e-02
+6.36830e-03 +2.81042e-03 +8.53745e-04 10r+0.00000e+00
+4.61645e-04 +.00000e+00 +1.91150e+01 2r+0.00000e+00
+5.62400e+00 +6.67311e+00 +3.67056e+00 +2.36190e+00
+1.25091e+00 +6.34987e-01 +2.37807e-01 +6.81944e-02
+3.18976e-02 +1.46332e-02 +6.83311e-03 +3.00852e-03
+1.32775e-03 +4.03369e-04 9r+0.00000e+00 +7.41258e-04
+.00000e+00 +1.97895e+01 2r+0.00000e+00 +5.84931e+00
+7.11797e+00 +3.15248e+00 +1.73403e+00 +1.11580e+00
+5.90949e-01 +2.99976e-01 +1.12343e-01 +3.22158e-02
+1.50688e-02 +6.91293e-03 +3.22810e-03 +1.42131e-03
+6.27277e-04 +1.90571e-04 8r+0.00000e+00 +1.13954e-03
+.00000e+00 +2.00756e+01 2r+0.00000e+00 +5.94053e+00
+7.35486e+00 +3.36238e+00 +1.48917e+00 +8.19124e-01
+5.27081e-01 +2.79152e-01 +1.41702e-01 +5.30685e-02
+1.52180e-02 +7.11816e-03 +3.26553e-03 +1.52489e-03
+6.71408e-04 +2.96319e-04 +9.00259e-05 7r+0.00000e+00
+1.83192e-03 +.00000e+00 +2.03314e+01 2r+0.00000e+00
+8.71590e+00 +1.00844e+01 +4.69805e+00 +2.14778e+00
+9.51233e-01 +5.23229e-01 +3.36682e-01 +1.78313e-01
+9.05147e-02 +3.38983e-02 +9.72075e-03 +4.54684e-03
+2.08591e-03 +9.74056e-04 +4.28872e-04 +1.89281e-04
+5.75067e-05 6r+0.00000e+00 +3.01563e-03 +.00000e+00
+2.04077e+01 2r+0.00000e+00 +6.04837e+00 +6.12785e+00
+2.13669e+00 +9.95423e-01 +4.55073e-01 +2.01547e-01
+1.10862e-01 +7.13364e-02 +3.77810e-02 +1.91783e-02
+7.18239e-03 +2.05963e-03 +9.63387e-04 +4.41961e-04

+2.06382e-04 +9.08718e-05 +4.01054e-05 +1.21839e-05
5r+0.00000e+00 +4.36153e-03 +.00000e+00 +2.04481e+01
2r+0.00000e+00 +6.05989e+00 +7.57479e+00 +2.89445e+00
+1.00925e+00 +4.70182e-01 +2.14951e-01 +9.51999e-02
+5.23651e-02 +3.36953e-02 +1.78457e-02 +9.05876e-03
+3.39255e-03 +9.72857e-04 +4.55048e-04 +2.08760e-04
+9.74848e-05 +4.29219e-05 +1.89437e-05 +5.75550e-06
4r+0.00000e+00 +6.83460e-03 +.00000e+00 +2.04716e+01
2r+0.00000e+00 +7.52899e+00 +9.09224e+00 +4.28667e+00
+1.63801e+00 +5.71149e-01 +2.66082e-01 +1.21644e-01
+5.38749e-02 +2.96340e-02 +1.90687e-02 +1.00991e-02
+5.12647e-03 +1.91990e-03 +5.50552e-04 +2.57519e-04
+1.18138e-04 +5.51672e-05 +2.42908e-05 +1.07199e-05
+4.38973e-06 3r+0.00000e+00 +1.20303e-02 +.00000e+00
+2.04788e+01 2r+0.00000e+00 +8.78529e+00 +9.22970e+00
+3.77560e+00 +1.78006e+00 +6.80191e-01 +2.37173e-01
+1.10492e-01 +5.05131e-02 +2.23718e-02 +1.23057e-02
+7.91834e-03 +4.19370e-03 +2.12879e-03 +7.97243e-04
+2.28620e-04 +1.06935e-04 +4.90598e-05 +2.29087e-05
+1.28864e-05 +6.02566e-06 +6.38292e-07 2r+0.00000e+00
+1.95977e-02 +.00000e+00 +2.04880e+01 2r+0.00000e+00
+6.06895e+00 +6.16347e+00 +1.95546e+00 +7.99918e-01
+3.77133e-01 +1.44109e-01 +5.02487e-02 +2.34094e-02
+1.07020e-02 +4.73981e-03 +2.60717e-03 +1.67762e-03
+8.88498e-04 +4.51023e-04 +1.68912e-04 +4.84372e-05
+2.26570e-05 +1.27240e-05 +8.78543e-06 +9.48712e-07
3r+0.00000e+00 +3.05522e-02 +.00000e+00 +2.05004e+01
2r+0.00000e+00 +7.53106e+00 +9.10220e+00 +3.48802e+00
+1.10663e+00 +4.52688e-01 +2.13426e-01 +8.15540e-02
+2.84366e-02 +1.32478e-02 +6.05645e-03 +2.68235e-03
+1.47542e-03 +9.49402e-04 +5.02822e-04 +2.55234e-04
+9.55880e-05 +3.12766e-05 +1.95643e-05 +6.42808e-06
4r+0.00000e+00 +4.70872e-02 +.00000e+00 +2.05185e+01
+1.15253e-10 +.00000e+00 +6.06997e+00 +6.82702e+00
+2.79504e+00 +1.07108e+00 +3.39816e-01 +1.39008e-01
+6.55375e-02 +2.50430e-02 +8.73213e-03 +4.06806e-03
+1.85979e-03 +8.23669e-04 +4.53068e-04 +2.91523e-04
+1.54407e-04 +7.83820e-05 +3.44941e-05 +1.11556e-05
5r+0.00000e+00 +6.84951e-02 +.00000e+00 +2.05408e+01
+1.00139e-05 +1.11121e-03 +6.07027e+00 +7.59869e+00
+3.22481e+00 +1.32026e+00 +5.05933e-01 +1.60515e-01
+6.56619e-02 +3.09573e-02 +1.18293e-02 +4.12470e-03

+1.92157e-03 +8.78461e-04 +3.89075e-04 +2.14003e-04
+1.37707e-04 +7.29308e-05 +4.46917e-05 +1.97326e-05
5r+0.00000e+00 +1.48150e-01 +.00000e+00 +2.26927e+01
+.00000e+00 +1.57982e+00 +8.39202e+00 +1.09365e+01
+5.16579e+00 +2.19230e+00 +8.97547e-01 +3.43944e-01
+1.09120e-01 +4.46360e-02 +2.10429e-02 +8.03920e-03
+2.80145e-03 +1.30594e-03 +5.97867e-04 +2.65222e-04
+1.46399e-04 +9.45605e-05 +5.03504e-05 +1.94609e-05
5r+0.00000e+00 +3.08010e-01 +.00000e+00 +2.98959e+01
2r+0.00000e+00 +2.80081e+01 +1.41514e+01 +3.46555e+00
+1.63693e+00 +6.94695e-01 +2.84414e-01 +1.08989e-01
+3.45777e-02 +1.41442e-02 +6.66804e-03 +2.54746e-03
+8.87722e-04 +4.10950e-04 +1.85312e-04 +8.00105e-05
+4.23281e-05 +2.60783e-05 +1.26360e-05 +4.08413e-06
4r+0.00000e+00
14** 5r+0.00000e+00 +1.69223e-01 27r+0.00000e+00 +2.00379e-01
+1.46122e-01 26r+0.00000e+00 +3.23489e-01 +3.04772e-01
+7.04046e-02 25r+0.00000e+00 +4.48075e-01 +4.19570e-01
+1.45985e-01 +3.39601e-02 24r+0.00000e+00 +6.42187e-01
+5.88885e-01 +1.99995e-01 +6.99093e-02 +1.63363e-02
23r+0.00000e+00 +8.66871e-01 +7.55538e-01 +2.79777e-01
+9.52653e-02 +3.33941e-02 +7.83165e-03 22r+0.00000e+00
+1.05436e+00 +9.75785e-01 +3.58166e-01 +1.32775e-01
+4.52920e-02 +1.59097e-02 +3.74364e-03 21r+0.00000e+00
+2.19839e+00 +1.97069e+00 +6.80802e-01 +2.50066e-01
+9.28194e-02 +3.17287e-02 +1.11758e-02 +2.64370e-03
20r+0.00000e+00 +2.10717e+00 +1.76116e+00 +2.99495e-01
+1.03538e-01 +3.80779e-02 +1.41628e-02 +4.85807e-03
+1.71961e-03 +4.11112e-04 19r+0.00000e+00 +2.56299e+00
+2.82583e+00 +8.32744e-01 +1.41704e-01 +4.90274e-02
+1.80538e-02 +6.72871e-03 +2.31602e-03 +8.23991e-04
+1.99202e-04 18r+0.00000e+00 +2.97868e+00 +3.36109e+00
+1.33583e+00 +3.93786e-01 +6.70828e-02 +2.32399e-02
+8.57536e-03 +3.20633e-03 +1.10961e-03 +3.97934e-04
+9.78753e-05 17r+0.00000e+00 +1.82812e+00 +2.27410e+00
+9.41473e-01 +3.74251e-01 +1.10370e-01 +1.88274e-02
+6.53280e-03 +2.41642e-03 +9.06928e-04 +3.15855e-04
+1.14326e-04 +2.86734e-05 16r+0.00000e+00 +4.70471e+00
+6.25317e+00 +3.37714e+00 +1.39843e+00 +5.56098e-01
+1.64123e-01 +2.80651e-02 +9.76549e-03 +3.62772e-03
+1.37061e-03 +4.82600e-04 +1.77438e-04 +4.59429e-05
15r+0.00000e+00 +5.05729e+00 +4.87183e+00 +2.03169e+00

+1.09759e+00 +4.54799e-01 +1.81049e-01 +5.35563e-02
+9.22563e-03 +3.23698e-03 +1.21768e-03 +4.68870e-04
+1.70170e-04 +6.52031e-05 +1.82394e-05 14r+0.00000e+00
+5.25767e+00 +5.19276e+00 +1.58323e+00 +6.60679e-01
+3.57153e-01 +1.48198e-01 +5.91299e-02 +1.75755e-02
+3.07373e-03 +1.09669e-03 +4.22771e-04 +1.68641e-04
+6.45161e-05 +2.63879e-05 +8.20524e-06 13r+0.00000e+00
+5.33901e+00 +5.36115e+00 +1.68739e+00 +5.14982e-01
+2.15192e-01 +1.16489e-01 +4.84781e-02 +1.94346e-02
+5.83424e-03 +1.05173e-03 +3.87456e-04 +1.56095e-04
+6.60254e-05 +2.73126e-05 +1.21526e-05 +4.23299e-06
12r+0.00000e+00 +7.42645e+00 +6.81444e+00 +2.18463e+00
+6.88524e-01 +2.10726e-01 +8.83937e-02 +4.80350e-02
+2.01547e-02 +8.18649e-03 +2.52381e-03 +4.90728e-04
+1.94264e-04 +8.54666e-05 +4.00010e-05 +1.85297e-05
+9.12122e-06 +3.54987e-06 11r+0.00000e+00 +5.43633e+00
+4.14067e+00 +8.35161e-01 +2.68293e-01 +8.49207e-02
+2.62237e-02 +1.11336e-02 +6.12276e-03 +2.63320e-03
+1.11081e-03 +3.67758e-04 +8.48111e-05 +3.82238e-05
+1.91283e-05 +1.00841e-05 +5.19803e-06 +2.76652e-06
+1.15658e-06 10r+0.00000e+00 +5.44673e+00 +5.51788e+00
+1.34563e+00 +2.71967e-01 +8.76693e-02 +2.79483e-02
+8.75764e-03 +3.79018e-03 +2.12304e-03 +9.46884e-04
+4.20650e-04 +1.51794e-04 +4.11397e-05 +2.03486e-05
+1.09724e-05 +6.12396e-06 +3.29710e-06 +1.80445e-06
+7.71740e-07 9r+0.00000e+00 +6.57839e+00 +6.36000e+00
+2.06288e+00 +5.03866e-01 +1.02355e-01 +3.32735e-02
+1.07914e-02 +3.49828e-03 +1.57920e-03 +9.18927e-04
+4.39340e-04 +2.13005e-04 +8.68654e-05 +2.80342e-05
+1.49923e-05 +8.53236e-06 +4.94088e-06 +2.72907e-06
+1.51690e-06 +1.07833e-06 8r+0.00000e+00 +7.48531e+00
+5.98590e+00 +1.54927e+00 +5.03462e-01 +1.23635e-01
+2.55452e-02 +8.53496e-03 +2.91895e-03 +1.04033e-03
+5.20400e-04 +3.28462e-04 +1.78236e-04 +9.83672e-05
+4.62581e-05 +1.73705e-05 +9.80225e-06 +5.76624e-06
+3.40973e-06 +3.13247e-06 +1.86065e-06 +3.21375e-07
7r+0.00000e+00 +5.45484e+00 +4.16262e+00 +7.33692e-01
+1.90461e-01 +6.22358e-02 +1.55210e-02 +3.36037e-03
+1.20369e-03 +4.63155e-04 +1.95526e-04 +1.12756e-04
+7.79810e-05 +4.75074e-05 +2.87984e-05 +1.47079e-05
+5.92117e-06 +3.41394e-06 +3.10401e-06 +3.01945e-06
+3.43790e-07 8r+0.00000e+00 +6.58023e+00 +6.36654e+00

+1.55653e+00 +2.75106e-01 +7.18358e-02 +2.37270e-02
+6.09225e-03 +1.43027e-03 +5.68327e-04 +2.51912e-04
+1.23816e-04 +7.86388e-05 +5.72482e-05 +3.68675e-05
+2.32276e-05 +1.22200e-05 +6.67233e-06 +5.95267e-06
+2.25196e-06 7r+0.00000e+00 +8.25162e-11 +.00000e+00
+5.45574e+00 +4.77510e+00 +1.23654e+00 +3.02908e-01
+5.39203e-02 +1.42920e-02 +4.84786e-03 +1.33168e-03
+3.66316e-04 +1.70474e-04 +8.88904e-05 +4.97697e-05
+3.37750e-05 +2.53649e-05 +1.68432e-05 +1.08244e-05
+7.60763e-06 +4.13594e-06 8r+0.00000e+00 +2.26680e-06
+1.03146e-03 +5.45603e+00 +5.53487e+00 +1.55173e+00
+4.02412e-01 +9.89348e-02 +1.78432e-02 +4.85701e-03
+1.72280e-03 +5.23321e-04 +1.72857e-04 +9.18923e-05
+5.31432e-05 +3.17858e-05 +2.21985e-05 +1.68784e-05
+1.13449e-05 +1.04453e-05 +7.81376e-06 9r+0.00000e+00
+7.33060e-01 +6.16816e+00 +7.23738e+00 +2.35874e+00
+6.65062e-01 +1.74997e-01 +4.46558e-02 +9.29426e-03
+3.75397e-03 -6.32230e-05 +1.35824e-04 +1.11673e-04
+7.56182e-05 +5.05926e-05 +3.28835e-05 +2.40485e-05
+1.87873e-05 +1.29540e-05 +6.38207e-06 10r+0.00000e+00
+1.02507e+01 +5.75320e+00 +9.67476e-01 +3.12878e-01
+8.64970e-02 +2.15616e-02 +4.68764e-03 +2.61662e-04
-7.96518e-04 +1.31700e-03 +3.74993e-04 +1.24451e-04
+7.16843e-05 +4.26877e-05 +2.49650e-05 +1.63935e-05
+1.15810e-05 +6.77510e-06 +2.56857e-06 4r+0.00000e+00
14** 5r+0.00000e+00 +1.40339e-01 27r+0.00000e+00 +1.77099e-01
+7.52869e-02 26r+0.00000e+00 +2.87618e-01 +1.83523e-01
+4.82017e-03 25r+0.00000e+00 +3.80790e-01 +2.35590e-01
+2.36266e-02 -1.26737e-02 24r+0.00000e+00 +5.62913e-01
+3.54668e-01 +2.59267e-02 -1.87079e-02 -1.36744e-02
23r+0.00000e+00 +7.35643e-01 +4.16160e-01 +4.27551e-02
-2.79681e-02 -2.38066e-02 -1.05814e-02 22r+0.00000e+00
+9.19897e-01 +5.54072e-01 +4.18861e-02 -3.80459e-02
-3.32595e-02 -1.91090e-02 -7.28187e-03 21r+0.00000e+00
+1.71537e+00 +8.54437e-01 -1.18873e-02 -1.13020e-01
-8.39134e-02 -4.43791e-02 -2.20623e-02 -7.73654e-03
20r+0.00000e+00 +1.82923e+00 +9.54956e-01 -8.81419e-02
-7.96628e-02 -4.73461e-02 -2.57597e-02 -1.18384e-02
-5.53513e-03 -1.86194e-03 19r+0.00000e+00 +2.21175e+00
+1.67282e+00 +7.13600e-02 -1.05117e-01 -6.23218e-02
-3.26243e-02 -1.68158e-02 -7.48568e-03 -3.44525e-03
-1.14578e-03 18r+0.00000e+00 +2.56002e+00 +1.98749e+00

+1.99033e-01 -1.43699e-01 -8.27734e-02 -4.29553e-02
-2.12261e-02 -1.06380e-02 -4.65265e-03 -2.12202e-03
-7.00986e-04 17r+0.00000e+00 +1.68775e+00 +1.55360e+00
+2.21757e-01 -7.29978e-02 -8.12957e-02 -3.15098e-02
-1.55380e-02 -7.48647e-03 -3.70328e-03 -1.60594e-03
-7.29180e-04 -2.40070e-04 16r+0.00000e+00 +3.77827e+00
+3.75660e+00 +9.74790e-01 -2.03796e-01 -3.25845e-01
-1.94640e-01 -6.29730e-02 -3.00681e-02 -1.42435e-02
-6.98204e-03 -3.00958e-03 -1.36213e-03 -4.47358e-04
15r+0.00000e+00 +4.05595e+00 +2.11496e+00 -1.27700e-01
-4.03892e-01 -3.74698e-01 -2.39926e-01 -1.11654e-01
-3.17494e-02 -1.47455e-02 -6.87914e-03 -3.34392e-03
-1.43323e-03 -6.46683e-04 -2.11869e-04 14r+0.00000e+00
+4.21354e+00 +2.24711e+00 -3.56846e-01 -4.84817e-01
-3.83686e-01 -2.39142e-01 -1.32535e-01 -5.71442e-02
-1.54450e-02 -7.08653e-03 -3.28317e-03 -1.58972e-03
-6.79514e-04 -3.06125e-04 -1.00152e-04 13r+0.00000e+00
+4.27663e+00 +2.31207e+00 -3.83261e-01 -4.71145e-01
-3.23738e-01 -2.24285e-01 -1.26828e-01 -6.68876e-02
-2.79743e-02 -7.39506e-03 -3.37410e-03 -1.55810e-03
-7.52990e-04 -3.21397e-04 -1.44648e-04 -4.72650e-05
12r+0.00000e+00 +5.28536e+00 +2.13364e+00 -7.66374e-01
-7.30003e-01 -4.02564e-01 -2.38601e-01 -1.57717e-01
-8.56668e-02 -4.41614e-02 -1.81969e-02 -4.75612e-03
-2.16351e-03 -9.97165e-04 -4.81276e-04 -2.05149e-04
-9.22070e-05 -3.00539e-05 11r+0.00000e+00 +4.35330e+00
+1.29592e+00 -5.68060e-01 -3.86894e-01 -2.03232e-01
-9.54634e-02 -5.37366e-02 -3.48619e-02 -1.86154e-02
-9.49947e-03 -3.88751e-03 -1.01040e-03 -4.58799e-04
-2.11139e-04 -1.01749e-04 -4.32719e-05 -1.93884e-05
-6.27554e-06 10r+0.00000e+00 +4.36162e+00 +2.37546e+00
-4.72630e-01 -3.92357e-01 -2.10044e-01 -1.01898e-01
-4.63264e-02 -2.57676e-02 -1.66411e-02 -8.84818e-03
-4.50338e-03 -1.83939e-03 -4.77115e-04 -2.16402e-04
-9.94428e-05 -4.78258e-05 -2.02655e-05 -9.03291e-06
-2.88898e-06 9r+0.00000e+00 +4.95095e+00 +2.32722e+00
-6.09790e-01 -5.75851e-01 -2.57300e-01 -1.26625e-01
-5.93411e-02 -2.65656e-02 -1.46898e-02 -9.46517e-03
-5.02142e-03 -2.55183e-03 -1.04083e-03 -2.69321e-04
-1.21886e-04 -5.58196e-05 -2.67115e-05 -1.12141e-05
-4.92928e-06 -1.72957e-06 8r+0.00000e+00 +5.32504e+00
+1.48225e+00 -8.97180e-01 -6.68241e-01 -3.04619e-01

-1.14330e-01 -5.42255e-02 -2.49941e-02 -1.11023e-02
-6.11979e-03 -3.93775e-03 -2.08570e-03 -1.05830e-03
-4.30639e-04 -1.10700e-04 -4.97361e-05 -2.25095e-05
-1.05775e-05 -4.80910e-06 -1.91394e-06 -2.24460e-07
7r+0.00000e+00 +4.36793e+00 +1.30013e+00 -5.52530e-01
-3.30471e-01 -1.72841e-01 -6.94698e-02 -2.47843e-02
-1.16102e-02 -5.31984e-03 -2.35558e-03 -1.29626e-03
-8.33146e-04 -4.40465e-04 -2.22899e-04 -9.02058e-05
-2.27819e-05 -1.00256e-05 -4.95875e-06 -2.50311e-06
-1.77576e-07 8r+0.00000e+00 +4.95228e+00 +2.32889e+00
-6.53328e-01 -4.46939e-01 -2.08767e-01 -1.02655e-01
-4.00757e-02 -1.41103e-02 -6.58672e-03 -3.01192e-03
-1.33128e-03 -7.31367e-04 -4.69334e-04 -2.47317e-04
-1.24488e-04 -4.98040e-05 -1.29628e-05 -5.93947e-06
-1.43232e-06 9r+0.00000e+00 +4.36863e+00 +1.74663e+00
-5.58847e-01 -4.02110e-01 -1.56715e-01 -6.72593e-02
-3.22227e-02 -1.24147e-02 -4.34329e-03 -2.02313e-03
-9.23304e-04 -4.06878e-04 -2.22723e-04 -1.42372e-04
-7.44213e-05 -3.69544e-05 -1.50890e-05 -2.73053e-06
10r+0.00000e+00 +4.36886e+00 +2.38215e+00 -4.58927e-01
-4.72133e-01 -2.22860e-01 -7.72055e-02 -3.22839e-02
-1.53334e-02 -5.88025e-03 -2.05161e-03 -9.54073e-04
-4.34262e-04 -1.90391e-04 -1.03510e-04 -6.56875e-05
-3.37860e-05 -1.79200e-05 -6.61501e-06 11r+0.00000e+00
+7.61983e-01 -1.62017e+00 -1.10974e+00 -5.35965e-01
-2.17416e-01 -7.08299e-02 -2.91626e-02 -1.37696e-02
-5.25412e-03 -1.81820e-03 -8.35260e-04 -3.70807e-04
-1.54382e-04 -7.84967e-05 -4.64393e-05 -2.05722e-05
-6.08759e-06 33r+0.00000e+00
14** 5r+0.00000e+00 +1.05802e-01 27r+0.00000e+00 +1.41695e-01
+4.75085e-04 26r+0.00000e+00 +2.31705e-01 +5.65226e-02
-4.13248e-02 25r+0.00000e+00 +2.91810e-01 +4.15938e-02
-6.83283e-02 -3.20816e-02 24r+0.00000e+00 +4.58582e-01
+1.14487e-01 -9.86007e-02 -6.04079e-02 -1.89766e-02
23r+0.00000e+00 +5.87132e-01 +3.90869e-02 -1.38388e-01
-8.11829e-02 -3.68764e-02 -1.01279e-02 22r+0.00000e+00
+7.02097e-01 +8.04800e-02 -1.82877e-01 -1.21155e-01
-4.84668e-02 -1.98871e-02 -5.14013e-03 21r+0.00000e+00
+1.17701e+00 -1.02744e-01 -4.35020e-01 -2.29613e-01
-1.12802e-01 -3.89687e-02 -1.51510e-02 -3.78306e-03
20r+0.00000e+00 +1.44515e+00 +1.21462e-01 -2.68852e-01
-1.14898e-01 -4.50936e-02 -2.00072e-02 -6.46833e-03

-2.44982e-03 -6.03793e-04 19r+0.00000e+00 +1.74690e+00
+4.53819e-01 -4.71850e-01 -1.61501e-01 -6.10150e-02
-2.27577e-02 -9.88486e-03 -3.15280e-03 -1.19023e-03
-2.94725e-04 18r+0.00000e+00 +2.01204e+00 +5.23547e-01
-6.52123e-01 -3.74927e-01 -8.63011e-02 -3.08232e-02
-1.12081e-02 -4.81948e-03 -1.53096e-03 -5.79640e-04
-1.45455e-04 17r+0.00000e+00 +1.49247e+00 +7.24329e-01
-3.70277e-01 -3.07483e-01 -1.26948e-01 -2.56410e-02
-8.93931e-03 -3.21647e-03 -1.37893e-03 -4.38899e-04
-1.67255e-04 -4.27100e-05 16r+0.00000e+00 +2.64657e+00
+1.11905e+00 -1.02864e+00 -1.07674e+00 -5.84094e-01
-2.11079e-01 -3.96744e-02 -1.36460e-02 -4.89029e-03
-2.09990e-03 -6.74197e-04 -2.60404e-04 -6.85441e-05
15r+0.00000e+00 +2.83654e+00 -3.86374e-01 -1.43408e+00
-1.02529e+00 -5.23250e-01 -2.32004e-01 -7.62269e-02
-1.35233e-02 -4.61891e-03 -1.66375e-03 -7.23417e-04
-2.39324e-04 -9.60254e-05 -2.72562e-05 14r+0.00000e+00
+2.94296e+00 -4.22534e-01 -1.30823e+00 -7.42469e-01
-4.39831e-01 -1.97142e-01 -8.22272e-02 -2.61512e-02
-4.58085e-03 -1.58093e-03 -5.82421e-04 -2.60736e-04
-9.12490e-05 -3.89470e-05 -1.22692e-05 13r+0.00000e+00
+2.98525e+00 -4.48081e-01 -1.39760e+00 -6.07252e-01
-2.84317e-01 -1.59818e-01 -6.86061e-02 -2.80292e-02
-8.85694e-03 -1.57926e-03 -5.61675e-04 -2.16567e-04
-1.01989e-04 -3.88528e-05 -1.79618e-05 -6.32787e-06
12r+0.00000e+00 +2.96403e+00 -1.52690e+00 -1.95689e+00
-8.34828e-01 -2.86743e-01 -1.25769e-01 -6.93753e-02
-2.94056e-02 -1.20255e-02 -3.86816e-03 -7.39335e-04
-2.82924e-04 -1.19702e-04 -6.15664e-05 -2.65221e-05
-1.34833e-05 -5.29342e-06 11r+0.00000e+00 +3.03725e+00
-9.29039e-01 -9.12609e-01 -3.50342e-01 -1.19434e-01
-3.80857e-02 -1.64110e-02 -9.06559e-03 -3.90011e-03
-1.64689e-03 -5.65352e-04 -1.27838e-04 -5.59233e-05
-2.70732e-05 -1.54367e-05 -7.46203e-06 -4.07590e-06
-1.71087e-06 10r+0.00000e+00 +3.04308e+00 -4.66819e-01
-1.20616e+00 -3.55333e-01 -1.23329e-01 -4.06414e-02
-1.29167e-02 -5.63439e-03 -3.16237e-03 -1.40778e-03
-6.25210e-04 -2.33075e-04 -6.19460e-05 -2.98238e-05
-1.55912e-05 -9.33130e-06 -4.71977e-06 -2.63861e-06
-1.12505e-06 9r+0.00000e+00 +3.08810e+00 -1.05517e+00
-1.79219e+00 -6.19828e-01 -1.44601e-01 -4.84764e-02
-1.59485e-02 -5.19905e-03 -2.35732e-03 -1.37274e-03

-6.54494e-04 -3.17027e-04 -1.32997e-04 -4.21163e-05
-2.19554e-05 -1.21110e-05 -7.46321e-06 -3.85940e-06
-2.17226e-06 -1.28894e-06 8r+0.00000e+00 +2.98379e+00
-1.78580e+00 -1.59531e+00 -6.42837e-01 -1.73564e-01
-3.75006e-02 -1.26573e-02 -4.34981e-03 -1.55220e-03
-7.78264e-04 -4.91214e-04 -2.65731e-04 -1.46417e-04
-7.04651e-05 -2.59231e-05 -1.42213e-05 -8.05621e-06
-5.00640e-06 -3.63809e-06 -1.96970e-06 -3.13827e-07
7r+0.00000e+00 +3.04723e+00 -9.37115e-01 -8.19119e-01
-2.56938e-01 -8.88491e-02 -2.27839e-02 -5.00118e-03
-1.79645e-03 -6.92153e-04 -2.92065e-04 -1.68604e-04
-1.16533e-04 -7.07356e-05 -4.27459e-05 -2.22256e-05
-8.69452e-06 -4.81934e-06 -3.91349e-06 -3.12868e-06
-2.33408e-07 8r+0.00000e+00 +3.08888e+00 -1.05724e+00
-1.44974e+00 -3.65390e-01 -1.02848e-01 -3.47996e-02
-9.04417e-03 -2.13600e-03 -8.49472e-04 -3.76596e-04
-1.84845e-04 -1.17384e-04 -8.53213e-05 -5.46531e-05
-3.42190e-05 -1.81880e-05 -8.54082e-06 -6.17344e-06
-1.73108e-06 9r+0.00000e+00 +3.04769e+00 -7.93115e-01
-1.20947e+00 -3.86777e-01 -7.71986e-02 -2.10390e-02
-7.20235e-03 -1.98751e-03 -5.47836e-04 -2.54866e-04
-1.32767e-04 -7.41124e-05 -5.01802e-05 -3.75448e-05
-2.46883e-05 -1.56491e-05 -9.73844e-06 -4.06999e-06
10r+0.00000e+00 +3.04786e+00 -4.69207e-01 -1.34827e+00
-5.03993e-01 -1.37875e-01 -2.61703e-02 -7.21598e-03
-2.57044e-03 -7.82323e-04 -2.58515e-04 -1.37261e-04
-7.91829e-05 -4.70783e-05 -3.26806e-05 -2.46526e-05
-1.62642e-05 -1.30864e-05 -8.21756e-06 11r+0.00000e+00
-3.04989e+00 -2.58357e+00 -9.48511e-01 -2.76410e-01
-7.20104e-02 -1.42060e-02 -4.41630e-03 -1.87404e-03
-7.62441e-04 -3.50261e-04 -2.15979e-04 -1.33576e-04
-7.89791e-05 -5.22884e-05 -3.70968e-05 -2.16045e-05
-8.52723e-06 33r+0.00000e+00
14** -1.82649e-01 +.00000e+00 +7.90175e-01 2r+0.00000e+00
+3.71574e-01 22r+0.00000e+00 -9.49081e-02 +.00000e+00
+1.27857e+00 2r+0.00000e+00 +4.14615e-01 +2.06621e-01
21r+0.00000e+00 -3.13465e-02 +.00000e+00 +1.72030e+00
2r+0.00000e+00 +5.96345e-01 +4.16118e-01 +1.22538e-01
20r+0.00000e+00 -5.50986e-04 +.00000e+00 +2.21108e+00
2r+0.00000e+00 +6.64002e-01 +4.93560e-01 +1.55711e-01
+1.11271e-01 21r+0.00000e+00 +2.62734e+00 2r+0.00000e+00
+5.72253e-01 +5.88887e-01 +1.93805e-01 +1.50460e-01

+9.77999e-02 20r+0.00000e+00 +2.85514e+00 2r+0.00000e+00
+4.48971e-01 +5.95838e-01 +3.09818e-01 +2.18048e-01
+1.71840e-01 +3.16489e-02 19r+0.00000e+00 +2.95569e+00
2r+0.00000e+00 +3.91049e-01 +6.44190e-01 +4.78046e-01
+3.31658e-01 +2.11337e-01 +4.03422e-02 +1.57868e-02
18r+0.00000e+00 +3.06029e+00 2r+0.00000e+00 +8.35007e-01
+1.40876e+00 +1.25008e+00 +9.42627e-01 +3.17179e-01
+3.42624e-02 +1.78464e-02 +1.19699e-02 17r+0.00000e+00
+3.17469e+00 2r+0.00000e+00 +6.04077e-01 +8.58139e-01
+6.56165e-01 +4.70485e-01 +3.85771e-02 +5.69495e-05
+2.24840e-03 +3.31676e-03 +1.89675e-03 16r+0.00000e+00
+3.23499e+00 2r+0.00000e+00 +6.77637e-01 +1.03906e+00
+6.85061e-01 +4.60660e-01 +4.14158e-02 +.00000e+00
+2.21327e-05 +1.08389e-03 +1.66420e-03 +9.03843e-04
15r+0.00000e+00 +3.28105e+00 2r+0.00000e+00 +7.25804e-01
+1.08566e+00 +7.35484e-01 +4.79454e-01 +3.90582e-02
2r+0.00000e+00 +7.24992e-06 +5.09885e-04 +8.18267e-04
+4.29714e-04 14r+0.00000e+00 +3.30935e+00 2r+0.00000e+00
+4.04312e-01 +6.19273e-01 +3.99620e-01 +2.73624e-01
+1.27027e-01 3r+0.00000e+00 +1.30339e-06 +1.41245e-04
+2.32096e-04 +1.21246e-04 13r+0.00000e+00 +3.33743e+00
2r+0.00000e+00 +1.08036e+00 +1.70563e+00 +1.21609e+00
+7.93471e-01 +5.00107e-01 +7.56002e-02 3r+0.00000e+00
+8.46930e-07 +2.04734e-04 +3.49314e-04 +1.79814e-04
12r+0.00000e+00 +3.36635e+00 2r+0.00000e+00 +1.10669e+00
+1.39622e+00 +8.52764e-01 +6.11730e-01 +2.78602e-01
+2.23364e-02 4r+0.00000e+00 +1.56200e-09 +6.74224e-05
+1.14776e-04 +5.85159e-05 11r+0.00000e+00 +3.38544e+00
2r+0.00000e+00 +1.12130e+00 +1.40670e+00 +6.78665e-01
+3.46646e-01 +1.08158e-01 7r+0.00000e+00 +2.31616e-05
+3.74710e-05 +1.86411e-05 8r+0.00000e+00 +1.10614e-06
+.00000e+00 +3.39452e+00 2r+0.00000e+00 +1.12825e+00
+1.41375e+00 +6.73239e-01 +1.82187e-01 9r+0.00000e+00
+7.46253e-06 +1.12256e-05 +4.62747e-06 7r+0.00000e+00
+2.91951e-07 +.00000e+00 +3.39492e+00 2r+0.00000e+00
+1.63702e+00 +1.91770e+00 +8.38067e-01 +1.79717e-01
10r+0.00000e+00 +2.09253e-06 +3.01789e-06 +1.21999e-06
6r+0.00000e+00 +7.13671e-06 +.00000e+00 +3.39499e+00
2r+0.00000e+00 +1.13142e+00 +1.15022e+00 +3.36281e-01
+1.23245e-02 11r+0.00000e+00 +1.45377e-07 +2.09665e-07
+8.47577e-08 5r+0.00000e+00 +1.05104e-05 +.00000e+00
+3.39502e+00 2r+0.00000e+00 +1.13164e+00 +1.41696e+00

+5.01017e-01 +1.22904e-02 12r+0.00000e+00 +3.24361e-08
+4.67799e-08 +1.89109e-08 4r+0.00000e+00 +1.38597e-05
+.00000e+00 +3.39502e+00 2r+0.00000e+00 +1.40432e+00
+1.69760e+00 +7.79457e-01 +1.06658e-01 13r+0.00000e+00
+7.47831e-09 +1.16178e-08 +1.04115e-08 3r+0.00000e+00
+1.87822e-05 +.00000e+00 +3.39503e+00 2r+0.00000e+00
+1.63858e+00 +1.72120e+00 +5.65765e-01 +6.71458e-02
19r+0.00000e+00 +3.03387e-05 +.00000e+00 +3.39503e+00
2r+0.00000e+00 +1.13185e+00 +1.14958e+00 +2.60303e-01
20r+0.00000e+00 +4.86612e-05 +.00000e+00 +3.39505e+00
2r+0.00000e+00 +1.40445e+00 +1.69755e+00 +5.66595e-01
+9.17828e-03 19r+0.00000e+00 +7.04168e-05 +.00000e+00
+3.39507e+00 +1.10207e-12 +.00000e+00 +1.13189e+00
+1.27313e+00 +4.98505e-01 +4.02530e-02 19r+0.00000e+00
+1.03703e-04 +.00000e+00 +3.39510e+00 +5.65611e-07
+2.59297e-04 +1.13188e+00 +1.41694e+00 +5.84297e-01
+6.70939e-02 19r+0.00000e+00 +2.25794e-04 +.00000e+00
+4.14321e+00 +.00000e+00 +1.90204e-01 +2.45155e+00
+2.03518e+00 +8.45725e-01 +1.33124e-01 19r+0.00000e+00
+4.69325e-04 +.00000e+00 +5.42118e+00 2r+0.00000e+00
+5.23051e+00 +1.69117e+00 +2.27941e-01 +4.48536e-04
19r+0.00000e+00

14** 5r+0.00000e+00 +3.12823e-01 27r+0.00000e+00 +3.74556e-01
+1.45900e-01 26r+0.00000e+00 +5.39150e-01 +2.77042e-01
+6.98302e-02 25r+0.00000e+00 +5.98526e-01 +3.04634e-01
+5.64641e-02 +2.36881e-02 24r+0.00000e+00 +5.18447e-01
+3.53956e-01 +3.18645e-02 -2.72642e-03 -2.30889e-02
23r+0.00000e+00 +4.22642e-01 +3.23523e-01 +3.29624e-02
-5.69219e-02 -8.31352e-02 +4.67511e-03 22r+0.00000e+00
+3.31969e-01 +3.27912e-01 +3.50389e-02 -1.14482e-01
-1.32109e-01 -8.00195e-03 +2.71782e-03 21r+0.00000e+00
+5.61818e-01 +4.35250e-01 -1.96265e-01 -4.94915e-01
-2.32264e-01 -9.14120e-03 +6.05118e-03 +1.20865e-03
20r+0.00000e+00 +5.05939e-01 +3.68839e-01 -2.28517e-01
-3.35036e-01 -3.12795e-02 +5.08007e-05 +1.35497e-03
+6.24697e-04 +1.11387e-04 19r+0.00000e+00 +5.72650e-01
+5.83081e-01 -1.77996e-02 -3.38494e-01 -2.92816e-02
+.00000e+00 +1.99138e-05 +5.74610e-04 +2.21809e-04
+4.03633e-05 18r+0.00000e+00 +6.16672e-01 +6.11378e-01
+8.67859e-02 -2.20478e-01 -3.55562e-02 2r+0.00000e+00
+6.67329e-06 +2.25821e-04 +7.78740e-05 +1.47008e-05
17r+0.00000e+00 +3.72576e-01 +4.12097e-01 +8.66771e-02

-5.97859e-02 -9.82470e-02 3r+0.00000e+00 +1.24022e-06
+5.35287e-05 +1.70783e-05 +3.35010e-06 16r+0.00000e+00
+8.50689e-01 +9.77684e-01 +3.04506e-01 -1.48768e-01
-2.99551e-01 -7.50913e-02 3r+0.00000e+00 +8.19542e-07
+6.39812e-05 +2.00640e-05 +4.00020e-06 15r+0.00000e+00
+8.71657e-01 +5.40651e-01 -7.49238e-02 -2.47821e-01
-2.06026e-01 -2.13305e-02 4r+0.00000e+00 +1.62136e-09
+1.45064e-05 +4.38385e-06 +8.89454e-07 14r+0.00000e+00
+8.83381e-01 +5.47672e-01 -1.84166e-01 -2.40130e-01
-9.12040e-02 7r+0.00000e+00 +3.10495e-06 +9.69734e-07
+1.98206e-07 13r+0.00000e+00 +8.88971e-01 +5.51563e-01
-1.81531e-01 -1.36399e-01 9r+0.00000e+00 +6.46711e-07
+2.15607e-07 +4.42068e-08 12r+0.00000e+00 +1.11441e+00
+4.62766e-01 -3.03017e-01 -1.34605e-01 10r+0.00000e+00
+1.68505e-07 +5.68238e-08 +1.16547e-08 11r+0.00000e+00
+8.91733e-01 +2.78004e-01 -2.11625e-01 -1.14837e-02
11r+0.00000e+00 +1.17068e-08 +3.94779e-09 +8.09701e-10
10r+0.00000e+00 +8.91931e-01 +5.53613e-01 -1.80874e-01
-1.14547e-02 12r+0.00000e+00 +2.61198e-09 +8.80819e-10
+1.80658e-10 9r+0.00000e+00 +1.02758e+00 +5.29793e-01
-2.55934e-01 -7.98723e-02 13r+0.00000e+00 +5.90798e-10
+2.18752e-10 +5.63971e-09 8r+0.00000e+00 +1.11577e+00
+2.80861e-01 -2.88541e-01 -5.65690e-02 24r+0.00000e+00
+8.92116e-01 +2.77954e-01 -1.66532e-01 25r+0.00000e+00
+1.02767e+00 +5.29804e-01 -2.26372e-01 -8.54986e-03
22r+0.00000e+00 +9.32982e-14 +.00000e+00 +8.92139e-01
+3.97310e-01 -2.31930e-01 -3.39115e-02 22r+0.00000e+00
-9.20229e-08 +1.55614e-04 +8.92138e-01 +5.53648e-01
-1.91848e-01 -5.65241e-02 23r+0.00000e+00 +3.20690e-03
+9.37991e-01 +4.06935e-01 -3.11868e-01 -9.96593e-02
24r+0.00000e+00 +7.00362e-01 -4.26589e-03 -1.65593e-01
-4.41640e-04 19r+0.00000e+00
14** 5r+0.00000e+00 +2.23298e-01 27r+0.00000e+00 +2.95869e-01
+1.02517e-02 26r+0.00000e+00 +4.20049e-01 +7.79880e-02
-1.31254e-02 25r+0.00000e+00 +4.51996e-01 +6.19358e-02
-4.30597e-02 -4.83560e-03 24r+0.00000e+00 +3.87467e-01
+7.42979e-02 -7.51088e-02 -2.75637e-02 +2.80182e-02
23r+0.00000e+00 +2.96109e-01 -1.45622e-03 -1.33026e-01
-4.91106e-02 +5.16192e-02 +3.05005e-03 22r+0.00000e+00
+2.31793e-01 -2.65170e-02 -2.09952e-01 -8.95907e-02
+6.99648e-02 +1.44380e-02 22r+0.00000e+00 +2.87549e-01
-3.37007e-01 -4.29033e-01 +3.30875e-02 +1.20216e-01

+1.36281e-02 22r+0.00000e+00 +3.57790e-01 -1.02599e-01
-1.72419e-01 +1.71731e-01 +2.41097e-02 23r+0.00000e+00
+4.05342e-01 +1.79022e-02 -2.82253e-01 +1.63465e-01
+2.56150e-02 23r+0.00000e+00 +4.36398e-01 +2.61402e-02
-3.18609e-01 -6.38057e-02 +2.90634e-02 23r+0.00000e+00
+3.14565e-01 +1.21849e-01 -1.60140e-01 -1.08748e-01
+4.00450e-02 23r+0.00000e+00 +5.03898e-01 +9.59124e-02
-4.00378e-01 -2.93721e-01 +4.97871e-02 +5.43703e-02
22r+0.00000e+00 +5.17617e-01 -2.32290e-01 -3.67218e-01
-1.06691e-01 +9.85995e-02 +1.80298e-02 22r+0.00000e+00
+5.25116e-01 -2.30757e-01 -1.91471e-01 +9.00821e-02
+6.29588e-02 23r+0.00000e+00 +5.28611e-01 -2.30684e-01
-1.91391e-01 +6.93763e-02 24r+0.00000e+00 +4.66109e-01
-4.18093e-01 -1.33404e-01 +6.83606e-02 24r+0.00000e+00
+5.30407e-01 -2.50533e-01 +5.39114e-02 +9.91167e-03
24r+0.00000e+00 +5.30549e-01 -2.30118e-01 -8.01267e-02
+9.89705e-03 24r+0.00000e+00 +5.11704e-01 -3.51183e-01
-1.62685e-01 +4.05142e-02 24r+0.00000e+00 +4.66883e-01
-3.89779e-01 -2.55991e-03 +3.90137e-02 24r+0.00000e+00
+5.30670e-01 -2.50296e-01 +4.75891e-02 25r+0.00000e+00
+5.11753e-01 -3.51144e-01 -6.30257e-02 +7.38782e-03
24r+0.00000e+00 +5.30676e-01 -2.63376e-01 -4.15459e-02
+2.33883e-02 24r+0.00000e+00 +5.30678e-01 -2.30056e-01
-1.21956e-01 +3.89846e-02 25r+0.00000e+00 -3.53705e-01
-1.23648e-01 +5.05494e-02 47r+0.00000e+00
14** 5r+0.00000e+00 +1.36616e-01 27r+0.00000e+00 +1.98805e-01
-3.50963e-02 26r+0.00000e+00 +2.66835e-01 -4.40452e-02
-3.85721e-03 25r+0.00000e+00 +2.89894e-01 -8.28025e-02
-2.08494e-02 +1.32185e-02 24r+0.00000e+00 +2.31646e-01
-9.76783e-02 -1.68458e-02 +3.40332e-02 -1.22375e-02
23r+0.00000e+00 +1.63877e-01 -1.63300e-01 -4.67635e-02
+6.77003e-02 -7.79305e-03 -2.08626e-03 22r+0.00000e+00
+1.16545e-01 -1.89801e-01 -2.06923e-02 +1.08152e-01
-1.37412e-02 -1.11993e-02 22r+0.00000e+00 +7.61481e-02
-2.81916e-01 +1.81387e-01 +1.32503e-01 -1.86306e-02
-8.97518e-03 22r+0.00000e+00 +1.93976e-01 -2.10326e-01
+2.16823e-01 -3.78342e-02 -1.32765e-02 23r+0.00000e+00
+2.22923e-01 -2.71083e-01 -5.30358e-03 -7.59612e-03
-1.70008e-02 23r+0.00000e+00 +2.41614e-01 -2.78980e-01
-1.04547e-01 +1.20085e-01 -2.55214e-02 23r+0.00000e+00
+2.40313e-01 -9.40803e-02 -1.06070e-01 +7.41574e-02
+1.05022e-02 23r+0.00000e+00 +1.91036e-01 -3.59066e-01

-2.96293e-01 +1.50180e-01 +8.70492e-02 -2.86842e-02
22r+0.00000e+00 +1.98315e-01 -3.20791e-01 +8.58458e-02
+1.68185e-01 -9.53178e-03 -1.42436e-02 22r+0.00000e+00
+2.01859e-01 -3.24018e-01 +1.37087e-01 +2.38148e-02
-3.26314e-02 23r+0.00000e+00 +2.03678e-01 -3.25799e-01
+1.35556e-01 -1.30141e-02 24r+0.00000e+00 +7.06538e-02
-2.35713e-01 +1.30510e-01 -1.25573e-02 24r+0.00000e+00
+2.04570e-01 -1.41580e-01 +3.92817e-02 -7.85508e-03
24r+0.00000e+00 +2.04654e-01 -3.26780e-01 +7.80218e-02
-7.85479e-03 24r+0.00000e+00 +1.27146e-01 -2.99541e-01
+1.42214e-01 -7.32893e-03 24r+0.00000e+00 +7.09807e-02
-1.44815e-01 +9.48473e-02 -2.00861e-02 24r+0.00000e+00
+2.04714e-01 -1.41598e-01 +2.35156e-02 25r+0.00000e+00
+1.27162e-01 -2.99539e-01 +8.26536e-02 -5.86354e-03
24r+0.00000e+00 +2.04710e-01 -2.24629e-01 +1.14896e-01
-1.20418e-02 24r+0.00000e+00 +2.04712e-01 -3.26781e-01
+1.06604e-01 -2.00726e-02 25r+0.00000e+00 -2.04712e-01
+1.22073e-01 -9.13820e-03 47r+0.00000e+00
14** +6.78031e-02 +.00000e+00 +1.41147e+00 2r+0.00000e+00
+9.50612e-01 22r+0.00000e+00 +7.05034e-02 +.00000e+00
+1.30263e+00 2r+0.00000e+00 +6.83617e-01 +1.44575e-01
21r+0.00000e+00 +2.03670e-05 +.00000e+00 +1.55869e+00
2r+0.00000e+00 +1.03169e+00 +3.05296e-01 +8.49519e-02
20r+0.00000e+00 +1.19426e-05 +.00000e+00 +1.95762e+00
2r+0.00000e+00 +1.34267e+00 +4.75637e-01 +1.26177e-01
+3.85345e-02 19r+0.00000e+00 +5.94246e-06 +.00000e+00
+1.90406e+00 2r+0.00000e+00 +1.33818e+00 +6.14936e-01
+1.01878e-03 +7.95260e-02 +2.62243e-02 18r+0.00000e+00
+5.96494e-06 +.00000e+00 +2.50080e+00 2r+0.00000e+00
+1.72085e+00 +5.65875e-01 +.00000e+00 +1.72789e-02
+3.37621e-02 +2.58019e-02 17r+0.00000e+00 +6.50756e-06
+.00000e+00 +3.12373e+00 2r+0.00000e+00 +2.17505e+00
+7.79940e-01 2r+0.00000e+00 +1.63359e-02 +2.31887e-03
+2.70635e-02 16r+0.00000e+00 +4.01579e-06 +.00000e+00
+3.85412e+00 2r+0.00000e+00 +3.15686e+00 +9.48673e-01
3r+0.00000e+00 +1.30646e-02 +1.06539e-03 +3.44267e-02
15r+0.00000e+00 +9.87636e-07 +.00000e+00 +4.29545e+00
2r+0.00000e+00 +2.92048e+00 +6.97255e-01 4r+0.00000e+00
+2.04581e-03 +2.01436e-04 +6.55914e-03 14r+0.00000e+00
+1.06092e-06 +.00000e+00 +4.44791e+00 2r+0.00000e+00
+3.02528e+00 +1.37497e+00 5r+0.00000e+00 +9.24382e-04
+9.25044e-05 +2.92318e-03 13r+0.00000e+00 +9.91388e-07

+.00000e+00 +4.55676e+00 2r+0.00000e+00 +3.10307e+00
+1.42263e+00 6r+0.00000e+00 +3.99577e-04 +3.94841e-05
+1.21324e-03 12r+0.00000e+00 +5.76911e-06 +.00000e+00
+4.61158e+00 2r+0.00000e+00 +1.86801e+00 +1.36521e+00
7r+0.00000e+00 +9.82425e-05 +1.01975e-05 +2.96602e-04
11r+0.00000e+00 +4.42349e-06 +.00000e+00 +4.65736e+00
2r+0.00000e+00 +3.66623e+00 +2.74356e+00 +8.84741e-02
7r+0.00000e+00 +1.28069e-04 +1.32575e-05 +3.72046e-04
10r+0.00000e+00 +2.90725e-06 +.00000e+00 +4.69714e+00
2r+0.00000e+00 +3.69976e+00 +9.91128e-01 9r+0.00000e+00
+3.55503e-05 +3.53485e-06 +8.80620e-05 9r+0.00000e+00
+6.15362e-06 +.00000e+00 +4.71669e+00 2r+0.00000e+00
+3.71618e+00 +9.97380e-01 10r+0.00000e+00 +9.77237e-06
+9.47407e-07 +2.06371e-05 8r+0.00000e+00 +1.73958e-05
+.00000e+00 +4.72831e+00 2r+0.00000e+00 +3.72497e+00
+1.00050e+00 11r+0.00000e+00 +3.16502e-06 +2.41843e-07
+4.83855e-06 7r+0.00000e+00 +1.72921e-05 +.00000e+00
+4.73504e+00 2r+0.00000e+00 +4.13231e+00 +1.00332e+00
12r+0.00000e+00 +1.42811e-06 +8.80201e-08 +1.35096e-06
6r+0.00000e+00 +3.09162e-05 +.00000e+00 +4.73776e+00
2r+0.00000e+00 +3.73310e+00 +6.02716e-01 13r+0.00000e+00
+2.24257e-07 +1.01512e-08 +1.04295e-07 5r+0.00000e+00
+4.53057e-05 +.00000e+00 +4.73856e+00 2r+0.00000e+00
+3.73373e+00 +1.00463e+00 14r+0.00000e+00 +9.21174e-08
+3.28773e-09 +2.65032e-08 4r+0.00000e+00 +6.49856e-05
+.00000e+00 +4.73898e+00 2r+0.00000e+00 +3.98534e+00
+1.00478e+00 15r+0.00000e+00 +4.66910e-08 +5.92580e-10
+3.51187e-09 3r+0.00000e+00 +1.24331e-04 +.00000e+00
+4.73922e+00 2r+0.00000e+00 +4.13630e+00 +7.53572e-01
16r+0.00000e+00 +1.76577e-08 4r+0.00000e+00 +1.98708e-04
+.00000e+00 +4.73936e+00 2r+0.00000e+00 +3.73431e+00
+6.02798e-01 17r+0.00000e+00 +3.52685e-09 3r+0.00000e+00
+3.14273e-04 +.00000e+00 +4.73950e+00 2r+0.00000e+00
+3.98562e+00 +1.00485e+00 18r+0.00000e+00 +6.86480e-10
2r+0.00000e+00 +4.80439e-04 +.00000e+00 +4.73967e+00
+5.52831e-10 +.00000e+00 +3.73436e+00 +7.53567e-01
21r+0.00000e+00 +7.00547e-04 +.00000e+00 +4.73989e+00
+2.52411e-10 +5.62739e-04 +3.73436e+00 +1.00483e+00
21r+0.00000e+00 +1.51463e-03 +.00000e+00 +4.78098e+00
+.00000e+00 +1.75170e-01 +3.25451e+00 +1.00483e+00
21r+0.00000e+00 +3.12700e-03 +.00000e+00 +4.95174e+00
2r+0.00000e+00 +4.77344e+00 +1.52439e+00 21r+0.00000e+00

```
14**  5r+0.00000e+00   +6.32843e-01 27r+0.00000e+00   +4.61543e-01
     +1.86516e-02 26r+0.00000e+00   +5.02697e-01   -3.92455e-02
     +1.59806e-02 25r+0.00000e+00   +3.11945e-01   -1.38958e-01
     +5.43594e-03   +4.91003e-03 24r+0.00000e+00   +3.16016e-01
     -2.62223e-01   +9.99198e-04   +4.86469e-03   +1.40896e-03
    23r+0.00000e+00   +4.57869e-01   -1.36212e-01   +.00000e+00
     +9.89452e-03   -1.10195e-02   -5.82083e-04 22r+0.00000e+00
     +5.85951e-01   -1.63461e-01  2r+0.00000e+00   +2.29776e-03
     -1.15368e-03   -5.05336e-04 21r+0.00000e+00   +5.68654e-01
     -2.41931e-01  3r+0.00000e+00   +5.14932e-04   -1.69674e-05
     -1.51430e-04 20r+0.00000e+00   +7.11775e-01   -2.26718e-01
    4r+0.00000e+00   +2.17460e-07   -8.29428e-06   -3.60260e-05
    19r+0.00000e+00   +7.08544e-01   -3.96183e-01  5r+0.00000e+00
     -9.86258e-05   -5.37480e-06   -1.45909e-05 18r+0.00000e+00
     +7.08288e-01   -4.10985e-01  6r+0.00000e+00   -8.90558e-05
     -2.95492e-06   -6.82647e-06 17r+0.00000e+00   +9.85471e-01
     -3.48554e-01  7r+0.00000e+00   -2.52722e-05   -8.07404e-07
     -1.81884e-06 16r+0.00000e+00   +5.64884e-01   -7.05082e-01
     -7.30277e-02  7r+0.00000e+00   -3.34725e-05   -1.03089e-06
     -2.40632e-06 15r+0.00000e+00   +5.63279e-01   -2.90063e-01
    9r+0.00000e+00   -8.28001e-06   -2.06401e-07   -5.11694e-07
    14r+0.00000e+00   +5.62331e-01   -2.93337e-01 10r+0.00000e+00
     -3.11799e-06   -5.62490e-08   -2.71305e-08 13r+0.00000e+00
     +5.62316e-01   -2.94781e-01 11r+0.00000e+00   -9.02536e-07
     -2.98649e-08   +1.82802e-08 12r+0.00000e+00   +4.43698e-01
     -2.95827e-01 12r+0.00000e+00   -3.30168e-07   -1.45402e-08
     -1.79647e-09 11r+0.00000e+00   +5.61961e-01   -1.77788e-01
    13r+0.00000e+00   -3.64607e-08   -1.67991e-09   -3.00778e-09
    10r+0.00000e+00   +5.61949e-01   -2.96288e-01 14r+0.00000e+00
     -1.11906e-08   -5.26172e-10   -4.87678e-10  9r+0.00000e+00
     +4.87829e-01   -2.96342e-01 15r+0.00000e+00   -3.89740e-09
     -7.65706e-11   -9.91888e-11  8r+0.00000e+00   +4.43344e-01
     -2.22258e-01 16r+0.00000e+00   -7.81803e-10  9r+0.00000e+00
     +5.61923e-01   -1.77790e-01 17r+0.00000e+00   -4.06048e-11
    8r+0.00000e+00   +4.87806e-01   -2.96373e-01 18r+0.00000e+00
     +2.72694e-12  5r+0.00000e+00   -4.54140e-10   +.00000e+00
     +5.61910e-01   -2.22257e-01 24r+0.00000e+00   -2.33702e-10
     +9.05731e-05   +5.61911e-01   -2.96364e-01 25r+0.00000e+00
     -2.38452e-02   +4.63442e-01   -2.96365e-01 26r+0.00000e+00
     +2.94357e-01   -1.86862e-01 21r+0.00000e+00
14**  5r+0.00000e+00   +4.40352e-01 27r+0.00000e+00   +3.35566e-01
     +2.62005e-03 26r+0.00000e+00   +2.49729e-01   +7.28206e-03
```

```
    26r+0.00000e+00   +4.18396e-01   +4.39004e-02 26r+0.00000e+00
     +1.12344e-01   +9.47590e-02 26r+0.00000e+00   +5.89408e-02
     -2.54630e-03 26r+0.00000e+00   +6.73290e-02   -1.37943e-02
    26r+0.00000e+00   +5.40070e-02   -2.78892e-02 26r+0.00000e+00
     +5.66384e-02   -2.91877e-02 26r+0.00000e+00   +5.03656e-02
     -3.93379e-02 26r+0.00000e+00   +4.63208e-02   -3.81653e-02
    26r+0.00000e+00   +1.75322e-01   -8.42714e-02 26r+0.00000e+00
     +3.09127e-02   -1.66354e-01   +4.79783e-02 25r+0.00000e+00
     +2.99386e-02   -2.28180e-02 26r+0.00000e+00   +2.94496e-02
     -2.26018e-02 26r+0.00000e+00   +2.93146e-02   -2.24493e-02
    26r+0.00000e+00   +2.01906e-02   -2.24705e-02 26r+0.00000e+00
     +2.90874e-02   -1.34339e-02 26r+0.00000e+00   +2.90708e-02
     -2.23654e-02 26r+0.00000e+00   +2.34709e-02   -2.23595e-02
    26r+0.00000e+00   +2.01129e-02   -1.67647e-02 26r+0.00000e+00
     +2.90549e-02   -1.34092e-02 26r+0.00000e+00   +2.34643e-02
     -2.23521e-02 26r+0.00000e+00   +2.90531e-02   -1.67616e-02
    26r+0.00000e+00   +2.90523e-02   -2.23504e-02 27r+0.00000e+00
     -2.23499e-02 49r+0.00000e+00
14**  5r+0.00000e+00   +3.21913e-01 27r+0.00000e+00   +2.53141e-01
     +4.38647e-03 26r+0.00000e+00   +1.73964e-01   +4.56739e-03
    26r+0.00000e+00   +1.04617e-01   -3.40548e-03 26r+0.00000e+00
     +2.49180e-02   -3.44643e-02 26r+0.00000e+00   +1.80660e-02
     -1.18580e-02 26r+0.00000e+00   +9.55391e-03   -1.07347e-02
    26r+0.00000e+00   +1.67196e-03   -4.84898e-03 26r+0.00000e+00
     +2.69323e-03   +1.26739e-04 26r+0.00000e+00   +1.76579e-03
     -1.80232e-03 26r+0.00000e+00   +1.14381e-03   -1.38261e-03
    26r+0.00000e+00   -4.28342e-02   +2.17396e-02 26r+0.00000e+00
     +8.03229e-04   +4.29732e-02   -2.26716e-02 25r+0.00000e+00
     +6.78520e-04   -7.20320e-04 26r+0.00000e+00   +6.38102e-04
     -6.43506e-04 26r+0.00000e+00   +5.76425e-04   -6.21337e-04
    26r+0.00000e+00   +3.48806e-04   -5.67995e-04 26r+0.00000e+00
     +5.77016e-04   -3.44952e-04 26r+0.00000e+00   +5.76518e-04
     -5.75046e-04 26r+0.00000e+00   +4.32616e-04   -5.75077e-04
    26r+0.00000e+00   +3.46121e-04   -4.31467e-04 26r+0.00000e+00
     +5.76370e-04   -3.45178e-04 26r+0.00000e+00   +4.32626e-04
     -5.75406e-04 26r+0.00000e+00   +5.76607e-04   -4.31671e-04
    26r+0.00000e+00   +5.76836e-04   -5.75671e-04 27r+0.00000e+00
     -5.75029e-04 49r+0.00000e+00
14**   +1.98628e-01   +.00000e+00   +1.62288e+00  2r+0.00000e+00
     +9.41251e-01 22r+0.00000e+00   +1.64183e-01   +.00000e+00
     +1.13548e+00  2r+0.00000e+00   +5.52356e-01   +1.75472e-01
    21r+0.00000e+00   +7.14987e-02   +.00000e+00   +1.63074e+00
```

2r+0.00000e+00 +1.20616e+00 +2.03738e-01 +1.23453e-01
20r+0.00000e+00 +5.08645e-04 +.00000e+00 +1.51112e+00
2r+0.00000e+00 +1.33968e+00 +3.53084e-01 +2.99457e-02
+8.20423e-02 19r+0.00000e+00 +2.51149e-06 +.00000e+00
+1.91054e+00 2r+0.00000e+00 +1.46677e+00 +1.70931e-01
+.00000e+00 +8.24394e-02 +4.51164e-02 18r+0.00000e+00
+1.77503e-06 +.00000e+00 +3.98629e+00 2r+0.00000e+00
+2.93384e+00 +4.43765e-01 2r+0.00000e+00 +5.73541e-02
+3.08011e-02 19r+0.00000e+00 +3.07551e+00 2r+0.00000e+00
+2.48940e+00 +1.05245e+00 3r+0.00000e+00 +2.54838e-02
+1.53025e-02 16r+0.00000e+00 +4.37700e-06 +.00000e+00
+4.61109e+00 2r+0.00000e+00 +4.10157e+00 +5.86107e-01
4r+0.00000e+00 +1.68932e-02 +9.00569e-03 15r+0.00000e+00
+1.56648e-06 +.00000e+00 +3.59163e+00 2r+0.00000e+00
+2.65608e+00 +5.09517e-01 5r+0.00000e+00 +2.12027e-03
+1.06089e-03 14r+0.00000e+00 +1.65232e-06 +.00000e+00
+3.69934e+00 2r+0.00000e+00 +2.76383e+00 +9.35545e-01
6r+0.00000e+00 +6.32822e-04 +4.23011e-04 13r+0.00000e+00
+5.10172e-06 +.00000e+00 +3.77000e+00 2r+0.00000e+00
+2.83382e+00 +9.35506e-01 7r+0.00000e+00 +1.98628e-04
+1.77028e-04 12r+0.00000e+00 +4.26831e-06 +.00000e+00
+3.80631e+00 2r+0.00000e+00 +1.93700e+00 +9.36076e-01
8r+0.00000e+00 +4.81698e-05 +4.65881e-05 11r+0.00000e+00
+4.97744e-07 +.00000e+00 +3.83727e+00 2r+0.00000e+00
+3.20988e+00 +1.86931e+00 +9.72393e-05 8r+0.00000e+00
+6.45854e-05 +6.63084e-05 10r+0.00000e+00 +4.60077e-07
+.00000e+00 +3.86386e+00 2r+0.00000e+00 +3.23735e+00
+6.27391e-01 10r+0.00000e+00 +1.87409e-05 +2.12445e-05
9r+0.00000e+00 +2.49338e-06 +.00000e+00 +3.87672e+00
2r+0.00000e+00 +3.25004e+00 +6.26508e-01 11r+0.00000e+00
+5.78548e-06 +6.92369e-06 8r+0.00000e+00 +5.69372e-07
+.00000e+00 +3.88284e+00 2r+0.00000e+00 +3.25541e+00
+6.26677e-01 12r+0.00000e+00 +1.85287e-06 +2.49395e-06
7r+0.00000e+00 +1.97053e-06 +.00000e+00 +3.88622e+00
2r+0.00000e+00 +3.50978e+00 +6.27425e-01 13r+0.00000e+00
+7.87737e-07 +1.17935e-06 6r+0.00000e+00 +6.09854e-06
+.00000e+00 +3.88757e+00 2r+0.00000e+00 +3.26026e+00
+3.76435e-01 14r+0.00000e+00 +1.02255e-07 +1.83774e-07
5r+0.00000e+00 +4.77364e-06 +.00000e+00 +3.88795e+00
2r+0.00000e+00 +3.26066e+00 +6.27304e-01 15r+0.00000e+00
+3.87604e-08 +7.43842e-08 4r+0.00000e+00 +2.40832e-06
+.00000e+00 +3.88815e+00 2r+0.00000e+00 +3.41772e+00

+6.27288e-01 16r+0.00000e+00 +1.52119e-08 +3.54278e-08
3r+0.00000e+00 +9.70276e-06 +.00000e+00 +3.88826e+00
2r+0.00000e+00 +3.51196e+00 +4.70428e-01 17r+0.00000e+00
+2.14038e-09 +4.14354e-09 2r+0.00000e+00 +9.29943e-06
+.00000e+00 +3.88829e+00 2r+0.00000e+00 +3.26101e+00
+3.76294e-01 21r+0.00000e+00 +1.44061e-05 +.00000e+00
+3.88831e+00 2r+0.00000e+00 +3.41789e+00 +6.27274e-01
21r+0.00000e+00 +2.69680e-05 +.00000e+00 +3.88833e+00
+7.86228e-11 +.00000e+00 +3.26105e+00 +4.70408e-01
21r+0.00000e+00 +4.00550e-05 +.00000e+00 +3.88833e+00
+1.51864e-09 +4.94279e-04 +3.26104e+00 +6.27252e-01
21r+0.00000e+00 +8.47716e-05 +.00000e+00 +3.91326e+00
+.00000e+00 +1.27258e-01 +2.80613e+00 +6.27254e-01
21r+0.00000e+00 +1.76324e-04 +.00000e+00 +4.01849e+00
2r+0.00000e+00 +3.89106e+00 +1.10655e+00 21r+0.00000e+00
14** 5r+0.00000e+00 +6.23435e-01 27r+0.00000e+00 +2.08906e-01
+3.20293e-02 26r+0.00000e+00 +5.03688e-01 -4.23855e-02
+1.07109e-02 25r+0.00000e+00 +3.51035e-01 -5.65563e-02
+1.32351e-02 +8.83050e-04 24r+0.00000e+00 +3.36041e-01
-4.61429e-02 +.00000e+00 +1.31341e-02 +4.05641e-03
23r+0.00000e+00 +5.80957e-01 -1.04861e-01 2r+0.00000e+00
-3.84412e-03 +1.30084e-03 22r+0.00000e+00 +7.39651e-01
-2.93974e-01 3r+0.00000e+00 -7.70573e-04 -4.73653e-04
21r+0.00000e+00 +1.58249e-01 -9.87251e-03 4r+0.00000e+00
-2.83671e-04 -7.18408e-04 20r+0.00000e+00 +2.69510e-01
-2.19988e-01 5r+0.00000e+00 -5.59984e-04 -1.21800e-04
19r+0.00000e+00 +3.43953e-01 -3.20066e-01 6r+0.00000e+00
-1.67516e-04 -6.15982e-05 18r+0.00000e+00 +3.84462e-01
-3.04184e-01 7r+0.00000e+00 -3.41054e-05 -2.89016e-05
17r+0.00000e+00 +6.94094e-01 -2.94607e-01 8r+0.00000e+00
-8.11632e-06 -7.99925e-06 16r+0.00000e+00 +3.18899e-01
-5.85492e-01 -9.65195e-05 8r+0.00000e+00 -1.12567e-05
-1.14843e-05 15r+0.00000e+00 +3.39799e-01 -1.93755e-01
10r+0.00000e+00 -3.34227e-06 -3.14193e-06 14r+0.00000e+00
+3.48307e-01 -1.91965e-01 11r+0.00000e+00 -9.35278e-07
-1.08784e-06 13r+0.00000e+00 +3.51235e-01 -1.91577e-01
12r+0.00000e+00 -2.65458e-07 -2.79512e-07 12r+0.00000e+00
+2.76918e-01 -1.91583e-01 13r+0.00000e+00 -7.73265e-08
-9.58323e-08 11r+0.00000e+00 +3.54056e-01 -1.14802e-01
14r+0.00000e+00 -1.00355e-08 -1.36479e-08 10r+0.00000e+00
+3.54373e-01 -1.91214e-01 15r+0.00000e+00 -1.19418e-09
-6.09669e-09 9r+0.00000e+00 +3.06770e-01 -1.91169e-01

16r+0.00000e+00 +1.07625e-10 -1.65182e-09 8r+0.00000e+00
+2.78133e-01 -1.43356e-01 17r+0.00000e+00 -6.12855e-11
-2.70906e-11 7r+0.00000e+00 +3.54644e-01 -1.14665e-01
26r+0.00000e+00 +3.06849e-01 -1.91142e-01 24r+0.00000e+00
-6.93324e-11 +.00000e+00 +3.54647e-01 -1.43341e-01
24r+0.00000e+00 -1.51236e-09 +4.93749e-05 +3.54647e-01
-1.91134e-01 25r+0.00000e+00 -1.91903e-02 +3.19628e-01
-1.91135e-01 26r+0.00000e+00 +1.83887e-01 -1.50116e-01
21r+0.00000e+00
14** 5r+0.00000e+00 +4.36278e-01 27r+0.00000e+00 +1.22135e-01
+1.70794e-03 26r+0.00000e+00 +2.61655e-01 -1.62374e-02
26r+0.00000e+00 +2.26746e-01 +7.31554e-03 26r+0.00000e+00
+1.73966e-01 +8.58991e-04 26r+0.00000e+00 +6.82632e-01
+1.88525e-02 26r+0.00000e+00 +8.54147e-02 +2.92014e-02
26r+0.00000e+00 +8.20533e-02 -5.32649e-02 26r+0.00000e+00
-1.21491e-02 +8.83089e-03 26r+0.00000e+00 +4.54541e-04
-3.49706e-04 26r+0.00000e+00 +8.10013e-03 -6.64330e-03
26r+0.00000e+00 +2.15478e-02 -1.05901e-02 26r+0.00000e+00
+9.02446e-03 -2.25406e-02 +9.48538e-05 25r+0.00000e+00
+1.18399e-02 -8.79276e-03 26r+0.00000e+00 +1.27913e-02
-9.88794e-03 26r+0.00000e+00 +1.31484e-02 -1.01823e-02
26r+0.00000e+00 +9.26421e-03 -1.03320e-02 26r+0.00000e+00
+1.35114e-02 -6.26912e-03 26r+0.00000e+00 +1.35577e-02
-1.04644e-02 26r+0.00000e+00 +1.09559e-02 -1.04843e-02
26r+0.00000e+00 +9.38749e-03 -7.86704e-03 26r+0.00000e+00
+1.35890e-02 -6.29472e-03 26r+0.00000e+00 +1.09653e-02
-1.04939e-02 26r+0.00000e+00 +1.35899e-02 -7.86976e-03
26r+0.00000e+00 +1.35899e-02 -1.04940e-02 27r+0.00000e+00
-1.04939e-02 49r+0.00000e+00
14** 5r+0.00000e+00 +3.41641e-01 27r+0.00000e+00 +1.23238e-01
-1.26526e-03 26r+0.00000e+00 +1.76109e-01 +1.89478e-02
26r+0.00000e+00 +7.33683e-02 +1.43113e-03 26r+0.00000e+00
+4.11444e-02 -2.52456e-03 26r+0.00000e+00 +3.97154e-02
-3.98441e-03 26r+0.00000e+00 -9.63776e-03 -3.21950e-02
26r+0.00000e+00 +1.24107e-02 -2.35939e-02 26r+0.00000e+00
-8.16755e-04 +6.10343e-04 26r+0.00000e+00 -5.49794e-04
+5.50586e-04 26r+0.00000e+00 -2.65568e-04 +2.52954e-04
26r+0.00000e+00 -3.84918e-04 +1.62504e-04 26r+0.00000e+00
+1.26220e-07 +2.34052e-04 -9.28939e-05 25r+0.00000e+00
+1.21254e-04 -1.05779e-04 26r+0.00000e+00 +1.60887e-04
-1.62057e-04 26r+0.00000e+00 +1.79955e-04 -1.77207e-04
26r+0.00000e+00 +1.14220e-04 -1.88972e-04 26r+0.00000e+00

+1.95694e-04 -1.16881e-04 26r+0.00000e+00 +1.98426e-04
-1.96530e-04 26r+0.00000e+00 +1.49197e-04 -1.98314e-04
26r+0.00000e+00 +1.19819e-04 -1.48553e-04 26r+0.00000e+00
+1.99256e-04 -1.19011e-04 26r+0.00000e+00 +1.49695e-04
-1.98359e-04 26r+0.00000e+00 +1.99316e-04 -1.48765e-04
26r+0.00000e+00 +1.99318e-04 -1.98364e-04 27r+0.00000e+00
-1.98386e-04 49r+0.00000e+00
14** -1.51326e+00 +.00000e+00 +4.56758e+00 2r+0.00000e+00
+2.62047e+00 22r+0.00000e+00 -2.94625e-02 +.00000e+00
+4.15820e+00 2r+0.00000e+00 +2.07426e+00 +2.46037e-02
23r+0.00000e+00 +4.04134e+00 2r+0.00000e+00 +1.90134e+00
+9.09078e-02 +1.68632e-01 20r+0.00000e+00 +1.57339e-02
+.00000e+00 +4.62358e+00 2r+0.00000e+00 +2.62594e+00
+1.76646e-01 +2.79179e-01 +4.23325e-01 19r+0.00000e+00
+2.78805e-02 +.00000e+00 +5.57840e+00 2r+0.00000e+00
+3.90415e+00 +1.50619e-01 +4.42472e-01 +5.10921e-01
+5.13868e-01 18r+0.00000e+00 +4.81149e-02 +.00000e+00
+6.32547e+00 2r+0.00000e+00 +5.17018e+00 +1.59464e-01
+4.28446e-01 +5.67412e-01 +5.13228e-01 +3.95583e-01
17r+0.00000e+00 +8.12692e-02 +.00000e+00 +6.89593e+00
2r+0.00000e+00 +6.21263e+00 +6.31946e-01 +1.64981e-01
+5.96860e-01 +4.53756e-01 +3.51313e-01 +2.29115e-01
16r+0.00000e+00 +1.07856e-01 +.00000e+00 +7.25667e+00
2r+0.00000e+00 +7.00136e+00 +4.61083e-01 +4.57412e-01
+6.25438e-01 +6.32195e-01 +4.02145e-01 +2.78119e-01
+4.12151e-01 15r+0.00000e+00 +1.29642e-01 +.00000e+00
+7.23159e+00 2r+0.00000e+00 +6.87837e+00 +1.31845e-01
+8.62512e-02 +7.06080e-03 +2.70377e-01 +1.02311e-01
+5.84210e-02 +3.82304e-02 +2.42925e-01 14r+0.00000e+00
+1.62746e-01 +.00000e+00 +7.13206e+00 2r+0.00000e+00
+6.73319e+00 +2.23581e-01 +8.82558e-03 +3.50586e-02
+5.51470e-03 +1.69871e-01 +4.33173e-02 +2.39601e-02
+1.57140e-02 +1.82049e-01 13r+0.00000e+00 +2.19187e-01
+.00000e+00 +6.96433e+00 2r+0.00000e+00 +6.50665e+00
+2.36127e-01 +.00000e+00 +4.13509e-03 +1.26580e-02
+2.76702e-03 +1.03712e-01 +1.73574e-02 +9.41647e-03
+1.79259e-02 +3.99246e-01 12r+0.00000e+00 +2.84226e-01
+.00000e+00 +6.87801e+00 2r+0.00000e+00 +6.12671e+00
+2.38495e-01 2r+0.00000e+00 +9.98707e-04 +2.72864e-03
+9.70396e-04 +3.30784e-02 +4.15611e-03 +2.23201e-03
+5.43819e-03 +1.33299e-01 11r+0.00000e+00 +4.44182e-01
+.00000e+00 +6.77993e+00 2r+0.00000e+00 +6.18949e+00

+4.67074e-01 3r+0.00000e+00 +1.26473e-03 +3.27363e-03
+1.17217e-03 +6.20914e-02 +5.12387e-03 +2.73360e-03
+8.55885e-03 +2.25250e-01 10r+0.00000e+00 +8.24890e-01
+.00000e+00 +6.69019e+00 2r+0.00000e+00 +5.73226e+00
+1.46258e-01 4r+0.00000e+00 +2.99414e-04 +7.55658e-04
+2.61060e-04 +3.42379e-02 +1.17900e-03 +6.24607e-04
+2.93563e-03 +8.33991e-02 9r+0.00000e+00 +1.20282e+00
+.00000e+00 +6.49863e+00 2r+0.00000e+00 +5.17552e+00
+1.33040e-01 5r+0.00000e+00 +6.87066e-05 +1.72025e-04
+5.63977e-05 +7.78942e-03 +2.66951e-04 +1.40956e-04
+7.26619e-04 +2.09129e-02 8r+0.00000e+00 +1.46100e+00
+.00000e+00 +6.33874e+00 2r+0.00000e+00 +4.75867e+00
+1.20289e-01 6r+0.00000e+00 +1.56287e-05 +3.87290e-05
+1.15825e-05 +1.75404e-03 +5.99766e-05 +3.16192e-05
+1.62210e-04 +4.66631e-03 7r+0.00000e+00 +1.29391e+00
+.00000e+00 +1.02607e+01 2r+0.00000e+00 +8.87932e+00
+1.19069e-01 7r+0.00000e+00 +4.29138e-06 +1.03231e-05
+2.35191e-06 +4.64579e-04 +1.58673e-05 +8.35854e-06
+4.27756e-05 +1.23023e-03 6r+0.00000e+00 +4.48059e+00
+.00000e+00 +1.87552e+01 2r+0.00000e+00 +1.40783e+01
+8.75029e-02 8r+0.00000e+00 +2.83791e-07 +7.39260e-07
+6.46634e-08 +7.99143e-03 +1.10442e-06 +5.81537e-07
+2.97220e-06 +8.54695e-05 5r+0.00000e+00 +6.82966e+00
+.00000e+00 +1.58424e+01 2r+0.00000e+00 +8.88355e+00
+1.96260e-01 9r+0.00000e+00 +5.77365e-08 +1.74002e-07
+3.55685e-09 +3.97686e-03 +2.46524e-07 +1.29795e-07
+6.63169e-07 +1.90697e-05 4r+0.00000e+00 +1.19758e+01
+.00000e+00 +2.11899e+01 2r+0.00000e+00 +9.12918e+00
+1.29190e-01 10r+0.00000e+00 +1.17412e-08 +4.68719e-08
+.00000e+00 +9.87946e-04 +6.12378e-08 +3.22404e-08
+1.63957e-07 +4.73457e-06 3r+0.00000e+00 +2.39921e+00
+.00000e+00 +7.33081e+00 2r+0.00000e+00 +4.86199e+00
+8.49546e-02 11r+0.00000e+00 +9.05054e-10 +8.75599e-09
+.00000e+00 +1.41973e-04 +7.96103e-09 +3.19047e-09
+2.15235e-08 +6.80126e-07 2r+0.00000e+00 +1.19616e-01
+.00000e+00 +5.04036e+00 2r+0.00000e+00 +4.80270e+00
+6.96140e-02 15r+0.00000e+00 +9.86221e-06 2r+0.00000e+00
+7.33100e-10 +4.72477e-08 +.00000e+00 +9.95808e-01
+.00000e+00 +6.06196e+00 2r+0.00000e+00 +4.97334e+00
+1.18047e-01 16r+0.00000e+00 +2.44930e-06 3r+0.00000e+00
+1.16591e-08 +9.33226e+00 +.00000e+00 +1.47962e+01
2r+0.00000e+00 +5.32499e+00 +9.28088e-02 17r+0.00000e+00

+2.97822e-07 3r+0.00000e+00 +9.94455e+01 +.00000e+00
+1.06496e+02 2r+0.00000e+00 +6.82933e+00 +1.38946e-01
18r+0.00000e+00 +6.64513e-08 2r+0.00000e+00 +4.93914e+03
+.00000e+00 +4.96468e+03 2r+0.00000e+00 +2.55402e+01
+2.21575e-01 21r+0.00000e+00 +2.68224e+03 +.00000e+00
+2.69081e+03 2r+0.00000e+00 +8.56555e+00 22r+0.00000e+00
14** 5r+0.00000e+00 +2.28193e+00 27r+0.00000e+00 +1.53382e+00
+7.61297e-04 26r+0.00000e+00 +1.21237e+00 +9.90577e-04
26r+0.00000e+00 +1.60219e+00 -5.50923e-03 26r+0.00000e+00
+2.14663e+00 -9.88301e-04 26r+0.00000e+00 +2.32121e+00
+1.41067e-04 26r+0.00000e+00 +2.40278e+00 +6.13373e-03
-4.72475e-03 25r+0.00000e+00 +1.82089e+00 -1.12009e-02
-5.47264e-03 +2.11498e-03 24r+0.00000e+00 +1.14221e+00
-3.17197e-02 -2.98408e-04 +6.05210e-04 -7.80377e-04
23r+0.00000e+00 +7.06443e-01 -5.97511e-02 +7.38945e-05
-2.96718e-04 -1.04217e-04 -1.08723e-04 22r+0.00000e+00
+1.96446e-01 -7.35073e-02 +.00000e+00 -2.87541e-05
-1.62538e-04 +1.15888e-04 -1.36732e-04 21r+0.00000e+00
+1.93318e-01 -7.86220e-02 2r+0.00000e+00 -6.59618e-06
-6.99368e-05 -2.01561e-05 21r+0.00000e+00 +8.60018e-02
-1.53879e-01 3r+0.00000e+00 -1.10767e-05 -4.49396e-05
-3.12515e-05 20r+0.00000e+00 +7.89413e-02 -4.81054e-02
4r+0.00000e+00 -4.07938e-06 -1.55103e-05 -1.06218e-05
19r+0.00000e+00 +7.13330e-02 -4.38600e-02 5r+0.00000e+00
-1.41587e-06 -5.19808e-06 -3.63267e-06 18r+0.00000e+00
+6.82572e-02 -3.96578e-02 6r+0.00000e+00 -3.01986e-07
-1.72076e-06 -1.27246e-06 17r+0.00000e+00 +8.20453e-02
-3.90821e-02 7r+0.00000e+00 -2.40554e-07 -6.98791e-07
-5.93207e-07 16r+0.00000e+00 +1.37060e-01 -2.84131e-02
8r+0.00000e+00 -3.12329e-08 -8.42958e-08 -4.49773e-08
15r+0.00000e+00 +9.59822e-02 -5.16824e-02 9r+0.00000e+00
-1.10323e-08 -2.55869e-08 -3.26316e-09 14r+0.00000e+00
+8.30726e-02 -4.20746e-02 10r+0.00000e+00 -4.19975e-09
-1.01457e-08 14r+0.00000e+00 +5.24208e-02 -2.79612e-02
11r+0.00000e+00 -4.71053e-10 -2.16606e-09 13r+0.00000e+00
+6.83022e-02 -2.29233e-02 26r+0.00000e+00 +6.08565e-02
-3.88699e-02 26r+0.00000e+00 +7.83524e-02 -3.05546e-02
26r+0.00000e+00 +1.14652e-01 -4.56718e-02 26r+0.00000e+00
+1.54440e-01 -7.24788e-02 26r+0.00000e+00 +5.27805e-02
22r+0.00000e+00
14** 5r+0.00000e+00 +2.00387e+00 27r+0.00000e+00 +1.21886e+00
+8.67534e-05 26r+0.00000e+00 +8.93157e-01 -1.45523e-03

26r+0.00000e+00 +1.16714e+00 +1.46544e-03 26r+0.00000e+00
+1.38577e+00 +1.08911e-02 26r+0.00000e+00 +1.27956e+00
+7.69302e-03 26r+0.00000e+00 +8.64435e-01 -4.92164e-04
26r+0.00000e+00 +5.44046e-01 -5.85073e-03 26r+0.00000e+00
+3.11445e-01 -3.71806e-03 26r+0.00000e+00 +1.69332e-01
-4.59379e-03 26r+0.00000e+00 +2.25178e-02 -1.97760e-03
26r+0.00000e+00 +1.18954e-03 -5.53827e-04 26r+0.00000e+00
+4.36869e-04 -1.08327e-03 26r+0.00000e+00 +3.89797e-04
-3.34761e-04 26r+0.00000e+00 +3.58338e-04 -2.95276e-04
26r+0.00000e+00 +4.34121e-04 -2.72993e-04 26r+0.00000e+00
+5.75911e-04 -3.55518e-04 26r+0.00000e+00 +9.23780e-03
-4.31428e-04 26r+0.00000e+00 +6.86470e-04 -9.00774e-03
26r+0.00000e+00 +3.62167e-04 -5.41235e-04 26r+0.00000e+00
+2.47717e-04 -2.13683e-04 26r+0.00000e+00 +3.65768e-04
-1.68248e-04 26r+0.00000e+00 +3.09733e-04 -2.86475e-04
26r+0.00000e+00 +4.72583e-04 -2.28098e-04 26r+0.00000e+00
+9.27972e-04 -3.84535e-04 27r+0.00000e+00 -8.14360e-04
49r+0.00000e+00
14** 5r+0.00000e+00 +1.74072e+00 27r+0.00000e+00 +1.03081e+00
+2.03030e-04 26r+0.00000e+00 +6.74310e-01 +2.25142e-04
26r+0.00000e+00 +5.82016e-01 -2.02183e-03 26r+0.00000e+00
+3.79726e-01 -9.99004e-03 26r+0.00000e+00 +2.14829e-01
-6.71344e-03 26r+0.00000e+00 +5.82526e-02 -7.60693e-03
26r+0.00000e+00 +3.17467e-02 -1.02782e-02 26r+0.00000e+00
+1.84928e-02 -3.47690e-03 26r+0.00000e+00 +9.00146e-03
-3.30086e-03 26r+0.00000e+00 +1.03823e-03 -1.02238e-03
26r+0.00000e+00 +2.83077e-06 -2.03066e-06 26r+0.00000e+00
+9.51281e-07 -3.19113e-06 26r+0.00000e+00 +4.51064e-07
-1.30363e-06 26r+0.00000e+00 +5.52417e-07 -7.79834e-07
26r+0.00000e+00 +9.76460e-06 -8.46758e-07 26r+0.00000e+00
+2.10222e-05 -1.00364e-05 26r+0.00000e+00 +3.20659e-03
-2.15341e-05 26r+0.00000e+00 -3.73384e-05 -3.20742e-03
26r+0.00000e+00 +7.37864e-08 +3.68026e-05 26r+0.00000e+00
+3.53980e-07 -6.25725e-07 26r+0.00000e+00 +6.21078e-07
-6.28171e-07 26r+0.00000e+00 +4.41033e-07 -9.01403e-07
26r+0.00000e+00 +1.12439e-06 -7.17341e-07 26r+0.00000e+00
+8.24881e-06 -1.42491e-06 27r+0.00000e+00 -8.62516e-06
49r+0.00000e+00
14** +2.33807e-03 +.00000e+00 +4.58821e+00 2r+0.00000e+00
+3.16468e+00 22r+0.00000e+00 +4.97793e-03 +.00000e+00
+3.98562e+00 2r+0.00000e+00 +2.16818e+00 +3.02631e-02
21r+0.00000e+00 +7.20503e-02 +.00000e+00 +3.82548e+00

2r+0.00000e+00 +1.95097e+00 +1.31138e-01 +2.09414e-02
20r+0.00000e+00 +1.87095e-01 +.00000e+00 +4.31204e+00
2r+0.00000e+00 +2.74703e+00 +2.54970e-01 +1.69052e-01
+1.37748e-01 19r+0.00000e+00 +2.76544e-01 +.00000e+00
+5.36863e+00 2r+0.00000e+00 +4.41511e+00 +3.58176e-01
+3.96206e-01 +3.87186e-01 +3.15489e-01 18r+0.00000e+00
+3.10575e-01 +.00000e+00 +6.28125e+00 2r+0.00000e+00
+5.70751e+00 +2.75027e-01 +4.06666e-01 +4.57330e-01
+4.46922e-01 +3.64164e-01 17r+0.00000e+00 +2.83639e-01
+.00000e+00 +6.83293e+00 2r+0.00000e+00 +6.31431e+00
+2.31870e-01 +1.59122e-01 +3.01284e-01 +3.41034e-01
+3.33273e-01 +2.71559e-01 16r+0.00000e+00 +2.97547e-01
+.00000e+00 +7.20394e+00 2r+0.00000e+00 +6.77104e+00
+2.30843e-01 +2.43838e-02 +1.80707e-01 +2.52945e-01
+2.86317e-01 +2.79801e-01 +2.27989e-01 15r+0.00000e+00
+3.92001e-01 +.00000e+00 +7.21258e+00 2r+0.00000e+00
+6.57824e+00 +1.35155e-01 +2.28993e-03 +4.42581e-03
+3.32731e-02 +3.54312e-02 +4.01058e-02 +3.91931e-02
+3.19355e-02 14r+0.00000e+00 +5.09779e-01 +.00000e+00
+7.08459e+00 2r+0.00000e+00 +6.34503e+00 +2.42338e-01
+9.91533e-05 +1.08089e-03 +1.54613e-03 +1.61019e-02
+1.43763e-02 +1.62730e-02 +1.59027e-02 +1.29579e-02
13r+0.00000e+00 +6.61791e-01 +.00000e+00 +6.89524e+00
2r+0.00000e+00 +6.01664e+00 +2.29785e-01 +.00000e+00
+6.04173e-05 +4.62435e-04 +5.87517e-04 +7.30225e-03
+5.61304e-03 +6.35359e-03 +6.20900e-03 +5.05926e-03
12r+0.00000e+00 +7.73218e-01 +.00000e+00 +6.75335e+00
2r+0.00000e+00 +5.56060e+00 +2.16806e-01 2r+0.00000e+00
+1.47527e-05 +1.17557e-04 +1.36917e-04 +1.91959e-03
+1.32593e-03 +1.50086e-03 +1.46670e-03 +1.19511e-03
11r+0.00000e+00 +9.34776e-01 +.00000e+00 +6.60172e+00
2r+0.00000e+00 +5.53690e+00 +4.19535e-01 3r+0.00000e+00
+1.81891e-05 +1.43381e-04 +1.65801e-04 +2.58542e-03
+1.62026e-03 +1.83402e-03 +1.79228e-03 +1.46040e-03
10r+0.00000e+00 +1.16813e+00 +.00000e+00 +6.50810e+00
2r+0.00000e+00 +5.21507e+00 +1.30046e-01 4r+0.00000e+00
+4.19041e-06 +3.26453e-05 +3.59075e-05 +7.14040e-04
+3.69336e-04 +4.18064e-04 +4.08550e-04 +3.32897e-04
9r+0.00000e+00 +1.40282e+00 +.00000e+00 +6.63965e+00
2r+0.00000e+00 +5.11359e+00 +1.24897e-01 5r+0.00000e+00
+9.50453e-07 +7.36538e-06 +8.02049e-06 +1.60921e-04
+8.32547e-05 +9.42387e-05 +9.20941e-05 +7.50407e-05

8r+0.00000e+00 +1.75164e+00 +.00000e+00 +6.96009e+00
2r+0.00000e+00 +5.08467e+00 +1.23238e-01 6r+0.00000e+00
+2.14081e-07 +1.65650e-06 +1.80441e-06 +4.15616e-05
+1.86658e-05 +2.11284e-05 +2.06476e-05 +1.68242e-05
7r+0.00000e+00 +2.69711e+00 +.00000e+00 +7.95104e+00
2r+0.00000e+00 +5.17891e+00 +1.23778e-01 7r+0.00000e+00
+5.69706e-08 +4.41773e-07 +4.83403e-07 +1.62006e-05
+4.93297e-06 +5.58379e-06 +5.45672e-06 +4.44628e-06
6r+0.00000e+00 +4.41257e+00 +.00000e+00 +9.70833e+00
2r+0.00000e+00 +5.17002e+00 +7.50251e-02 8r+0.00000e+00
+4.04321e-09 +3.17056e-08 +3.45120e-08 +1.12678e-06
+3.43158e-07 +3.88431e-07 +3.79592e-07 +3.09302e-07
5r+0.00000e+00 +6.47348e+00 +.00000e+00 +1.18004e+01
2r+0.00000e+00 +5.20041e+00 +1.25743e-01 9r+0.00000e+00
+7.53851e-10 +7.49486e-09 +7.42976e-09 +2.51514e-07
+7.65878e-08 +8.66923e-08 +8.47194e-08 +6.90315e-08
4r+0.00000e+00 +1.03461e+01 +.00000e+00 +1.56532e+01
2r+0.00000e+00 +5.21549e+00 +1.26465e-01 11r+0.00000e+00
+1.44489e-09 +1.50472e-09 +6.17903e-08 +1.90237e-08
+2.15335e-08 +2.10435e-08 +1.71468e-08 3r+0.00000e+00
+3.69010e+01 +.00000e+00 +4.45409e+01 2r+0.00000e+00
+7.59612e+00 +9.16285e-02 14r+0.00000e+00 +7.60306e-09
+1.17183e-09 +1.32644e-09 +1.29625e-09 +1.05622e-09
2r+0.00000e+00 +7.91427e-01 +.00000e+00 +4.28871e+00
2r+0.00000e+00 +3.39955e+00 +4.37574e-02 21r+0.00000e+00
+1.81667e+01 +.00000e+00 +2.18929e+01 2r+0.00000e+00
+3.64617e+00 +9.77316e-02 16r+0.00000e+00 +1.25192e-09
4r+0.00000e+00 +4.18903e+01 +.00000e+00 +4.51148e+01
2r+0.00000e+00 +3.13256e+00 +8.00752e-02 21r+0.00000e+00
+2.16304e+00 +.00000e+00 +5.79010e+00 2r+0.00000e+00
+3.52636e+00 +9.19122e-02 21r+0.00000e+00 +5.29591e+00
+.00000e+00 +8.98790e+00 2r+0.00000e+00 +3.69199e+00
+1.00698e-01 21r+0.00000e+00 +1.05989e+01 +.00000e+00
+1.43117e+01 2r+0.00000e+00 +3.71281e+00 22r+0.00000e+00
14** 5r+0.00000e+00 +3.13029e-02 27r+0.00000e+00 +4.65348e-02
-1.24531e-02 26r+0.00000e+00 +3.86620e-02 -3.29578e-02
26r+0.00000e+00 +5.88381e-02 -2.63970e-02 26r+0.00000e+00
+7.86285e-02 -3.93163e-02 -3.22972e-06 25r+0.00000e+00
+8.93125e-02 -4.78000e-02 -1.22265e-03 25r+0.00000e+00
+1.12042e-01 -5.38697e-02 -4.68204e-04 25r+0.00000e+00
+9.48453e-02 -7.30389e-02 +2.52002e-04 -6.70610e-04
24r+0.00000e+00 +1.22539e-01 -5.36612e-02 +6.66270e-05

-6.82563e-05 -3.29861e-05 23r+0.00000e+00 +1.15686e-01
-8.19241e-02 +2.92127e-06 -1.25739e-05 -1.84281e-05
-1.06339e-05 22r+0.00000e+00 +1.08624e-01 -7.65321e-02
+.00000e+00 -2.03115e-07 -1.16400e-06 -9.11752e-06
-5.21513e-06 21r+0.00000e+00 +1.73890e-01 -7.14990e-02
2r+0.00000e+00 -9.65326e-08 -1.45768e-06 -2.61997e-06
-1.49024e-06 20r+0.00000e+00 +7.65294e-02 -1.38272e-01
3r+0.00000e+00 -1.49873e-07 -2.22550e-06 -4.65105e-06
-2.24189e-06 19r+0.00000e+00 +7.29499e-02 -4.27767e-02
4r+0.00000e+00 -5.09479e-08 -7.42932e-07 -2.21087e-06
-7.38935e-07 18r+0.00000e+00 +7.18016e-02 -4.11459e-02
5r+0.00000e+00 -1.69089e-08 -2.44399e-07 -2.70771e-07
-2.42046e-07 17r+0.00000e+00 +7.18062e-02 -4.06116e-02
6r+0.00000e+00 -5.54132e-09 -7.97440e-08 -8.79743e-08
-7.91213e-08 16r+0.00000e+00 +5.60077e-02 -4.07848e-02
7r+0.00000e+00 -2.26134e-09 -3.23551e-08 -3.55621e-08
-3.26560e-08 15r+0.00000e+00 +7.29506e-02 -2.47160e-02
8r+0.00000e+00 -2.74166e-10 -3.89407e-09 -3.92512e-09
-4.11747e-09 14r+0.00000e+00 +7.33681e-02 -4.14093e-02
9r+0.00000e+00 -6.85938e-11 -1.18132e-09 -1.13461e-09
-1.32052e-09 13r+0.00000e+00 +6.20308e-02 -4.16418e-02
11r+0.00000e+00 -3.22057e-10 -2.80052e-10 -1.79110e-10
12r+0.00000e+00 +5.96748e-02 -3.05098e-02 26r+0.00000e+00
+5.00148e-02 -1.41725e-02 26r+0.00000e+00 +4.47826e-02
-2.91853e-02 26r+0.00000e+00 +4.65193e-02 -2.25895e-02
26r+0.00000e+00 +4.84826e-02 -2.73147e-02 26r+0.00000e+00
+2.19884e-02 -2.68802e-02 26r+0.00000e+00 +2.20949e-02
22r+0.00000e+00

14** 5r+0.00000e+00 +3.56556e-04 27r+0.00000e+00 +5.44568e-04
-3.05957e-04 26r+0.00000e+00 +3.54387e-04 -5.07938e-04
26r+0.00000e+00 +5.37608e-04 -3.22129e-04 26r+0.00000e+00
+4.93263e-04 -4.91912e-04 26r+0.00000e+00 +5.31165e-04
-4.21355e-04 26r+0.00000e+00 +6.26577e-04 -4.36990e-04
26r+0.00000e+00 +4.97741e-04 -5.21830e-04 26r+0.00000e+00
+6.71747e-04 -3.86793e-04 26r+0.00000e+00 +6.23697e-04
-5.62404e-04 26r+0.00000e+00 +5.87261e-04 -5.18301e-04
26r+0.00000e+00 +1.03701e-03 -4.87327e-04 26r+0.00000e+00
+3.86414e-04 -9.41138e-04 26r+0.00000e+00 +3.80154e-04
-2.95557e-04 26r+0.00000e+00 +3.74581e-04 -2.94550e-04
26r+0.00000e+00 +3.79547e-04 -2.90630e-04 26r+0.00000e+00
+2.63364e-04 -2.96053e-04 26r+0.00000e+00 +3.84724e-04
-1.79138e-04 26r+0.00000e+00 +3.86089e-04 -2.99825e-04

```
   26r+0.00000e+00    +4.16834e-04    -3.00695e-04 26r+0.00000e+00
     +2.34865e-04    -3.32156e-04 26r+0.00000e+00    +3.33179e-04
     -1.44688e-04 26r+0.00000e+00    -8.68080e-04    -2.77015e-04
   26r+0.00000e+00    +2.63013e-04    +9.29629e-04 26r+0.00000e+00
     +2.65954e-04    -2.07868e-04 27r+0.00000e+00    -2.07546e-04
   49r+0.00000e+00
14**  5r+0.00000e+00    +4.81009e-06 27r+0.00000e+00    +3.30530e-06
     -4.82424e-06 26r+0.00000e+00    +1.64500e-06    -3.30973e-06
   26r+0.00000e+00    +1.49279e-06    -1.65109e-06 26r+0.00000e+00
     +7.17867e-07    -1.50459e-06 26r+0.00000e+00    +1.69431e-06
     -7.24386e-07 26r+0.00000e+00    +1.72855e-06    -1.71175e-06
   26r+0.00000e+00    +1.41343e-06    -1.75333e-06 26r+0.00000e+00
     +1.72796e-06    -1.43830e-06 26r+0.00000e+00    +1.49681e-06
     -1.74069e-06 26r+0.00000e+00    +1.53818e-06    -1.51352e-06
   26r+0.00000e+00    +2.97909e-06    -1.55089e-06 26r+0.00000e+00
     +8.82337e-07    -3.00178e-06 26r+0.00000e+00    +8.27434e-07
     -9.03008e-07 26r+0.00000e+00    +1.07027e-06    -8.43488e-07
   26r+0.00000e+00    +1.07197e-06    -1.09011e-06 26r+0.00000e+00
     +5.25024e-07    -1.08916e-06 26r+0.00000e+00    +8.70291e-07
     -5.45039e-07 26r+0.00000e+00    +1.15855e-06    -8.81177e-07
   26r+0.00000e+00    +3.52312e-06    -1.17776e-06 26r+0.00000e+00
     +7.66101e-08    -3.53545e-06 26r+0.00000e+00    +3.24751e-07
     -9.35408e-08 26r+0.00000e+00    -6.65119e-05    -3.35728e-07
   26r+0.00000e+00    +7.11654e-07    +6.65008e-05 26r+0.00000e+00
     +6.80182e-07    -7.22405e-07 27r+0.00000e+00    -6.92759e-07
   49r+0.00000e+00
14** 448r+0.00000e+00    +1.14756e+00    +.00000e+00    +1.14756e+00
   25r+0.00000e+00    +6.49561e+00    +.00000e+00    +6.49561e+00
   25r+0.00000e+00    +6.51133e+00    +.00000e+00    +6.51133e+00
   25r+0.00000e+00    +9.16486e+00    +.00000e+00    +9.16486e+00
   25r+0.00000e+00    +8.28887e+00    +.00000e+00    +8.28887e+00
   25r+0.00000e+00    +5.30738e+01    +.00000e+00    +5.30738e+01
   25r+0.00000e+00    +8.45222e+01    +.00000e+00    +8.45222e+01
   25r+0.00000e+00    +2.13587e+03    +.00000e+00    +2.13587e+03
   25r+0.00000e+00    +1.25329e+02    +.00000e+00    +1.25329e+02
   25r+0.00000e+00    +1.08769e+02    +.00000e+00    +1.08769e+02
   25r+0.00000e+00    +1.97672e+02    +.00000e+00    +1.97672e+02
   25r+0.00000e+00
14**   756r0.00000e+00
14**   756r0.00000e+00
14**   756r0.00000e+00
14**   756r0.00000e+00
```

14** 756r0.00000e+00
14** 756r0.00000e+00
14** 756r0.00000e+00
14** 756r0.00000e+00
14** 756r0.00000e+00
14** 756r0.00000e+00
14** 756r0.00000e+00
14** 756r0.00000e+00
14** 756r0.00000e+00
14** 756r0.00000e+00
14** 756r0.00000e+00
14** 756r0.00000e+00
14** 756r0.00000e+00
14** 756r0.00000e+00
14** 756r0.00000e+00
14** 756r0.00000e+00
14** 756r0.00000e+00
14** 756r0.00000e+00
14** 756r0.00000e+00
14** 756r0.00000e+00
14** 756r0.00000e+00
14** 756r0.00000e+00
14** 756r0.00000e+00
14** 756r0.00000e+00
14** 756r0.00000e+00
14** 756r0.00000e+00
14** 756r0.00000e+00
14** 756r0.00000e+00
14** 756r0.00000e+00
14** 756r0.00000e+00
14** 756r0.00000e+00
14** 756r0.00000e+00
14** 756r0.00000e+00
14** 756r0.00000e+00
14** 756r0.00000e+00
14** 756r0.00000e+00
14** 756r0.00000e+00
14** 756r0.00000e+00
14** 756r0.00000e+00
14** 756r0.00000e+00
14** 756r0.00000e+00
14** 756r0.00000e+00
14** 756r0.00000e+00
14** 756r0.00000e+00
14** 756r0.00000e+00
14** 756r0.00000e+00

```
14**   756r0.00000e+00
14**   756r0.00000e+00
14**   756r0.00000e+00
14**   756r0.00000e+00
14**   756r0.00000e+00
14**   756r0.00000e+00
14**   756r0.00000e+00
14**   756r0.00000e+00
14**   756r0.00000e+00
14**   756r0.00000e+00
14**   756r0.00000e+00
14**   756r0.00000e+00
14**   756r0.00000e+00
14**   756r0.00000e+00
14**   756r0.00000e+00
14**   756r0.00000e+00
14**   756r0.00000e+00
14**   756r0.00000e+00
14**   756r0.00000e+00
14**   756r0.00000e+00
14**   756r0.00000e+00
14**   756r0.00000e+00
14**   756r0.00000e+00
14**   756r0.00000e+00
14**   756r0.00000e+00
14**   756r0.00000e+00
14**   756r0.00000e+00
14**   756r0.00000e+00
14**   756r0.00000e+00
14**   756r0.00000e+00
14**   756r0.00000e+00
14**   756r0.00000e+00
14**   756r0.00000e+00
14**   756r0.00000e+00
  t
```

C.3 DORT Input for 6 MeV Run on $Al/AlF_3/LiF$ Geometry

```
Electron Accelerator Experiment pnv8f10p
' Unperturbed Flux
' Varitron June 15, 1995.    6 MeV.
' Library from pnvgip1
' Nominal 8 MeV Source
' Add polyethylene envelope
'
61$$  0  0  8  0 19  0  0  0  0  0
     0  e
62$$   0  3  14 110 148  27   3   6  30   0
      14  64  64   0 166   1   1   0   0   0
       1  99  99   2   0   1   1   0   0   3
       0   0   0   0   0  14   0   1   1   0
       0   0   0  11   0   0   1   1   1   1
       4 100   2   0   5 101   1   0   0   0
       1   2   0   0   0   4  27   0   0   0e
63** 0.0 1.0 0.001 0.001 0.0 0.0 0.0 0.0 0.0 0.0
    1.0 1.0 -1.0 0.3 1.2 3.0-2 1.0-4 0.0 0.3 0.5
    1.0 0.6 0.0 1.0e-30 0.0 0.001 0.1 0.9 e
 t
 t
/ u 166 upward bias
82*
                                                0 -22698- 5
0 -14889- 5 0 +14889- 5 0 -50167- 5 0 -43340- 5 0 -14888- 5 0 +14888- 5
0 +43340- 5 0 -73377- 5 0 -67942- 5 0 -43340- 5 0 -14888- 5 0 +14888- 5
0 +43340- 5 0 +67942- 5 0 -90121- 5 0 -86507- 5 0 -67941- 5 0 -43340- 5
0 -14887- 5 0 +14887- 5 0 +43340- 5 0 +67941- 5 0 +86507- 5 0 -98886- 5
0 -97391- 5 0 -86506- 5 0 -67941- 5 0 -43340- 5 0 -14887- 5 0 +14887- 5
0 +43340- 5 0 +67941- 5 0 +86506- 5 0 +97391- 5
0 -25298- 6 0 -19937- 6 0 -46106- 7 0 -22051- 7 0 -66232- 8 0 +66232- 8
0 +22051- 7 0 +46106- 7 0 +19937- 6 0 -57248- 6 0 -45113- 6 0 -10433- 6
0 -49897- 7 0 -14987- 7 0 +14987- 7 0 +49897- 7 0 +10433- 6 0 +45113- 6
0 -89576- 6 0 -70587- 6 0 -16324- 6 0 -78072- 7 0 -23450- 7 0 +23450- 7
0 +78072- 7 0 +16324- 6 0 +70587- 6 0 -12192- 5 0 -96074- 6 0 -22218- 6
0 -10626- 6 0 -31917- 7 0 +31917- 7 0 +10626- 6 0 +22218- 6 0 +96074- 6
0 -15413- 5 0 -12146- 5 0 -28089- 6 0 -13434- 6 0 -40350- 7 0 +40350- 7
0 +13434- 6 0 +28089- 6 0 +12146- 5 0 -18621- 5 0 -14674- 5 0 -33934- 6
```

0 -16230- 6 0 -48747- 7 0 +48747- 7 0 +16230- 6 0 +33934- 6 0 +14674- 5
0 -21808- 5 0 -17185- 5 0 -39743- 6 0 -19008- 6 0 -57091- 7 0 +57091- 7
0 +19008- 6 0 +39743- 6 0 +17185- 5 0 -24971- 5 0 -19678- 5 0 -45507- 6
0 -21764- 6 0 -65371- 7 0 +65371- 7 0 +21764- 6 0 +45507- 6 0 +19678- 5
0 -28110- 5 0 -22151- 5 0 -51226- 6 0 -24500- 6 0 -73587- 7 0 +73587- 7
0 +24500- 6 0 +51226- 6 0 +22151- 5 0 -31216- 5 0 -24598- 5 0 -56887- 6
0 -27207- 6 0 -81719- 7 0 +81719- 7 0 +27207- 6 0 +56887- 6 0 +24598- 5
0 -34291- 5 0 -27021- 5 0 -62490- 6 0 -29887- 6 0 -89768- 7 0 +89768- 7
0 +29887- 6 0 +62490- 6 0 +27021- 5 0 -50167- 5 0 -43340- 5 0 -14888- 5
0 +14888- 5 0 +43340- 5 0 -73377- 5 0 -67942- 5 0 -43340- 5 0 -14888- 5
0 +14888- 5 0 +43340- 5 0 +67942- 5 0 -90121- 5 0 -86507- 5 0 -67941- 5
0 -43340- 5 0 -14887- 5 0 +14887- 5 0 +43340- 5 0 +67941- 5 0 +86507- 5
0 -98886- 5 0 -97391- 5 0 -86506- 5 0 -67941- 5 0 -43340- 5 0 -14887- 5
0 +14887- 5 0 +43340- 5 0 +67941- 5 0 +86506- 5 0 +97391- 5
83*
3r-97390- 5 5r-86506- 5 7r-67940- 5
9r-43339- 511r-14887- 5
9r+99968- 5 9r+99836- 5 9r+99598- 5 9r+99254- 5 9r+98805- 5 9r+98251- 5
9r+97593- 5 9r+96832- 5 9r+95968- 5 9r+95003- 5 9r+93937- 5 5r+86506- 5
7r+67940- 5 9r+43339- 511r+14887- 5
81*
0 + 0+ 0 2r+16672- 6 0 + 0+ 0 0 +24447- 6
2r+12924- 6 0 +24447- 6 0 + 0+ 0 0 +27017- 6 0 +85519- 7 2r+19214- 6
0 +85519- 7 0 +27017- 6 0 + 0+ 0 0 +24447- 6 0 +85519- 7 0 +27474- 6
2r+68585- 7 0 +27474- 6 0 +85519- 7 0 +24447- 6 0 + 0+ 0 0 +16672- 6
0 +12924- 6 0 +19215- 6 0 +68586- 7 2r+18229- 6 0 +68586- 7 0 +19215- 6
0 +12924- 6 0 +16672- 6
0 + 0+ 0 0 +16682- 8 0 +15365- 9 0 +87799-10 2r+65851-10 0 +87799-10
0 +15365- 9 0 +16682- 8 0 + 0+ 0 0 +39065- 8 0 +35981- 9 0 +20560- 9
2r+15421- 9 0 +20560- 9 0 +35981- 9 0 +39065- 8 0 + 0+ 0 0 +61448- 8
0 +56597- 9 0 +32341- 9 2r+24256- 9 0 +32341- 9 0 +56597- 9 0 +61448- 8
0 + 0+ 0 0 +83620- 8 0 +77018- 9 0 +44010- 9 2r+33008- 9 0 +44010- 9
0 +77018- 9 0 +83620- 8 0 + 0+ 0 0 +10579- 7 0 +97439- 9 0 +55680- 9
2r+41761- 9 0 +55680- 9 0 +97439- 9 0 +10579- 7 0 + 0+ 0 0 +12776- 7
0 +11767- 8 0 +67240- 9 2r+50431- 9 0 +67240- 9 0 +11767- 8 0 +12776- 7
0 + 0+ 0 0 +14971- 7 0 +13789- 8 0 +78795- 9 2r+59097- 9 0 +78795- 9
0 +13789- 8 0 +14971- 7 0 + 0+ 0 0 +17146- 7 0 +15793- 8 0 +90244- 9
2r+67684- 9 0 +90244- 9 0 +15793- 8 0 +17146- 7 0 + 0+ 0 0 +19301- 7
0 +17777- 8 0 +10158- 8 2r+76187- 9 0 +10158- 8 0 +17777- 8 0 +19301- 7
0 + 0+ 0 0 +21454- 7 0 +19760- 8 0 +11291- 8 2r+84688- 9 0 +11291- 8
0 +19760- 8 0 +21454- 7 0 + 0+ 0 0 +23566- 7 0 +21705- 8 0 +12403- 8
2r+93024- 9 0 +12403- 8 0 +21705- 8 0 +23566- 7 0 + 0+ 0 0 +24447- 6

```
2r+12924- 6 0 +24447- 6 0 +    0+ 0 0 +27017- 6 0 +85519- 7 2r+19214- 6
0 +85519- 7 0 +27017- 6 0 +    0+ 0 0 +24447- 6 0 +85519- 7 0 +27474- 6
2r+68585- 7 0 +27474- 6 0 +85519- 7 0 +24447- 6 0 +    0+ 0 0 +16672- 6
0 +12924- 6 0 +19215- 6 0 +68586- 7 2r+18229- 6 0 +68586- 7 0 +19215- 6
0 +12924- 6 0 +16672- 6
 t
1**  f0.0
2**  1i0.0 19i0.3175
    1i9.8425 3i10.16 7i10.2108 3i10.236 i59i10.2868 3i40.2868
    7i40.3396 3i40.3648 23i40.4176 7i70.2868 72.8268
4**  19i0.0 3i1.27 24i1.3208 14i4.0328 11i5.7032 1i6.9850 23i7.3025
    7i19.5441 22.0841
'
'  1    Lucite
'  5    D2O
'  9    Void
' 13    Cadmium
' 17    Indium
' 21    Aluminum 100%
' 25    AlF3 100%
' 29    Teflon (CF2) 100%
' 33    Al-AlF3 (+LiF)  30%-69%-1% (VTT)
' 37    Al-Teflon 50%-50%
' 41    Cu63-65   69.17%-30.83%
' 45    W182-183-184-186   26.3% 14.28% 30.7% 28.6%
' 49    Gold 100%
' 53    Lead
' 57    Upstream Indium
' 61    Lithiated Poly
'
9$$  1 5 5 5 9   9  9 53 33 9   9  9 61 61
31$$ 1 2 3 4 5 6 7 8 9 10 11 12 13 14
32**  0.0     0.0     0.0     0.0     0.0     0.0     0.0
    7.3025  0.0     0.0     0.0     0.0    19.5441  0.0
33**  7.3025  6.9850  5.7032  4.0328 22.0841  1.3208  1.27
   22.0841 19.5441 19.5441  1.3208  1.27   22.0841 22.0841
34**  0.0    0.3175  0.3175  0.3175 10.16   10.16   10.2108
    0.0    10.2868 40.2868 40.2868 40.3396 10.2868 70.2868
35** 10.16   9.8425  9.8425  9.8425 10.2868 10.2868 10.236
   10.16   40.2868 70.2868 40.4176 40.3648 70.2868 72.8268
 t
96**  49r0.8135 15r0.1637 12r0.0228 f0.0
```

t
97** 2r0.0 20r1.0 f0.0
t
98**
.00000e+00
.00000e+00
.00000e+00
1.15566e+10
2.16707e+10
2.03474e+10
1.45454e+10
2.94866e+10
1.20222e+10
6.07141e+09
2.80555e+09
1.70160e+09
1.21903e+09
4.39057e+08
5.09150e+08
2.40505e+08
1.13607e+08
7.25672e+07
1.53750e+07
7.26262e+06
4.10999e+06
1.70662e+06
3.61582e+05
2.04625e+05
6.28336e+04
2.96813e+04
2.01532e+04
t

C.4 DORT Input for 6 MeV Run on Aluminum/Teflon Geometry

```
Electron Accelerator Experiment pnv8t33p
' Indium (Cd) Upstream (T=0.013)
' Indium (Cd) Downstream (3xT=0.013, 1xT=0.025)
' Copper  After Indium (T=0.05096)
' Varitron Nov 21, 1995.   Nominal 6 MeV.
' Library from pnvgip1
' Nominal 8 MeV Source
' Add Polyethylene Reflector
'
61$$  0  0  8  0 19  0  0  0  0  0
    0  e
62$$   0  3  18 110 172  27   3   6  30   0
     18  68  68   0 166   1   1   0   0   0
      1  99  99   2   0   1   1   0   0   3
      0   0   0   0   0  18   0   1   1   0
      0   0   0  11   0   0   1   1   1   1
      4 100   2   0   5 101   1   0   0   0
      1   2   0   0   0   4  27   0   0   0e
63** 0.0 1.0 0.001 0.001 0.0 0.0 0.0 0.0 0.0 0.0
   1.0 1.0 -1.0 0.3 1.2 3.0-2 1.0-4 0.0 0.3 0.5
   1.0 0.6 0.0 1.0e-30 0.0 0.001 0.1 0.9 e
 t
 t
/ u 166 upward bias
82*
                                        0 -22698- 5
0 -14889- 5 0 +14889- 5 0 -50167- 5 0 -43340- 5 0 -14888- 5 0 +14888- 5
0 +43340- 5 0 -73377- 5 0 -67942- 5 0 -43340- 5 0 -14888- 5 0 +14888- 5
0 +43340- 5 0 +67942- 5 0 -90121- 5 0 -86507- 5 0 -67941- 5 0 -43340- 5
0 -14887- 5 0 +14887- 5 0 +43340- 5 0 +67941- 5 0 +86507- 5 0 -98886- 5
0 -97391- 5 0 -86506- 5 0 -67941- 5 0 -43340- 5 0 -14887- 5 0 +14887- 5
0 +43340- 5 0 +67941- 5 0 +86506- 5 0 +97391- 5
0 -25298- 6 0 -19937- 6 0 -46106- 7 0 -22051- 7 0 -66232- 8 0 +66232- 8
0 +22051- 7 0 +46106- 7 0 +19937- 6 0 -57248- 6 0 -45113- 6 0 -10433- 6
0 -49897- 7 0 -14987- 7 0 +14987- 7 0 +49897- 7 0 +10433- 6 0 +45113- 6
0 -89576- 6 0 -70587- 6 0 -16324- 6 0 -78072- 7 0 -23450- 7 0 +23450- 7
0 +78072- 7 0 +16324- 6 0 +70587- 6 0 -12192- 5 0 -96074- 6 0 -22218- 6
0 -10626- 6 0 -31917- 7 0 +31917- 7 0 +10626- 6 0 +22218- 6 0 +96074- 6
```

0 -15413- 5 0 -12146- 5 0 -28089- 6 0 -13434- 6 0 -40350- 7 0 +40350- 7
0 +13434- 6 0 +28089- 6 0 +12146- 5 0 -18621- 5 0 -14674- 5 0 -33934- 6
0 -16230- 6 0 -48747- 7 0 +48747- 7 0 +16230- 6 0 +33934- 6 0 +14674- 5
0 -21808- 5 0 -17185- 5 0 -39743- 6 0 -19008- 6 0 -57091- 7 0 +57091- 7
0 +19008- 6 0 +39743- 6 0 +17185- 5 0 -24971- 5 0 -19678- 5 0 -45507- 6
0 -21764- 6 0 -65371- 7 0 +65371- 7 0 +21764- 6 0 +45507- 6 0 +19678- 5
0 -28110- 5 0 -22151- 5 0 -51226- 6 0 -24500- 6 0 -73587- 7 0 +73587- 7
0 +24500- 6 0 +51226- 6 0 +22151- 5 0 -31216- 5 0 -24598- 5 0 -56887- 6
0 -27207- 6 0 -81719- 7 0 +81719- 7 0 +27207- 6 0 +56887- 6 0 +24598- 5
0 -34291- 5 0 -27021- 5 0 -62490- 6 0 -29887- 6 0 -89768- 7 0 +89768- 7
0 +29887- 6 0 +62490- 6 0 +27021- 5 0 -50167- 5 0 -43340- 5 0 -14888- 5
0 +14888- 5 0 +43340- 5 0 -73377- 5 0 -67942- 5 0 -43340- 5 0 -14888- 5
0 +14888- 5 0 +43340- 5 0 +67942- 5 0 -90121- 5 0 -86507- 5 0 -67941- 5
0 -43340- 5 0 -14887- 5 0 +14887- 5 0 +43340- 5 0 +67941- 5 0 +86507- 5
0 -98886- 5 0 -97391- 5 0 -86506- 5 0 -67941- 5 0 -43340- 5 0 -14887- 5
0 +14887- 5 0 +43340- 5 0 +67941- 5 0 +86506- 5 0 +97391- 5
83*
3r-97390- 5 5r-86506- 5 7r-67940- 5
9r-43339- 511r-14887- 5
9r+99968- 5 9r+99836- 5 9r+99598- 5 9r+99254- 5 9r+98805- 5 9r+98251- 5
9r+97593- 5 9r+96832- 5 9r+95968- 5 9r+95003- 5 9r+93937- 5 5r+86506- 5
7r+67940- 5 9r+43339- 511r+14887- 5
81*
0 + 0+ 0 2r+16672- 6 0 + 0+ 0 0 +24447- 6
2r+12924- 6 0 +24447- 6 0 + 0+ 0 0 +27017- 6 0 +85519- 7 2r+19214- 6
0 +85519- 7 0 +27017- 6 0 + 0+ 0 0 +24447- 6 0 +85519- 7 0 +27474- 6
2r+68585- 7 0 +27474- 6 0 +85519- 7 0 +24447- 6 0 + 0+ 0 0 +16672- 6
0 +12924- 6 0 +19215- 6 0 +68586- 7 2r+18229- 6 0 +68586- 7 0 +19215- 6
0 +12924- 6 0 +16672- 6
0 + 0+ 0 0 +16682- 8 0 +15365- 9 0 +87799-10 2r+65851-10 0 +87799-10
0 +15365- 9 0 +16682- 8 0 + 0+ 0 0 +39065- 8 0 +35981- 9 0 +20560- 9
2r+15421- 9 0 +20560- 9 0 +35981- 9 0 +39065- 8 0 + 0+ 0 0 +61448- 8
0 +56597- 9 0 +32341- 9 2r+24256- 9 0 +32341- 9 0 +56597- 9 0 +61448- 8
0 + 0+ 0 0 +83620- 8 0 +77018- 9 0 +44010- 9 2r+33008- 9 0 +44010- 9
0 +77018- 9 0 +83620- 8 0 + 0+ 0 0 +10579- 7 0 +97439- 9 0 +55680- 9
2r+41761- 9 0 +55680- 9 0 +97439- 9 0 +10579- 7 0 + 0+ 0 0 +12776- 7
0 +11767- 8 0 +67240- 9 2r+50431- 9 0 +67240- 9 0 +11767- 8 0 +12776- 7
0 + 0+ 0 0 +14971- 7 0 +13789- 8 0 +78795- 9 2r+59097- 9 0 +78795- 9
0 +13789- 8 0 +14971- 7 0 + 0+ 0 0 +17146- 7 0 +15793- 8 0 +90244- 9
2r+67684- 9 0 +90244- 9 0 +15793- 8 0 +17146- 7 0 + 0+ 0 0 +19301- 7
0 +17777- 8 0 +10158- 8 2r+76187- 9 0 +10158- 8 0 +17777- 8 0 +19301- 7
0 + 0+ 0 0 +21454- 7 0 +19760- 8 0 +11291- 8 2r+84688- 9 0 +11291- 8

```
 0 +19760- 8 0 +21454- 7 0 +    0+ 0 0 +23566- 7 0 +21705- 8 0 +12403- 8
 2r+93024- 9 0 +12403- 8 0 +21705- 8 0 +23566- 7 0 +    0+ 0 0 +24447- 6
 2r+12924- 6 0 +24447- 6 0 +    0+ 0 0 +27017- 6 0 +85519- 7 2r+19214- 6
 0 +85519- 7 0 +27017- 6 0 +    0+ 0 0 +24447- 6 0 +85519- 7 0 +27474- 6
 2r+68585- 7 0 +27474- 6 0 +85519- 7 0 +24447- 6 0 +    0+ 0 0 +16672- 6
 0 +12924- 6 0 +19215- 6 0 +68586- 7 2r+18229- 6 0 +68586- 7 0 +19215- 6
 0 +12924- 6 0 +16672- 6
  t
1**  f0.0
2**  1i0.0 19i0.3175
     1i9.8425 3i10.16 7i10.2108 3i10.22385 i59i10.2868 3i40.2868
     7i40.3396 7i40.35265 7i40.3657 15i40.37875 15i40.40485
     3i40.45581 7i40.50861 43.04861
4**  19i0.0 3i1.27 24i1.3208 14i4.0328 11i5.7032 1i6.9850 23i7.3025
     7i19.5441 22.0841
'
'  1    Lucite
'  5    D2O
'  9    Void
' 13    Cadmium
' 17    Indium Down Stream T=0.025
' 21    Aluminum 100%
' 25    AlF3 100%
' 29    Teflon (CF2) 100%
' 33    Al-AlF3 (+LiF)  30%-69%-1% (VTT)
' 37    Al-Teflon 50%-50%
' 41    Cu63-65   69.17%-30.83%  (T=0.05096)
' 45    W182-183-184-186   26.3% 14.28% 30.7% 28.6%
' 49    Gold 100%
' 53    Lead
' 57    Upstream Indium (T=0.013).
' 61    Down Stream Indium (T=0.013)
' 65    Lithiated Poly
'
9$$  1 5 5 5 9   13 57 53 37 9   13 61 61 61 17   41 65 65
31$$  1 2 3 4 5 6 7 8 9 10 11 12 13 14 15 16 17 18
32**  0.0     0.0     0.0     0.0     0.0     0.0     0.0
      7.3025  0.0     0.0     0.0     0.0     0.0     0.0
      0.0     0.0     19.5441  0.0
33**  7.3025  6.9850  5.7032  4.0328  22.0841  1.3208  1.27
     22.0841  19.5441  19.5441  1.3208  1.27     1.27     1.27
      1.27     1.27    22.0841  22.0841
```

```
34**  0.0     0.3175   0.3175   0.3175  10.16    10.16    10.2108
     0.0     10.2868  40.2868  40.2868  40.3396  40.35265 40.36570
     40.37875 40.40485 10.2868  40.50861
35**  10.16    9.8425   9.8425   9.8425  10.2868  10.2868  10.22385
     10.16    40.2868  40.50861 40.50861 40.35265 40.36570 40.37875
     40.40485 40.45581 40.50861 43.04861
 t
96**  49r0.8135 15r0.1637 12r0.0228 f0.0
 t
97**  2r0.0 20r1.0 f0.0
 t
98**
 .00000e+00
 .00000e+00
 .00000e+00
 1.15566e+10
 2.16707e+10
 2.03474e+10
 1.45454e+10
 2.94866e+10
 1.20222e+10
 6.07141e+09
 2.80555e+09
 1.70160e+09
 1.21903e+09
 4.39057e+08
 5.09150e+08
 2.40505e+08
 1.13607e+08
 7.25672e+07
 1.53750e+07
 7.26262e+06
 4.10999e+06
 1.70662e+06
 3.61582e+05
 2.04625e+05
 6.28336e+04
 2.96813e+04
 2.01532e+04
 t
```

APPENDIX D

EXPERIMENTAL FOIL DATA

The information provided in this appendix is pertinent to data collection, detectors, and foil analyses. Included in this section are raw data (reaction rates) from foil counting as well as information on the detectors used and derivations and methodologies used.

The first section, D.1, shows a derivation of the activation equation as it is employed in this thesis. Section D.2 describes alternate methods of neutron detection. D.3 is a program listing used to determine activities of radionuclides. D.4 lists raw data from some of the experiments as listed in spreadsheet format. D.5 is a detector specification and performance data sheet. (Although several detectors were employed, this is typical of those used.) D.6 is a detector calibration curve used in determining the detector efficiency. Tables D.1 - D.4 of section D.7 show reaction rate data obtained on several of the final runs completed. Section D.8 is a listing of the fine-group and broad group energy structures used. Although many experiments were carried out, these are the data are used in the final beam analyses presented.

D.1 Activation Equation Derivation

The activation equation used in the reduction of the collected foil data is derived as follows. Beginning with the equation below indicating the change in the number of atoms with time as the atoms of interest, N_{115}, are activated at the rate of $\sigma\varphi$ while, at the same time, decaying with a decay constant, λ.

$$\frac{dN_{116}}{dt} = N_{115}\sigma\varphi - \lambda N_{116} \tag{D.1}$$

This equation can be integrated to yield:

$$N_{116} = \frac{N_{115}\sigma\varphi}{\lambda}\left(1 - e^{-\lambda t}\right) + N_{116}e^{-\lambda t} \tag{D.2}$$

If it is assumed that there are no N_{116} atoms at the start of activation process and if activation occurs for time t_i, then the number of atoms upon completion of activation is:

$$N_{116} = \frac{N_{115}\sigma\varphi}{\lambda}\left(1 - e^{-\lambda t_i}\right) \tag{D.3}$$

Compensating for a wait time, t_w, before counting commences yields:

$$N_{116} = \frac{N_{115}\sigma\varphi}{\lambda}\left(1 - e^{-\lambda t_i}\right)e^{-\lambda t_w} \tag{D.4}$$

Activity is written as:

$$A_{116} = \lambda N_{116} = N_{115}\sigma\varphi\left(1 - e^{-\lambda t_i}\right)e^{-\lambda t_w} \tag{D.5}$$

In order to compensate for decay during the count time, a time t_c is introduced. Integrating over t_c to obtain the total counts yields:

$$\int_0^{t_c} A_{116}(t) = \int_0^{t_c} N_{115}\sigma\varphi\left(1 - e^{-\lambda t_i}\right)e^{-\lambda t_w}e^{-\lambda t} \tag{D.6}$$

This integration gives a total counts measured of:

$$C = \frac{N_{115}\sigma\varphi}{\lambda}\left(1 - e^{-\lambda t_i}\right)e^{-\lambda t_w}\left(1 - e^{-\lambda t_c}\right) \tag{D.7}$$

which, when efficiency and branching ratios are considered, yields total counts of:

$$C = \varepsilon b_\gamma \frac{N_{115}\sigma\varphi}{\lambda}\left(1 - e^{-\lambda t_i}\right)e^{-\lambda t_w}\left(1 - e^{-\lambda t_c}\right) \tag{D.8}$$

This can then be rewritten in terms of activation rate as:

$$\sigma\phi = \frac{C\lambda}{\varepsilon b\gamma N_{115}} \cdot \left(1 - e^{-\lambda t_i}\right)^{-1} \cdot e^{\lambda t_w} \cdot \left(1 - e^{-\lambda t_c}\right)^{-1} \tag{D.9}$$

D.2 Alternate Neutron Detection Methods

In proton recoil counting, advantage is taken of the fact that, in a hydrogenous medium, fast neutrons are scattered by the hydrogen atoms, transferring energy elastically according to the recoil equation:

$$E_n = E_i \frac{m_1 m_2}{m_1 + m_2} \cos\Theta \tag{D.10}$$

where m_1 and m_2 are the masses of the two particles and E_n and E_i are the energies of the scattered and incident neutrons, respectively. In the case of hydrogen, the masses are approximately equal and the maximum energy transfer (in a head-on collision with an incident angle of $\Theta = 0$) is $E_{nmax} = 1/2E_i$. This effect can be used for detecting neutron energies, in photographic emulsions, damage-track detectors or gas-filled detectors.

Time-of-flight measurements are based on the detection of a measured flight path of a neutron and the time required for the neutron to reach the end of this flight path. Because thermal neutrons travel at an average velocity of approximately 2200 meters per second, it is feasible to detect their velocities. The kinetic energy for neutrons can be expressed as:

$$E = 1/2mv^2 \tag{D.11}$$

If the time t is described as d/v (distance travelled over velocity), then the time for a neutron's arrival at the detector is:

$$t = \frac{d}{\sqrt{2E/m}} \tag{D.12}$$

A neutron pulse can be detected with this method using a He-3 detector or a surface-barrier detector in which a layer of boron is employed that allows detection of the resultant secondary alpha particles as opposed to the incident neutrons.

D.3 Program Listing to Determine Activities

```
/* This program finds the activities of decay radionuclides, given a production rate
    and time thereafter. */

#include<stdio.h>
#include<math.h>
#define SIZE 4
main()
{
    int i, j, k;
    double p, L[SIZE], t, N, A, S, M;
    printf("Enter the production \n");
    scanf("%lf", &p);
/*  printf("Enter the lambdas 1-4\n"); */
    /*for (i = 0; i<SIZE; i++) */
    /*scanf("%lf", &L[i]); */
    L[0] = .02145;
    L[1] = .00453;
    L[2] = 7.63e-10;
    L[3] = 3.002e-6;
    printf("Enter the time\n");
    scanf("%lf", &t);
    printf("Enter the value for k, where k is the kth nuclide of interest:\n");
    scanf("%d", &k);
    N = 1;
    M = 1;
    S = 0;
    for (i = 0; i<k-1; i++)
    N *=L[i];
    N *= p;
/*  printf("N with p and Ls is: %lf\n", N); */
    for (i = 0; i<k; i++)
    {
    for (j = 0; j<k; j++)

    if (i!=j)
    M *= (L[j] - L[i]);
    printf("M is: %lf\n", M);
    S += (1 - exp(-L[i]*t))/fabs(M);
    printf("S is: %lf\n", S);
    M = 1;
    }
    N *= S;
    A = N*L[k-1];
    printf("The activity is: %lf\n", A);
}
```

D.4 Spreadsheet Data

	A	B	C	D	E	F	G	H	I	J	K
1											
2	Foil/Line	Reaction Rate	Uncert.(units-1)	Tw	Ti	Tc	N(Atoms)	branching ratio	efficiency	counts	Uncert.(sec-1)
3											
4	6/11 MeV Lines										
5	In UP 416	1.25137632E-17	0.0122400	23.00	120.00	24.31	4.75E+21	0.2350000	0.0173	185501.00	2.1332E-04
6	In UP 1037	1.48554702E-17	0.0122400	23.00	120.00	24.31	4.75E+21	0.51100	0.0101	179315.00	2.1332E-04
7	In UP 1234	3.2555564E-18	0.0122400	23.00	120.00	24.31	4.75E+21	0.41900	0.0092	212451.00	2.1332E-04
8	In UP 316	4.18290232E-19	0.0123150	23.00	120.00	24.31	4.75E+21	0.47000	0.0134	7233.00	4.2917E-05
9	In DOW N 416	3.41140332E-19	0.0122400	10.00	120.00	20.23	4.65E+21	0.23500	0.0173	5668.00	2.1332E-04
10	In DOW N 1037	4.1827224E-19	0.0122400	10.00	120.00	20.23	4.65E+21	0.51100	0.0101	8271.00	2.1332E-04
11	In DOW N 1234	9.31140403E-19	0.0122400	10.00	120.00	20.23	4.65E+21	0.41900	0.0092	18595.00	2.1332E-04
12	In DOW N 316	7.4687452E-21	0.0123750	10.00	120.00	20.23	4.65E+21	0.47000	0.0134	97.00	4.2917E-05
13	Au 411	5.5464064E-18	0.0123123	120.00	120.00	162.55	1.11E+21	0.33000	0.0174	121114.00	2.9722E-04
14	Cu 811	1.3250724E-20	0.0123100	93.00	120.00	40.00	4.65E+22	0.23900	0.0154	532.00	1.5107E-05
15											
16											
17											
18											
19											
20											
21	6/11 MeV										
22	In UP 416	2.7725533E-17	0.0122400	93.00	93.00	28.21	4.75E+21	0.2350000	0.0173	346115.00	2.1332E-04
23	In UP 1037	2.3147541E-17	0.0122400	93.00	93.00	28.21	4.75E+21	0.51100	0.0101	281004.00	2.1332E-04
24	In UP 1234	2.03187222E-17	0.0122400	93.00	93.00	28.21	4.75E+21	0.41900	0.0092	344172.00	2.1332E-04
25	In UP 316	5.0283593E-18	0.0123750	93.00	93.00	28.21	4.75E+21	0.47000	0.0134	37245.00	4.2917E-05
26	In DOW N 416	1.2556972E-18	0.0122400	93.15	93.00	28.21	4.65E+21	0.23500	0.0173	6617.00	2.1332E-04
27	In DOW N 1037	1.4035492E-18	0.0122400	93.15	93.00	28.17	4.65E+21	0.51100	0.0101	6035.00	2.1332E-04
28	In DOW N 1234	3.0316031E-18	0.0122400	93.15	93.00	28.17	4.65E+21	0.41900	0.0092	7272.00	2.1332E-04
29	In DOW N 316	6.6814268E-20	0.0123750	93.15	93.00	28.17	4.65E+21	0.47000	0.0134	510.00	4.2917E-05
30	Au 411 *	1.2346533E-17	0.0123123	124.59	93.00	162.55	1.11E+21	0.33000	0.0174	210325.00	2.9722E-04
31	Cu 811	1.1729406E-20	0.0123100	122.59	93.00	40.07	4.65E+22	0.23900	0.0154	458.00	1.5107E-05
32											
33											
34											
35											
36											
37											
38											
39											
40	11/12 MeV Al-Tcd										
41	In UP 416	8.5676743E-18	0.0122400	41.77	41.00	20.00	4.71E+21	0.2350000	0.0173	42560.00	2.1332E-04
42	In UP 1037	8.3600427E-18	0.0122400	41.77	41.00	20.00	4.71E+21	0.51100	0.0101	59460.00	2.1332E-04
43	In UP 1234	7.4183221E-18	0.0122400	41.77	41.00	20.00	4.71E+21	0.41900	0.0092	113100.00	2.1332E-04
44	In UP 316	3.5141222E-19	0.0123750	41.77	41.00	20.00	4.71E+21	0.47000	0.0134	2329.00	4.2917E-05
45	In DOW N 416	7.4035972E-19	0.0122400	13.78	41.00	20.00	4.71E+21	0.23500	0.0173	10400.00	2.1332E-04
46	In DOW N 1037	8.3104032E-19	0.0122400	13.78	41.00	20.00	4.71E+21	0.51100	0.0101	3350.00	2.1332E-04
47	In DOW N 1234	5.9053032E-19	0.0122400	13.78	41.00	20.00	4.71E+21	0.41900	0.0092	11700.00	2.1332E-04
48	In DOW N 316	N/A	0.0123750	13.78	41.00	20.00	4.71E+21	0.47000	0.0134	N/A	4.2917E-05
49	Au 411	2.6655253E-17	0.0123123	188.00	41.00	265.00	1.11E+21	0.33000	0.0174	123331.71	2.9722E-04
50	Cu 811	2.4918154E-20	0.0123100	74.25	41.00	66.00	5.03E+22	0.23900	0.0154	452.00	1.5107E-05
51	W 416	1.2313104E-18	0.0124823	187.00	41.00	160.00	7.23E+19	0.28000	0.0158	2312.35	0.0558E-06
..											

	A	B	C	D	E	F	G	H	I	J	K
59	Foil/Line	Reaction Rate	lambda (min-1)	Tw	Ti	Tc	N (atms)	branching ratio	efficiency	counts	lamda (sec-1)
60											
61	10/25 6MeV Al-Tef										
62	In UP 416	5.5042128E-17	0.0128000	168.40	105.00	15.00	2.40E+21	0.2950000	0.0285	49674.05	2.1333E-04
63	In UP 1097	3.4570605E-17	0.0128000	168.40	105.00	15.00	2.40E+21	0.56800	0.0148	48999.23	2.1333E-04
64	In UP 1294	7.0743724E-17	0.0128000	168.40	105.00	15.00	2.40E+21	0.84900	0.0133	58531.28	2.1333E-04
65	In UP 336	1.3009554E-18	0.0025750	168.40	105.00	15.00	2.40E+21	0.47000	0.0329	6557.17	4.2917E-05
66	A: In DOWN 416	1.0951451E-18	0.0128000	12.03	105.00	25.00	2.41E+21	0.2950000	0.0285	18087.85	2.1333E-04
67	A: In DOWN 1097	1.0756635E-18	0.0128000	12.03	105.00	25.00	2.41E+21	0.56800	0.0148	17765.76	2.1333E-04
68	A: In DOWN 1294	9.6116961E-19	0.0128000	12.03	105.00	25.00	2.41E+21	0.84900	0.0133	21321.01	2.1333E-04
69	A: In DOWN 336	2.8672053E-20	0.0025750	12.03	105.00	25.00	2.41E+21	0.47000	0.0329	357.26	4.2917E-05
70	B: In DOWN 416	6.2043827E-19	0.0128000	44.33	105.00	25.00	2.50E+21	0.2950000	0.0285	7030.96	2.1333E-04
71	B: In DOWN 1097	6.1296745E-19	0.0128000	44.33	105.00	25.00	2.50E+21	0.56800	0.0148	6945.39	2.1333E-04
72	B: In DOWN 1294	5.4016862E-19	0.0128000	44.33	105.00	25.00	2.50E+21	0.84900	0.0133	8221.25	2.1333E-04
73	B: In DOWN 336	2.6019619E-20	0.0025750	44.33	105.00	25.00	2.50E+21	0.47000	0.0329	309.50	4.2917E-05
74	C: In DOWN 416	5.3604785E-19	0.0128000	72.30	105.00	25.00	2.47E+21	0.2950000	0.0285	4185.85	2.1333E-04
75	C: In DOWN 1097	5.4759200E-19	0.0128000	72.30	105.00	25.00	2.47E+21	0.56800	0.0148	4278.50	2.1333E-04
76	C: In DOWN 1294	4.8545851E-19	0.0128000	72.30	105.00	25.00	2.47E+21	0.84900	0.0133	5084.90	2.1333E-04
77	C: In DOWN 336	1.9374300E-20	0.0025750	72.30	105.00	25.00	2.47E+21	0.47000	0.0329	211.52	4.2917E-05
78	D: In DOWN 416	5.5143476E-19	0.0128000	101.57	105.00	25.00	2.43E+21	0.2950000	0.0285	2920.60	2.1333E-04
79	D: In DOWN 1097	5.1875942E-19	0.0128000	101.57	105.00	25.00	2.43E+21	0.56800	0.0148	2747.18	2.1333E-04
80	D: In DOWN 1294	4.8154805E-19	0.0128000	101.57	105.00	25.00	2.43E+21	0.84900	0.0133	3425.39	2.1333E-04
81	D: In DOWN 336	2.0423740E-20	0.0025750	101.57	105.00	25.00	2.43E+21	0.47000	0.0329	209.85	4.2917E-05
82	F: In DOWN 416	7.9965597E-19	0.0128000	134.17	105.00	25.00	2.47E+21	0.2950000	0.0285	2838.58	2.1333E-04
83	F: In DOWN 1097	7.3991979E-19	0.0128000	134.17	105.00	25.00	2.47E+21	0.56800	0.0148	2626.26	2.1333E-04
84	F: In DOWN 1294	6.6313060E-19	0.0128000	134.17	105.00	25.00	2.47E+21	0.84900	0.0133	3161.56	2.1333E-04
85	F: In DOWN 336	2.2570064E-20	0.0025750	134.17	105.00	25.00	2.47E+21	0.47000	0.0329	210.72	4.2917E-05
86											

	A	B	C	D	E	F	G	H	I	J	K
93	Foil/Line	Reaction Rate	lambda (min-1)	Tw	Ti	Tc	N (atoms)	branching ratio	efficiency	counts	lamda (sec-1)
94											
95	11/3 6MeV Fastest										
96	D2O UP 416	1.07687911E-17	0.0128000	160.00	105.00	20.00	4.66E+21	0.2950000	0.0285	42539.51	2.1333E-04
97	D2O UP 1097	1.0539991E-17	0.0128000	160.00	105.00	20.00	4.66E+21	0.56800	0.0148	41688.96	2.1333E-04
98	D2O UP 1294	9.5669933E-18	0.0128000	160.00	105.00	20.00	4.66E+21	0.84900	0.0133	50828.50	2.1333E-04
99	D2O UP 336	4.5054005E-19	0.0025750	160.00	105.00	20.00	4.66E+21	0.47000	0.0329	5359.21	4.2917E-05
100	D2O DOWN 416	7.4464745E-19	0.0128000	85.00	105.00	30.00	4.71E+21	0.2950000	0.0285	10935.99	2.1333E-04
101	D2O DOWN 1097	7.2795557E-19	0.0128000	85.00	105.00	30.00	4.71E+21	0.56800	0.0148	10748.07	2.1333E-04
102	D2O DOWN 1294	6.4229978E-19	0.0128000	85.00	105.00	30.00	4.71E+21	0.84900	0.0133	12738.57	2.1333E-04
103	D2O DOWN 336	1.5291541E-20	0.0025750	85.00	105.00	30.00	4.71E+21	0.47000	0.0329	319.75	4.2917E-05
104	NADA UP 416	0.0000000E+00	0.0128000	126.00	60.00	20.00	4.69E+21	0.2950000	0.0285	0.00	2.1333E-04
105	NADA UP 1097	0.0000000E+00	0.0128000	126.00	60.00	20.00	4.69E+21	0.56800	0.0148	0.00	2.1333E-04
106	NADA UP 1294	0.0000000E+00	0.0128000	126.00	60.00	20.00	4.69E+21	0.84900	0.0133	0.00	2.1333E-04
107	NADA UP 336	5.1549488E-19	0.0025750	126.00	60.00	20.00	4.69E+21	0.47000	0.0329	4531.53	4.2917E-05
108	NADA DOWN 416	0.0000000E+00	0.0128000	152.00	60.00	20.00	4.75E+21	0.2950000	0.0285	0.00	2.1333E-04
109	NADA DOWN 1097	0.0000000E+00	0.0128000	152.00	60.00	20.00	4.75E+21	0.56800	0.0148	0.00	2.1333E-04
110	NADA DOWN 1294	0.0000000E+00	0.0128000	152.00	60.00	20.00	4.75E+21	0.84900	0.0133	0.00	2.1333E-04
111	NADA DOWN 336	1.9596125E-20	0.0025750	152.00	60.00	20.00	4.75E+21	0.47000	0.0329	162.95	4.2917E-05
112	H2O UP 416	0.0000000E+00	0.0128000	109.17	59.32	20.00	4.68E+21	0.2950000	0.0285	0.00	2.1333E-04
113	H2O UP 1097	0.0000000E+00	0.0128000	109.17	59.32	20.00	4.68E+21	0.56800	0.0148	0.00	2.1333E-04
114	H2O UP 1294	0.0000000E+00	0.0128000	109.17	59.32	20.00	4.68E+21	0.84900	0.0133	0.00	2.1333E-04
115	H2O UP 336	3.8131545E-19	0.0025750	109.17	59.32	20.00	4.68E+21	0.47000	0.0329	3452.12	4.2917E-05
116	H2O DOWN 416	0.0000000E+00	0.0128000	131.04	59.32	20.00	4.70E+21	0.2950000	0.0285	0.00	2.1333E-04
117	H2O DOWN 1097	0.0000000E+00	0.0128000	131.04	59.32	20.00	4.70E+21	0.56800	0.0148	0.00	2.1333E-04
118	H2O DOWN 1294	0.0000000E+00	0.0128000	131.04	59.32	20.00	4.70E+21	0.84900	0.0133	0.00	2.1333E-04
119	H2O DOWN 336	0.0000000E+00	0.0025750	131.04	59.32	20.00	4.70E+21	0.47000	0.0329	0.00	4.2917E-05
120											
121											
122											
123											
124											
125											
126	09/26 6MeV Al-Tef										
127	In UP 416 no cd	1.2649295E-17	0.0128000	95.25	30.00	20.00	4.75E+21	0.2950000	0.0285	48000.00	2.1333E-04
128	In UP 1097 no cd	1.1699588E-17	0.0128000	95.25	30.00	20.00	4.75E+21	0.56800	0.0148	46600.00	2.1333E-04
129	In UP 1294 no cd	1.0541613E-17	0.0128000	95.25	30.00	20.00	4.75E+21	0.84900	0.0133	56400.00	2.1333E-04
130	In UP 336 no cd	5.2415006E-19	0.0025750	95.25	30.00	20.00	4.75E+21	0.47000	0.0329	1620.00	4.2917E-05
131	In DOWN 416 no cd	5.9777310E-19	0.0128000	11.50	30.00	20.00	4.71E+21	0.29500	0.0285	6910.00	2.1333E-04
132	In DOWN 1097 no cd	5.9871651E-19	0.0128000	11.50	30.00	20.00	4.71E+21	0.56800	0.0148	6920.00	2.1333E-04
133	In DOWN 1294 no cd	5.2173609E-19	0.0128000	11.50	30.00	20.00	4.71E+21	0.84900	0.0133	8100.00	2.1333E-04
134	In DOWN 336 no cd	N/A	0.0025750	11.50	30.00	20.00	4.71E+21	0.47000	0.0329	0.00	4.2917E-05
135											

D.5 Detector Specification Sheet

Specifications

Model GC3318 Serial Number 8902320

The purchase specifications and therefore the warranted performance of this detector are as follows:

Active volume _____ cc Relative efficiency 33 %

Resolution 1.80 keV(FWHM) at 1.33 MeV

3.25 keV(FWTM) at 1.33 MeV

0.90 keV(FWHM) at 122 keV

1.70 keV(FWTM) at 122 keV

Peak/Compton 60 : 1 Cryostat well diameter _____ mm Well depth _____ mm

Cryostat description of Drawing Number if special 7905-30/S

Physical Characteristics

Geometry Closed-end coaxial

Diameter 58.5 mm Active volume 122.7 cc

Length 49.5 mm Well depth _____ mm

Distance from window 5 mm Well diameter _____ mm

Electrical Characteristics

Depletion voltage (+) 2000 V dc

Recommended bias voltage V dc (+) 2500 V dc

Leakage current at recommended bias 0.04 nA

Preamplifier test point voltage at recommended voltage (-) 1.48 V dc

Capacitance at recommended bias ~ 20 pF

Resolution and Efficiency

With amp time constant of 4 µs

Isotope	^{57}Co	^{60}Co			
Energy (keV)	122	1332			
FWHM (keV)	0.89	1.77			
FWTM (keV)	1.65	3.23			
Peak/Compton		60.6:1			
Rel. Efficiency		33.1			

Tested by: _____ Date: August 8, 1990

Approved by: _____ Date: August 8, 1990

D.6 Detector Calibration Curve

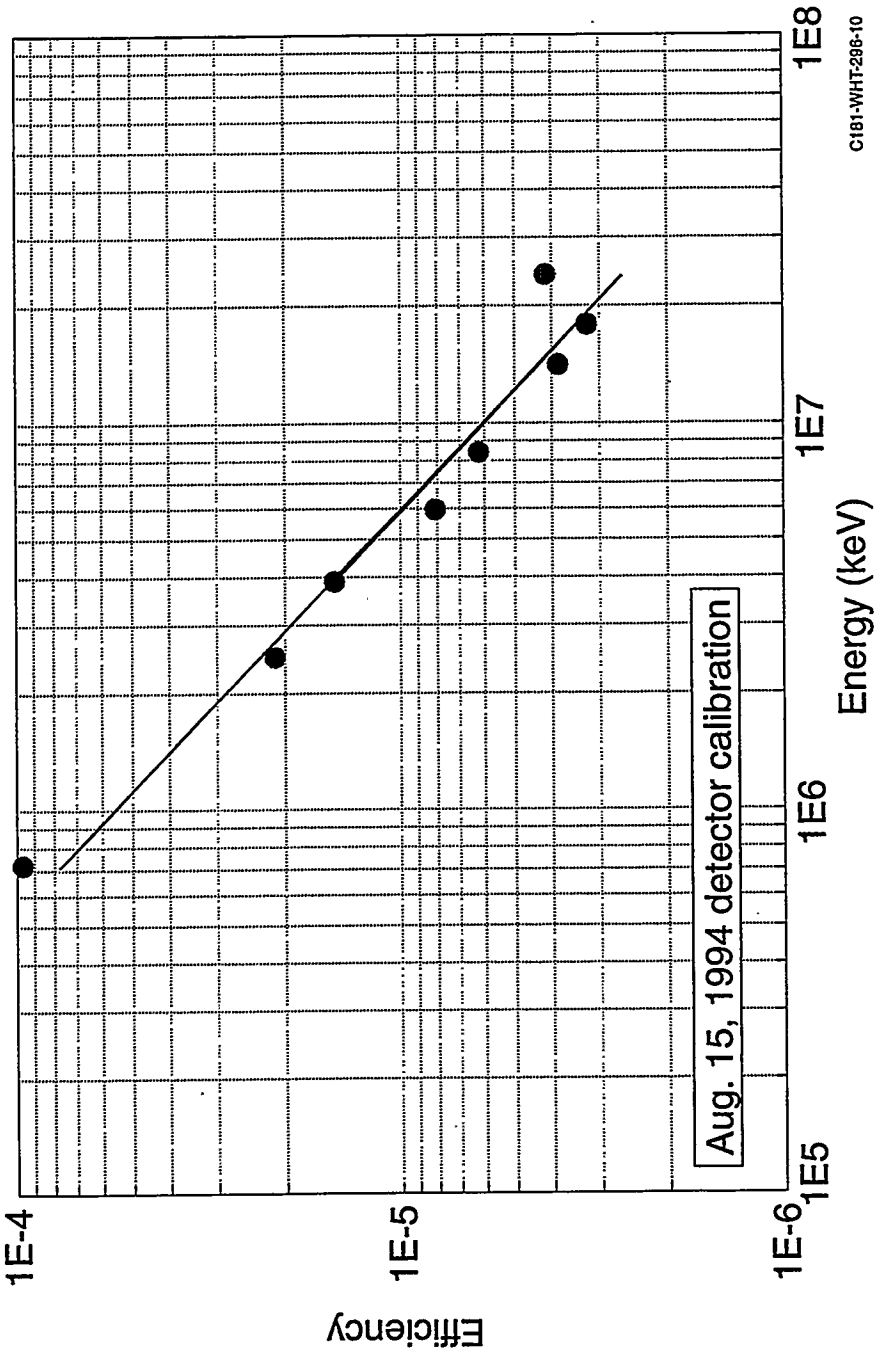

D.7 Reaction Rate Data Tables

Table D.1: Reaction rate data for 6 MeV Al/AlF_3 filter upstream

Foil reaction	Measured reaction rate
$^{115}In(n,n')^{115m}In$	1.0800×10^{-19}
$^{115}In(n,\gamma)^{116}In$	1.0960×10^{-17}
$^{115}In(n,\gamma)^{116}In$	1.8480×10^{-17}

Table D.2: Reaction rate data for 6 MeV Al/AlF_3 filter downstream

Foil reaction	Measured reaction rate
$^{115}In(n,n')^{115m}In$	7.4860×10^{-23}
$^{63}Cu(n,\gamma)^{64}Cu$	1.5175×10^{-20}
$^{197}Au(n,\gamma)^{198}Au$	5.7780×10^{-19}
$^{115}In(n,\gamma)^{116}In$	4.6430×10^{-19}
$^{115}In(n,\gamma)^{116}In$	5.4320×10^{-19}

Table D.3: Reaction rate data for 6 MeV Al/Teflon filter upstream

Foil reaction	Measured reaction rate
$^{115}In(n,n')^{115m}In$	2.1490×10^{-19}
$^{115}In(n,\gamma)^{116}In$	2.0000×10^{-17}

Table D.4: Reaction rate data (stacked foil assemblies) for 6 MeV Al/Teflon filter downstream

Foil reaction	Measured reaction rate
$^{115}In(n,n')^{115m}In$	1.0690×10^{-21}
$^{63}Cu(n,\gamma)^{64}Cu$	4.1870×10^{-20}
$^{115}In(n,\gamma)^{116}In$	5.5720×10^{-19}
$^{115}In(n,\gamma)^{116}In$	9.2510×10^{-19}

D.8 Fine-Group and Broad-Group Energy Structures Used

Energy breakpoints for fine-group structure (eV):

3.6800e+06	2.2300e+06	1.3500e+06	8.2100e+05	4.9800e+05
1.8300e+05	1.1100e+05	6.7400e+04	4.0900e+04	3.1800e+04
1.5000e+04	7.1000e+03	3.3600e+03	1.5900e+03	4.5400e+02
2.1450e+02	1.0130e+02	3.7300e+01	1.0680e+01	5.0400e+00
1.8600e+00	8.7600e-01	4.1400e-01	1.0000e-01	1.0000e-03

Lower energies of broad-groups for downstream Al/Teflon (eV):

4.9800e+05	3.7300e+01	1.8600e+00	1.0000e-03

Lower energies of broad-groups for downstream AlF_3 (eV):

4.9800e+05	4.5400e+02	1.8600e+00	4.1400e-01	1.0000e-03

Lower energies of broad-groups for upstream Al/Teflon (eV):

4.9800e+05	1.0000e-03

Lower energies of broad-groups for upstream AlF_3 (eV):

4.9800e+05	4.1400e-01	1.0000e-03

BIBLIOGRAPHY

Aizawa, O. and Yamada, H., "Study on the Best Design of Neutron Irradiation Facility for BNCT." In: Progress in Neutron Capture Therapy for Cancer. New York: Plenum, 1992.

Alsmiller, R.G. and Morán, H.S., "Electron-Photon Cascade Calculations and Neutron Yields from Electrons in Thick Targets," Oak Ridge National Laboratory, Report No. ORNL-TM-1502, 1966.

Asbury, A. K., Ojeman, R. C., Nielsen, S. L., and Sweet, W. H., "Neuropathological Study of 14 Cases of Malignant Brain Tumor Treated by B-10 Slow Neutron Capture Radiation." *J. of Neuropath. & Expt. Neurol.* 31: 278-303, 1972.

Auterinen, I. and Hiismaki, P., "Epithermal BNCT Neutron Beam Design for a TRIGA II Reactor." In: Advances in Neutron Capture Therapy. New York: Plenum, 1993.

Auterinen, I. and Hiismaki, P., "Epithermal BNCT Neutron Beam Design for a TRIGA II Reactor", Advances in Neutron Capture Therapy, R. Barth and A. Soloway, Editors, Plenum Press, New York, 81-84, 1993.

Barth, R. F., Soloway, A. H. and Fairchild, R. G., "Boron Neutron Capture Therapy for Cancer," *Scientific American* 100-107, October 1990.

Berger, M. J. and Seltzer, S. M., "Tables of Energy Losses and Ranges of Electrons and Positrons," NASA SP-3012, National Bureau of Standards, 1964.

Berger, M. J. and Seltzer, S. M., "Bremsstrahlung and Photoneutrons from Thick Tungsten and Tantalum Targets," *Physical Review C*, 2:2, 621-631, August 1970.

Berger, M. J. and Seltzer, S. M., "ETRAN Monte Carlo Code System for Electron and Photon Transport Through Extended Media," CCC-107, Radiation Shielding Information Center, Computer Code Collection, Oak Ridge National Laboratory, June 1968.

Berman, B. L., Van Hemert, R. L. and Bowman, C. D., "Threshold Photoneutron Cross Section for Be^9," *Phys. Rev.* 163:4, 958-963, 1967.

Beth, H.A. and Bacher, R.E., *Rev. Mod. Phys.* 8:125, 1936.

Bethe, H. A. and Heitler, W., *Proc. Roy. Soc. (London)*, A146: 83, 1934.

Biggs, F. and Lighthill, R., "Analytical Approximations for X-Ray Cross Sections II," SC-RR-71 0507, Sandia National Laboratories, December 1971.

Briesmeister, J. F., ed., "MCNP - A General Monte Carlo Code for Neutron and Photon Transport, Version 3B," LA-7396-M, Los Alamos National Laboratory, 1989.

Brownell, G. L. and Sweet, W. H., "Studies on Neutron Capture Therapy." In: Proceedings of the Second United Nations International Conference on the Peaceful Uses of Atomic Energy, 26: 444-450, 1958.

Brugger, R. M., Shih, J. A. and Liu, H. B., "An Epithermal Neutron Beam for Neutron Capture Therapy at the Missouri Univerisity Research Reactor," *Nuclear Technology*, 98: 322-332, 1992.

Burian, J., Marek, M., and Rataj, J., "Neutron Beam Parameters on LVR--15 Reactor for Neutron Capture THerapy." In: Progress in Neutron Capture Therapy for Cancer. New York: Plenum, 1992.

Choi, J. R., Zamenhof, R. G., Yanch, J. C. et al. "Performance of the Currently Available Epithermal Neutron Beam at the Massachusetts Institute of Technology Reseaerch Reactor (MITR-II)." In: Progress in Neutron Capture Therapy for Cancer. New York: Plenum, 1992.

Cierjacks, S., ed. Neutron Sources for Basic Physics and Applications: Oxford, England: Pergamon Press, 1983.

Corder, A., Whittaker, A., et al. "Evaluation of a ^{10}B-Labelled DNA Ligand," In: Advances in Neutron Capture Therapy, New York: Plenum, 1993.

Cokinos, D. M. and van Tuyle, G. J., "A High-Intensity Accelerator-Based Neutron Source," In: *Transactions American Nuclear Society* 69: 423-424, November 1993.

Crawford, J. F., Reist, H., Conde, H. B., Larsson, J. et al. "Neutrons for Capture Therapy Produced by 72 MeV Protons." In: Progress in Neutron Capture Therapy for Cancer. New York: Plenum, 1992.

Crawford, J. G., Larsson, B., Reist, H., Conde, et al. "High Energy Accelerator Technology in Radiology," Presentationn at IEEE Particle Accelerator Conference, Washington, D. C., May 1993.

Evans, R. D., "Radiative Collisions of Electrons with Atomic Nuclei," The Atomic Nucleus, New York: McGraw-Hill, 1955.

Evans, R. D., "Stopping of Electrons by Thick Absorbers," The Atomic Nucleus, New York: McGraw-Hill, 1955.

Fairchild, R. G., "Recent Advances in Neutron Capture Therapy (NCT)," In: Neutron Capture Therapy (Hatanaka, H. ed.), Norwell, MA: MTP Press, 1986

Fairchild, R. G. and Bond, V. P., Eds., Workshop on Neutron Capture Therapy. Report BNL-51994, Brookhaven National Laboratory, Upton, NY, 1986.

Fairchild, R. G., "Development of Boronated Compounds for NCT." In: Boron Compounds Suitable for Neutron Capture Therapy for the Treatment of Cancer. NCI: Bethesda, MD, 1988.

Farr, L. E., Sweet, W. H., et al. "Neutron Capture Therapy of Gliomas Using Boron-10." *Transactions of the American Neurological Association*, 79: 110-113, 1954.

Farr, L. E., "The Physics & Physiology of NCT." *Proc. National Acad. Sci.* 40: 1088-1093, 1954.

Gabel, D., Bond, V. P., Kalef-Ezra, J. and Fairchild, R. G., "The Necessity of Stochastic Radiobiology in BNCT, or, What is the RBE of the $^{10}B(n,)^{7}Li$ Reaction?" In: Progress in Neutron Capture Therapy for Cancer, New York: Plenum, 1992.

Glover, G.H., Pauley, J.M. and Bradshaw, K. M., "Boron-11 Imaging with a 3-dimensional Reconstruction Method," *J. Magn. Reson. Imaging*. 2:47, 1992.

Grimesey, R.A., Nigg, D.W., Curtis, R.L., "COMBINE/PC - A Portable ENDF/B Version 5 Neutron Spectrum and Cross-Section Generation Program", EGG-2589 (Rev 1), Idaho National Engineering Laboratory, February, 1991.

Grusell, Erik, "Accelerator Based Neutron Sources for Neutron Capture Therapy." In: Progress in Neutron Capture Therapy for Cancer. New York: Plenum 1992.

Hablieb, J. A. and Mehlhorn, T. A., "ITS - The Integrated TIGER Series of Coupled Electron/Photon Monte Carlo Transport Codes", SAND91-1634, Sandia National Laboratory, March, 1992.

Harling, O. K. et al., "Boron Neutron Capture Therapy and Radiation Synovectomy Research at the Massachussetts Institute of Technology Research Reactor," *Nuclear Science and Engineering*, 110:330, 1992.

Hatanaka, H., "Experience of Boron-Neutron Capture Therapy for Malignant Brain Tumours--with Special Reference to the Problems of Post-operative CT Follow-ups," *Acta Neurochir. Suppl. Wein.* 42: 187-192, 1988.

Hisdal, E., *Phys. Rev.*, 105:1821, 1957.

Jakobson, M. J., "Photodisintegration of Be^9 from Threshold to 5 MeV," *Phys. Rev.* 123:1, 229-230, 1961.

Jupiter, C.P., Hatcher, C.R. and Hansen, N.E., "Measurement of the Angular Distribution of Bremsstrahlung Intensity for 10 MeV and 20 MeV electrons on Thick Targets," CONF-452-14, American Physical Society, Washington, D.C., April 1964.

Jones, J.L. and Yoon, W.Y., "Feasibility Study of the Application of a Linear Electron Accelerator to BNCT", Proceedings of the 12th International Conference on the Application of Accelerators in Research and Industry, University of North Texas, Denton TX, November, 1992.

Jones, J. L. and Yoon, W. Y., "Feasibility Study of the Application of a Linear Electron Accelerator to BNCT," Proceedings of the 12th International Conference on the Application of Accelerators in Research and Industry, University of North Texas, Denton TX, November, 1992.

Khandelwal, G. S., Pritchard, W. M. and Singh, J. J., "An Estimate of the Yield of Photoneutrons from Beryllium Using a LINAC as the X-Ray Source," *Nucl. Sci. Eng.*, 60:481-486, 1976.

Klee, K., "Optimization of an Epithermal Neutron Beam and Beam Dosimetry for Boron Neutron Capture Therapy at the Georgia Tech Research Reactor," Doctoral Thesis, Georgia Institute of Technology, 1994.

Klee, K., Nigg, D., Wheeler, F. and Karam, R., "Conceptual Design for an Advanced Epithermal Neutron Beam for Boron Neutron Capture Therapy at the Georgia Institute of Technology Research Reactor," ANS Topical Meeting on Advances in Reactor Physics, Knoxville, TN, April 1994.

Koch, H. W. and Motz, J. W., "Bremsstrahlung Cross-Section Formulas and Related Data," *Review of Modern Physics*, 31:920-955, 1959.

Koch, H.W. and Motz, J.W., "Bremsstrahlung Cross-Section Formulas and Related Data," *Rev. Mod. Phys.* 31: 920, 1959.

Kruger, P. G., "Some Biological Effects of Nuclear Disintegration Products on Neoplastic Tissue." Proceedings of the National Academy of Sciences of the USA. 26: 181-192, 1940.

Locher, G. L., "Biological Effects and Therapeutic Possibilities of Neutrons." *American Journal of Roentgenology*, 36: 1-13, 1936.

Marion, J. B. and Levin, J. S., "Investigation of the $^{9}Be(p,n)^{9}B$ and $^{9}Be(p,\alpha\gamma)^{6}Li$ reactions," *Physics Review*, 115:144, 1959.

McEligot, D.M., "Accelerator Target Cooling for the BNCT Epithermal Source", In: J.R. Venhuizen (ed), 1995 INEL BNCT Program Annual Report, 1996.

Mobley, R. C. and Laubenstein, R. A., "Photoneutron Thresholds of Beryllium and Deuterium," Argonne National Laboratory ANL-4468, 1950.

Moran, J. M., Nigg, D. W., Wheeler, F. J. and Bauer, W. F., "Macroscopic geometric heterogeneity effects in radiation dose distribution analysis for boron neutron capture therapy," *Medical Physics* 19:3, 723-732, May/June 1992.

Moss, R. L., "Progress Towards Boron Neutron Capture THerapy at the High-Flux Reactor Petten," Neutron Beam Design, Development and Performance for Neutron Capture Therapy, New York: Plenum Press, 1990.

Nakagawa, Y., "Recent Study of Boron Neutron Capture Therapy for Brain Tumors," Proceedings of the First International Workshop on Accelerator-Based Neutron Sources for Boron Neutron Capture Therapy, Vol. I, 11, Jackson, Wyoming, Sept. 1994.

Nigg, D. W., Randolph, P. D. and Wheeler, F. J., "Demonstration of three-dimensional deterministic radiation transport theory dose distribution analysis for boron neutron capture therapy," *Medical Physics* 18:1, 43-53, Jan/Feb 1991.

Nigg, D.W., Mitchell, H.E., et al., "Epithermal Photoneutron Source Studies for BNCT," Proceedings of the First International Workshop on Accelerator-Based Neutron Sources for Boron Neutron CaptureTherapy, 373, Sept. 1994.

O'Dell, A. A., et al. *Nucl. Instr. Methods* 61:340, 1968.

O'Dell, A. A., Sandifer, C. W. et al. *Nucl. Instr. Methods* 61:340, 1968.

Parsons, D.K., "ANISN/PC Manual," EGG-2500, INEL, Dec. 1988.

Pettersson, O., Svensson, P., Larsson, B. and Grusell, E., "Studsvik Thermal Neutron Facility." In: Progress in Neutron Capture Therapy for Cancer. New York: Plenum, 1992.

Rarita, W., "Deuteron and Triton Methods", *Physical Review*, 1799-1801, Dec. 15, 1948.

Rhoades, W. A. and Childs, R. L., "An Updated Version of the DOT-4 One- and Two-Dimensional Neutron/Photon Transport Code, ORNL-5851, Oak Ridge National Laboratory, 1982.

Rief, H. et al. "Generating Epi-thermal Neutron Beams for BNCT at TRIGA reactors." In: Abstract Book - 5th International Symposium on Neutron Capture Therapy for Cancer. Columbus, OH, 1992.

Roussin, R. W., "BUGLE-80 Coupled 47-Neutron, 20 Gamma-Ray P_3 Cross Section for LWR Shielding Calculations", DLC-75, Radiation Shielding Information Center, Oak Ridge National Laboratory, 1980.

Sakurai, Y., Kobayashi, T., Kanda, K., et al. "Improvement of Thermal Neutron Fluence for BNCT Treatment of Deep-seated Tumors: Simulation Calculation and Phantom Experiments." In: Advances in Neutron Capture Therapy. New York: Plenum, 1993.

Schiff, L. I., "Energy-Angle Distribution of Thin Target Bremsstrahlung," *Phys. Rev.* 83:2, 252-256, 1951.

Seltzer, S. M. and Berger, M. J., "Energy Deposition by Electron, Bremsstrahlung, and ^{60}Co Gamma-Ray Beams in Multi-Layer Media," *Appl. Radiat. Isot.* Vol 38:5, 349-364, 1987.

Shefer, R. E., Klinkowstein, R. E., Yanch, J. C., and Brownell, G. L., "A Versatile, New Accelerator Design for Boron Neutron Capture Therapy: Accelerator Design and Neutron Energy Considerations," In: Neutron Beam Design, Development, and Performance for Neutron Capture Therapy, New York: Plenum, 1990.

Sirlin, A., *Phys. Rev.*, 106:637, 1957.

Soloway, A. H., "Presentation at the National Cancer Institute Board of Scientific Counsellors." In: Boron Compounds Suitable for Neutron Capture Therapy for the Treatment of Cancer. NCI: Bethesda, MD, 1988.

Starfelt, N. and Koch, H. W., *Phys. Rev.* 102:1598, 1956.

Storr, G. J., Allen, B. J. et al. "Design Considerations for the Proposed HIFAR Thermal and Epithermal Neutron Capture Therapy Facilities." In: Progress in Neutron Capture Therapy for Cancer. New York: Plenum, 1992.

Ulrey, C. T., *Physics Review* 11:401, 1918.

Vroegindeweij, C., "Micro-dosimetry Model: A Preparatory Study," ECN-I-93-010 ECN Netherlands Energy Research Foundation, March 1993.

Wang, C.-K. Ch., Blue, Th. E., Gahbauer, A., "A design study of an accelerator-based epithermal neutron source for boron neutron capture therapy." *Strahlentherapie und Onkologie* 165: 75-78, Februar/Marz 1989.

Wang, C.-K. Ch., and Moore, B. R., "On the Study of Energy Spectra and Angular Distriibutions of the Neutrons Emitted from a Beryllium Target Bombarded with 4-MeV Protons for Neutron Capture Therapy," In: Advances in Neutron Capture Therapy. New York: Plenum, 1993.

Wang, C.K., "Thick Beryllium Target as an Accelerator-Based Neutron Source for Neutron Capture Therapy," Proceedings of the First International Workshop on Accelerator-Based Neutron Sources for Boron Neutron Capture-Therapy, 161, Sept. 1994.

Wattenberg, A., "Photo-Neutron Sources," *Preliminary Report No. 6 Nuclear Science Series*, July, 1949.

Whittemore, W. L., "A Compact TRIGA Reactor for Boron Neutron Capture Therapy." In: Progress in Neutron Capture Therapy for Cancer. New York: Plenum, 1992.

Wu, T. H., "A Low Energy Accelerator-Based Neutron Source for Boron Neutron Capture Therapy," Dissertation in Nuclear Engineering Program of University of Missouri-Columbia, Aug. 1992.

Wu, T. H., Brugger, R. and Kunze, J. F., "Low Energy Accelerator-based Neutron Sources for Neutron Capture Therapy," In: Advances in Neutron Capture Therapy. New York: Plenum, 1993.

Yanch, J. C., Zhou, X-L, and Klinkowstein, R. E., "Accelerator-Based Epithermal Neutron Beam Design for Neutron Capture Therapy," *Medical Physics*, 19:3, 709-721, May/June 1992.

Yanch, J. C., Zhou, X-L, et al. "Design of an Accelerator-Based Epithermal Neutron Beam for Boron Neutron Capture Therapy." In: Progress in Neutron Capture Therapy for Cancer. New York: Plenum, 1992.

Yoshizaki, T., Ikeuchi, I. and Nagasawa, K., "Quality Control of $Na_2{}^{10}B_{12}H_{11}SH$ for Neutron Capture Therapy," In: Neutron Capture Therapy (Hatanaka, H. ed.), Norwell, MA: MTP Press, 1986.

VITA

Hannah Elizabeth Mitchell was [redacted] vania. She attended high school in Bartlesville, Oklahoma, graduating in 1985. Following graduation, Hannah went on to obtain her Bachelor of Science from Carnegie Mellon in 1989 with a double major in electrical engineering and physics and a minor in music. After six months as an engineer for Digital Equipment Corporation in Vermont, Hannah enrolled in January of 1990 at the Georgia Institute of Technology, where she obtained her Master's degree in medical health physics one year later. She was awarded a scholarship to study at the Eidgenössische Technische Hochschule in Zürich, Switzerland for 1991-1992; in addition, she spent the first half of 1992 working at a large consulting firm in Zürich until her return to Georgia Tech in Atlanta in the fall of 1992. She then entered the Ph.D. program under the guidance of Dr. Ratib Karam. Much of her thesis research was conducted at the Idaho National Engineering Laboratory in Idaho Falls, Idaho beginning in late 1993. She also spent three months on an American Nuclear Society graduate student fellowship at the Kernforschungsanlage in Jülich, Germany. Following a March 1996 defense, she intends to spend several weeks at a JSPS-funded post-doctoral position in the physics department of Kyoto University in Kyoto, Japan. Upon her return, she will continue in BNCT research as a postdoctoral research at the Idaho State University in Pocatello, Idaho under the guidance of Dr. Frank Harmon. She is currently a member of both the American Association of

Physicists in Medicine and the Health Physics Society. Other interests and hobbies of hers include: piano, languages, rock climbing, hiking, reading, travelling, running, skiing, sky diving, juggling, and board games.

Publication List

- "Apparent Dose Equivalents Resulting from Severe Heating of Film Dosimeters", *Health Physics* Vol. 60, No. 4 (April) pp. 597-601, 1991 (Kearfott, K., Mitchell, H.E, et al.)
- "Development of Automated System for Phase Inversion Temperature Measurement", *Topical Report, U. S. DOE* (R. M. Llave, H. E. Mitchell, Ed Norman, D. Olsen), 1987
- "Epithermal Photoneutron Source Studies for BNCT", *Proceedings of the First International Workshop on Accelerator-Based Neutron Sources for BNCT*, Sept. 1994, Jackson, WY
- Ph.D. Thesis: (completed 1996) "An Accelerator-Based Epithermal Photoneutron Source for Boron Neutron Capture Therapy", Georgia Institute of Technology, Atlanta, GA, advisors: Dr. Ratib Karam/Dr. David W. Nigg
- pending article in *Medical Physics* journal 1996